A PHYSICALLY MEANINGFUL MODEL OF VERTICAL CRUSTAL MOVEMENTS IN CANADA USING SMOOTH PIECEWISE ALGEBRAIC APPROXIMATION: CONSTRAINTS FOR GLACIAL ISOSTATIC ADJUSTMENT MODELS

AZADEH KOOHZARE

April 2007

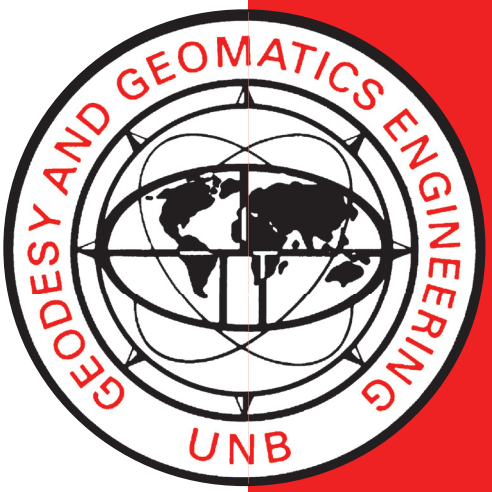

TECHNICAL REPORT
NO. 246

A PHYSICALLY MEANINGFUL MODEL OF VERTICAL CRUSTAL MOVEMENTS IN CANADA USING SMOOTH PIECEWISE ALGEBRAIC APPROXIMATION: CONSTRAINTS FOR GLACIAL ISOSTATIC ADJUSTMENT MODELS

Azadeh Koohzare

Department of Geodesy and Geomatics Engineering
University of New Brunswick
P.O. Box 4400
Fredericton, N.B.
Canada
E3B 5A3

April 2007

PREFACE

This technical report is a reproduction of a dissertation submitted in partial fulfillment of the requirements for the degree of Doctor of Philosophy in the Department of Geodesy and Geomatics Engineering, April 2007. The research was supervised by Dr. Petr Vaníček and Dr. Marcelo Santos, and funding was provided by the GEOIDE Network of Centres of Excellence.

As with any copyrighted material, permission to reprint or quote extensively from this report must be received from the author. The citation to this work should appear as follows:

Koohzare, A. (2007). *A Physically Meaningful Model of Vertical Crustal Movements in Canada Using Smooth Piecewise Algebraic Approximation: Constraints for Glacial Isostatic Adjustment Models*. Ph.D. dissertation, Department of Geodesy and Geomatics Engineering, Technical Report No. 246, University of New Brunswick, Fredericton, New Brunswick, Canada, 174 pp.

DEDICATION

To my supportive parents

for giving me a
chance to prove and improve myself through all my walks of life.

ABSTRACT

Different kinds of analytical models of crustal deformation have both advantages and limitations, and are appropriate to different deformation patterns. However, in wide areas where multiple geophysical phenomenon are responsible for the deformation, such as in Canada, it would be a challenge to infer a physically meaningful model that accommodates different kinds of scattered geodetic data, while offering the optimum approximation to them.

We develop an efficient method to automatically compute a smooth approximation of large functional scattered re-levelling data and historical tide gauge records given over Canada and northern US to thereby compile a unified map of Vertical Crustal Movements (VCM). The area of study is divided into patches and piecewise algebraic surfaces are fitted to 2D observation points and tilt between them, where constraints are enforced between the parameters of the surfaces. When the surfaces are fitted to the data, the set of constraints is imposed in such a way that rather than the surfaces being fitted sequentially, they are fitted simultaneously.

The VCM model accomplished in this research is computationally demanding and numerically manageable. Enforcing the continuity and smoothness in the first derivatives throughout the surfaces, the VCM model highlights the long wavelength spatial variations of the crust in Canada, mainly due to Post Glacial Rebound (PGR).

The rate of changes of orthometric height obtained from the map of VCM ($\dot{H}$) is compared with the map of rate of gravity changes ($\dot{g}$) in Canada (Pagiatakis and Salib, 2003). The PGR hinge line follows the same pattern in both maps and the close correlation between the map of VCM and $\dot{g}$ map is easily traceable and is in a fairly good agreement with theoretical model of Jachens (1978) in different areas.

The VCM is also compared to geodetic height changes based on GPS solutions in Canadian Base Network (CBN) stations (Henton et al., 2006). This investigation shows disagreement with the GPS solution in Canadian prairies. In this study, some of the probable causes of such inconsistencies are explored.

VCM is also collated to theoretical predictions based on the published ICE-3G and ICE-4G loading history and on a model of Earth rheology characterized by stratified viscosity variations (Tushingham and Peltier, 1991; Peltier, 1994).

In this study, a map of ratio between gravity changes to height changes is compiled and physically interpreted. Using VCM and geodetic height changes from CBN-GPS solution, a map of rate of geoidal height changes is also compiled and interpreted in some areas in Canada.

The VCM constraints on Glacial Isostatic Adjustment (GIA) model parameters are investigated by varying, one at a time, two key parameters: 1) viscosity in different layers, and 2) the thickness of Laurentide ice over individual ice disks in Eastern Canada, and the Prairies, to obtain better fits to the VCM. In Eastern Canada, the VCM is consistent with an increase in the upper mantle viscosity. In The Great Lakes, the VCM has a better agreement with the predictions of GIA computed considering a lower viscosity for different layers of mantle. This study shows also that near the center of rebound at Churchill, present day vertical crustal movement is most sensitive to the viscosity in the shallow part of the lower mantle and the transition zone (UM2). The VCM is consistent with a thinning of the Laurentide ice-sheet over the Prairies relative to both standard ice models. These analyses leads to better understanding of the trade-offs between Earth rheology and ice sheet history and hence some suggestions are made to improve postglacial rebound model.

ACKNOWLEDGEMENTS

This work is dedicated to my parents. It simply would not have been done without their support from far away.

In a project spanning so many years, there are countless people to whom thanks are due. First and foremost, I am deeply indebted to my supervisors, Professor Petr Vaníček and Professor Marcelo Santos for all their guidance, advices and preserving supports. Their efforts in reviewing my manuscripts and patience in dealing with my stubbornness and ambitiousness are gratefully appreciated.

I would like to thank the members of my Examination Committee, specially my Internal Appraiser, Professor Karl Butler (Geology) and my External Examiner, Professor Zdenek Martinec (GeoForschungsZentrum Potsdam). Their constructive comments and recommendations, together with those from the other members of my Examination Committee, are greatly appreciated. Dr. Anna Szostak-Chrzanowski is acknowledged for her insights, advice and friendship. Her comments are greatly appreciated.

I also thank Professor Patrick Wu from the University of Calgary. The discussion I had with him, during my stay in Calgary, was really helpful. Professor Spiros Pagiatakis, from York University, and Dr. Mike Craymer and Dr. Joe Henton from Geodetic Survey Division, NR Canada are acknowledged for spending time and opening the discussion door to me. Dr. Hugh Thomas in the Department of Mathematics and Statistics is acknowledged for his time and constructive comments in the mathematical discussion. I also express my thanks to Professor W.R. Peltier from the University of Toronto and Dr. Tony Lambert from Pacific GeoScience Center, Geological Survey of Canada for sending my copies of their publications.

I thank the Department of Geodesy and Geomatics Engineering, especially the chair of the department, Professor Peter Dare and the chair of the graduate studies in my department, Professor Sue Nichols, and also the kindness of Sylvia Whitaker, the secretary of graduate studies. Special thanks go to Nicole, Felipe, Robbie, Artu, Sam, Garret, Jason and many others for their friendship. I express my gratitude to GEOIDE Network (Geomatics for Informed Decisions) for funding this work.

The Canadian re-levelling Data was provided to me by Dr. Andre Maninville from the Geodetic Survey Division, N.R. Canada and the U.S. levelling information were provided by Dr. Dave Zilkoski from U.S. Geological Survey. The tide gauge data were provided by Dr. Thomson from Marine Environmental Data Service (MEDS) in Canada.

Last but not least, I deeply thank my best friend, Sasan, for his unfailing support, encouragement and advices throughout my degree. I owe him a huge debt of gratitude.

Table of Contents

List of Tables

List of Figures

List of Symbols, Nomenclature or Abbreviations

ACS	…Active Control System
BM	…Bench Mark
BP	…Before Present
CBN	…Canadian Base Network
CGSN	…Canadian Gravity Standardization Network
CORS	…Continuously Operating Reference Station network
CSZ	…Charlevoix Seismic Zone
ESS	…Earth Science Sector
GC	…Geoid Change
GIA	…Glacial Isostatic Adjustment
GSD	…Geodetic Survey Division
IAG	… International Association of Geodesy
IGS	… International GNSS Service
ITRF	…International Terrestrial Reference Frame
Kyr	…1000 years
LM	…Lower Mantle
MEDS	…Marine Environmental Data Service
MQ	…Multiquadric
MSL	…mean sea level
Mod	…Model of Earth rheology
NGS	…National Geodetic Survey
NRCan	…National Resources Canada
PCG	…Pacific Geosciences Center
PGR	…Post Glacial Rebound
RD	…Radial Displacement
RSL	…Relative Sea Level
SINEX	…Independent Exchange Format
SNARF	…Stable North American Reference Frame

SPAA	…Smooth Piecewise Algebraic Approximation
VCM	…Vertical Crustal Movement
VM	…Viscosity Model
UM	…Upper Mantle

Throughout this dissertation, the following notation is used:

variables/ observables	italic
vector	lower case, boldface letters
matrices/operators	upper case, boldface letters
functions	upper or lower case letters, no boldface
< , >	Inner product

Chapter 1

Introduction

Geodetic observations play an important role in detecting and qualifying the vertical crustal movements (VCM), which are in turn, of great importance in geosciences. In geophysics, for example, VCM are of primary interest in the study of the rheology of the mantle and lithosphere, which is crucial in understanding geodynamical processes (for recent reviews, see Peltier (1998), Lambert et al. (2001) and Wahr and Davis (2002)). In geodesy, VCM are important in the definition of vertical datum that is required in many application areas such as navigation, mapping, and environmental studies (See for instance Rapp (1994), Pan and Sjöberg (1998), Henton et al. (2006)).

There are different kinds of geodetic data with vastly different accuracies, which contain information on the vertical movements of the crust. Therefore, the main problem is to put together the various types of available data with VCM models designed to detect and describe the crustal movements. The VCM model should also be physically meaningful so that it not only describes the actual movements of the crust, but also opens doors to the study of the causes of the movements, validates the geophysical models of the movements and perhaps, as an independent constraint, resolves the trade-off in some of the geophysical models (Velicogna and Wahr, 2002).

During the past few decades, intensive research and progress have been made on the development of vertical crustal deformation models. Very comprehensive reviews of modeling strategies for vertical crustal deformation are presented by, e.g., Vaníček and Christodulides (1974), Holdahl (1978), Gubler (1984), Chrzanowski et al. (1986), Vaníček and Sjöberg (1987), Carrera et al. (1991), Liu and Parm (1996), Liu and Chen. (1998). All of the models can estimate deformation parameters for multi-epoch observations. They provide the convenience of predicting deformation in time-space domains, which is very important for studying the time and areal distribution of deformation (Liu and Chen, 1998). However, since a crustal deformation is a complex

process and should be analyzed by choosing different models for different deformation areas of interest, and since selecting a particular deformation model for a particular deformation area is very difficult, the above models cannot be used in their current form over a wide area of interest such as Canada where different geophysical phenomena contribute to the deformation.

The first VCM model which covered the whole of Canada was compiled by Vaníček and Nagy (1981) using precise re-leveled segments and tide gauge records. The country was divided into regions and polynomial surfaces of order 2, 3 and 4 were calculated by the method of least squares for each region to obtain representations of the vertical movements. A considerably larger database has been gathered since then, and this, together with additional insight into the nature of the data, led to the recompilation of the map of VCM of Canada by Carrera et al. (1991) in which a polynomial surface was fitted to the data. Those models also have some limitations. A significant limitation is that to get the details needed for the map to be meaningful, the order of the velocity surface would have to be too high. This would cause wild oscillations (artifacts) where there is no data. Other limitations are severe restrictions on the number and distribution of data and limitation to handle large linear equation systems (Haber et al. 2001).

In this work, we divide the area of interest into patches and fit a piecewise surface to 2D observation points and tilt between them, where constraints are enforced between the parameters of the surfaces. When the surfaces are fitted to the data, the set of constraints is imposed in such a way that rather than the surfaces being fitted sequentially, they are fitted simultaneously, using the constraints as a set-condition which the parameters of the surfaces must also satisfy. Enforcing the constraints guarantees a certain degree of smoothness (differentiability) of the resulting function.

The compiled surface should also be physically meaningful. In order to infer such a VCM, it is necessary to combine the geodetic and geophysical data, theories, methodologies and techniques that are linked together. Hence, the study of different geodynamical processes that contribute to the deformation of the crust, the interaction between them, and finally finding the best approach to reconcile geodetic data with geological phenomena, are required.

In North America, the most significant geophysical process that has an evident effect on the shape of the viscoelastic earth is Post-Glacial Rebound (PGR) or Glacial Isostatic Adjustment (GIA), arising from the melting of the ice sheets, that began at Last Glacial maximum (LGM), some 21000 years before present (21ka BP) and was completed at approximately 7ka BP (Peltier, 1994). PGR manifests itself through a 3-D displacement of the Earth's crust in the vicinity of the LGM, along with a change of gravity arising from the crustal uplift and mantle flow (Wahr et al., 1995; Ekman and Makinen, 1996).

The global theory of the GIA was first formulated by Farrell and Clark (1976), Peltier and Andrews (1976). A method was developed for constructing the impulse-response (Green) functions, that are required to compute the visco-elastic response of the Earth to an arbitrary variation of surface mass load. Since then, more intensive research has been conducted to improve the model either by modifying the Earth rheology parameters e.g., Peltier (1998), Martinec (2000), Wu (2002); Velímský and Martinec (2005) or by implementing different mathematical approaches for computing the Earth response to surface load (e.g., Le Meur and Hindmarsh, 2000). Parallel to these developments, the long period ($10^3 - 10^4$ years) and small steady deformations of the crust due to GIA have been detected by precise geodetic observations. However, no significant attempt has been made to employ geodetic observations for refining the geophysical model of GIA to thereby provide a physical meaningful VCM model. The main problem with observed geodetic variations in GIA contexts is that of the time-scale. Geodetic observations can reveal the variations of the shape and the gravity field of the Earth over relatively short time intervals, i.e. several decades, while postglacial rebound has been ongoing on time scale of 10^3-10^4 years. Another problem is that of interpretation: How can we interpret them in terms of different earth parameters, lithosphere thickness, and the ice sheet history? How much of the observed changes are due to GIA process? How much are the contribution of plate tectonic movements, intraplate deformations, tidal deformations and the Earth's rotation or polar motion?

In this work, some ideas are explored in an effort to obtain a more physically meaningful VCM model for Canada. Using Smooth Piecewise Algebraic Approximation (SPPA) method, the velocity surfaces are computed in pieces, and then they are tied together to guarantee their continuity across the pieces boundaries. We then compare this

model with other geodynamical studies in Canada and show how the VCM constrains the GIA models.

1.1 Research objective

The ultimate goal of this study is to infer a physically meaningful VCM model for Canada using physical models and geodetic observations in the same frame. This is conducted by modeling the vertical crustal movements using smooth piecewise algebraic approximation to the scattered data of tide gauge linear records and re-levelling data. The rate of height changes with respect to geoid obtained from the model of VCM is then compared with other studies of geodynamics in the region, and the misfits are interpreted. Then the sensitivity of the VCM to uncertain physical parameters in the GIA models (mainly viscosity and ice thickness) is investigated, and the physical parameters in the GIA models that make a best fit with VCM are discussed.

1.2 Thesis contributions and its outline

The main contributions of this work are summarized as follow:

- Developing a method for the surface fitting to scattered data of different types (SPAA).

  In this work, we develop a method for the surface fitting to scattered data of different types in the form of a VCM not only in which the details of the movements can be predicted with reasonable accuracy, but also which compiled as a unified surface in a simultaneous solution.

- The compilation of a physically meaningful map of VCM using the SPAA.

  The map of VCM in Canada is complied using SPAA, and in spite of the sparse data in some areas, we manage to obtain a stable solution for Canada.

- Comparison of VCM with other studies and physical interpretation in different areas.

The VCM solution is compared with other geophysical and geodetic solutions of the crustal movements, including GIA models, rate of gravity changes, and rate of geodetic height changes. The map of VCM in Canada is physically interpreted in different regions and the probable sources of the movements in each area in Canada are investigated.

- The compilation of a map of ratio between gravity changes to height changes in Canada and its physical interpretation.

For the first time in Canada, a map of ratio between gravity changes to height changes is compiled using the VCM and rate of gravity changes from Pagiatakis and Salib (2003). The map of ratio between gravity changes to height changes is discussed and compared with stochastic model of Jachen (1978).

- The compilation of a map of geoidal height in Canada and its physical interpretation.

The map of rate of geoidal height changes is compiled using the VCM and the GPS solution in Canadian Base Network. This map is further interpreted and the probable sources responsible for the geoidal height changes in some areas are discussed.

- Investigation of the use of VCM as constraint for the GIA models

The sensitivity of the VCM to the radial viscosity changes and ice thickness as two key parameters in the GIA models is tested, and some modifications are recommended. In particular, this study suggests the consideration of the lateral viscosity in the GIA modeling and it indicates that a thinner ice in the Praries gives a better fit with VCM.

The secondary contributions of this work are summarized as:

- Analysis of the available historical tide gauges in Canada.

In this research, the historical tide gauge records are analyzed after the last study by Carrera et al. (1991). The monthly mean sea level record from each individual historical tide gauge in Canada is analyzed to detect the probable systematic errors and datum biases and linear trends of the records of the tide gauges are calculated.

- Desigining the optimum differencing tree in Atlantic and Pacific.

In this study, the differencing method is used to cancel out the effect of oceanic noises in the records of the tide gauges. The optimum networks for the differencing method in Atlantic and Pacific is designed.

- Developing an algorithm to retrieve the re-leveling data.

An algorithm is developed by which nearly 50,000 re-leveling data from the 1st order Canadian network is retrieved. The algorithm is then used to retrieve the U.S. re-leveled segments for further analysis.

- The use of GIS as a tool for geodetic analysis

Throughout this research, GIS is used extensively in geodetic spatial analysis. For example, spatial analysis in GIS is used to determine the optimum differencing network for the tide gauges.

- Organizing a data bank for geodynamics studies.

A database of re-leveled segments, tide gauge records, rates of gravity changes, geoidal changes, geodetic changes and orthometric changes up to 2006, is organized. Other data that would be available in future can be simply added to the database and used to improve the model.

- Identifying the leveling lines in 1st order Canadian leveling network that need to be re-leveled to help in crustal motion studies.

In chapter 2, an overview is given of the methodology used to model VCM. The first sections of the chapter describe the general procedures normally adhered to when performing a scattered data fitting task, and discuss the advantages and limitations of different fitting approaches, when dealing with geodetic data. This is followed by the mathematical formulation of our method of smooth piecewise algebraic approximation to model VCM and to assess the computed unknown parameters. Chapter 3 is concerned with the characteristics of observable quantities, i.e. those data that determine the unknown parameters of VCM. It is shown how geodetic observables are introduced into the VCM model. This includes 1) the utilization of GIS to accommodate all data in the same framework, 2) error analysis or assessment of re-levelling data; and, 3) detection of the secular variations of the movements from the tide gauge records. In chapter 4, the VCM in Canada are computed using SPAA and the pre-analyzed geodetic data. The problems in the compilation are discussed and the prescribed remedies are presented. The resulting VCM is then compared with GIA models. To do GIA models the justice they deserve in the context of VCM in Canada, and since these models are going to be constrained with geodetic VCM, the whole of chapter 5 is devoted to the concepts of GIA modeling needed in our research.

One of the main contributions of this work is the physical interpretation of the results and the comparisons with other studies. This includes the comparison of the VCM with 1) GIA models based on the ICE-3G and ICE-4G ice history and an approximation to the standard Earth rheology models; 2) The map of temporary changes of gravity; 3) The rate of changes of the geodetic heights in GPS stations. Moreover, the sensitivity of the VCM to different uncertain parameters of GIA models such as viscosity and ice thickness are studied for different areas of Canada, and the GIA models are modified using the new parameters and forward modeling. Furthermore, the amount of the misfit between VCM and the modified GIA models are discussed. These are all the contents of chapter 6 of this

dissertation. Finally, the conclusions and recommendations for future investigations are given.

Chapter 2

Mathematical Model

2.1 Introduction

In order to predict the spatial vertical velocities, or uplift rates, a vertical velocity surface should be fitted to the scattered geodetic data which are both the point rates and the gradients. The point rates are determined from some of the tide gauge data which are used in the point velocity mode, and the gradients come from re-levelled segments and tide gauge pairs.

In this chapter, the focus is on the problem of functional scattered data fitting. Two sets of pairs of points and a set of individual points are given as follows:

$$\begin{aligned} &\{(x_i, y_i), (x_j, y_j)\} \in \Omega, i = 1,..., N, j = 1,..., N \\ &(x_t, y_t) \in \Omega, t = 1,..., p \end{aligned}, \tag{2.1}$$

where Ω is a bounded domain in the plane of observations. Their corresponding values $\Delta V_{ij} = V_j - V_i, i, j = 1,..., N,$ and $V_t, t = 1,..., p,$ are the relative and absolute vertical velocities, respectively, which are determined from geodetic data. We want to find a method to construct a velocity surface $S : \Omega \mapsto R$ that meets as many as possible of the following goals:

- Approximation: S should approximate different types of data while satisfying least square approximation .i.e.,

$$\begin{aligned} &\{S(x_j, y_j) - S(x_i, y_i)\} \approx \Delta V_{ij} (i, j = 1,..., N). \\ &S(x_t, y_t) \approx V_t (t = 1,..., p). \end{aligned} \tag{2.2}$$

- Quality: S should be of high visual quality (i.e., S should be continuous and smooth) and have convenient properties for further processing.
- Independency: the method should be independent of the choice of *nodal points*.
- Usability: large number of geodetic data, where N is typically of the order of 10^5, should be manageable.
- Stability: the computation of S should be numerically stable, i.e., the method should work for any distributions of scattered points.
- Adaptiveness: the local variation and distribution of the data should be taken into account.
- Simplicity: the method should be easy to implement.

Although many approaches have been developed mainly in mathematics and computer sciences, the literature show that it is a difficult task to meet all of the above goals by using one single method. The main limitation of all the methods is that they can not be used for different types of data, point values and relative values (tilt) between points. Other limitations are severe restrictions on the number of data, restriction on the domain and distribution of the data and a limitation to handle large linear equation systems (Haber et al. 2001). Some of the methods are reviewed and their limitations are discussed in section 2.2. In section 2.3, our method of Smooth Piecewise Algebraic Approximation (SPAA) which will be proved useful in global approximation is presented. This method is based on simultaneous fitting of piecewise surfaces to 2D observation point field and tilt between them, where constraints are forced on the parameters of the surfaces. When the surfaces are fitted to the data, the set of constraints is imposed in such a way that rather than the surfaces being fitted sequentially, they are fitted simultaneously, using the constraints as a set-conditions which the parameters must also satisfy.

2.2 Review of existing models of VCM

There are many different approaches to scattered data fitting in the computer science literature, where the data are the point values (scattered point fitting); see for instance the survey and overview in Frank (1982), Lancaster and Salkauska (1986), Lodha and Franke (1999); however, when dealing with the scattered tilt data, those methods cannot be used directly and need to be modified in such a way as to be able to fit with these types of data. In this section, all the methods of data fitting are classified into two groups and the advantages and limitations of each method are discussed. These methods are: 1) fitting a unified surface to the data in one stage; and, 2) fitting piecewise surfaces.

2.2.1 Unified surface fitting to the data

The main idea is to provide an approximation surface, $V(x, y)$, to the data. Generally, the velocity surface can be expressed as:

$$V(x, y) = \sum_{i=1}^{I} c_i \psi_i (x, y), \tag{2.3}$$

where ψ_i are some basis functions of position and c_i are the best fitting coefficients to the observations (Vaníček and Christodulids, 1974).

Different models can be produced by choosing different suitable basis functions. All of them have their own advantages and disadvantages and are appropriate to different deformation behaviours. Practically, the two dimensional algebraic functions would be used in most cases. The basic equation then becomes:

$$V(x,y)=\sum_{i,j=0}^{n} c_{ij}x^{i}y^{j}, \tag{2.4}$$

where *n* is the degree of the polynomials, and c_{ij} are the sought coefficients (Vaníček and Nagy, 1981). Here, the algebraic functions are the simplest functions to deal with numerically and are adequate when the solution is confined to the regions where sufficient data exists; the poor behaviour appears only when the solution is used in an extrapolation mode. These models are more applicable in the compilation of a map of VCM as they can handle both point and tilt data. In other words, different types of input data can be used in one model. To get the details needed for the map to be meaningful, the order of the velocity surface would have to be too high to be numerically manageable. This would cause wild oscillations (artifacts) where there are no data.

Another active area of research for scattered point fitting is radial basis methods (Dyne et al., 1986). Generally, by a radial function, we mean a function:

$$g: R^{d} \to R: (x_1, x_2, ..., x_d) \mapsto \phi(\|x_1, x_2, ..., x_d\|_2), \tag{2.5}$$
$$\text{for some function } \phi: R \to R.$$

Here *d* represents the dimensionality of the problem, i.e., *d*=2 in our case. In other words, the function value of *g* at a point $\bar{x}=(x_1, x_2, ..., x_d)$ only depends on the L2-norm[1] of $\bar{x}$. An example of such a radial method is the Multi Quadric method (MQ) of Hardy (1978). This method considers the vertical crustal deformation as one kind of continuous change which can be approached precisely by the superposition of Multi Quadric functions:

[1] For the definition of L2-norm, Please see *MathWorld*--A Wolfram Web Resource. http://mathworld.wolfram.com/L2-Norm.html

$$V(x, y; t - t^0) = \sum_{i=1}^{k} c_i K(x, y, x_i, y_i)(t - t^0), \tag{2.6}$$

in which t is the present epoch; $t°$ is a pre-specified initial epoch, K is the kernel function, i is its running number and k is the total number of kernel functions; c_i is the unknown coefficients. The general form of K is:

$$K(x, y, x_i, y_i) = [(x - x_i)^2 + (y - y_i)^2 + \delta^2]^b, \tag{2.7}$$

where (x_i, y_i) is the nodal point, δ is the smoothing factor, b is selected to determine the form of the function; usually, it is chosen to be b=1, ½ or -½ , etc. (Liu and Chen, 1998). Special attention should be paid to the location of nodal points, which indeed controls the pattern of the surface. This method strongly depends on the choice of (x_i, y_i), and while dealing with tilt data, deciding about where to choose the nodal points is nontrivial. Figure 2.1a, b show how effectively the nodal points control the pattern of the surface.

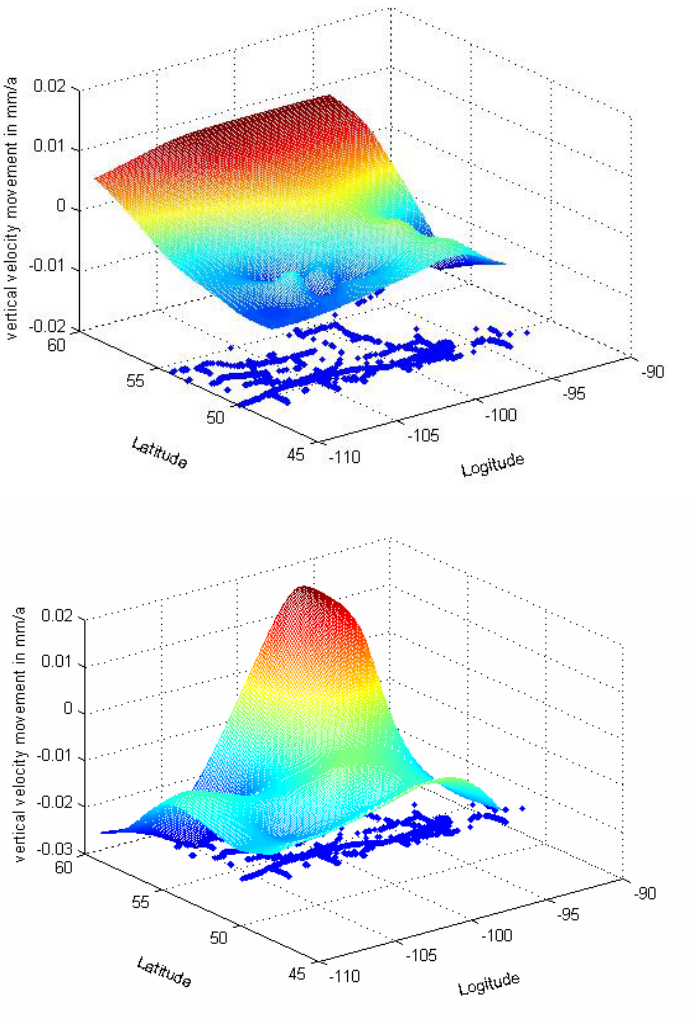

Figure 2.1: The vertical velocity surfaces obtained using the MQ analysis, using two different sets of nodal points. The blue dots show the location of data points (Here levelling BM).

Holdahl et al, (1978) suggested that the location of the nodal points can be determined by a review of leveling profiles to find the maxima and minima of the relative motion for each route of re-levelling. However, it would be an uncertain task to distinguish the maxima and minima of the point values from the highest and lowest tilt.

Another problem is that radial basis methods usually require solving large, ill-conditioned linear systems of equation. Therefore, sophisticated iterative techniques are needed for the computation of the radial function interpolants (Haber et al., 2001).

2.2.2 Piecewise fitting methods

A practical way to avoid the problem of wild oscillations due to using a unified surface is to divide the area of study into pieces, and seek the velocity surface piecewise. One of the most common methods in this area is the use of Free-form Blending (Moore and Warren, 1991). In this approach, the fitting is performed locally and the results are merged to form a global approximation. First, a uniform trianglar mesh of elements that cover the data is constructed, and then for each individual mesh element *E*, an algebraic surface that fits the scattered data is computed. For each vertex of *E*, the function and its derivatives are extracted from the computed fitting surface in each individual element. Then, the function and the derivatives of the fitting surface data from all touching elements are averaged at each vertex of the mesh. These averages values for the function and the derivatives are used to produce a continuous surface. This method was originally developed for surface reconstruction and was further developed in complicated objects (See for example Turk, 1992, Kobbelt et al., 2000). Figure 2.2 shows a continuous linear approximation to a simulated data using Free- form blending.

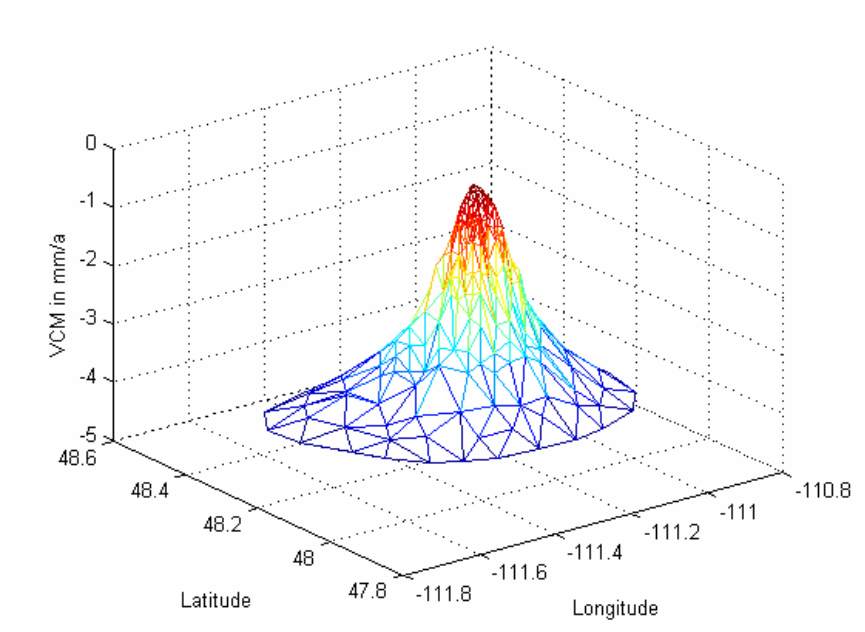

Figure 2.2: A continuous piecewise linear approximation to a simulated data using Free- form blending

These methods are fast and easy when there are dense data, but when the data is sparse, it would not be useful (Kobbelt et al., 2000). On the other hand, the functional value at each vertex is to be known, while in this study, the point values are available only in some of the elements.

Another common approach is the use of spline functions. Spline is a special function defined piecewise by polynomials. There are several types of splines that can be used. The simplest approach in data fitting using splines is to apply tensor product splines (Dierckx, 1993, Forsey and Bartels 1995, Greiner and Hormann, 1996, and Gregorski et al., 2000). In general, tensor product methods are straightforward to apply only for the data given on a grid (Haber et al., 2001). Parametric bicubic splines are subdivided to approximate 3D points with a regular quad-mesh[2] structure (Haber et al., 2001), and multilevel B-splines are used to approximate scattered data points (Lee et al., 1997). Other spline methods are based on simplex splines or splines of finite-element type (Zhou et al., 1997). The simplest example of finite element splines are continuous piecewise

[2] Quadmesh is a mesh made up of quadrilaterals.

linear functions with respect to a suitable triangulation of the planar domain. It is well-known that these methods which are based on piecewise linear functions can not exceed approximation order 2. To achieve higher smoothness and approximation order, polynomial patches of a higher degree have to be considered.

In particular, there are scattered data methods based on classical smooth finite elements such as Bell quintic element, Frajies de Veubecke-Sander and Clough-Tocher cubic elements, and Powell-Sabin quadratic element (see the above-mentioned surveys and more papers, Dahmen et al., 1990, Dierckx et al., 1992 and Morandi Cecchi et al., 1999). The above-mentioned methods based on finite elements require accurate estimates of derivatives at the data points, which is a nontrivial task by itself assuming that data points might be irregularly distributed (as it is the case in this study). To overcome these difficulties, global least squares approximation and other global methods were considered (Dierckx et al., 1992, Meyling and Pfluger 1990, Zhou et al., 1997)

The basic idea of the method used in this research is related to the approximation scheme of Vaníček and Christodulids (1974). Essential differences are, however, that the piecewise polynomials are used. This method, which we call Smooth Piecewise Algebraic Approximation (SPAA) is different from the standard spline , as the data points are neither triangulated (or quadrangulated), nor interpolated as for instance in (Dahmen et al., 1990) and (Morandi et al., 1999). In particular, there is no need of any pre-estimates of functional values at points different from the given data points. Instead, local least squares approximations are computed, directly in the polynomial form and then the remaining degrees of freedom are settled by continuity conditions, which results in very short computation time. Since this method does not even require a triangulation of the data points, it is very well suited for extremely large datasets. Theoretical aspects of the method are treated in the next section.

2.3 Smooth Piecewise Algebraic Approximation in Geodesy

The procedure of fitting a surface to the geodetic data involves the use of both the point rates and the gradients simultaneously, together with their proper weights. The point rates are determined from some of the tide gauge data which were selected to be used in the point velocity mode, and the gradients come from re-levelled segments and tide gauge pairs.

In order to fit a surface to the geodetic data, it is advantageous first to transform the geodetic coordinates of φ and λ to rectangular coordinates *x* and *y* related to an arbitrary origin located in the center of the region as

$$\begin{aligned} x &= R(\lambda - \lambda_0)\cos\varphi, \\ y &= R(\varphi - \varphi_0). \end{aligned} \tag{2.8}$$

Here, *x* and *y* are easting and northing in a local Cartesian system, *R* is the Gauss radius of curvature, φ_0 and λ_0 are the geodetic coordinates of the origin of the grid.

In general, if we divide the area of study into *p* patches, the resulting function is a polynomial function of degree *n* with *p* patches. A given polynomial in the m^{th} *(m=1, 2,..., p)* patch looks as follows:

$$V_m(x,y) = \sum_{i=0}^{n_x}\sum_{j=0}^{n_y} c_{ij,m}(x - x_{0m})^i (y - y_{0m})^j . \tag{2.9}$$

where V_m is the algebraic least squares velocity surface for patch *m*, fitted to the desired data (*x, y*). The pair (x_{0m}, y_{0m}) represents the position of the origin in patch *m* and $c_{ij,m}$ are the unknown coefficients in patch *m*.

If *m* and m' represent the two adjacent patches having common border mm' (Figure 2.3), then in order to piece the polynomials together, the following conditions should be satisfied:

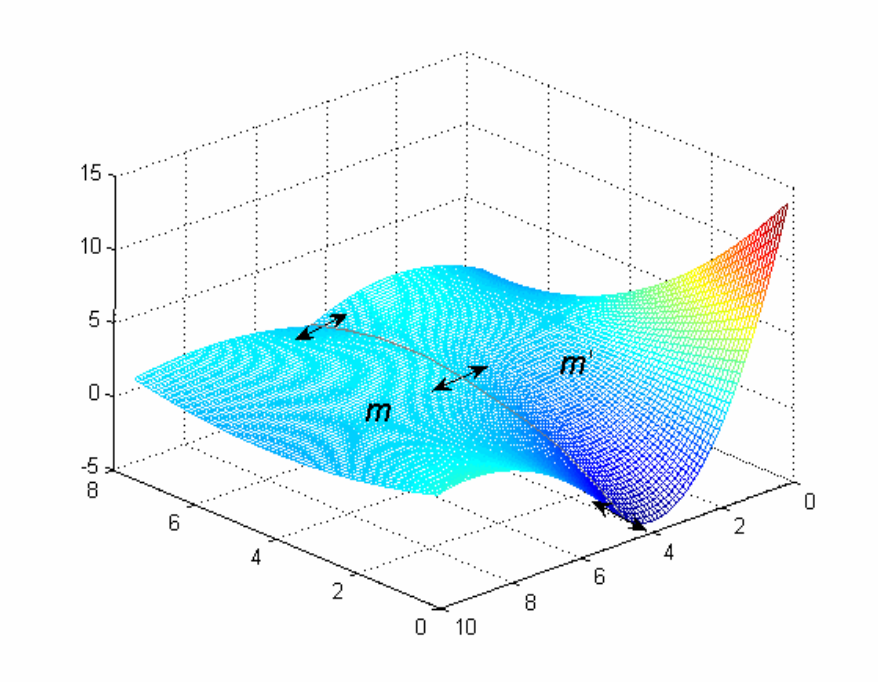

Figure 2.3: Two adjacent patches m and m' and the nodal points in the common border between two patches.

$$V_m(x_{mm',k}, y_{mm',k}) = V_{m'}(x_{mm',k}, y_{mm',k}) \qquad \forall k = 1,2,...,q\,; \tag{2.10.a}$$

$$\left.\frac{\partial V_m(x,y)}{\partial x}\right|_{\substack{x=x_{mm',k}\\ y=y_{mm',k}}} = \left.\frac{\partial V_{m'}(x,y)}{\partial x}\right|_{\substack{x=x_{mm',k}\\ y=y_{mm',k}}} \qquad \forall k = 1,2,...,q\,; \tag{2.10. b}$$

$$\left.\frac{\partial V_m(x,y)}{\partial y}\right|_{\substack{x=x_{mm',k}\\ y=y_{mm',k}}} = \left.\frac{\partial V_{m'}(x,y)}{\partial y}\right|_{\substack{x=x_{mm',k}\\ y=y_{mm',k}}} \qquad \forall k = 1,2,...,q\,. \tag{2.10. c}$$

$(x_{mm',k}, y_{mm',k})$ is the position of k^{th} nodal point in the border mm' joining patches m and m'.

Here, q represents the maximum number of the nodal points in the common border between patch m and patch m'.

Conditions (2.10.a) make sure that the piecewise polynomial fits to the nodal points (P *mm', 1*, P *mm', 2*, …, P *mm', k=q*) located in the predefined border *mm'* between two patches *m* and *m'*. These conditions imply that the surface is continuous everywhere in the region. Conditions (2.10.b) and (2.10.c) ensure that the polynomials are continuous in slope along *x* and *y* directions, respectively. The main mathematical model is given by equation (2.9) while all the conditions under (2.10) constitute the constraints on the main model. (Koohzare et al., 2006a).

Assuming the velocity to be constant in time, the difference of the two leveled height differences divided by the time span between the two levellings gives the velocity difference between the two levelling segment ends, i.e.,

$$V_B - V_A = \Delta V_{AB} = \frac{[H_B(t_2) - H_B(t_1)] - [H_A(t_2) - H_A(t_1)]}{t_2 - t_1} = \frac{\nabla \Delta H_{AB}}{\Delta t}, \qquad (2.11)$$

where V_B and V_A are the vertical velocities at bench marks *B* and *A*, respectively and $H_A(t_1), H_B(t_1), H_A(t_2), H_B(t_2)$ are the heights of the bench marks *A* and *B* determined at times t_1 and t_2. ΔH_{AB} is the height difference between the two bench marks *A* and *B*. Since the height differences obtained from the two levellings are known and so is the time interval Δt, the difference of vertical velocities of the two relevelled adjacent bench marks can be computed. Going back to model (2.9), one can rewrite it in a more suitable form for the velocity differences between two adjacent bench marks (tilt)

$$\Delta V_m(x_A, y_A, x_B, y_B) = \sum_{i=0}^{n_x} \sum_{j=0}^{n_y} c_{ij,m} [(x_B - x_{0m})^i (y_B - y_{0m})^j - (x_A - x_{0m})^i (y_A - y_{0m})^j]. \qquad (2.12)$$

The 'observations' on the left hand side of the equation are used to compute the coefficients by means of least-squares method.

To find the least square solutions, equations (2.12) and (2.10) can be written in a general form:

$$f(\mathbf{c},\mathbf{l}) = 0, \tag{2.13a}$$

$$f_c(\mathbf{c}) = 0. \tag{2.13b}$$

Here, **l** is the vector of observations which includes $V_m(x_t, y_t)$ from the tide gauge observations and $\Delta V_m(x_A, y_A, x_B, y_B)$ from re-levelling data and paired tide gauges. **c** is the vector of unknown coefficients. It is assumed to be possible to solve for **c**, using only the main model (2.13.a). The auxiliary model f_c consists of the constraint functions that are enforced. The above models are then linearized by Mikhail (1976) to yield:

$$\begin{aligned} \mathbf{A\delta} + \mathbf{Br} + \mathbf{w} &= 0, \\ \mathbf{D\delta} + \mathbf{w}_c &= 0. \end{aligned} \tag{2.14}$$

with:

$$rank\ (\mathbf{A})=u \quad rank\ (\mathbf{B})=c \quad \text{and } rank\ (\mathbf{D})=d$$

In equations (2.14), **r** is the vector of expected residuals, and **δ** is the vector of unknowns. Matrices **A** and **D** are the Jacobian matrices of transformation from parameters space to the two model spaces, valid for a small neighborhood of $\mathbf{c}^{(0)}$. Matrix **B** is the Jacobian matrix of transformation from observation space to the main model space. It is observed that equations (2.14) are merely the differentional form of the original non-linear mathematical model equations (2.13a) and(2.13b) and describe the relations of quantities in the neighborhoods of $\mathbf{c}^{(0)}$, the point of expansion in the parameters space, and $\mathbf{w}^{(0)}$, the misclosure vector, where,

$$\begin{aligned} \boldsymbol{\delta} &= \mathbf{c} - \mathbf{c}^{(0)}, \\ \mathbf{w}^{(0)} &= f(\mathbf{l}^{(0)}, \mathbf{c}^{(0)}). \end{aligned} \tag{2.15}$$

In the presence of constraints, it is, in general, possible that u>c leading to rank of **A** being c. In such situation, part of the development to follow (solution by partitioning) would not work. Therefore, we assume that u<c. Other possibilities (for u>c) has been

addressed as a special case in Mikhail (1976). The tasks of constrained fitting can now be formulated. The standard method for solving a minimization problem subject to a set of constraints is the use of Lagrangian multipliers. The constraints $f_c(\mathbf{c}) = 0$ are viewed as a hypersurface *S* upon which we wish to minimize $f(\mathbf{c},\mathbf{l}) = 0$. The variation function for finding the least-squares solution is written as:

$$\phi = \mathbf{r}^{\mathbf{T}}\mathbf{C}_{\mathbf{r}}^{-1}\mathbf{r} + 2\mathbf{k}^{\mathbf{T}}(\mathbf{A}\boldsymbol{\delta} + \mathbf{B}\mathbf{r} + \mathbf{w}) + 2\mathbf{k}_{\mathbf{c}}^{\mathbf{T}}(\mathbf{D}\boldsymbol{\delta} + \mathbf{w}_c),$$

where $\mathbf{C}_\mathbf{r}$ is equal to the covariance matrix of the observations. Here, there are two sets of Lagrange correlates: $\mathbf{k}$, $\mathbf{k}_\mathbf{c}$, reflecting the fact that two models are present. The minimum with respect to $\mathbf{r}$ is found by the Lagrange approach (Mikhail 1976; Vaníček and Krakiwsky, 1986) as

$$\hat{\boldsymbol{\delta}} = \boldsymbol{\delta}^{(1)} - \mathbf{N}^{-1}\mathbf{D}^{\mathbf{T}}(\mathbf{D}\mathbf{N}^{-1}\mathbf{D}^{\mathbf{T}})^{-1}(\mathbf{w}_\mathbf{c} + \mathbf{D}\boldsymbol{\delta}^{(1)}), \tag{2.16}$$

where

$$\mathbf{N} = (\mathbf{A}^{\mathbf{T}}(\mathbf{B}\mathbf{C}_\mathbf{r}\mathbf{B}^{\mathbf{T}})^{-1}\mathbf{A})^{-1}, \tag{2.17}$$

$$\mathbf{u} = \mathbf{A}^{\mathbf{T}}(\mathbf{B}\mathbf{C}_\mathbf{r}\mathbf{B}^{\mathbf{T}})^{-1}\mathbf{w}, \tag{2.18}$$

$$\boldsymbol{\delta}^{(1)} = -\mathbf{N}^{-1}\mathbf{u}. \tag{2.19}$$

Equation (2.19) represents the solution from the main model *f* alone, and the corrective term $\hat{\boldsymbol{\delta}} - \boldsymbol{\delta}^{(1)}$ in equation (2.16), arises from the enforcement of the constraints.

2.3.1 Sequential constraints

The Lagrangian-multiplier method works adequately when the constraints are independent, but is less useful when they are not (Benko et al., 2002). In this work, a sequential approach is used to select the optimum number of independent constraints. We assume that the constraints have been sorted into an order of priority: $f_c(\mathbf{c}) = (\mathbf{c}_1, \mathbf{c}_2, ..., \mathbf{c}_k)$, where $\mathbf{c}_1$ is a vector of highest priority constraints, and $\mathbf{c}_k$ is the lowest. We wish to solve the $f(\mathbf{c},\mathbf{l}) = 0,$ by sequentially attempting to satisfy the constraints in their priority order.

The two problems: $f(\mathbf{c},\mathbf{l}) = 0$ and $f_c(\mathbf{c}) = 0$ are solved simultaneously using Lagrangian-multiplier method (previous section) with more sets of constraints in different steps. Depending on the desired degree of freedom for the resulted velocity surface, while still securing the regular solutions, the computations end at that step.

2.3.2 Testing for errors

The next task is to obtain the covariance matrix of the parameters. It is given by Mikhail (1976) and Vaníček and Krakiwsky (1986) as:

$$\hat{\mathbf{C}}_{\hat{\boldsymbol{\delta}}} = \mathbf{N}^{-1} - \mathbf{N}^{-1}\mathbf{D}^{\mathbf{T}}(\mathbf{D}\mathbf{N}^{-1}\mathbf{D}^{\mathbf{T}})^{-1}\mathbf{D}\mathbf{N}^{-1}. \tag{2.20}$$

The appropriate degree of the velocity surface is determined by testing the estimated accuracy, or the ‘a posteriori standard deviation’. This is computed from

$$\hat{\sigma}_0^2 = \frac{\hat{\mathbf{r}}^{\mathbf{T}}\mathbf{C}_{\mathbf{l}}^{-\mathbf{1}}\hat{\mathbf{r}}}{v}, \tag{2.21}$$

where $\hat{\mathbf{r}}$ is the vector of least squares estimations of residuals and v denotes the number of degrees of freedom.

2.3.3 Filtering the solution

Some of the computed coefficients may not be statistically significant on a certain level of probability and they should be filtered out in the first stage. The logic behind this is that the existing data can only produce a surface with some of the bases, the statistically significant ones and the coefficients associated with those bases should remain, and other coefficients should be filtered out. In order to discard all the coefficients that are insignificantly different from zero, one way is to orthogonalize the basis. Then each of the coefficients can be tested for statistical significance against its own variance. A certain level of significance, in terms of a multiple of the standard deviation is assumed, and all the coefficients, insignificant on this level, are discarded. Here, the Gram-Schmidt's orthogonalization is applied to the polynomial basis ($\psi_i(\varphi,\lambda)$), the significance test for the coefficients is performed, and the solution is de-orthogonalized into the natural solution space (Vaníček, 1976).

The basis functions in Equation (2.12) can be presented as:

$$\mathbf{\Phi} \equiv \{\boldsymbol{\varphi}_1, \boldsymbol{\varphi}_2, ..., \boldsymbol{\varphi}_l\}. \tag{2.22}$$

The above bases are then orthogonalized to obtain:

$$\mathbf{\Phi}^* \equiv \{\boldsymbol{\varphi}_1^*, \boldsymbol{\varphi}_2^*, ..., \boldsymbol{\varphi}_l^*\}. \tag{2.23}$$

(See Appendix I for the method of Gram-Schmidt orthogonalization)

The coefficients for each individual patch are then evaluated in the orthogonal space as

$$\boldsymbol{\delta}^{*(1)} = \left[\left\langle \boldsymbol{\varphi}_i^*, \mathbf{w} \right\rangle / \left\| \boldsymbol{\varphi}_i^* \right\|^2 ; i = 1,...,l \right]. \tag{2.24}$$

These coefficients should be confirmed as significant. To test their significance, one can start from the following null hypothesis:

$$H_0 : E(\delta_i^{*(1)}) = 0; i = 1,...,l. \tag{2.25}$$

where $\delta_i^{*(1)}$ is the i^{th} coefficient for each patch, computed in the orthogonal space. It is therefore possible to define a statistic that, if H_0 is true, follows a *t* (Student) distribution (Crow et al., 1960; Vaníček and Krakiwsly, 1986):

$$-t_{\beta,\nu} < \frac{\delta_i^{*(1)}}{\sigma_{\delta_i^{*(1)}}} < t_{\beta,\nu}, \tag{2.26}$$

where $\sigma_{\delta_i^{*(1)}}$ is the standard deviation of $\delta_i^{*(1)}$ and v is the degree of freedom, i.e., the number of redundant observations. The hypothesis H_0 is accepted or rejected depending on whether the absolute value t_0 is smaller or greater than a boundary value t_β at a chosen confidence level $(1-\beta)$(Crow et al., 1960; Vaníček and Krakiswky, 1986; Liu and Chen, 1998). When H_0 is found valid, $\delta^{*(1)}$ should be rejected. Otherwise, $\delta^{*(1)}$ should remain in the model.

After discarding the insignificant coefficients from (2.24), we de-orthogonalize (2.24) into the natural space by

$$\boldsymbol{\delta}^{(1)} = \mathbf{T}^t \boldsymbol{\delta}^{*(1)}. \tag{2.27}$$

Here **T** is the transformation matrix from orthogonalized space to non-orthogonal space. The matrix for Gram-Schmidt approach is given in Appendix I.

Chapter 3

Data Treatment and Error Analysis

3.1 Introduction

The data used as input for the VCM model are of two kinds: re-levellings from the first-order levelling network and sea-level records. Other data, such as the rate of gravity changes ($\dot{g}$), geodetic height changes ($\dot{h}$), location of tectonic boundaries, and seismicity information are added in the database for further analysis and interpretation of the results. To integrate and analyze different spatially distributed data, ArcGIS was used throughout this research.

This chapter explores the data and the framework for VCM compilation. This includes the error analysis of the re-levelling data and the approach taken for the treatment of tide gauge records. The filtered rate of height differences between the levelling bench marks, and the monthly mean sea level trend of the tide gauges, which are used in the mathematical model of VCM, are presented here.

3.2 Data and GIS framework

The Canadian 1st order levelling database was provided to us by Geodetic Survey Division (GSD), Natural Resources Canada, in a format which allows the data to be categorized by provinces. Developing an efficient algorithm to retrieve the re-levelling data based on all the possible combinations of the levelling bench marks, the RE_LEVEL program was designed and used to retrieve all possible re-leveled information from the entire 1st order leveling data. A full description of the program is given in Appendix II.

The map of all the retrieved re-leveled data in Canada is given in Figure 3.1. It is apparent that the data in northern Canada, and in some areas such as western Ontario are sparse.

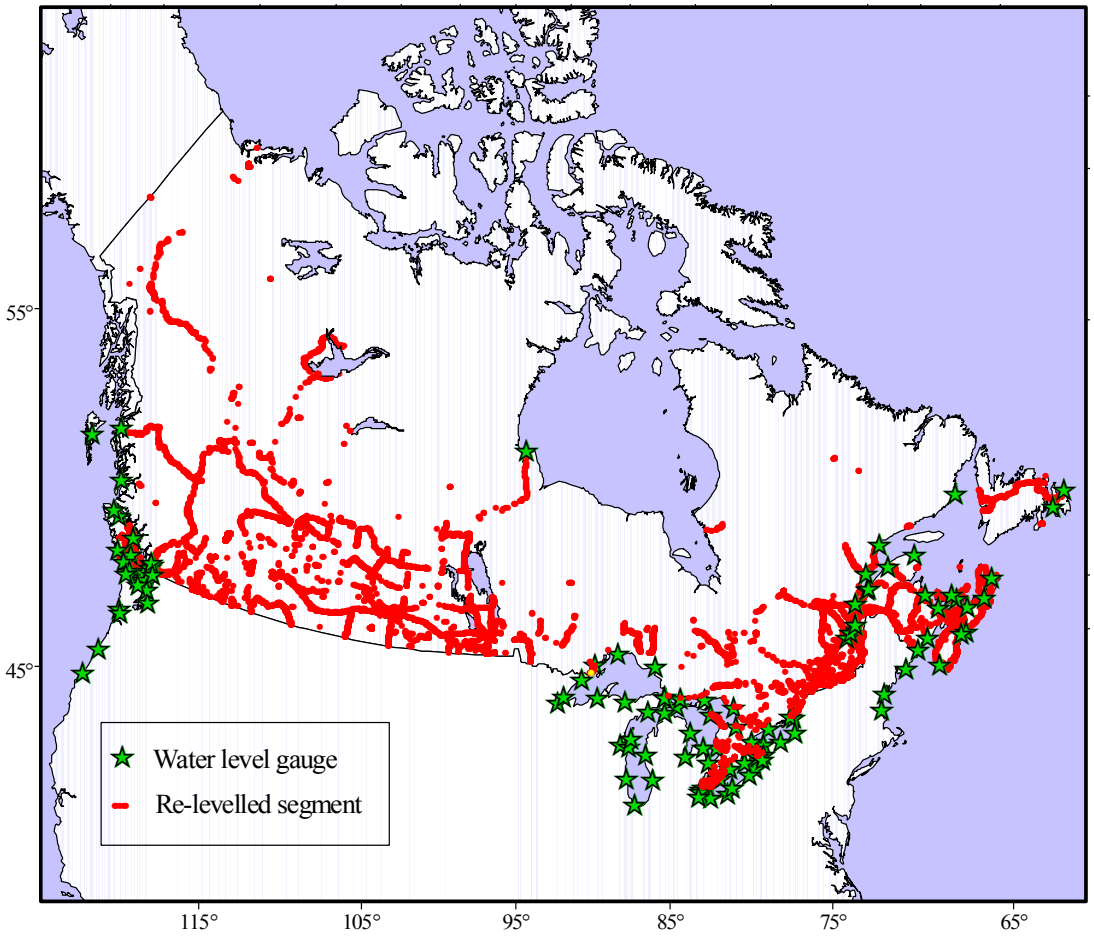

Figure 3.1 The distribution of data used in the computations. Red dot lines show re-leveled segments. Stars indicate the location of water level gauges.

The Canadian sea level information includes monthly mean sea and lake level values which were provided by the Marine Environmental Data Service (MEDS), and the U.S.monthly mean sea level records were downloaded from the NOAA website (http://tidesandcurrents.noaa.gov/station_retrieve.shtml?type=Historic+Tide+Data). The locations of the tide gauges analyzed in this study are also shown in Figure 3.1.

All available data compiled during the course of the study were integrated with the geological map of Canada in ArcGIS and subsequently formatted to meet the

requirements of the base map[1]. Other information including attribute data and information on sites which had come throughout the study were added to the project. As an example, the values of the rates of gravity variations were added in the map as different layer for further analysis and comparisons with the output map. Moreover, the "spatial analysis facilities" in the GIS were used in the analysis of data and the study of the impact of some physical effects in the data[2]. Figure 3.2 depicts the idea of utilizing GIS as a useful tool in our study.

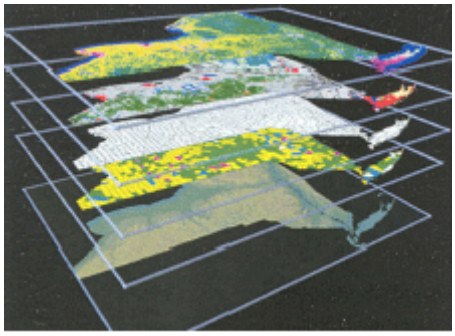

Figure 3.2: Different sources of data are integrated with the geological map of Canada in GIS.

3.3 Levelling data analysis

The 1st order levelling data used in this study are the precise leveling data corrected for systematic errors. Two adjacent permanent benchmarks, whose height difference is established using geodetic levelling, constitute a segment. Many of these segments have been leveled twice in different years. The re-leveled segments were pre-processed to eliminate the ones that showed high tilts that might have resulted from highly localized

[1] Base map is the most accurate spatial database within a data system. Because the base maps tend to serve as the point of reference when creating other spatial databases, they tend to have the highest level of accuracy. The base map in this study is the geological map of Canada, in *.shp format.

[2] For further discussion on how Spatial Analysis in GIS is utilized in compilation of a map of VCM, See Koohzare et al. (2006).

movements of one of the benchmarks in which we have no interest. The quality control criterion applied to the re-levelling segments was implemented by means of a rejection criterion for height difference differences per distance in time, greater than 0.1 millimetre per kilometre per year. By applying this criterion, 1882 Canadian re-leveled segments were eliminated. Most of them were removed because they were too short to contribute to the analysis. Table 3-1 shows the number of extracted relevelled data in each province in Canada.

Table 3-1: Number of re-leveled segments in Canada used in this study.

Province	**Number of 1st order re-levelling data**
Alberta(AB)	1498
British Columbia(BC)	10826
Manitoba(MB)	2213
New Brunswick(NB)	1294
Newfoundland(NF)	513
Northern Territories(NT)	492
Nova Scotia(NS)	2336
Ontario(ON)	15249
Prince Edward Island(PEI)	63
Quebec(QC)	10127
Saskatchewan(SK)	1681
Yukon(YK)	48
Total	**46340**

3.4 Sea level analysis

The long-periodic and, particularly, the secular changes in sea level are important in geodynamics when only linear movements are considered. The global mean secular sea level variations (eustatic) have been estimated by Carrera and Vaníček (1988), Douglas (1991), Peltier (1996, 2001), and Church et al. (2001). The most probable contributor to

the eustatic sea level variations[3] are the melting of Antarctica's, as well as other, permanent ice sheets on the surface of the earth, and the continuing adjustment of the lithosphere- asthenosphere system to the load of water freed after the last glacial melt (Vaníček and Krakiwsky, 1986). The apparent sea level rise left after removal of the global eustatic signal is assumed to represent a vertical motion of the crust of the same magnitude but of opposite sign.[4] The assumed global eustatic sea level rise in this study is the value of 1.8 mm per year from Douglas (2000).

The analysis of the tide gauge records was based on monthly mean sea level data, knowing that monthly averaging of sea level acts as an effective filter of high frequency oceanic signals (Godin, 1972 and Cartwright, 1983). Typically, monthly averages of sea level oscillate within the range of about 0.5 metre throughout the year of observations. Since the linear trend in which we are interested, is a fraction of a centimetre per year, it is important to have records that are as long as possible. In the studies of vertical crustal motions, tide gauge records with longer time spans are more reliable and thus more valuable. Sea level records with duration of a few tens of years may not be taken as representative for the sought secular trends, if they are studied individually. However, when they are treated in a differenced mode, the secular variations can be accurately estimated (Koohzare et al., 2006b; Vaníček and Carrera, 1993). Therefore, the subset of sites is selected to include all stations for which continuous records of at least 10 year duration are available.

Appling this criterion, a total amount of 106 tide gauges in Canada and Northern U.S. were selected and analyzed. A monthly mean value is published by MEDS if there are at least 21 continuous days of sea level record available in any one month. According to MEDS, these monthly values are derived from daily and hourly values, filtered by an outlier detection procedure. In spite of that, the Cartwright (1968) smoothness test was

---

[3] Eustatic sea level change (as opposed to local change) results in an alteration to the global sea levels, such as changes in the volume of water in the world oceans or changes in the volume of an ocean basin.

[4] The vertical crustal motion is the movement of the crust relative to geoid or mean sea level, and the isostatic relative sea level changes is referred to the position and height of sea relative to the land.

applied to detect possible outliers in monthly values. A quintic polynomial was used to interpolate sea level values:

$$s_n^{'} = 0.75(s_{n+1} + s_{n-1}) + 0.20(s_{n+2} + s_{n-2}) + 0.05(s_{n+3} + s_{n-3}), \tag{3.1}$$

where $s_n^{'}$ is the interpolated sea level values for the n^{th} month and s_n is the monthly mean sea level. The time series containing the differences between the observed s_n and interpolated $s_n^{'}$ sea level values $\delta s_n = s_n - s_n^{'}$ helps to detect potential isolated errors in the original data. An outlier in the original data produces a well defined sub-sequence of values. The local extreme of this sequence (spike) permits to find the location in time of such an isolated error.

To calculate the mean rate of the sea level change, linear regression of the filtered monthly mean values is used. Following Vaníček and Nagy (1979), one approximates the time series by

$$\forall n = 1,..., N : s_{RSL}(t_n) = a + \dot{\bar{s}}_{obs} t_n, \tag{3.2}$$

where s_{RSL} is the monthly mean sea level height with respect to the land, or relative sea level(RSL), a is the intercept, $\dot{\bar{s}}_{obs}$ the observational rate of mean sea level change or the linear trend, t_n is the reference time epoch, and N is the total number of monthly values. From linear regression one can write

$$a = \frac{\sum s_n - \dot{\bar{s}}_{obs} \sum t_n}{N}, \tag{3.3}$$

$$\dot{\bar{s}}_{obs} = \frac{N \sum t_n s_n - \sum t_n \sum s_n}{N \sum t_n^2 - (\sum t_n)^2}. \tag{3.4}$$

Here, s_n is the monthly RSL height for the nth month and t_n is the reference time epoch for s_n. If we assume that the linear model does fit well and that all observations have the

same standard deviation σ, the assumption that the residuals are normally distributed around the linear model implies that:

$$\sigma = \sqrt{\frac{\sum s_n^2 - a\sum s_n - \dot{\bar{s}}_{obs}\sum t_n s_n}{N-2}}. \tag{3.5}$$

The standard deviation of the regression coefficient $\dot{\bar{s}}_{obs}$ is then calculated according to Wolf et al., (2006):

$$\varepsilon = \sqrt{\frac{N\sigma^2}{N\sum t_n^2 - (\sum t_n)^2}}. \tag{3.6}$$

It is suspected that some local and regional effects such as plate tectonics, seasonal or interannual ocean effects, river discharge and sedimental subsidence contaminate the records of tide gauges. All of these impacts have the potential to obscure or even hide the long-term eustatic and isostatic relative sea level changes. Therefore, the effects should be eliminated from the records of each individual tide gauge. Another alternative is that the records contaminated by the above impacts are rejected from the trend analysis. In this study, the second approach was considered. As an example, the record of Port aux Basques station, in Newfoundland is depicted in Figure 3.3. The record shows an error, probably due to datum changes, which contaminated the records in the years of 1935 to 1980. For this reason, data from this period were rejected from the analysis.

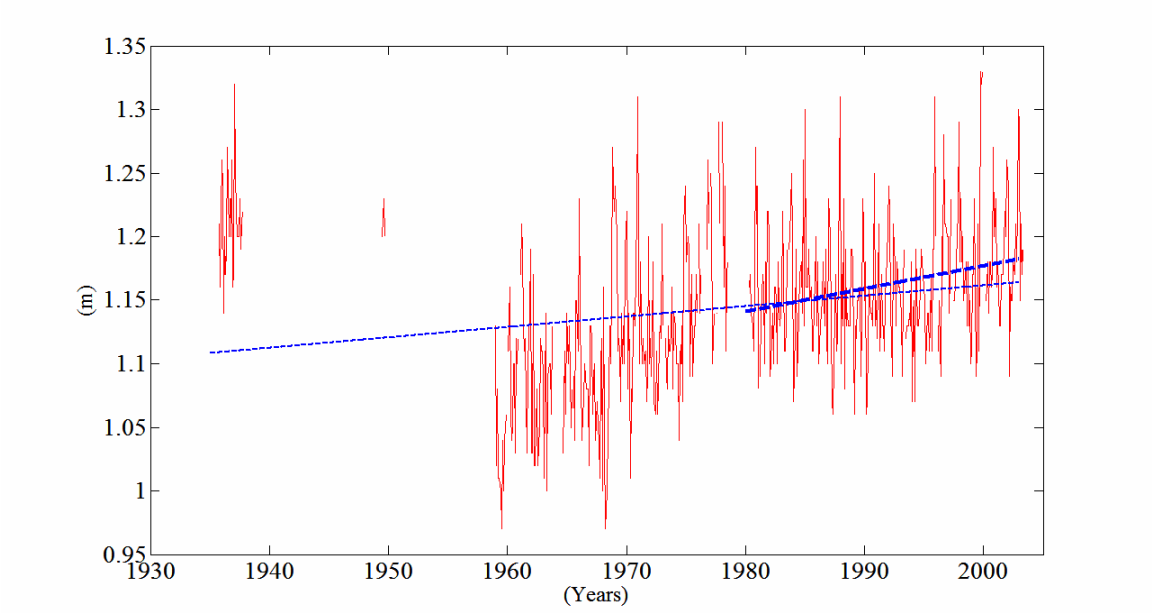

Figure 3.3: Monthly mean sea level record of Port aux Basque (NF). The monthly mean sea level trend is 0.61 mm/yr based on sea level data from 1935 to 2003. The record from 1935 to 1980 shows an error, and is thus rejected from the analysis. The monthly mean sea level trend is 1.8± 0.5 mm/yr based on the new set of data (1980-2003).

The plots of the time series of monthly mean sea level records of other tide gauges studied in this work, along with the linear trends and the standard deviations of the estimated trend are given in Appendix IV.

3.5 Treatment of tide gauge data for VCM model

There is another well documented feature of tide gauge records: their striking similarity when they are obtained at two close-by locations (Vaníček and Carrera, 1993). This spatial coherence is caused by common atmospheric and oceanic noise. Clearly, a large portion of these variations disappears when the records are differenced. This behaviour offers an alternative way of treating sea level trends in close-by tide gauges: mean sea level trend of only one tide gauge is used as a source of point velocity and the rest of tide gauge records are differenced to obtain velocity differences. The Pearson Linear correlation coefficient for any pair of series is computed to find out the optimum tree network of tide gauges for differencing. Denoting the corresponding parts of the two series, the data at common epoch, as $\mathbf{S}^i = (s_1^i, s_2^i, ..., s_n^i)$ and $\mathbf{S}^j = (s_1^j, s_2^j, ..., s_n^j)$, and n the

same number of elements in both series, the correlation coefficients are given by Vaníček and Carrera (1993) as

$$r_{ij} = \sum_k (s_k^i - s^i)(s_k^j - s^j) / \left[\sqrt{\sum_k (s_k^i - s^i)^2} \sqrt{\sum_k (s_k^j - s^j)^2} \right], \tag{3.7}$$

where s^i and s^j are the average values of two series. The correlation coefficient confidence interval can then be obtained by means of Fisher's Z-transformation and is given by David (1949) as:

$$< -1.96(n-3)^{-0.5}, 1.96(n-3)^{-0.5} > . \tag{3.8}$$

Correlation coefficients indicate which pairs of records should be differenced preferentially whereas confidence intervals of the correlation coefficient can be used to show which pairs of records have the longest common epochs. Having constructed the matrices of correlation and their confidence intervals, the optimum tree diagram for the differencing is defined. This is done in three steps:

- The linear trend with the smallest standard deviation is chosen as the absolute velocity datum for the solution of VCM.
- The adjacent locations that show the smallest confidence intervals for their correlation coefficients are selected to play the role of 'nodes' in the network of differenced velocities.
- The pairing of these nodal tide gauges and adjacent tide gauge is done on the basis of the highest correlations.

In this study, three network of differencing are considered: Atlantic, Pacific and Great Lakes differencing trees.

3.5.1 Atlantic Canada differencing tree

In Atlantic Canada, Halifax is selected to be used in the point velocity mode or the absolute velocity for the solution of VCM, and Charlottetown and Point au Père are defined as node points. Table 3-2 shows 95% correlation coefficient confidence intervals of the nodal tide gauges with respect to Halifax station. The next step is to find the pairing of these nodal sites with adjacent tide gauge based on the highest correlations. The matrix of correlation coefficients between each pairing tide gauges are given in Appendix IV. Figure 3.4 shows the map of differencing among tide gauges in Atlantic Canada.

Table 3-3 lists the linear trends of the tide gauges along Atlantic coast considered for this study and compares them with the results published in Carrera et al. (1991). The small differences between results of this work and the previous study are mainly due to the fact that only slightly more data in this study was used. However, the standard deviations of our trends are generally smaller than the standard deviations of the trends in the previous studies. There are some tide gauges whose records were not considered in the compilation of VCM in the previous work mainly because of the shortness of the data series or probable systematic errors reported in Carrera et al. (1991). In this study, those tide gauges are considered as their longer records do not show such systematic errors. It should be noted that short records display linear trend values which are close to their longer counterparts when the method of propagation of differences is used. As a way of an example, the linear trend in Pictou, NS, shows a value of 2.30 mm/yr when analyzed as a point value but when differenced acquires a value of very close to the value found for the gauge in Charlottetown (3.53 mm/yr) only a few tens of km away. The reason for this result is the attenuation of oceanic noises when differencing method is used.

Table 3-2: Correlation coefficient confidence intervals of node sites in Atlantic Canada with respect to Halifax tide gauge (Koohzare et al., 2006b).

Code	Tide gauge	Location		95% Correlation Coefficient Confidence Interval of each node site with respect to Halifax records
		Latitude	Longitude	
7	Charlottetown, PEI	46º 13´.8	63º 07´.2	<-0.0699,+0.0699>
18	Point au Père, QC	48º 31´.2	68º 28´.2	<-0.0725,+0.0725>

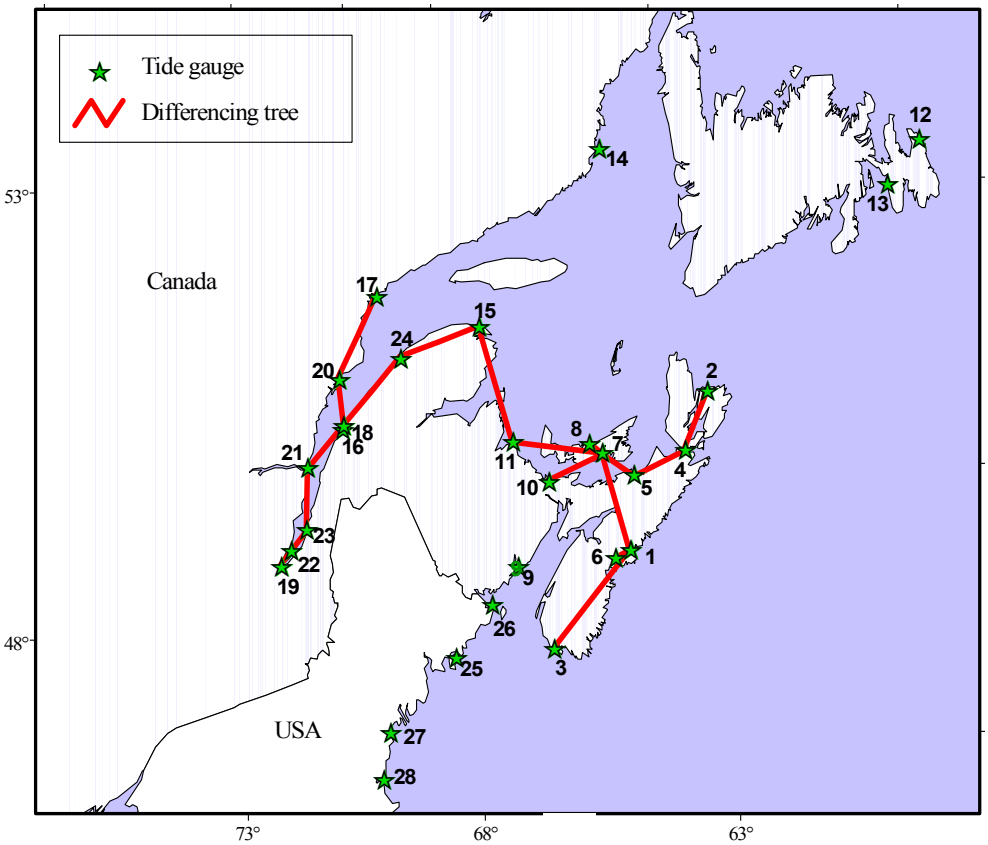

Figure 3.4: Tide gauge differencing tree in Eastern Canada.

Table 3-3: Sea level linear trends and their standard deviations of some of the tide gauges in Atlantic Canada and Northern U.S.in mm/yr.

code	Tide gauge	Location Latitude/ Longitude	Velocity based on differencing (mm/yr) from Carrera et al., 1991.[5]	Data available for this study	Point Velocity (mm/yr)	Velocity based on differencing (mm/yr) in this study
1	Halifax, NS	44º 39´.6 63º 35´.4	3.56± 0.08	1919-2003	3.27±0.05	3.27± 0.05
2	North Sydney, NS	46º 13´.2 60º 15´.0	3.87±0.46	1970-2003	3.07±0.54	3.42±0.37
3	Yarmouth, NS	43º 50´.4 66 º07´.2	4.75±0.35	1900-2003	2.85±0.15	4.17±0.18
4	Point Tupper, NS	45º 06´.0 61 º22´.2	4.31±0.79	1971-1992	1.67±0.70	3.12±0.80
5	Pictou, NS	45º 40´.8 62º 42´.0	3.68±0.33	1957-1996	2.30±0.35	3.70±0.21
6	Boutilier Point, NS	44º 39´.6 63º 57´.6	3.97±0.49	1970-1983	3.00±1.40	
7	Charlottetown, PEI	46º 13´.8 63º 07´.2	3.55±0.11	1905-2003	3.21±0.08	3.30±0.09
8	Rustico, PEI	46º 28´.2 63º 16´.8	3.28±0.47	1972-1996	3.92±0.68	3.92±0.68
9	Saint Jonh, NB	45º 16´.2 66º 03´.6	3.01±0.14	1905-2003	2.50±0.11	---
10	Shediac Bay, NB	46º 15´.0 64º 31´.8	---	1971-1992	1.23±0.70	2.50 ±0.14
11	Lower Escuminac, NB	47º 04´.8 64º 53´.4	2.12±0.48	1973-2003	1.98±0.66	2.10±0.31
12	St Johns,NF	47º 33´.6 52º 42´.6	1.93±0.36	1935-2003	2.10±0.25	---
13	Argentia, NF	47º 18´.0 53º 58´.8	---	1971-2003	1.70±0.50	---
14	Harrington Harbour, NF	50º 28´.8 59º 28´.2	0.13±0.16	1939-1989	-0.72±0.17	---
15	Riviere au Renard, QC	48º 58´.8 64º 22´.2	-0.32±0.77	1969-2003	-0.49±0.16	-0.32±0.15
16	Rimouski,, QC	48º 28´.8 68º 31´.2	---	1984-2003	-0.24±0.90	
17	Sept Illes, QC	50º 10´.8 66º 22´.2	1.87±0.41	1972-2003	2.01±0.25	0.19±0.11
18	Point au Pere, QC	48º 31´.2 68º 28´.2	-0.10±0.16	1900-2003	-0.31±0.07	-0.31±0.07
19	Quebec, QC	46º 49´.8 71º 10´.2	1.05±0.28	1900-2003	-0.52±0.16	
20	Baie Comeau,QC	49º 13´.8 68º 07´.8	-0.62±0.47	1964-1991	-5.77±0.72	-0.62±0.31
21	Tadoussac, QC	48º 08´.4 69º 42´.6	-1.21±0.80	1966-1995	-5.08±0.62	-1.21±0.21
22	St Francois, QC	47º 00´.0 70º 48´.6	1.70±0.28	1962-2003	-0.48±0.45	
23	St Jean Port Joli, QC	47º 13´.2 70º 16´.8	-0.88±1. 65	1968-1980	-5.38±2.18	-0.88±1. 64
24	St Anne des Monts, QC	49º 07´. 2 66º 28´.8	-0.55±0.60	1967-1997	-0.89±0.44	-0.40±0.49
25	Bar Harbour, ME[6]	44º 23´.5 68º 12´.3	---	1947-1999	2.18±0.16	---
26	Eastport, ME	44º 54´.2 66º 59´.1	---	1929-1999	2.21±0.13	---
27	Portland, ME	43º 43´.8 70º 12´.4	---	1912-1999	1.91±0.09	---
28	Seavey Island, ME	43º 05´.0 70º44´.0	---	1926-1999	1.75±0.17	---

[5] The signs are different from the original technical report due to different definitions.
[6] Tide gauges in the USA, Values taken from http://www.coops.nos.noaa.gov/sltrends/sltrends.html

3.5.2 Pacific coast differencing tree

In the Pacific coast, Seattle (USA) with more than 100 years of continuous record shows the smallest standard deviations for the linear trend and accordingly it is selected to be used in the point velocity mode or the absolute velocity for the solution of VCM. Tofino (BC), Vancouver (BC), and Port Hardy (BC) are defined as node points. Table 3-5 shows 95% correlation coefficient confidence intervals of the nodal tide gauges with respect to Seattle station. The next step is to find the pairing of these nodal sites with adjacent tide gauge based on the highest correlations. Figure 3.6 shows the map of differencing among tide gauges along Pacific Canada and Table 3.6 lists the linear trends of the tide gauges along Pacific coast studied in this research, and compares them with the previous study.

Table 3-4: Correlation coefficient confidence intervals of node sites in pacific Canada with respect to Seattle tide gauge.

Code	Tide gauge	Location		95% Correlation Coefficient Confidence Interval of each node site with respect to Seattle records
		Latitude	Longitude	
1	Tofino	49º 09´.0	-125º 54´.6	<-0.0702, +0.0702>
10	Vancouver	49º 17´.4	-123º 06´.6	<-0.0657,+ 0.0657>
14	Port Hardy	50º 43´.2	-127º 29´.4	<-0.0926,+ 0.0926 >

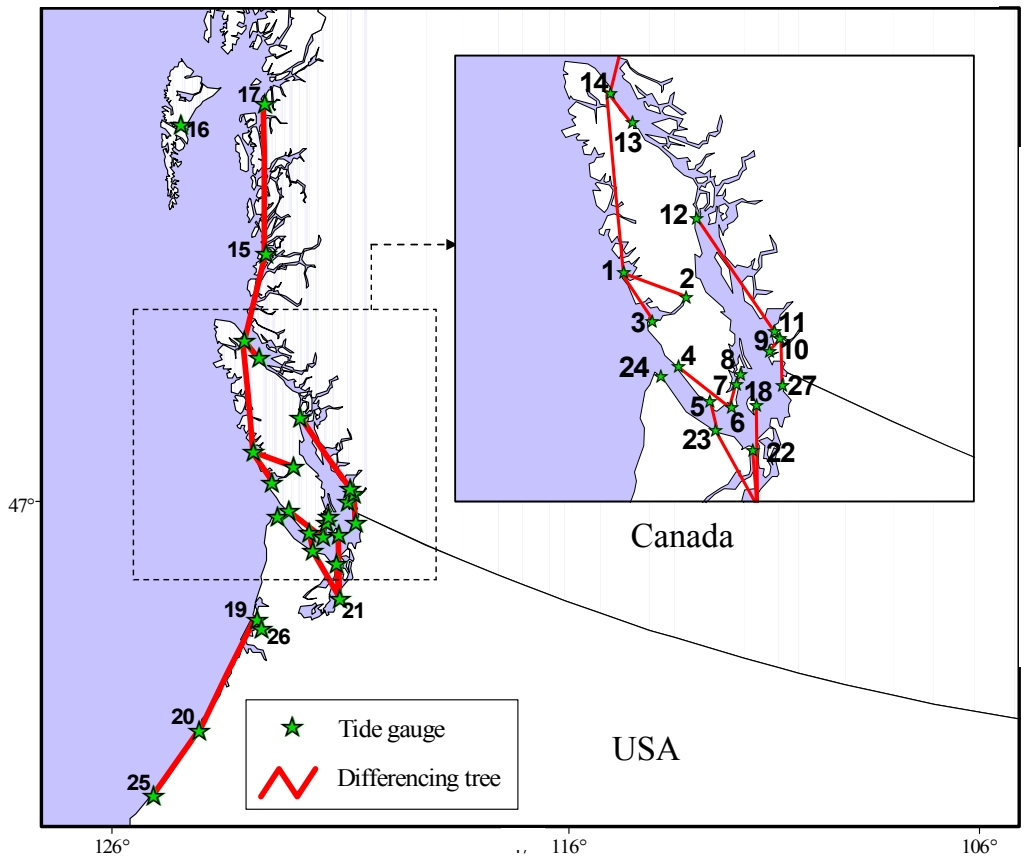

Figure 3.5: Tide gauge differencing tree in Pacific coast.

Table 3-5: Sea level linear trends and their standard deviations of some of the tide gauges in Pacific Canada and Northern U.S. in mm/yr .

code	Tide gauge	Location		Velocity based on differencing (mm/yr) from Carrera et al., 1991.[7]	Data available for this study	Point Velocity (mm/yr)	Velocity based on differencing (mm/yr) in this study
		Latitude	Longitude				
1	Tofino,BC	49º 09´.0	-125º 54´.6	-1.04±0.70	1909-2002	-1.55±0.16	-1.55±0.16
2	Port Alberni,BC	49º 13´.0	-124º 48´.6	+3.07±0.60	1970-1997	-0.01±0.78	-0.37±0.32
3	Bamfield,BC	48º 49´.8	-125º 07´.8	+1.05±0.46	1970-2002	+0.37±0.62	+0.92±0.19
4	Port Renfrew,BC	48º 33´.0	-124º 25´.2	+0.24±0.56	1957-1997	+1.24±0.69	+1.57±0.36
5	Sooke,BC	48º 22´.2	-123º 43´.2	-0.30±0.39	1958-1985	+1.95±1.41	+0.82±0.52
6	Victoria,BC	48º 25´.2	-123º 22´.2	+0.74±0.10	1925-2002	+0.08±0.36	+0.73±0.14

[7] The signs are different from the original technical report due to different definitions.

code	Tide gauge	Location Latitude	Longitude	Velocity based on differencing (mm/yr) from Carrera et al., 1991.[7]	Data available for this study	Point Velocity (mm/yr)	Velocity based on differencing (mm/yr) in this study
7	Patricia Bay,BC	48º 39´.0	-123º 27´.0	+0.66±0.48	1966-2002	-0.31±0.69	+1.01±0.19
8	Fulford Harbor,BC	48º 46´.2	-123º 27´.0	+0.20±0.13	1952-1992	+0.16±0.35	+0.24±0.36
9	Stevenson,BC	49º 07´.2	-123º 10´.8	+1.75±0.38	1969-1997	+2.10±0.60	+1.27±0.39
10	Vancouver,BC	49º 17´.4	-123º 06´.6	+0.24±0.10	1909-2002	+0.30±0.10	+0.30±0.10
11	Point Atkinson,BC	49º 20´.4	-123º 15´.0	+0.93±0.11	1914-2002	+0.85±0.12	+0.80±0.10
12	Campbell river,BC	50º 01´.2	-125º 13´.8	+0.09±0.23	1958-2003	-2.00±0.51	-1.58±0.20
13	Alert Bay,BC	50º 34´.8	-126º 55´.8	-1.06±0.22	1948-1979	-1.62±0.62	-1.22±0.63
14	Port Hardy,BC	50º 43´.2	-127º 29´.4	+0.56±0.38	1964-2002	-1.06±0.44	-0.65±0.21
15	Bella Bella,BC	52º 09´.6	-128º 08´.4	+1.92±0.46	1906-2002	-0.34±0.31	-0.89±0.19
16	Qu.Charlotte City,BC	53º 15´.0	-132º 04´.2	+1.28±0.54	1957-2002	-0.88±0.34	-0.88±0.34
17	Prince Rupert,BC	54º 19´.2	-130º 19´.2	+3.32±0.53	1909-2002	+1.04±0.14	+1.04±0.14
18	Friday Harbor,WA	48º 33´.0	-123º 00´.6	+0.63+0.12	1934-1999	+1.24±0.20	+1.07±0.19
19	Toke Point,WA	46º 42´.6	-123º 57´.9	---	1973-1999	+2.82±1.05	+1.20±0.47
20	South Beach, OR	44º 37´.2	-124º 02´.5	---	1967-1999	+3.51±0.73	+2.34±0.54
21	Seattle,WA	47º 36´.3	-122º 20´.4	+1.98+0.13	1898-1999	+2.11±0.10	+2.11±0.10
22	Port Townsend, WA	48º 06´.6	-122º 45´.6	---	1972-1999	+2.82±0.88	+2.13±0.12
23	Port Angeles, WA	48º 07´.5	-123º 26´.4	---	1975-1999	+1.49±1.10	+0.37±0.17
24	Neah Bay,WA	48º 22´.2	-124º 37´.2	---	1934-1999	-1.41±0.22	-1.41±0.22
25	Charleston, OR	43º 20´.7	-124º 19´.2	---	1970-1999	+1.74±0.87	+0.48±0.55
26	Astoria, OR	46º 36´.3	-123º 46´.2	---	1925-1999	-0.16±0.24	-0.16±0.34
27	Cherry Point,WA	48º 51´.6	-122º 45´.6	---	1973-1999	+1.39±0.94	-0.03±0.14

3.5.3 Great Lakes differencing tree

The differencing tree of lake level differences is formed based on the same method that was explained for the sea level differences. Except that none of the tide gauge linear trends were used as point velocity mode.

Recently, in addition to the Great Lakes Coordinating Committee's 1977 report, Tai and Bolduc (1985), Carrera et al. (1991), and Tushingham (1992), Mainville and Craymer (2005) used additional years of water level data to compute the movements between pairs of tide gauges. Moreover, the inconsistencies due to random errors in the data were taken into account using least squares adjustment to obtain more precise

results. Figure 3.5 shows the location of water level gauges in the Great Lakes and Table 3-4 lists the linear trends of the lake gauges.

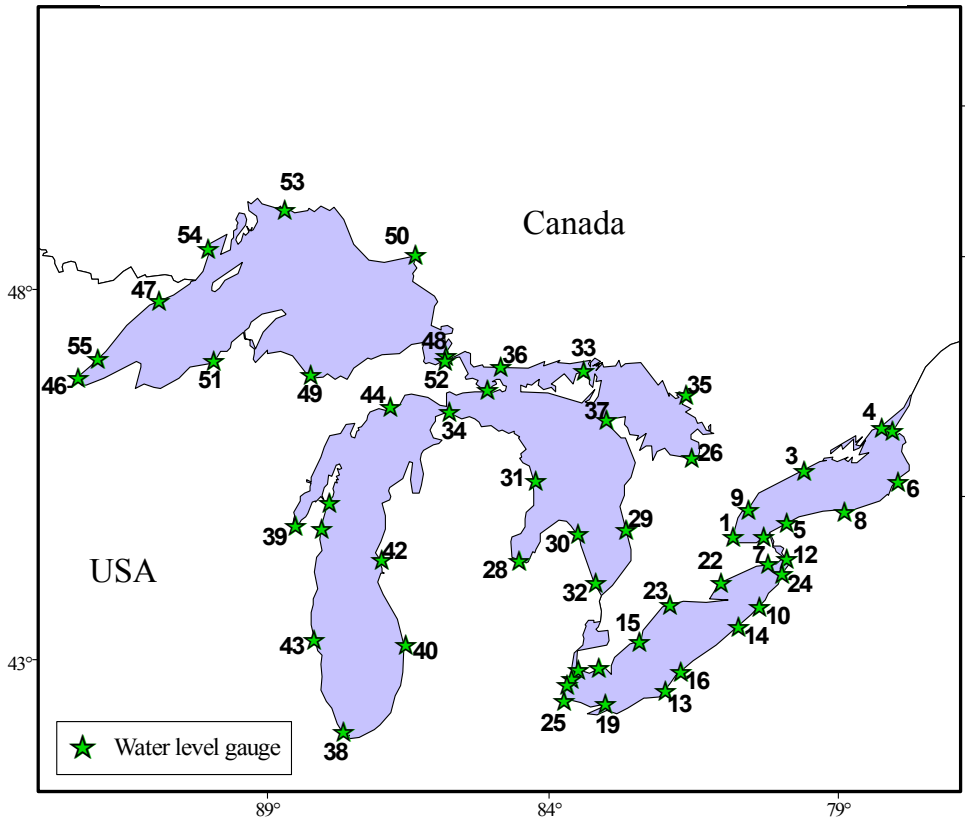

Figure 3.6: The location of water level gauges in the Great Lakes.

Table 3-6: Gauge vertical velocities from Mainville and Craymer (2005)

code	Tide gauge	Location		Vertical Velocity (mm/yr) from Mainville and Cramer , 2005.	Data available	comment
		Latitude	Longitude			
Lake Ontario-Relative to Cape Vincent						
1	Burlington	43º 20´20″	79º 46´08″	-2.00± 0.07	1970-2000	
2	Cape Vincent	44º 07´48″	76º 19´47″	0	1998-2000	outlet
3	Cobourg	43º 57´28″	78º 09´54″	-0.77±0.04	1956-2000	
4	Kingston	44º 13´01″	76º 31´01″	0.25±0.02	1916-2000	
5	Olcott	43º 20´24″	78º 43´48″	-1.13±0.06	1967-2000	
6	Oswego	43º 27´36″	76º 30´36″	0.45±0.02	1860-2000	

code	Tide gauge	Location		Vertical Velocity (mm/yr) from Mainville and Cramer , 2005.	Data available	comment
		Latitude	Longitude			
7	Port Weller	43º 14′13″	79º 13′11″	-1.47±0.03	1929-2000	
8	Rochester	43º 15′35″	77º 37′47″	-1.02±0.02	1860-2000	
9	Toronto	43º 38′24″	79º 22′51″	-1.21±0.02	1916-2000	
		Lake Erie-Relative to Buffalo				
10	Barcelona	42º 19′47″	79º 35′59″	-0.13±0.21	1960-1987	
11	Bar Point	42º 02′59″	83º 06′39″	-1.61±0.14	1966-2000	Rejected
12	Buffalo Har.	42º 53′24″	78º 53′24″	0	1860-2000	outlet
13	Cleveland	41º 31′48″	81º 38′24″	-0.98±0.03	1860-2000	
14	Erie	42º 08′59″	80º 04′47″	-1.21±0.12	1958-2000	
15	Erieau	42º 15′35″	81º 54′54″	-0.96±0.11	1957-2000	
16	Fairport Har.	41º 45′35″	81º 17′24″	-2.17±0.22	1975-2000	Rejected
17	Fermi Pow.	41º 58′00″	83º 15′00″	0.96±0.13	1963-2000	
18	Kingsville	42º 01′37″	82º 44′05″	1.03±0.12	1962-2000	
19	Marblehead	41º 32′59″	82º 43′48″	-0.84±0.12	1959-2000	
20	Monroe	41º 53′59″	83º 21′35″	-1.60±0.59	1975-2000	
21	Port Colbor	42º 52′26″	79º 15′10″	-0.57±0.05	1926-2000	
22	Port Dover	42º 46′51″	80º 12′07″	-0.18±0.11	1958-2000	
23	Port Standly	42º 39′32″	81º 12′46″	-0.74±0.05	1926-2000	
24	Sturgeon P.	42º 40′47″	79º 01′48″	0.21±0.16	1969-2000	
25	Toledo	41º 42′00″	83º 28′08″	-0.86±0.04	1877-2000	
		Lakes Heron- Michigan-Relative to Lake Port				
26	Collingwood	44º 30′18″	80º 13′01″	1.66± 0.07	1927-2000	
27	De Tour	46º 00′00″	83º 54′00″	1.73±0.08	1896-1983	
28	Essexville	43º 38′59″	83º 50′59″	-0.13±0.09	1953-1978	
29	Goderich	43º 44′45″	81º 43′44″	-0.15±0.07	1927-2000	
30	Harbor	43º 51′00″	82º 39′00″	0.01±0.07	1860-2000	
31	Harrisville	45º 40′12″	83º 16′48″	0.08±0.11	1970-2000	
32	Lakeport	45º 08′59″	82º 30′00″	0	1955-2000	outlet
33	Little Current	45º 58′51″	81º 55′40″	2.70±0.10	1959-2000	
34	Mackinaw	46º 46′48″	84º 43′11″	1.00±0.07	1899-2000	
35	Parry Sound	45º 20′16″	80º 02′09″	2.43±0.10	1960-2000	
36	Thessalon	41º 15′10″	83º 33′07″	2.08±0.07	1927-2000	
37	Tobermory	44º 15′32″	81º 39′57″	1.67±0.10	1962-2000	
38	Calumet	42º 42′00″	87º 30′00″	-1.04±0.07	1903-2000	
39	Green Bay	44º 30′00″	88º 05′59″	-0.62±0.09	1953-1981	
40	Holland	44º 23′59″	86º 12′00″	-0.79±0.08	1894-1997	
41	Kewaunee	43º 23′59″	87º 30′00″	-0.85±0.18	1974-1997	

code	Tide gauge	Location		Vertical Velocity (mm/yr) from Mainville and Cramer , 2005.	Data available	comment
		Latitude	Longitude			
42	Ludington	46º 00´00″	86º 30´00″	-1.22±0.08	1895-2000	
43	Milwaukee	44º 06´00″	87º 54´00″	-1.44±0.07	1860-1969	
44	Port Inland	43º 00´00″	85º 54´00″	0.94±0.11	1964-2000	
45	Sturgeon	43º 53´59″	87º 24´00″	-0.38±0.07	1905-2000	
		Lake Superior-Relative to Point Iroquois				
46	Duluth	46º 40´12″	92º 05´59″	-2.53±0.03	1860-2000	
47	Grand Mara.	47º 45´00″	90º 19´47″	-0.76±0.08	1966-2000	
48	Gros Cp.	46º 31´44″	84º 35´05″	0.16±0.07	1961-2000	
49	Marquette	46º 32´59″	87º 23´24″	-1.22±0.03	1860-1980	
50	Michipicoten	47º 57´43″	84º 54´03″	2.33±0.03	1931-2000	
51	Ontonagon	46º 52´11″	89º 18´36″	-1.87±0.07	1959-2000	
52	Point Iroqu.	46º 28´47″	84º 38´24″	0	1930-2000	outlet
53	Rossport	48º 50´02″	87º 31´11″	2.75±0.08	1967-2000	
54	Thunder	48º 24´32″	89º 13´01″	0.24±0.03	1931-2000	
55	Two Harb.	47º 00´35″	91º 40´12″	-2.12±0.05	1887-1988	

Chapter 4

Compilation of the map of VCM in Canada using SPAA

4.1 Introduction

As discussed before, most of the traditional methods of surface fitting reviewed in chapter 2, are significantly limited to the type of data (either point values or relative values), and the number and distribution of data, and ultimately the method of SPAA was developed to account for all the limitations, while securing the optimum approximation. However, this model should be used with certain caution, as imposing too many constraints results in excessive stiffening of the surface. Moreover, special attention should be paid to the selection of patches, and coordinate system to manage the solution numerically.

In this chapter, we will discuss some of the challenges with regard to the efficiency, stability, accuracy and robustness of SPAA method in the compilation of the map of VCM in Canada. In addition, the numerical problems which occurred in the modeling will be explained. At the end of the chapter the final map of VCM for Canada along with the map of standard deviations of the results will be depicted.

4.2 The Principle of modeling VCM in Canada using SPAA

The work of fitting a surface to the scattered height difference differences and the secular trends of tide gauge records was carried out from east to west. Due to the geophysical diversity in Eastern Canada, for example, different geological characteristics

and different seismicity rates, Eastern Canada was divided into two zones: the Maritimes zone, and the zone containing the southern part of St. Lawrence River (Figure 4.1). The border of these two zones is dictated by the actual data distribution and the present knowledge of the geodynamics of the area. For example, the estuary of the St. Lawrence River is an area where 50 to 100 earthquakes are detected yearly. The region, known as the Lower St. Lawrence Seismic Zone, was originally defined by spatial clustering of magnitude (M) <5 earthquakes (Basham et al., 1982 from Lemieux et al., 2003). This information was used to select the zone boundary[1].

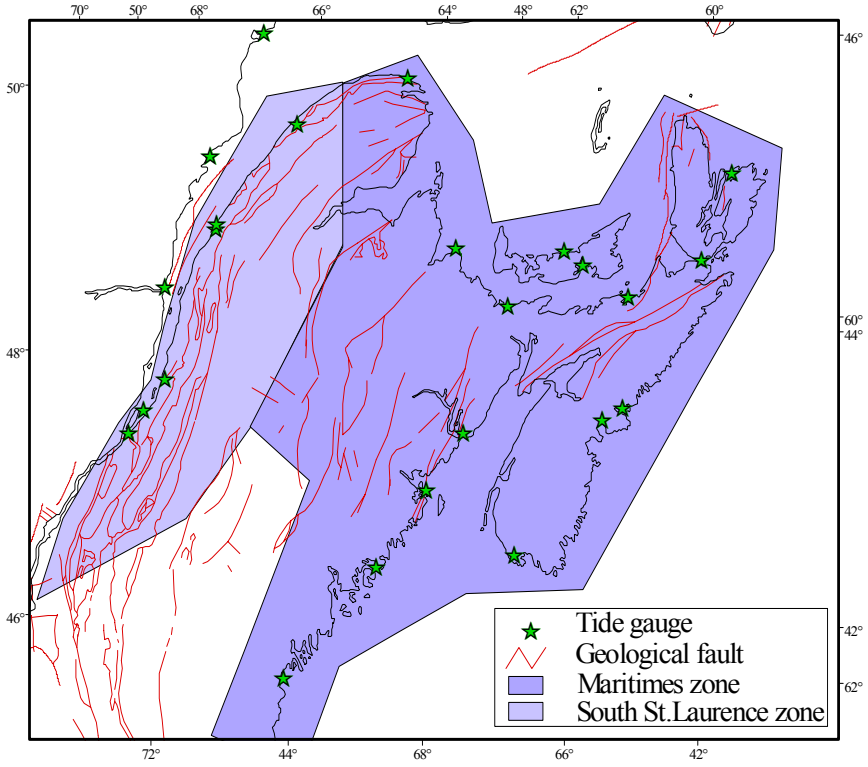

Figure 4.1: The polygonal subdivision used to compute the partial solutions describing the trends of VCM.

The locations of some points as nodal points on the zone boundary were then extracted. The next step was to seek the vertical movement by different polynomial surfaces in each zone. The polynomials were joined together at the nodal points in such a way that a desired degree of smoothness (differentiability) of the resulting function was guaranteed.

[1] More information on the geodynamics of Eastern Canada will be given in chapter 6.3 of this dissertation.

Due to irregular patches or zones, the constraints to be satisfied are determined manually and the satisfaction of continuity and smoothness is done step by step. We started to impose only the continuity conditions on a few nodal points along the border. We then increased the number of nodal points gradually and when we were assured that two surfaces have the same velocity values along the zones boundary, we started imposing the smoothness conditions on the same nodal points in a step by step approach.

Several tests were made to determine the appropriate degree of the velocity surface to be computed. Table 4-1 shows the a posteriori variance factors for the degrees 2, 3 and 4. All degrees of the polynomials yielded the a posteriori variance factors between 8.1-8.5. The value n=3 was finally selected as the highest degree compatible with data distribution.

Table 4-1: The a posteriori variance factors of polynomial surfaces of degree 2, 3 and 4.

Degree of polynomials	Degree 2	Degree 3	Degree 4
a posterior variance factor	8.4	8.1	8.3

The map of vertical crustal movements in Eastern Canada produced by SPAA is shown in Figure 4.2.

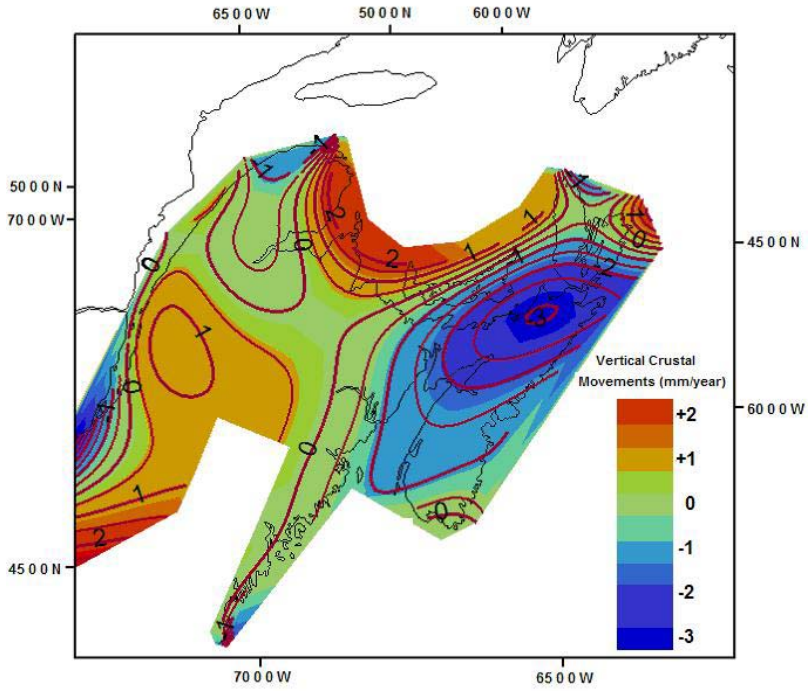

Figure 4.2: Pattern of vertical crustal movements in Eastern Canada. Contours are in millimetre/year (Koohzare et al., 2006a)

In order to fit a simultaneous surface to 2D measured data and the tilts between them in an automatic process, it was decided to divide the area of study into regular patches. In this study, some square and rectangular patches with different sizes were selected in which the border between two adjacent patches is always a straight line parallel to one of the coordinate axes. In this way, the number of constraints for the continuity and smoothness would be reduced and consequently a higher degree of freedom would be achieved. Another advantage is that when dealing with large numbers of data, this approach is computationally fast.

The region of study, Canada, was divided into patches of different sizes depending on the number and the distribution of data. The size of the patches was initially selected to be 2×2 degree and, if there were not enough data in a particular patch, or they were not well distributed, the adjacent patches would be combined to create a bigger patch. This was done automatically in the Program VCM-SPAA by checking the number of data, and

also by converting them to GIS for visualization. Figure 4.3 shows the selection of the patches and the combinations of some of them.

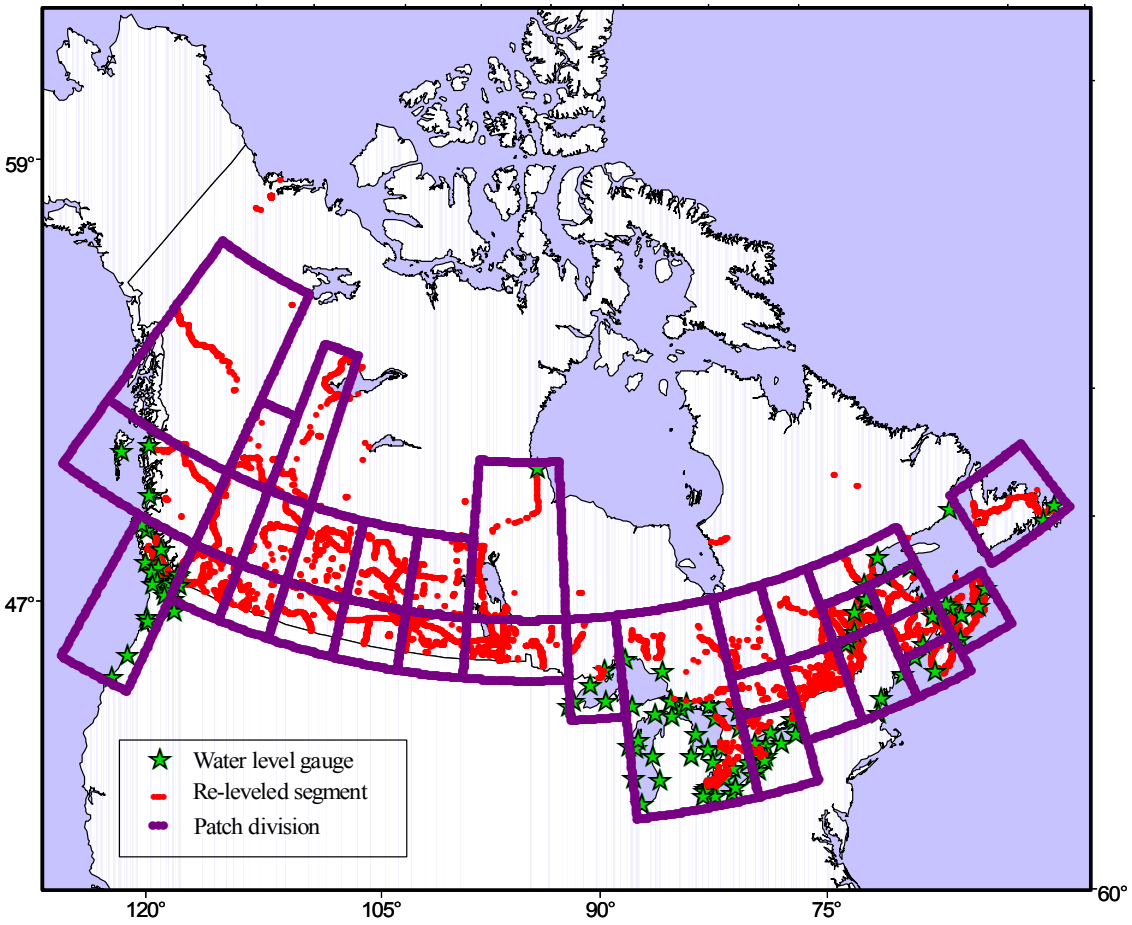

Figure 4.3: The selection of the patches and their combinations.

4.3 Numerical instabilities

One of the basic concepts that should be discussed before explaining the numerical problems is the notion of sensitivity to data distribution. We wish to solve a numerical problem that arises from a practical setting, say solve **Ac=l**, where **A** is a square matrix and **l** is the observed vector, and **c** is the vector of unknown coefficients. It is well-known

that there is a unique solution if and only if matrix **A** is nonsingular. Mathematically, there is no more to say. However, practically it is very important to know how sensitive the solution **c** is to perturbations in the data distribution which are presented in matrix **A**. If the mathematical solution is very sensitive to changes in the data distribution (i.e., the problem may be poorly conditioned) then it is not possible to guarantee that the computed solution is correct. Overdetermined systems of linear equations behave similarly. If the problem is poorly conditioned, we may not find the unknown coefficients such that **Ac** is 'close' to **l** (in the least squares sense).

One frequent problem in VCM modeling using SPAA is that the system of normal equations might be ill-conditioned, which means that the solution is hypersensitive to changes in the position of data. This is the case especially for the initial solutions in patches with poor distribution of data. For example in two adjacent patches, one 49°-51° North and 64°-68° West, and the other 49°-51° North and 68°-72° West, there are 106 and 101 observation equations, respectively (Figure 4.4). Theoretically, the system could be solved, with a reasonable number of degrees of freedom. However, due to the poor distribution of data (all along one line), the design matrix is ill-conditioned.

One remedy is to combine the patch with poor distribution of data with adjacent patch or patches, to create a patch with a more reasonable distribution of data. In Figure 4.4, two adjacent patches with green border are joined to make patch 7.

Following this, it was decided to identify the leveling lines in each patch that need to be re-leveled for a better distribution of data in the patch, which ultimately result in a more stable solution for that patch. This is done using ArcGIS software by putting the leveling and re-leveled lines in different layers and visually deciding which leveling line in each patch should be re-leveled to make a good distribution of data. The 1st order Canadian leveling lines that are recommended to be re-leveled are listed in Appendix VI.

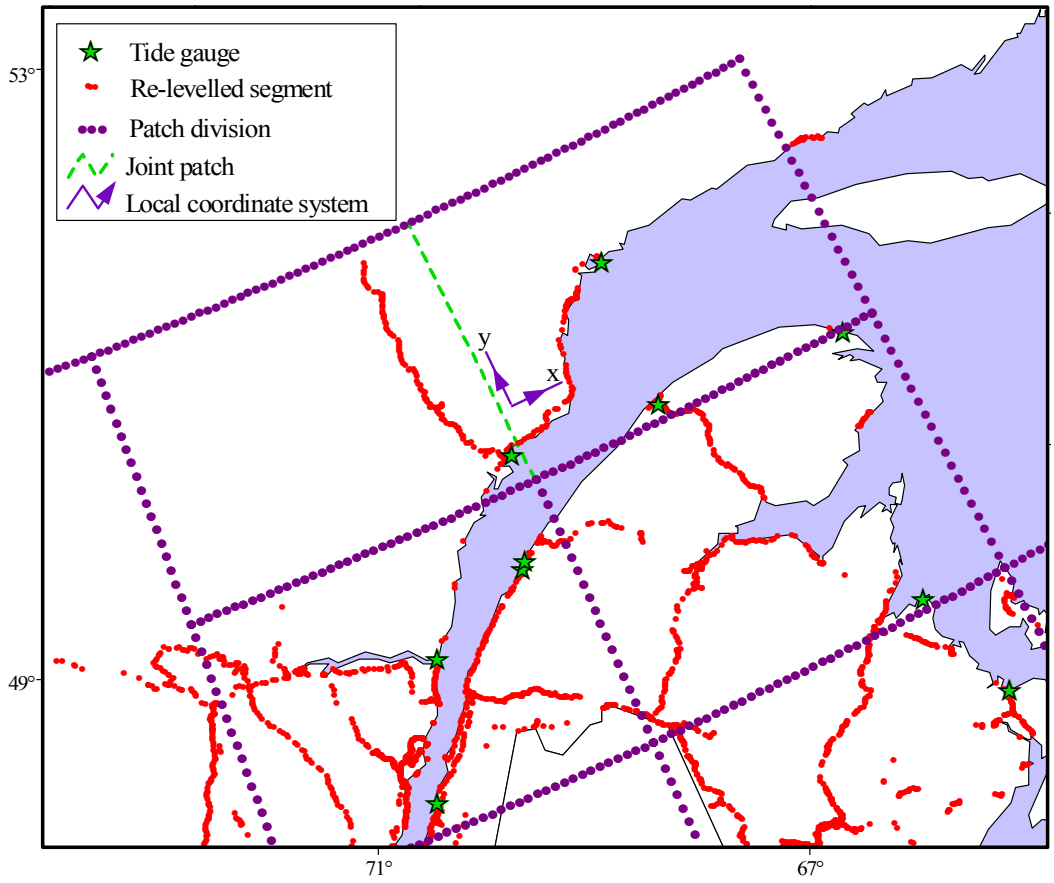

Figure 4.4: Data distribution in two adjacent patches (with green border) which are ultimately joined together to avoid ill-conditioned systems of equations.

In order to secure a numerically stable solution, the origin of the coordinate system should be chosen carefully. It was decided to choose the origin of the coordinate system of each patch either in the center of that patch itself or in the center of the mass point of the patch, depending on which leads to smaller standard deviation for the absolute term of the VCM surface.

To see the effect of different origins of coordinate systems on the standard deviation of the absolute term of the VCM in patch 7(as an example), the origin of the coordinate system for the computation, was assigned 1) outside the patch, 2) in the center of the patch, and 3) in the center of mass of the data in the patch. Three different solutions were obtained and the covariance matrices for the computed coefficients were calculated. Table 4-2 shows the standard deviation of the absolute term of VCM computed in patch 7

in three different coordinate systems. The tide gauges which supply the absolute vertical movements in this patch are Sept Iles, Baie Comeau and Saint Ann de Monts (See Table 3-3 for the vertical movements obtained from the records of these tide gauges along with the standard deviations).

Table 4-2: Standard deviation of the absolute term of VCM computed in patch 7 in three different coordinate systems.

The origin of the coordinate system	Standard deviation of the absolute term of VCM in Patch 7(mm/year)
Outside the Patch $\varphi_\circ$=46°00′00″, $\lambda_\circ$=79°00′00″	553
Center of the Patch $\varphi_\circ$=50°00′00″, $\lambda_\circ$=68°00′00″	0.52
Center of the mass $\varphi_\circ$=49°43′48″, $\lambda_\circ$=67°55′12″	0.39

The standard deviation of the absolute term for the VCM in this patch strongly depends on the location of the origin of the coordinate system, and this is mainly due to the poor distribution of data which appears in the design matrix, and makes it poorly conditioned.

4.4 Results

Figure 4.5 shows the contour map of VCM in Canada. The map of standard deviation of the computed VCM is depicted in figure 4.6. The final map is a patchwork of 33 patches, and cubic polynomials are used in most of the patches. A hypsometric representation of the VCM in Canada is illustrated in Figure 4.7.

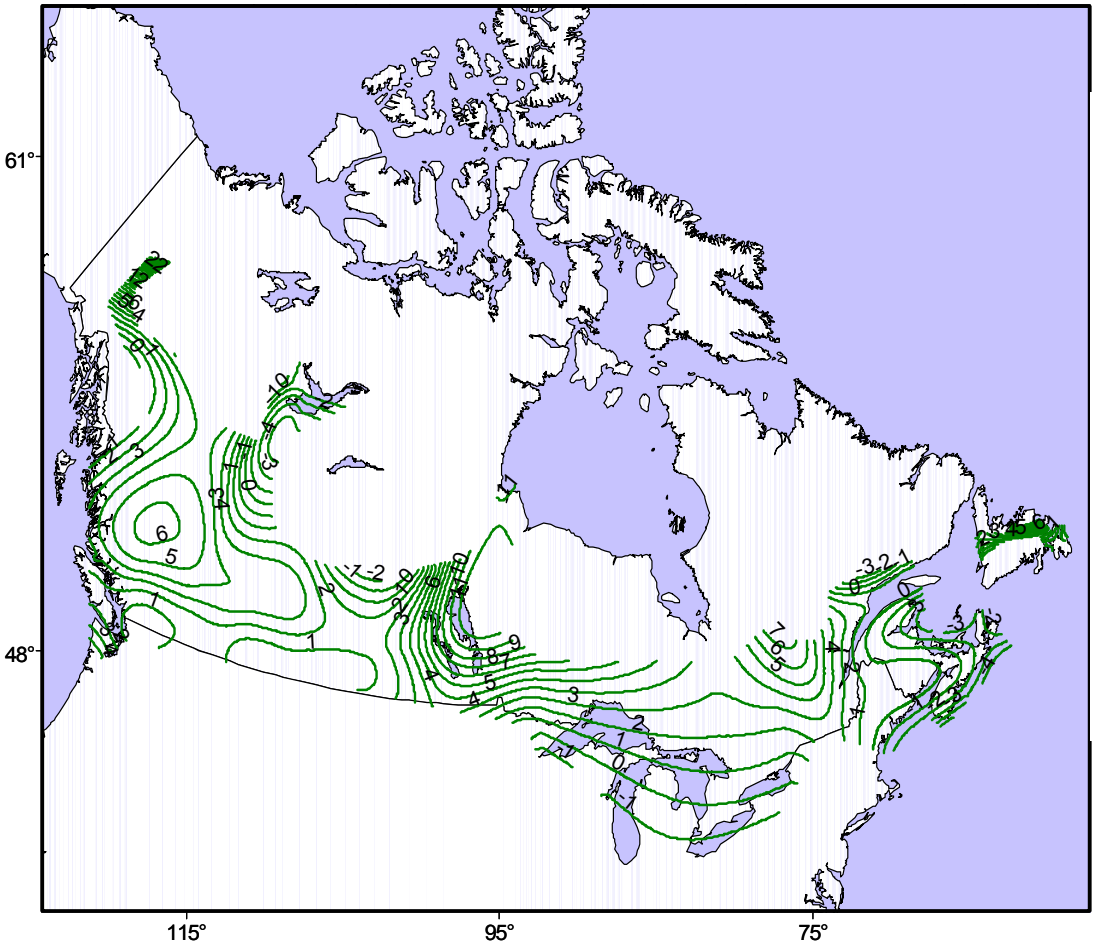

Figure 4.5 Pattern of vertical crustal movements in Canada using SPAA, in millimetre per year.

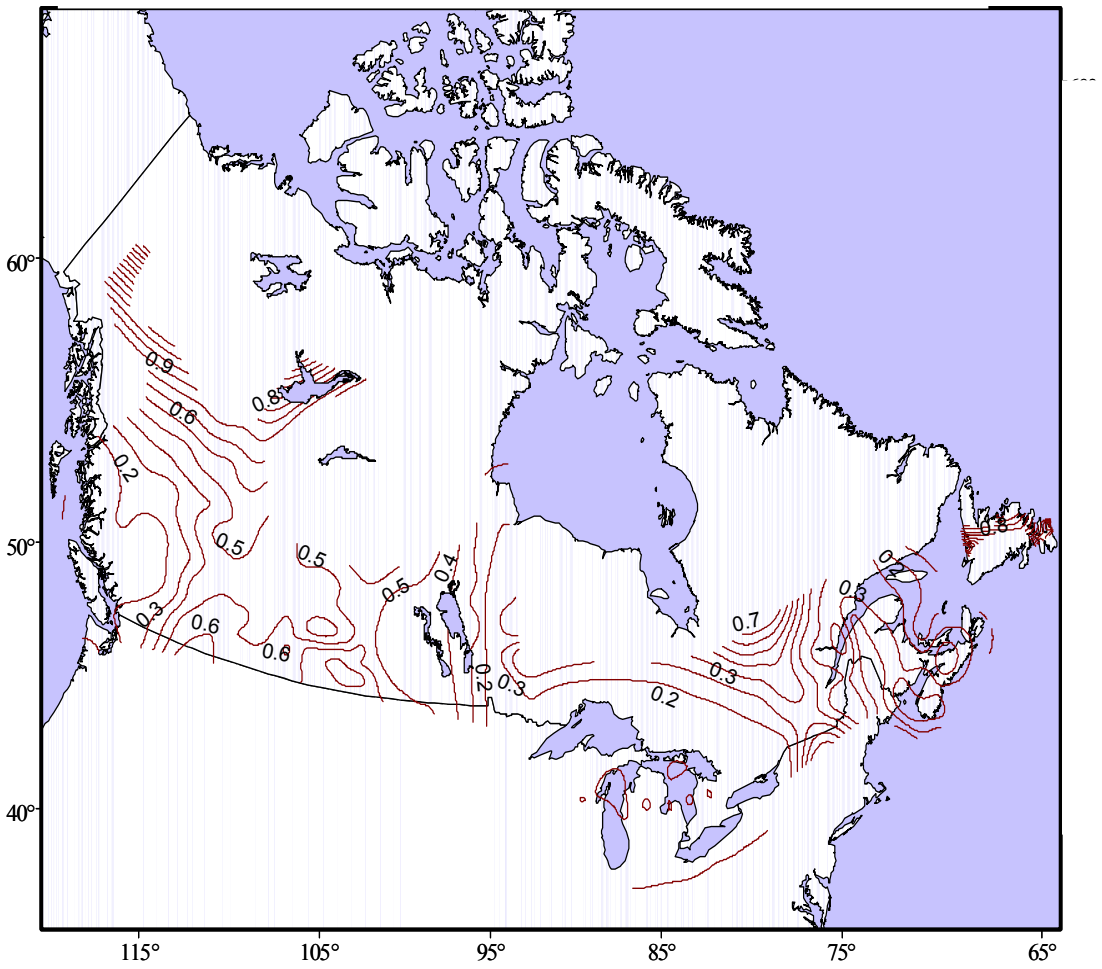

Figure 4.6: Pattern of the standard deviation of the predicted vertical crustal movements in Canada using SPAA, in millimetre per year.

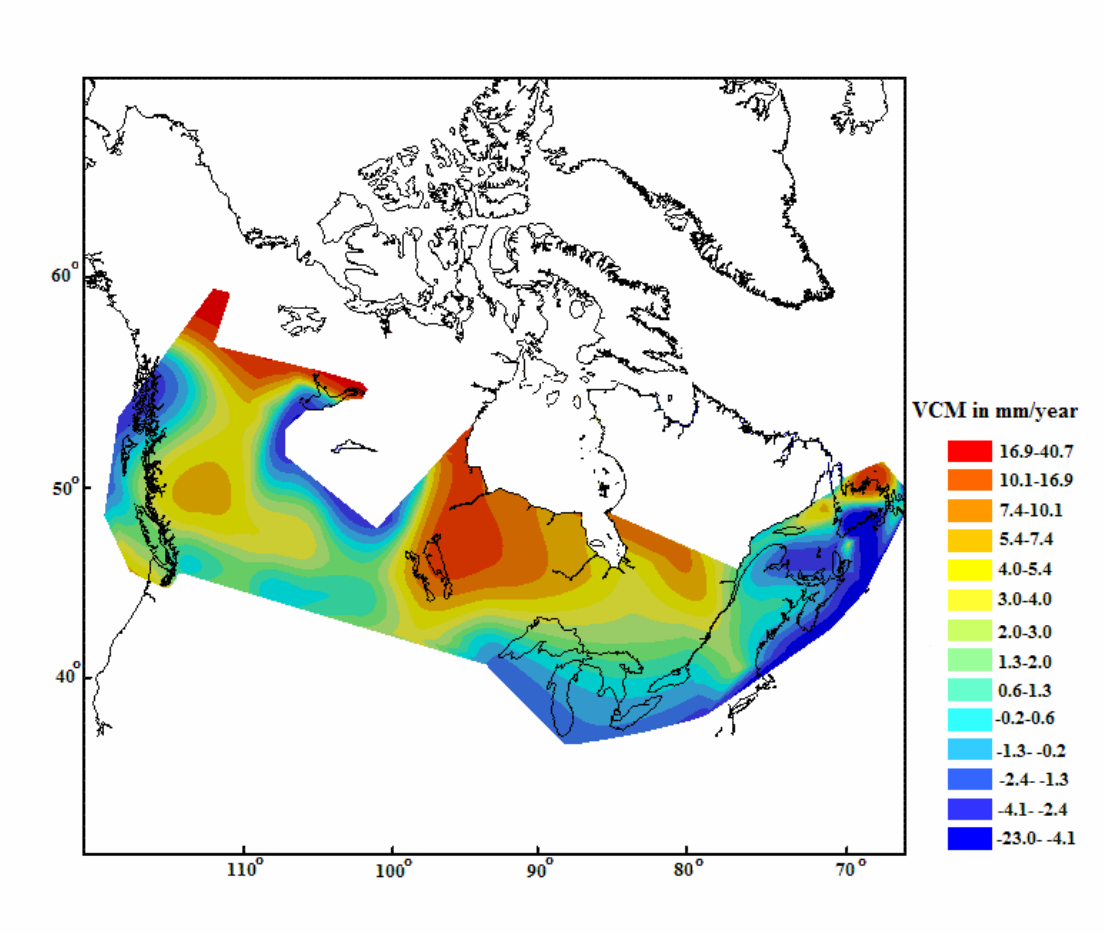

Figure 4.7: Hypsometric map of vertical crustal movements in Canada using SPAA.

Chapter 5

Glacial Isostatic Adjustment models

5.1 Introduction

As stated in the previous chapters, one goal in this research is to look into the relation between the geodetically compiled VCM and geophysical models. The aim of this chapter is to describe the geophysical models that geodesists need to know to interpret the geodetic results. In pursuit of this goal, we have decided to slant the chapter toward emphasizing the topic of particular importance in this work, i.e., Glacial Isostatic Adjustment (GIA). Those parts of the GIA topic that are very specialized, or considered clearly beyond the framework of this dissertation, are not discussed in here. Instead references are given, when it is necessary.

The GIA models consist of three key components: an ice loading model (evolution in time), Earth rheological model, and an algorithm to compute the sea level changes[1] and radial displacements[2] of the solid earth. In this chapter, the physical background of GIA and the mathematical model which is built up from the theory of the response of the Earth to a realistic model of ice sheet are reviewed. The so-called sea level equation is discussed. Then, the main input parameters for GIA models, i.e., the ice model and the radial viscosity profile of the Earth as one possibility of the Earth rheology model, are described. Moreover, the approximation to the standard Earth rheology model, which is used for sensitivity analysis in the subsequent chapter, is defined.

[1] It is equivalent to the changes of orthometric height in land with opposite sign.
[2] It is equivalent to the changes of geodetic heights.

5.2 Elements of the forward problem for GIA

Variations in the ice mass and sea level, together with the direct attraction of the surface load (ice plus water) perturb the gravitational field of the Earth. It is clear that these perturbations must, in turn, affect the sea level variations. In mathematical terms, this interrelation gives rise to an integral equation, known as the sea-level equation (Mitrovica and Peltier, 1991). This integral equation for the relative sea level history, $S(\theta,\lambda,t)$ may be written explicitly as

$$\begin{aligned} S(\theta,\lambda,t) &= C(\theta,\lambda,t)[G(\theta,\lambda,t) - R(\theta,\lambda,t)] \\ &= C(\theta,\lambda,t)\left[\int_{-\infty}^{t} dt' \iint_{\Omega} d\Omega L(\theta',\lambda',t') \times \left\{\frac{\phi(\gamma,t-t')}{g} - \Gamma(\gamma,t-t')\right\} + \frac{\Delta\Phi(t)}{g}\right]. \end{aligned} \tag{5.1}$$

in which $C(\theta,\lambda,t)$, with θ and λ, standing for latitude and longitude respectively, is the 'ocean function' which is, by definition, zero on land or land-locked lake or sea and unity at the oceans (Peltier et al. 1998). $G(\theta,\lambda,t)$ is the geoid and $R(\theta,\lambda,t)$ is simply the local radius of the Earth. Here, γ is the angular distance between (θ,λ) and (θ',λ').The two-dimensional time dependent fields $\phi(\gamma,t-t')$ and $\Gamma(\gamma,t-t')$ are, respectively, the geoidal perturbation and the perturbation to the local radius of the Earth surface. $L(\theta,\lambda,t)$ is the history of surface mass load or the ice thickness assumed known and *g* is the surface gravitational acceleration in the unperturbed and assumed spherically symmetric state. The remaining term in (5.1) is namely, $\Delta\Phi(t)$, is the mass conservation term.

The kernel in the above space-time convolution integral is represented by a system of Green functions for the gravitational potential and the radial displacements. These Green functions may be computed for a given radial viscoelastic structure of the earth using different methods discussed by Peltier (1985). The Green functions that appear in

equation (5.1), have simple expansions in terms of viscoelastic surface load Love numbers of the form

$$\begin{aligned} \phi\ (\gamma,t) &= \frac{ag}{m_e}\sum_{l=0}^{\infty}(1+k_l^L(t))P_l(\cos\gamma), \\ \Gamma\ (\gamma,t) &= \frac{a}{m_e}\sum_{l=0}^{\infty}h_l^L(t)P_l(\cos\gamma). \end{aligned} \tag{5.2}$$

in which a is the mean radius of the Earth, m_e is the mass of the Earth and P_l are the Legendre polynomials. k_l^L and h_l^L are the surface load numbers which generally have time-domain expansions:

$$\begin{aligned} h_l^L(t) &= h_l^E\delta(t)+\sum_{j=1}^{J}r_j^l e^{-s_j^l t}, \\ k_l^L(t) &= k_l^E\delta(t)+\sum_{j=1}^{J}r'^l{}_j e^{-s_j^l t}. \end{aligned} \tag{5.3}$$

These are discrete visco-elastic normal mode representations in which the h_l^E and k_l^E are precisely the elastic surface load Love numbers and $\delta(t)$ is the Dirac delta function. $r_j^l, r_j'^l$ are the amplitudes and s_j^l are the inverse relaxation times of the poles in the Laplace transform plane on the basis of which these expansions are constructed (For further details, see for instance Tushingham and Peltier, 1991; Mitrovica and Peltier, 1991; Peltier, 1998).

5.3 Model input

One of the main inputs of the GIA models is the Earth rheology. Glacial Isostatic Adjustment inversion studies provide a unique possibility to determine the mantle viscosity profile and this profile is used as one input to the GIA models. Besides Earth rheology models, the other input required for GIA study is a model of the formation and

retreat of the ice sheet. To this extent, GIA studies can be used in an inverse fashion to derive ice sheet chronology for a fixed viscosity profile[3].

Ocean function in equation (5.1) is another input described in section 5.3.3. Diagrammatically, Figure (5.1) gives an overall view on the input and output of the GIA models.

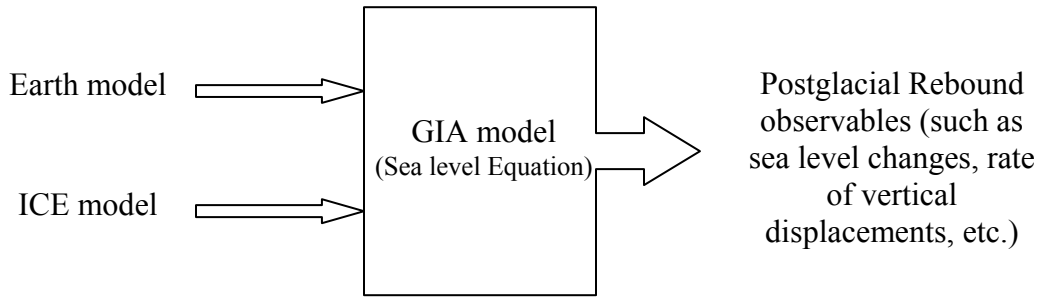

Figure 5.1: The input and output of the GIA model.

5.3.1 Earth rheological model

In the study of postglacial rebound, the most relevant rheological parameters is viscosity. There has been intensive research on the mantle viscosity. However, debates on mantle viscosity still exist and mostly concentrate on the increase which occurs at the upper-lower mantle transition at 670km depth (Peltier, 1998).

Using sensitivity kernels in a pseudo spectral formulation, Peltier (1976), Mitrovica and Peltier (1991, 1993, 1995), did a formal inversion of the viscosity profile in the mantle from postglacial sea levels and free-air gravity data, assuming that the Earth is laterally homogenous. Wu (2002, 2004) and Martinec (2000) carried on similar studies for the laterally heterogeneous earth.

[3] The procedure is based on laborious trial-and-error process of deriving a model of the ice sheets for all geological data.

The mantle viscosity profile from VM2 (Viscosity Model that are adopted in producing ICE-3G and ICE-4G ice history model) is depicted in Figure 5.2a. Figure 5.2b shows an approximation to the mantle viscosity which is used in next chapter.

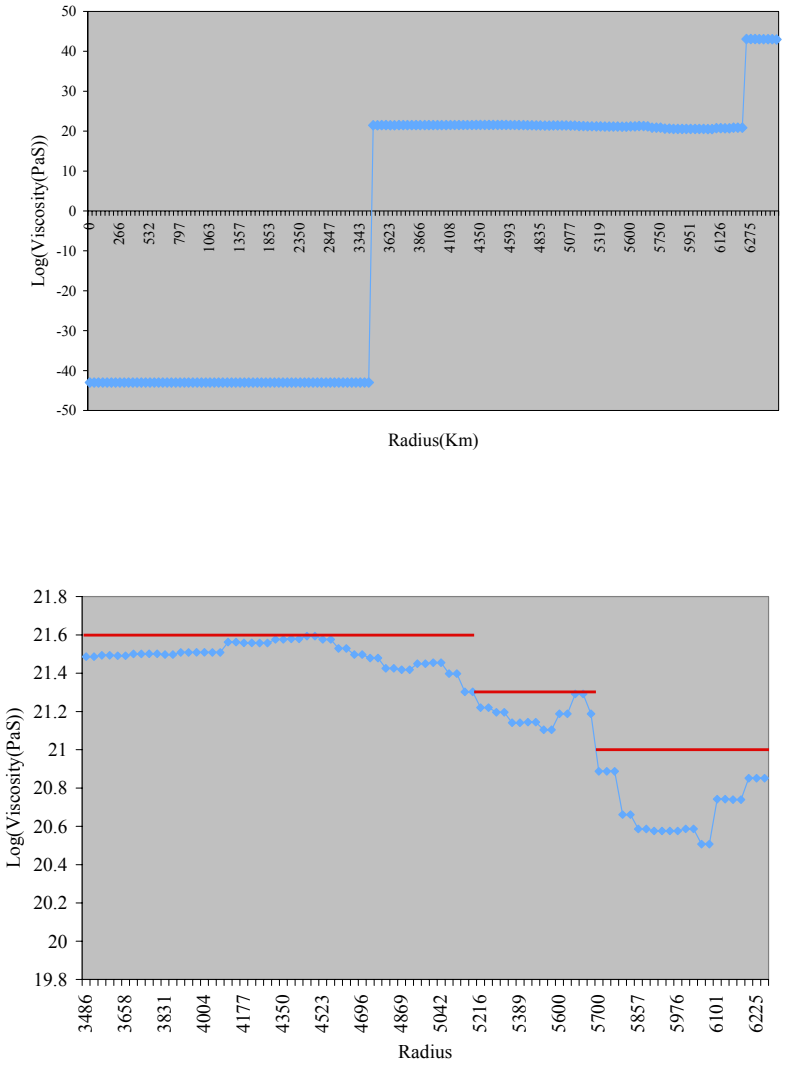

Figure 5.2: a) Viscosity model of VM2 in Pascal second. b) The viscosity model of lower and upper mantle, the blue line shows the viscosity values from VM2 model, and the red lines depict the values of viscosity from Mod17 Earth rheology model.

The Earth rheology model programs compute the response of a multi-layer, spherically symmetric Earth in terms of Love numbers, which are needed for the sea level equation. The starting point is the equation of conservation of momentum and Poisson's equation

for the gravity field. Eventually, they lead to a set of coupled differential equations. There are different ways of solving these differential equations. The technique which is mostly used in this field is Normal Mode Analysis (Peltier, 1974; Wu, 1978; Spada et al. 1992; Vermeersen and Sabadini, 1997 and Tromp and Mitrovica, 1999). The output of these programs is Love numbers for different spatial degrees (Equation 5.3).

5.3.2 ICE models

This section describes how ice models are constructed with the use of geological and sea level data. Some measure of the global ice-volume can be obtained from Oxygen isotope data[4] (Crowley and North, 1991). Geomorphological data yield information regarding the time-dependent geometry of the ice margins. Ice sheet reconstructions for the Late Pleistocene[5] can also incorporate the sea level records. The ICE-3G (Tushingham and Peltier, 1991) model and its descendants, use a global database of sea level records from the Late Pleistocene to obtain the deglaciation history. The global ice model at any epoch is represented by several hundred discrete ice elements, each of which can be varied until an adequate match with sea level history is obtained. A consistent solution is found for the sea level and the vertical deformation due to the viscoelastic response of the Earth to the changing ice. The criticism of such models is that they are non-unique, matched to a particular global mantle viscosity profile.
The properties of ICE3-G and ICE-4G are given in Table 5-1. Figure 5.3 illustrates the ice thickness in two ice models: ICE-3G, and ICE-4G.

[4] Oxygen isotope ratio cycles are cyclical variations in the ratio of the mass of oxygen with an atomic weight of 18 to the mass of oxygen with an atomic weight of 16 present in calcite of the oceanic floor as determined by core samples. The ratio is linked to water temperature of ancient oceans, which in turn reflects ancient climates. Cycles in the ratio mirror climate changes in geologic history.

[5] The Late Pleistocene is a stage of the Pleistocene Epoch. The beginning of the stage is defined by the base of Eemian interglacial phase before final glacial episode of Pleistocene 126,000 ± 5,000 years ago. The end of the stage is defined exactly at 10,000 Carbon-14 years BP.

Table 5-1: Data used to produce ICE3-G and ICE-4G.

ICE model	Data used
ICE3G (Tushingham and Peltier, 1991)	Geological evidence: features left by ice. Based on RSL history from sites in the near and far field.
ICE4G (Peltier, 1994)	Geological evidence: features left by ice. Based on RSL history from sites in the near and far field. Last Glacial Maximum shifted from 18,000 years to 21,000 years before present.

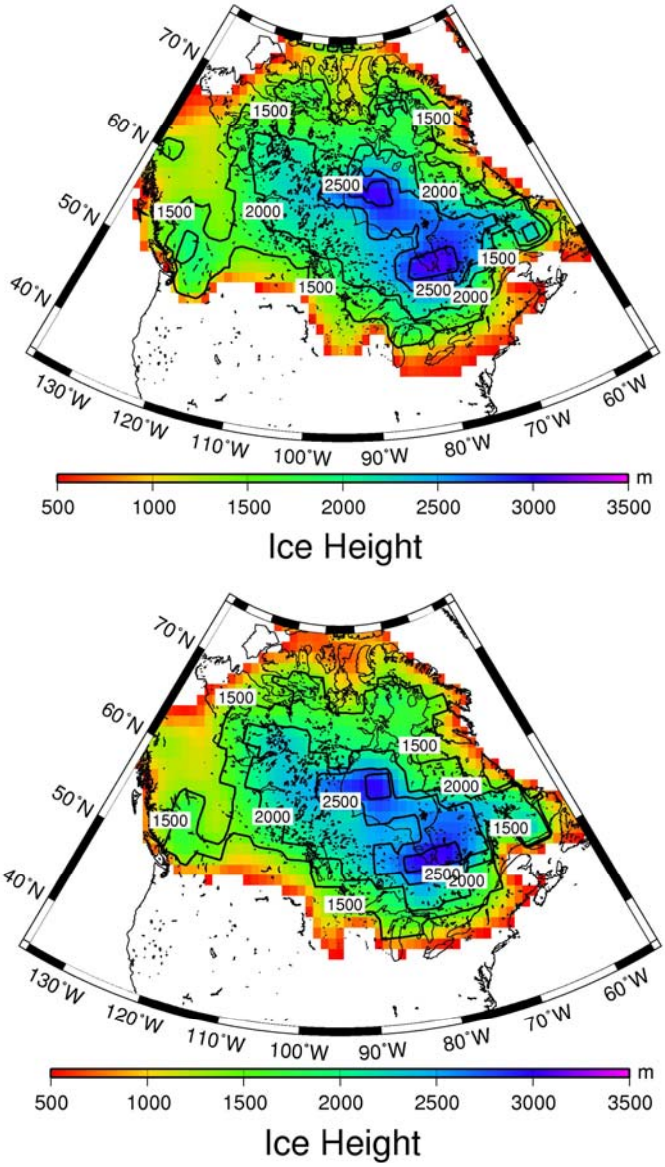

Figure 5.3: Ice thickness in (a) ICE-3G model and (b) ICE-4G model at the last glacial maximum at the time of Last Glacial Maximum.

The ICE-3G and ICE-4G provide the ice thickness in some discrete deglaciation times (e.g., in ICE-3G model every 9ky or 9000 year) in either disks (in ICE-3G) or in grids (in ICE-4G). The centers of the disks or the grids are given along with the size of the element. A sample of ICE models is given in Appendix VI.

5.3.3 Ocean Function

The ocean function assigns, for each node of computation, a value of 1 when it belongs to the oceans or a value of zero when it is on land. As will be noted in section 5.4, we use the pseudo-spectral method of Mitrovica and Peltier (1991) to obtain a gravitationally self-consistent solution of the sea level equation. In this method, the ocean function is required in spherical harmonic expansion as well as in spatial form (Motrovica and Peltier, 1991). The ocean function up to degree 128 is available as another input file for the computation.

5.4 Algorithm to solve the sea level equation

Mitrovica and Peltier (1991) presented two ways of obtaining a gravitationally self-consistent solution of the sea level equation (1): a full spectral and a pseudo-spectral method. A completely different method was presented in (Wu, 2002) and (Wu, 2003) as the Coupled Poisson Finite Element method. The latter doesn't follow the Love number approach. Instead, a grid of 18 layers and 360 elements is constructed. Therefore, the effect of lateral viscosity changes can be considered. However, the computation is very slow. In this research, the pseudo-spectral method of Mitrovica and Peltier (1991) was used to obtain the response of the Earth to the ice loads.

Chapter 6

Discussion and physical interpretation of the results

The study of geodynamics is interdisciplinary and hence requires creativity and the ability to integrate different sources of information about the temporal variation of the Earth crust and gravity and to interpret them. For this reason, the physical interpretations of the VCM cannot be conducted by itself, but its relationship with other geodynamics studies should be considered. In the first section of this chapter, some of the knowledge related to the temporal variations of heights in Canada from other fields, or other geodetic data than VCM is presented. This includes:

- Rate of vertical movements of the crust and the geoidal changes from GIA models
- Rate of gravity changes in Canada.
- Rate of changes of the geodetic heights from GPS solution.

Then, for different regions in Canada, the temporal variations of orthometric height are physically interpreted and compared with the above information. The ratios of gravity to height changes and the rate of geoid height changes in Canada are computed and discussed. The sensitivity of the VCM to uncertain parameters in GIA models (including the sensitivity of the computed VCM to the radial changes of viscosity and to the ice thickness) is also explored.

6.1 Rates of radial displacements and geoidal changes from GIA models

The present-day rate of geoidal and radial displacement of the surface of the solid Earth in North America due to PGR is shown in Figures 6.1a,b and 6.2a,b. It was computed using the Earth properties given in Table 6.1, and the ice history obtained from ICE-3G and ICE-4G models, respectively. These calculations are performed using the sea level program written by W. van del Wal, University of Calgary (Personal communications). The values of geoidal and radial displacements obtained from ICE-3G model are significantly higher than those computed using ICE-4G model, in most of the areas (see the color scale in Figures 6.1a,b and 6.2a,b). The sensitivity of the rates of the radial displacement and geoid to the ice thickness and other viscosity profiles will be discussed in section 6.4.

Table 6-1: Reference 6-layers Earth rheology model (Mod17).

Layer	R[*km*]	density $\rho\,(\mathrm{kg/m^3})$	rigidity μ (GPa)	viscosity υ (Pa.s)
1	6371000	3850.0	0.59485×10^{11}	0.10000×10^{44}
2	6256000	3850.0	0.73115×10^{11}	0.10000×10^{22}
3	5971000	4150.0	0.10950×10^{12}	0.10000×10^{22}
4	5701000	4630.0	0.18063×10^{12}	0.20000×10^{22}
5	5200000	4760.0	0.24145×10^{12}	0.40000×10^{22}
6	3480000	10910. 0	0.0000	0.0000

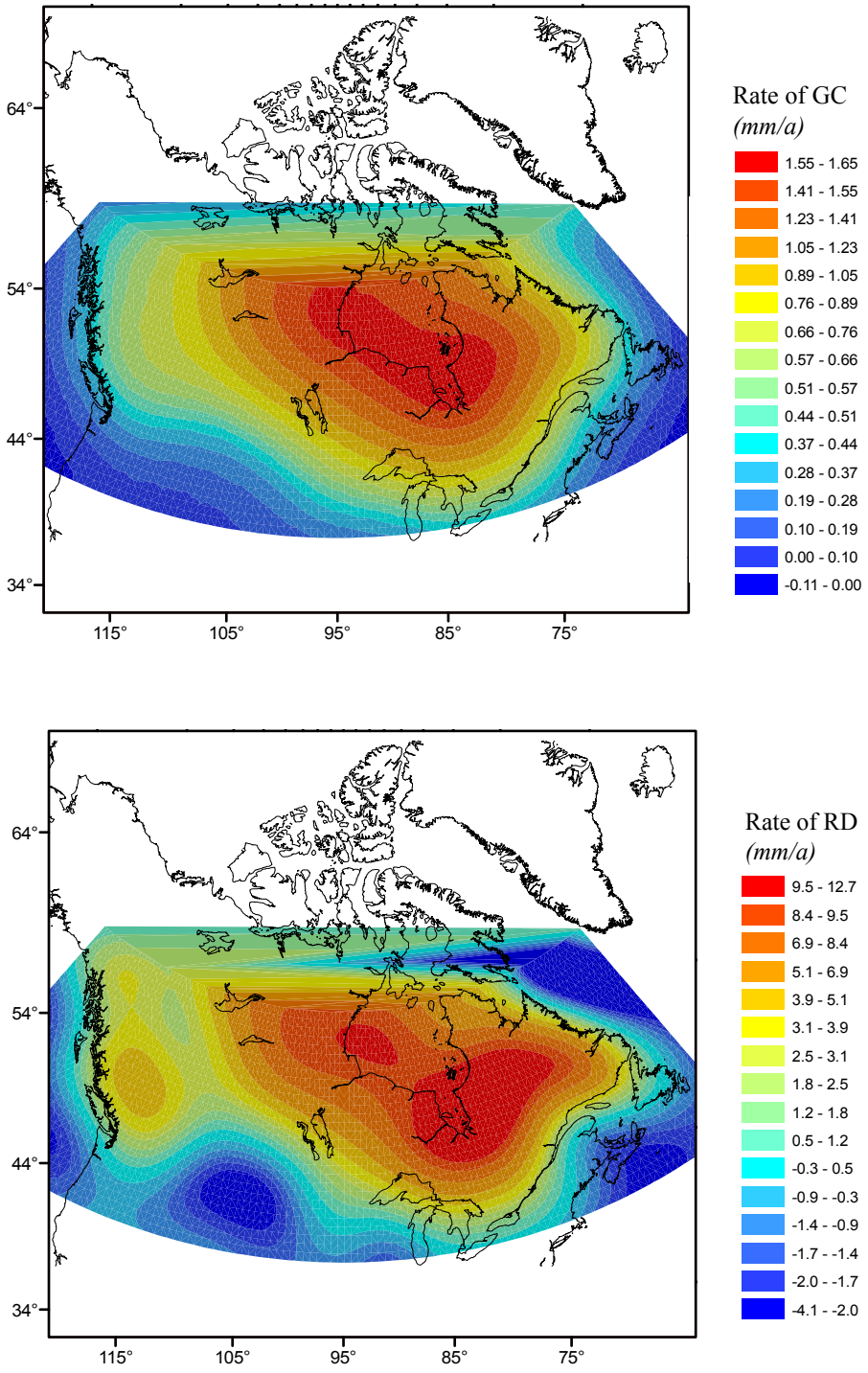

Figure 6.1 (a) The present-day rate of geoidal changes (GC) over North America using Mod17 viscosity model and ICE-3G deglaciation history. (b) The present-day rate of radial displacement (RD) of the surface of the solid Earth in North America using Mod17 viscosity model and ICE-3G deglaciation history. In the far north, the maps are merely an extrapolation based on the data in the further south and an artifact of the girding algorithm used.

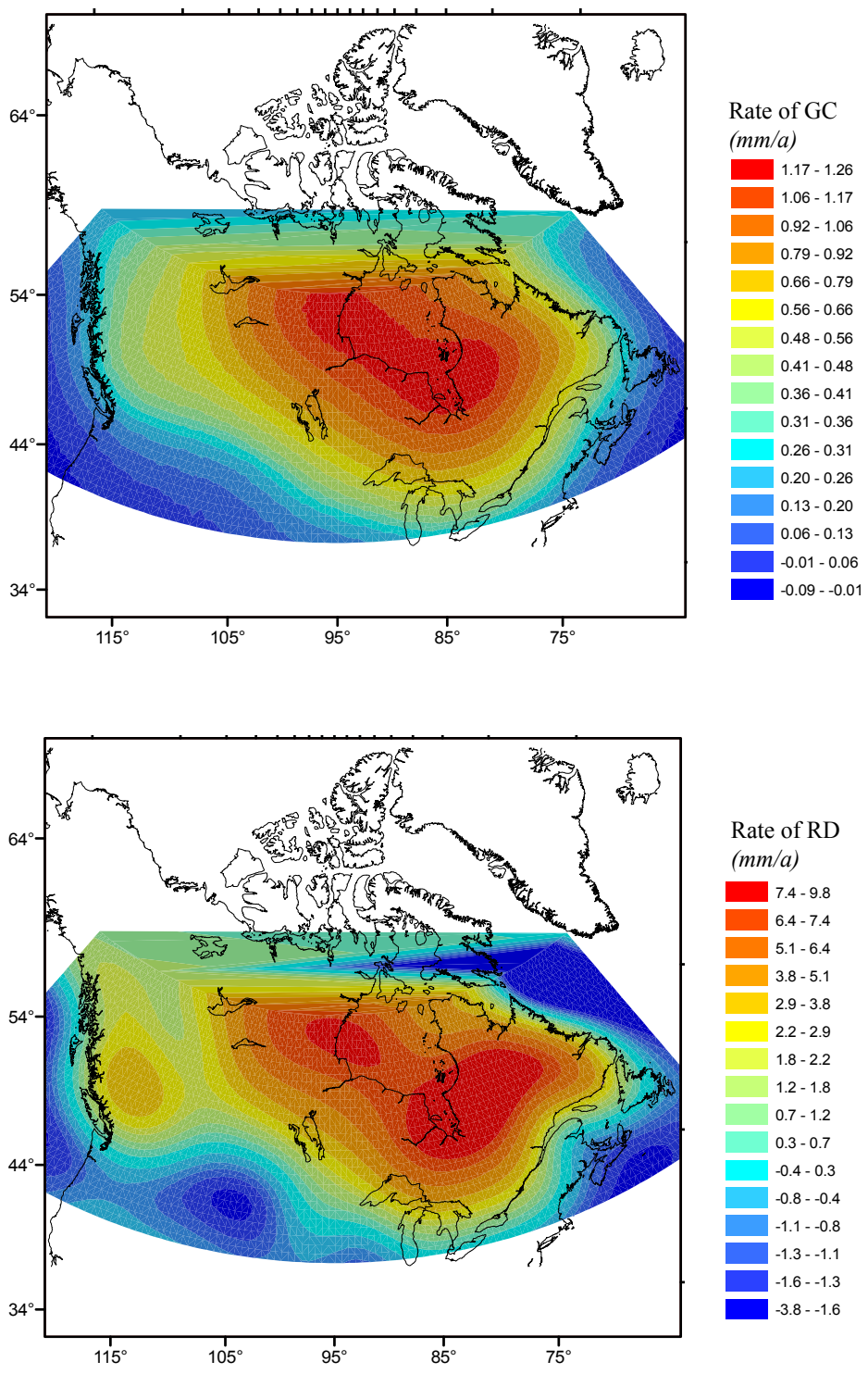

Figure 6.2: (a) The present-day rate of geoidal changes over North America using Mod17 viscosity model and ICE-4G deglaciation history. (b) The present-day rate of radial displacement of the surface of the solid Earth in North America using Mod17 viscosity model and ICE-4G deglaciation history. In the far north, the maps are merely an extrapolation based on the data in the further south and an artifact of the girding algorithm used.

6.2 The map of contemporary rate of gravity changes (ġ)

Over much of the Canadian landmass, the PGR signal may reach to 2 μGal/a or more, (Pagiatakis and Salib, 2003) and hence monitoring of temporal gravity changes in Canada in relation to the predicted crustal deformations using VCM-SPAA model provides an independent means of verifying the predicted crustal deformations from GIA models.

The most recent work on the time rate of changes of gravity in Canada was carried out based on the re-adjustment of the primary Canadian Gravity Standardization Network (CGSN) which consists of nearly 10,000 relative gravity observations obtained over a period of four decades (Pagiatakis and Salib 2003). The CGSN comprises over 1500 primary and secondary gravity reference stations that have been carefully maintained since 1950 and the gravity observations obtained using LaCoste- Romberg gravimeter.

The map of ġ produced by Pagiatakis and Salib (2003) is based on parametrizing the time rate of change of gravity into the observation equation and estimating it directly from a generalized least squares solution. Time rates of gravity changes from repeated absolute gravity observations, as well as absolute gravity values at selected sites are used as weighted constraint. Two least squares solutions for the rate of gravity changes, each using a different set of ġ constraints, namely Geodetic Survey Division solution (GSD solution) and Pacific Geosciences Center solution (PGC solution), are given by Pagaiatakis and Salib (2003). These solutions are presented in the form of a ġ map. Figures 6.3 and 6.4 show the map of ġ, produced using GSD solution and PGC solutions, respectively, for the areas where the map of VCM is valid. These maps also show the distribution of gravity stations in Canada with circles, in which 64 sites are classified as ‘Primary Gravity Control’ with good topological characteristic and relative gravity measurements spanning over 40 years.

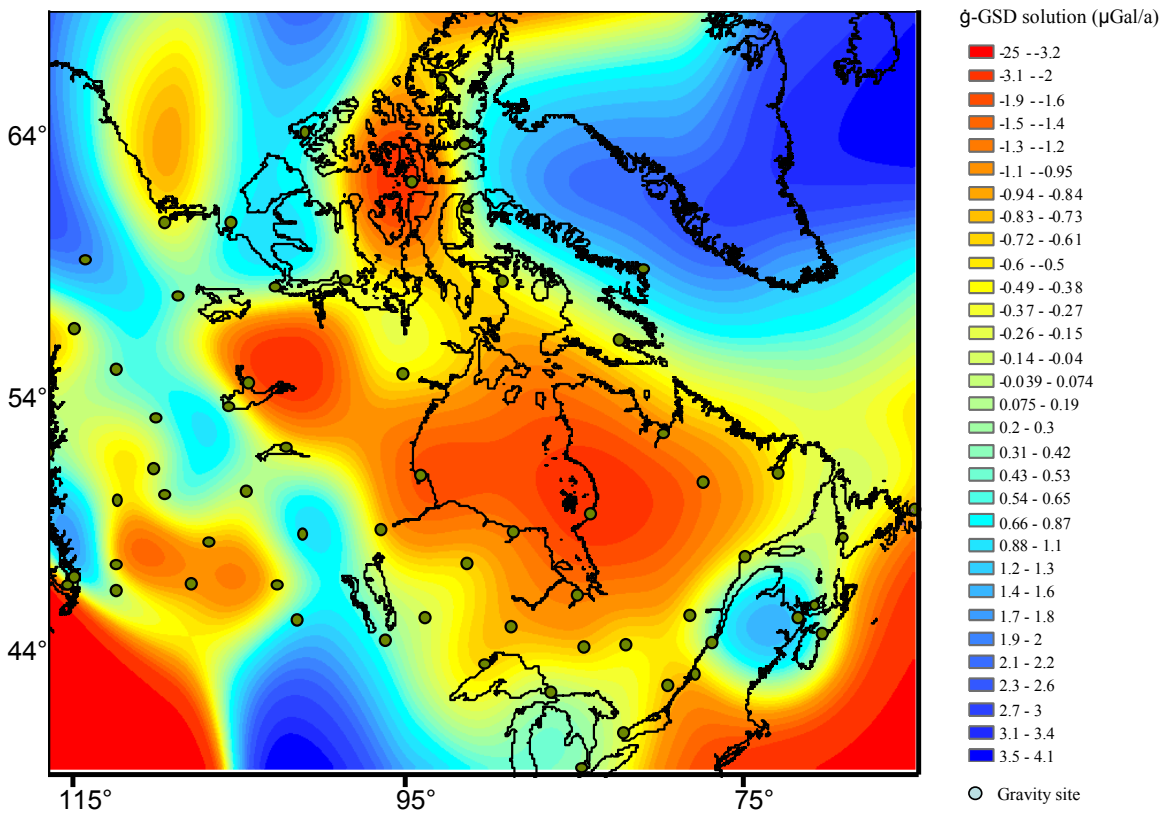

Figure 6.3: Map of ġ based on Geodetic Survey Division (GSD) Solution. Contour interval is 0.1 µGal/a. The circles depict the location of the gravity sites

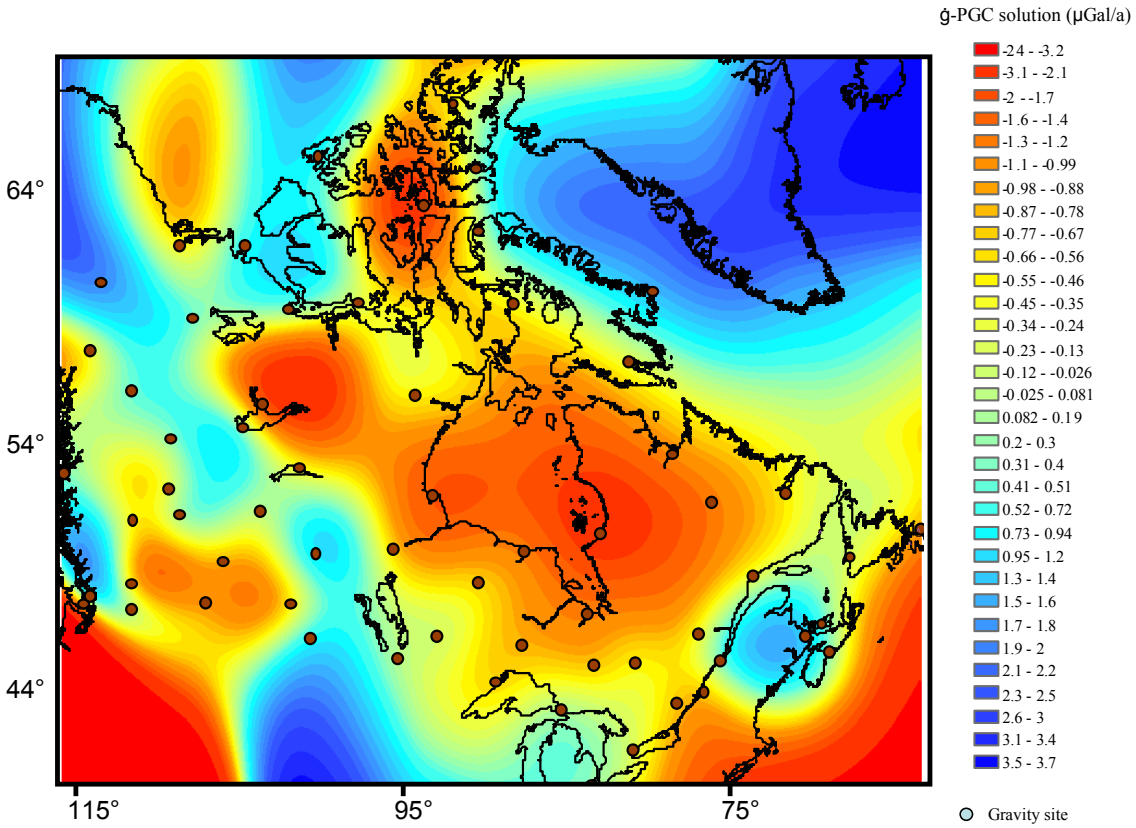

Figure 6.4: Map of ġ based on Pacific Geosciences Center (PGC) Solution. Contour interval is 0.1 µGal/a. The circles depict the location of the gravity sites.

6.3 Rate of change of the geodetic heights at GPS stations

There are a number of efforts within the Earth Science Sector (ESS) in NRCan, University of Wisconsin and Purdue University that contribute to monitoring crustal motion and deformation using GPS at different scales across the Canadian landmass. Progressing from larger to smaller spatial scales, these efforts can be summarized as

- Global-scale plate kinematics and ITRF.

- Continental and national scale monitoring efforts of a Stable North American Reference Frame (SNARF).
- Monitoring of the Canadian Base Network (CBN).
- GPS observations Campaigns on regional scales.

In addition, there are some more efforts by other institutes that contribute to the observation of deformation of the North American plate interior from continuous GPS measurements (See for example Calais et al., 2006; Sella et al., 2002). In the following, the velocity solutions computed by NRCan for SNARF and the solution from the CBN are presented.

6.3.1 NRCan velocity solution submitted to SNARF

Regional reference frames fixed to the stable part of a tectonic plate are often required to facilitate geophysical interpretation and inter-comparison of geodetic solutions of crustal motion. In 2003, the Stable North American Reference Frame (SNARF) Working Group was established under the auspices of UNAVCO, Inc. and International Association of Geodesy (IAG) Regional Sub-Commission 1.3c for North America especially to address needs for the US-led Earth Scope projects. The goal is to define a regional reference frame that is consistent and stable at sub-mm/year level throughout North America (Henton et al., 2006).

The first release of SNARF was computed using only stable sites from a combination of velocity solutions from GSD for the NAREF network and the Canadian Base Network, and a velocity solution from Purdue University for a selection of US Continuously Operating Reference Station network (CORS) stations. NRCan Velocity Solutions submitted for SNARF was made available on April 2005. It was computed based on NAREF weekly combinations 2001-2004 using Bernese & GIPSY software suite with respect to reference epoch 2002.0. However, there are some biases in Bernese solution for Canada which is due to Solid Earth tide error in Bernese GPS Software v4.2.(Craymer, personal communication). The offset is larger for stations farther from

fixed point DRAO and smaller in the far north where tides are smaller.[1] Therefore, the velocity solution computed for the SNARF is not considered in our comparisons.

6.3.2 NRCan velocity solution from CBN

Initiated in 1994, the Canadian Base Network (CBN) is a national network of high-stability passive pillar monuments for GPS receiver antennas. The initial role of the CBN was to complement the Active Control System (ACS) of the CSRS by providing easily accessible 3D reference coordinate sites, with a reasonable distribution across Canada.

By combining nearly 10 years of repeated multi-epoch (episodic) GPS measurements, GSD has begun to estimate velocities at the CBN sites in order to provide an increased spatial sampling of crustal deformation throughout Canada.

To determine individual station velocities, regional CBN solutions for each measurement epoch are systematically combined into a single Canada-wide, multi epoch cumulative solution by NRCan. (See Henton et al., 2006 for more details). This was based on the velocity estimations using 28 campaign surveys between 1994 and 2002. In order to generate time series of consistent, high accuracy coordinates for velocity estimation, it is necessary to ensure the consistency of the integration into the reference frame. This is accomplished by aligning each of the individual CBN solutions to a subset of stations from a recent cumulative solution for the IGS global network in ITRF. Consistent and realistic weighting of the individual CBN solutions is improved through the estimation of separate variance components relative to IGS global solution. After the individual CBN solutions are aligned and weighted, they are combined together in a simultaneous cumulative solution to produce velocities at each site (Henton et al., 2004). The CBN solution which is provided by GSD (CBN_cumu_r98_v0.snx), is based on 28 epoch surveys 1994-2002. The constraint station is ALGO in Ontario (See Figure 6.5) which is fixed to IGS05P01 position/velocity and the Reference epoch is 1998.0. There is no “Bernese bias” in this situation such that was present in the SNARF solution. The velocity solution is in a Solution Independent Exchange Format (SINEX) file that

[1] See the UNAVCO Scientific Workshop at http://www.unavco.org/research_science.

contains the estimated station positions, velocities and their covariance matrices for the entire time period considered. Figure 6.5 shows the observed CBN geodetic height changes in Canada.

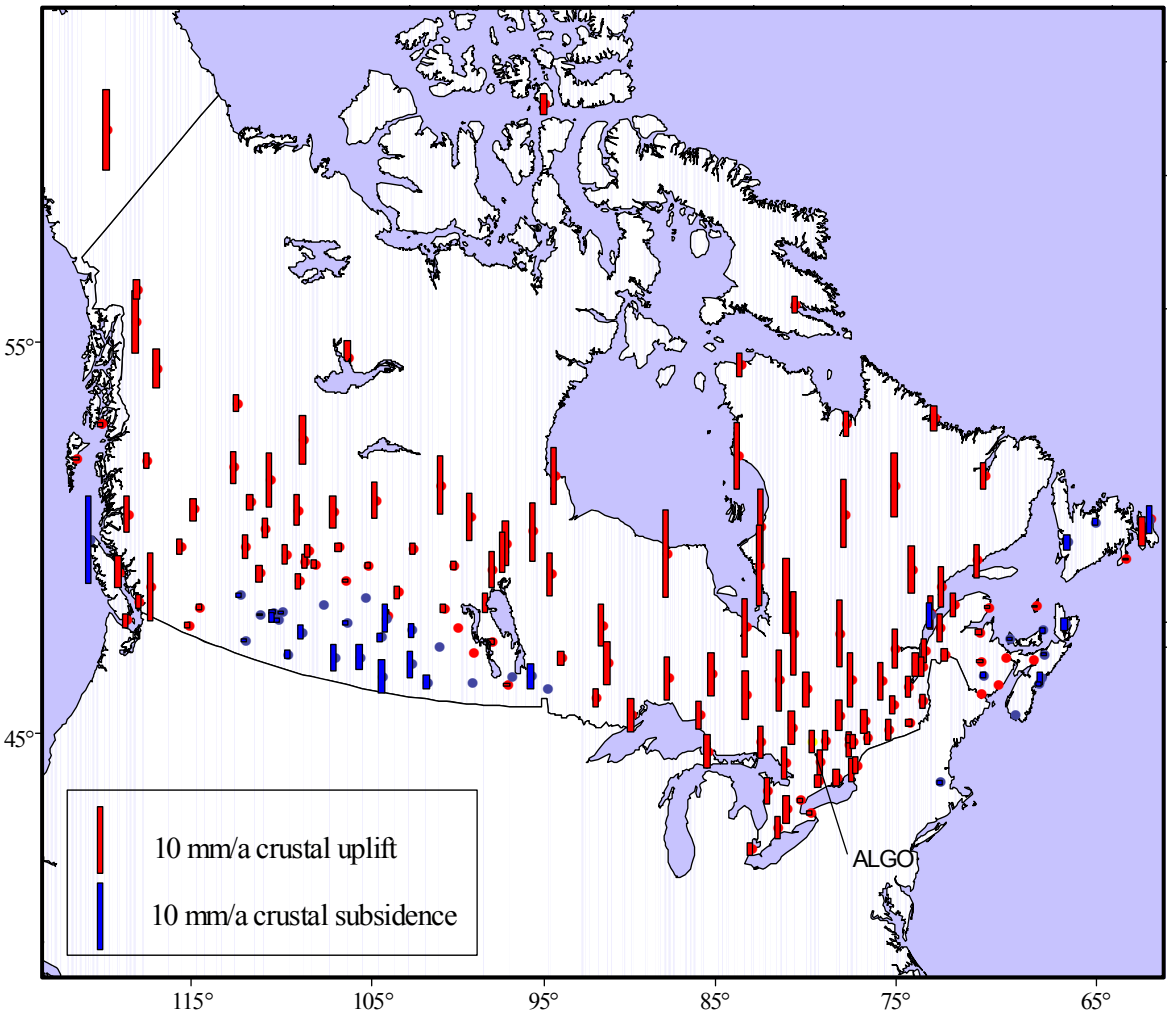

Figure 6.5: Observed CBN vertical rates. Red bars represent uplift and blue bars depict subsidence.

6.3.3 Velocity Solution from Purdue University

Purdue University velocity solution is based on data from more than 300 continuous GPS stations covering the central and eastern United States and Canada, spanning the

1993-2005 period. This includes the data from the CORS network coordinated by the National Geodetic Survey (NGS), and the data from sites that have been contributing to the International GPS Service for Geodynamics (IGS) since 1992 (in particular continuous sites in Canada operated by the Geodetic Survey Division of Natural Resources Canada and data from the GAMA network operated by the Center for Earthquake Research and Information, University of Memphis (Calais et al., 2006). Data have been processed using the GIPSY-OASIS and GAMIT-GLOBK software packages. The independent geodetic coordinate and velocity solutions were combined to average the random and systematic errors associated with individual processing strategies (Calais et al., 2006). Figure 6.6 shows the rate of geodetic height changes from this solution.

The CBN and Calais et al. (2006) solutions are compared in the common GPS sites in Table 6.2. The values of $\dot{h}$ from two different solutions are relatively close except for the HLFX and CAGS stations. Many reasons can be sought for such differences, including errors in the GPS observations, alignments, software biases or different constraint stations. The investigations about these causes are beyond the scope of this work. We decided to use CBN-solution for further comparison with the VCM, as this solution covers the whole Canada, and gives consistent solution.

Table 6-2: The CBN and Calais et al. (2006) solutions in the common GPS sites in Canada.

GPS site	Latitude (Degree)	Long (Degree)	$\dot{h}$ (mm/a) Calais solution	$\dot{h}$ (mm/a) CBN solution
ALGO	45.95	-78.07	2.48 ± 1.17	3.22 ± 0.01
CAGS	45.58	-75.80	5.50 ± 1.47	1.41 ±1.14
CHUR	58.76	-94.08	10.79 ±1.40	8.20 ± 0.60
HLFX	44.68	-63.61	5.82 ± 2.16	-1.56 ± 0.52
NRC1	45.45	-75.62	3.20 ± 1.24	2.32 ± 0.59
RESO	74.69	-94.89	5.51 ± 2.01	3.19 ± 3.65
SCH2	54.83	-66.83	10.26 ± 1.48	9.34 ± 0.47
WES2	42.61	-71.49	-0.81 ± 1.14	-0.62 ± 0.36

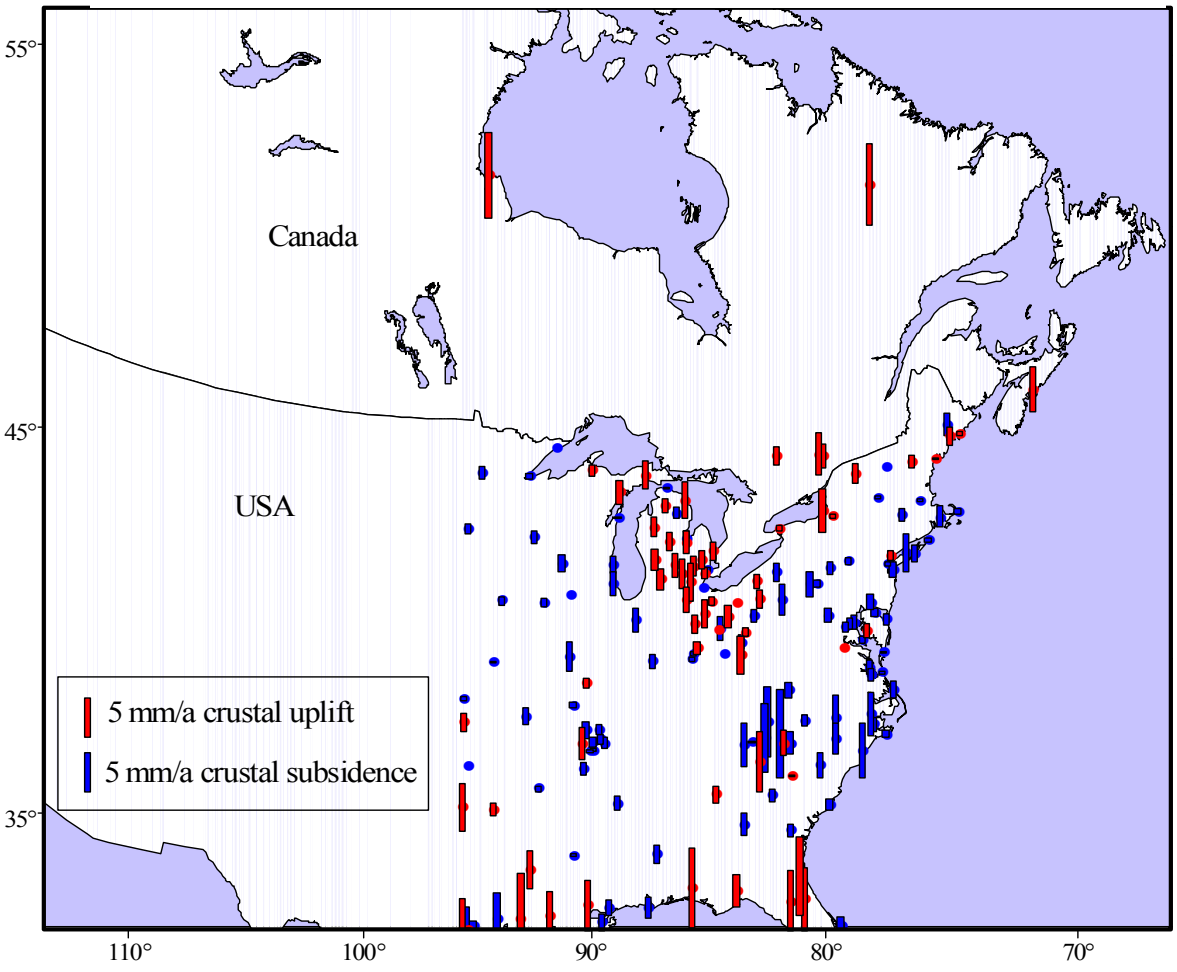

Figure 6.6: Vertical velocity from Calais et al. (2006) solution in central and eastern U.S. and Canada. Red bars represent uplift and blue bars depict subsidence.

6.4 Regional geophysical interpretation of VCM

In this section, the computed VCM presented in chapter 4 is compared with the rate of gravity changes, rate of changes of geodetic heights, and GIA models presented in section 6.3 as well as some regional geophysical evidence of deformations in each area.

6.4.1 Eastern Canada

There are different geophysical phenomena responsible for the crustal deformation in eastern Canada. These are global, regional and local phenomenon. During the last ice age (late Pleistocene), ice advanced over the Saint Lawrence River valley and extended east into the Maritime Provinces and south into New England. The weight of the ice depressed the surface of the Earth and flow of the incompressible fluid mantle created a peripheral bulge outside the glaciated region. Upon thinning and retreating of the ice sheet, the lithosphere began to rebound toward its former position of isostatic equilibrium and the peripheral bulge began to collapse and perhaps migrate toward the center of uplift. Some PGR models indicate that the hinge line between uplift to the north and subsidence to the south is near the Saint Lawrence valley (e.g., Tushingham and Peltier, 1991; Peltier, 2002). These first-order features of PGR-related crustal deformation are confirmed by various geodetic measurements in central and eastern North America (e.g., Lambert et al., 2001; Park et al., 2002; Sella et al., 2004 and Koohzare et al., 2006a). Therefore the subsidence in Maritimes predominantly in Nova Scotia and eastern New Brunswick seen in the VCM is presumably due to postglacial rebound. The map of VCM in this area which depicts this phenomenon is shown in Figure 6.7.

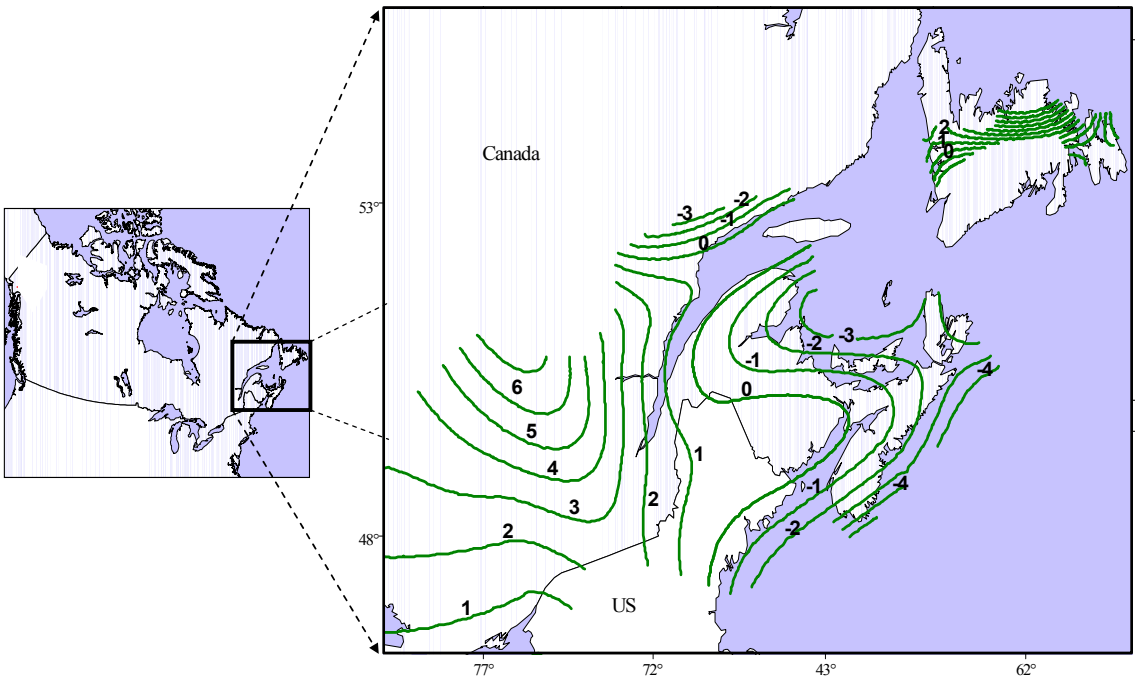

Figure 6.7: The contour map of VCM in Eastern Canada. The contours are in mm/year.

In Eastern Canada, there are also areas of substantial seismicity and earthquake hazard. The Saint Lawrence valley, eastern Quebec (Figure 6.8), is one of the most seismically active regions of eastern North America (Lemieux et al., 2003, Mazzotti et al., 2005). This area has a large range of intraplate earthquake patterns, from zones with large (M = 6–7) earthquakes to zones with very little background seismicity (e.g., Adams and Basham, 1991). The driving mechanism behind these earthquakes is difficult to be determined as the seismic activity does not seem to be directly correlated with plate interactions in this region. About 100 km downriver from Quebec City, the Charlevoix Seismic Zone (CSZ) is the strongest locus, with numerous small to medium earthquakes as well as five M > 6 events in the last 350 years (Mazzotti et al., 2005). In contrast, the area between Quebec City and Montreal shows very little seismic activity. Another seismic zone in Eastern Canada is Lower St Lawrence seismic zone. The Saint Lawrence valley is characterized by large eastward dipping normal faults with up to a few kilometres of motion documented in the Precambrian basement (Kumarapeli, 1985). The normal fault system is capped by westward verging thrust faults and napes of the

Appalachian orogen. This Paleozoic cover is only a few kilometres thick in most of the Saint Lawrence region.

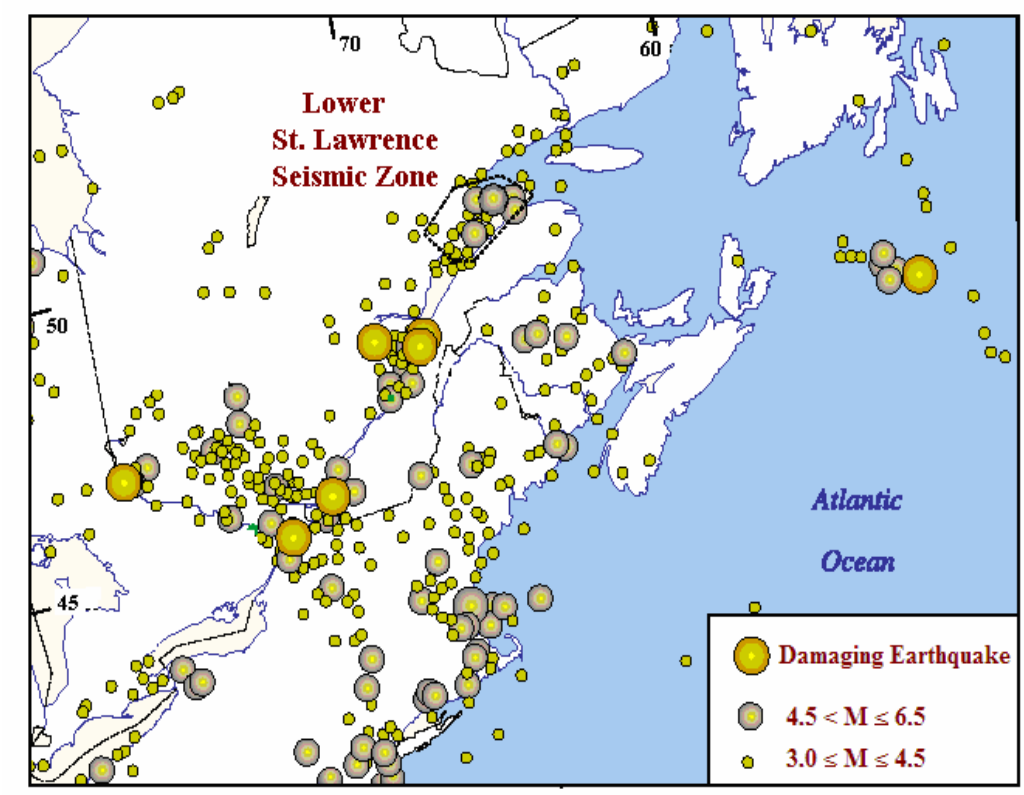

Figure 6.8: Seismicity map of Eastern Canada with an indication of the Lower St. Lawrence Seismic Zone (LSZ) (from Lamontagne et al., 2003).

A meteorite impact (-350 Ma) in the southern part of the Charlevoix seismic region contributes additional complexity by creating a 60 km diameter system of concentric faults and fractures (Rondot, 1968; Lemieux et al., 2003).

Although the VCM does not discriminate between various models of crustal deformation, it provides important constraints on GIA models, and large earthquake recurrence. In chapter 6.7, it will be explained how the computed vertical crustal deformations are sensitive to the viscosity of the mantle which could be correlated to the origin of the phenomenon producing such deformations.

The PGR hinge line appears from Gulf of St. Lawrence in the map of VCM. It follows the Atlantic coastline to the south of Canada (See Figure 6.7). This gives some

information about the formation and of ice model deglaciation. From $\dot{g}$ maps (Figures 6.3 and 6.4), it starts from the same region and follows roughly the Canadian East coast, along Labrador Sea and Buffin and Ellesmere Islands. The rate of geodetic height changes in Maritimes from GPS solution is also consistent with our results. The only difference is that the Maritimes experience all subsidence from the GPS solution and the probable PGR zero line follows the St. Lawrence River to the Great Lakes, while in VCM map, the PGR hinge line follows the coast line. It should be noted that the GPS solution gives the rate of height changes with respect to a reference ellipsoid. The difference between $\dot{H}$ and $\dot{h}$ reflects of course the temporal variations in the geoid.
The pattern shown in the north eastern margin of the former Laurentide ice sheet (the border of which has been postulated to have been parallel to St. Lawrence River) is complicated due to the probable fragmentation of the crust in this zone.

The earlier reported uplift of northern New Brunswick and the subsidence of the South St. Lawrence River (Carrera and Vaníček, 1994) are here more sharply defined.

Another interesting feature derived from VCM is a ridge across the St. Lawrence River, following the Hudson River path in US, which is hardly seen in the maps of $\dot{g}$ and $\dot{h}$ from GPS solution. The peak is in Charlevoix and might correspond to the seismic vertical strains, but it needs more investigation.

6.4.2 Great Lakes

Due to PGR, the land north of the Great Lakes is rising, while that south of the Great Lakes is subsiding to maintain equilibrium. Hence, residents on the south shores of the Great Lakes have noticed water level rising slowly over time, while those on the north shores have noticed declining water levels.

The location of postglacial rebound zero line (hinge line) derived from the VCM map (Figure 6.9) passes through the Great Lakes and is close to the location of zero line from GIA models. The best fit is with the GIA adopting ICE-3G ice history and the standard Earth rheology model (Figure 6.9). The VCM in this area is also in good agreement with the maps of $\dot{h}$ and $\dot{g}$.

Since the VCM is the result of simultaneous solution over the whole Canada, the absolute value for the vertical movements in The Great Lakes mainly is obtained from all the tide gauges which are used in the computation in the point velocity mode. The linear trend of the Churchill tide gauge in Hudson Bay, being the closest tide gauge to the Great Lakes controls the absolute term of the VCM in this area. The valley seen in figure 6.9, to the north of the Great Lakes, is an artifact resulted from sparse data in this area.

The relative movements or the tilt in this area varies slightly between 0.5-1.5mm/yr per hundred kilometres along north-south direction, toward the maximum ice location in Hudson Bay. The computed tilt is in a relatively good agreement with the tilt obtained from the GIA model of ICE-3G (Mod17) in this region (~1mm/year per hundred kilometres).

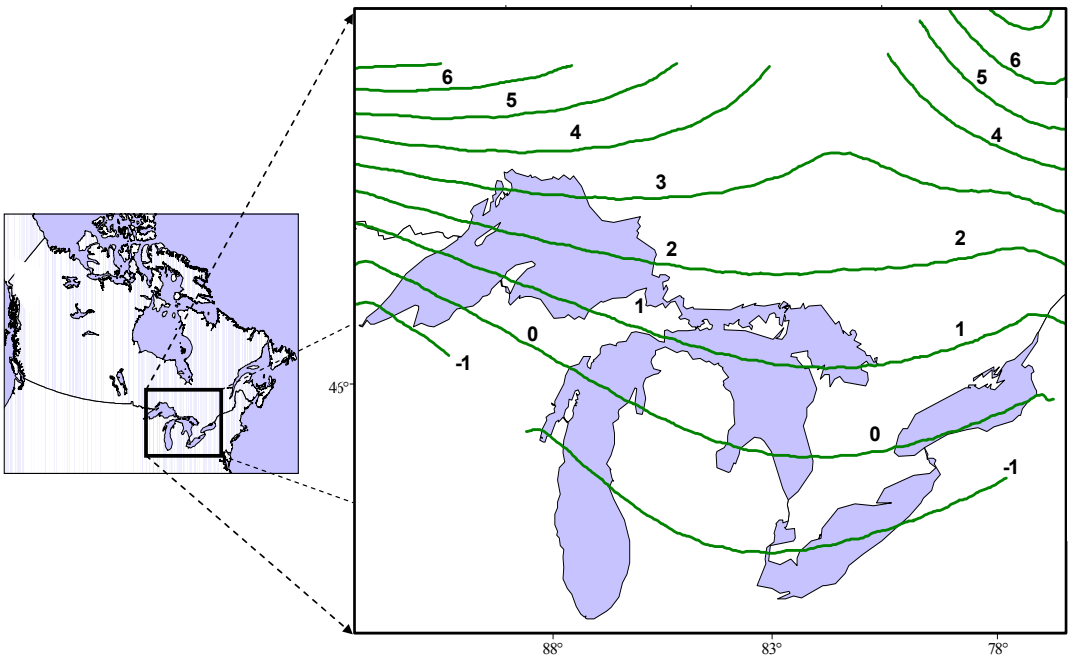

Figure 6.9: The contour map of VCM in the Great Lakes area. The contours are in mm/year.

6.4.3 Eastern Prairies

The predicted rate of relative uplift in Eastern prairies (Manitoba) from VCM is in the range of 1.5-2 mm/year per hundred kilometres in the direction toward Hudson Bay (See Figure 6.10). This is obtained from the computed coefficients in the SPAA model and it is significantly larger than the predicted tilt from GIA models using standard ICE and Earth rheology models which give ~1mm/year per hundred kilometres in Manitoba. However, it should be noted that the GIA models in this area are uncertain which is mainly due uncertainties in the ice models (Lambert et al., 1998). The difference between the predicted present-day crustal uplift rate for two models, ICE-3G (Tushingham and Peltier, 1991) and ICE-4G (Peltier, 1994) reaches to 1.5 mm/a in this area (Lambert et al., 1998).

The present-day relative heights of points along a continuously identifiable, dated strandline represent the total relative vertical movement since the strandline was formed. The relative uplift between two points on a strandline can be calculated by subtracting the uplift curve or tilt relative to the geoid for the two locations. Using the tilting of the 9.5 kyr before present Campbell strandline, south and west of Lake Winnipeg and the rate of decreasing in absolute gravity values measured from 1987 to 1995 at Churchill, and also the present-day regional tilt rate derived from water-level gauges in southern Manitoba lakes, Lambert et al. (1998) has indicated the 'disagreement' of all these data types in Manitoba with ICE-3G and the 'standard' Earth rheology model. Therefore, the map of VCM in this area plays an important role in the proper modifications of the uncertain parameters in the models, in such a way that a better fit with VCM is obtained. Either a further modification in the ice-sheet east of Manitoba or a thinner lithosphere (As recommended by Wolf, 1985 and Tackmam, 1997), or both, may be required to solve the disagreement. In section 6.7, the sensitivities of present-day rate of tilting in Manitoba from VCM to the changes of key parameters of the GIA models are discussed in more details.

The uplift around northern Winnipeg Lake seen in the map of VCM (Figure 6.11), and the negative values for the $\dot{g}$ in the same area are consistent. There is also a good agreement between the maps of VCM and the rate of geodetic height changes in this area.

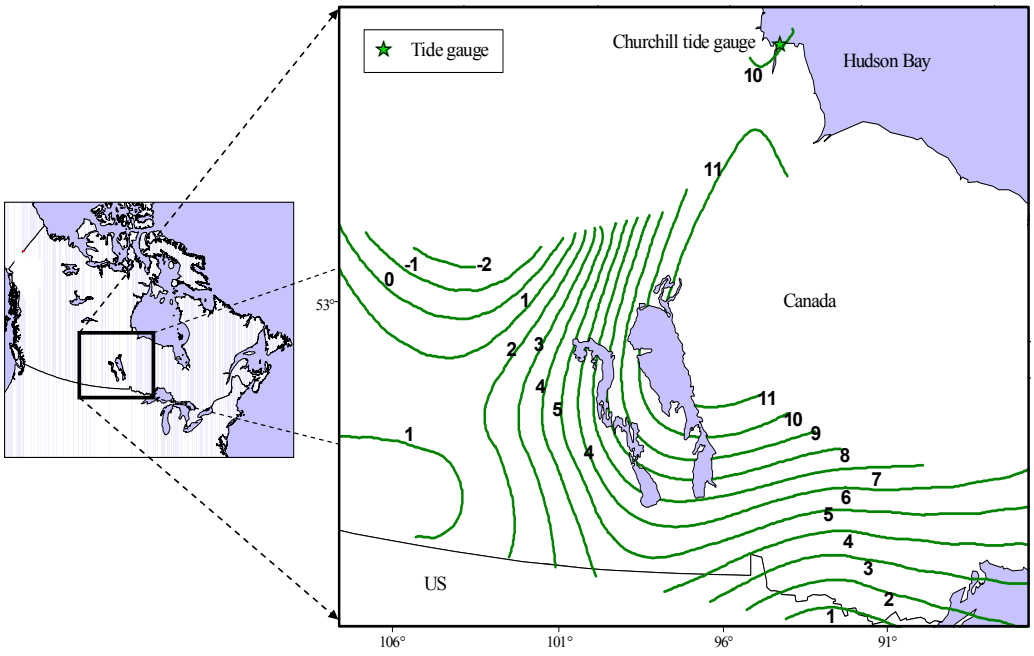

Figure 6.10: The contour map of VCM in Manitoba. The contours are in mm/year

6.4.4 Western and Central Prairies

The map VCM in western and central Prairies is shown in Figure (6.11). Another interesting feature seen from this map is the subsidence to the south of Lake Athabasca in Saskatchewan. While this is in good agreement with previous map of VCM (Carrera et al., 1991), GIA models and the pattern of $\dot{h}$ do not show such local subsidence. It is expected that the subsidence is due to some local movements in the area. The subsidence seen in southern Prairies might roughly correspond with the location of the prairie evaporate, a 100 m thick salt layer (Jim Merriam, Personal communications). This load causes local subsidence of the region. Distinction between different geophysical causes which are responsible for such movement, local load effect, PGR or both, needs further investigations.

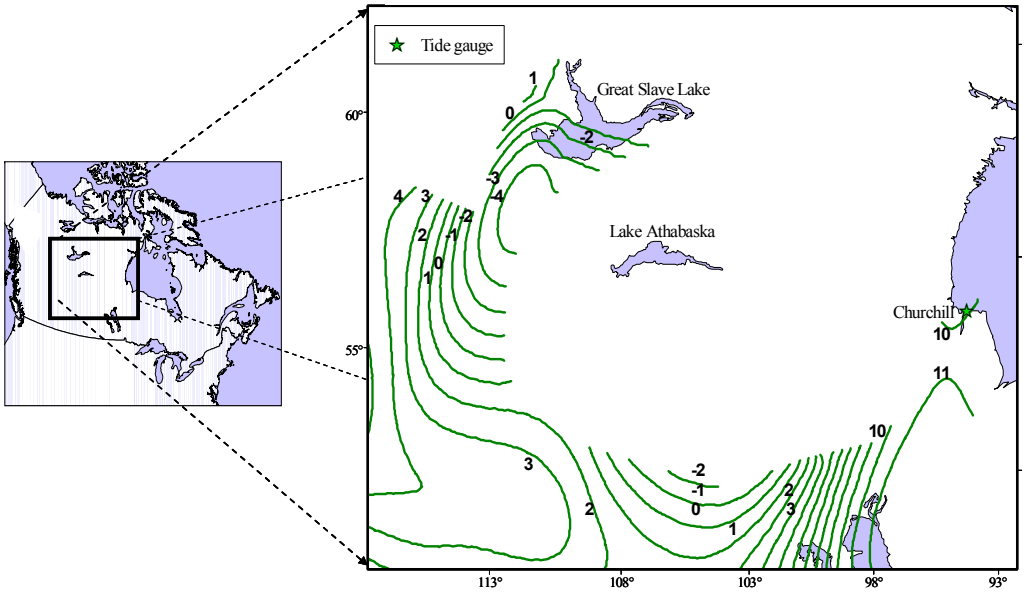

Figure 6.11: The contour map of VCM in southern, western Prairies and sub-arctic . The contours are in mm/year

6.4.5 British Columbia and Pacific coast

The zero line in VCM map loops around the Saskatchewan subsidence area, and creates an uplift dome like area in British Columbia (BC) (Figure 6.12). In ġ map, the uplift area of B.C, is also seen. This uplift is, partly, due to the PGR, and is consistent with GIA models (See Figures 6.1a and 6.2a). The location of such uplift in VCM map is in a better agreement with GIA models than with the map of ġ.

The zero line in the map of VCM nearly follows the Pacific coastline; with a little curve in the north (Fig 6.12). It is consistent in spatially long wavelengths with PGR models.

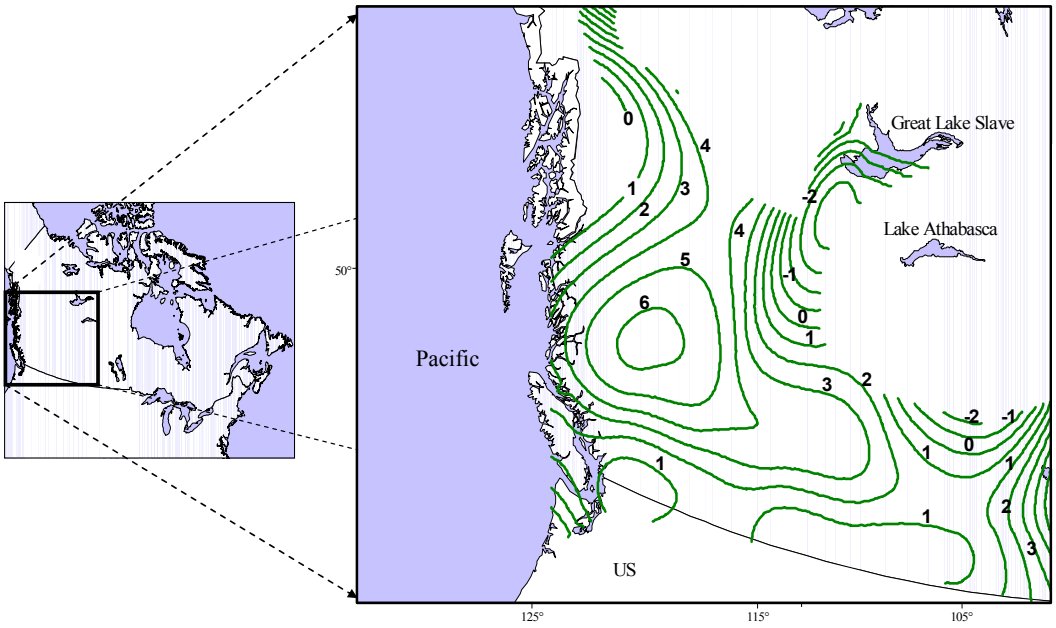

Figure 6.12: The contour map of VCM in British Colombia. The contours are in mm/year

The pacific coast of Canada is one of the few areas in the world where four tectonic plates meet and interact, and three different types of plate movements take place, resulting in significant earthquake activity. Plates move towards each other at converging boundary, apart from each other at diverging boundary and past each other at transform boundaries. All three of these boundary types occur in offshore B.C, (Figure 6.13).

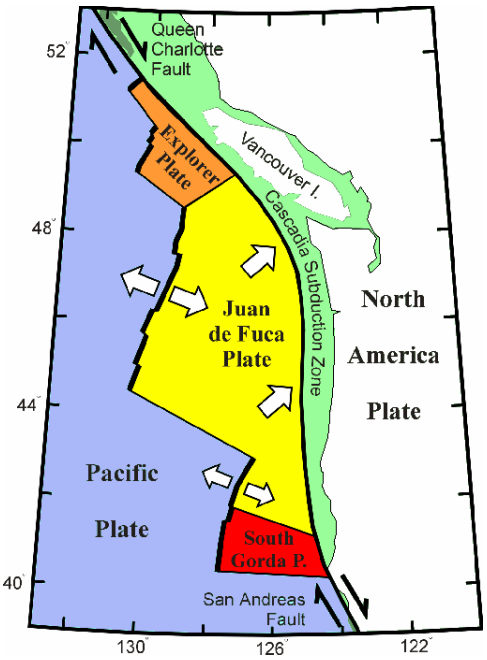

Figure 6.13: The interaction of four tectonic plates in offshore B.C.

About 200 kilometres off the west coast of Vancouver Island, the Juan de Fuca plate and Pacific plate are diverging or spreading apart along the Juan de Fuca ridge. Further east, the Juan de Fuca plate is converging with and sliding (subducting) beneath the North American plate at about 2-5 cm/year. This region is called the Cascadia subduction zone; it is located about 45 km southwest of Victoria, and about 70 km southwest of Vancouver (Figure 6.14). Periodic giant mega thrust earthquakes (approximately once every 500 years) exemplify a catastrophic sliding of the Juan de Fuca plate beneath the North American plate. In the period between the mega-earthquakes, the Juan de Fuca plate continues trying (unsuccessfully) to slide beneath the North American plate with the consequence that the rocks all along the edges of the plates are compressed or squeezed and uplifted, and these deformations are monitored using geodetic observations.

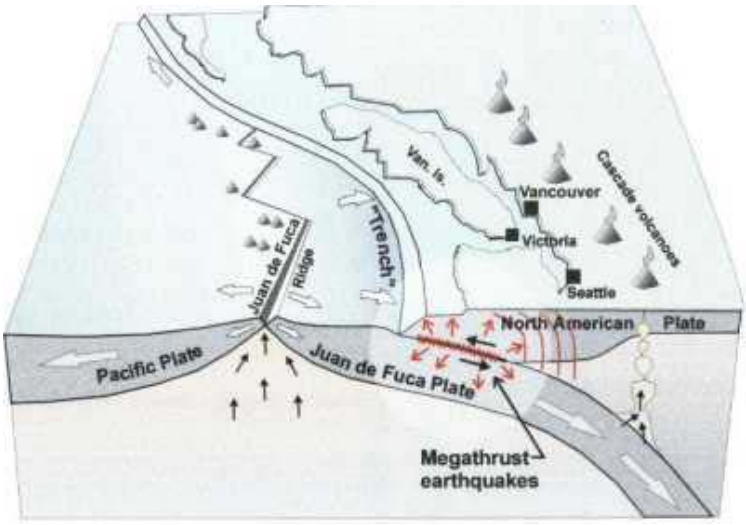

Figure 6.14: Cascadia Subduction Zone: Cross Section
(http://gsc.nrcan.gc.ca/geodyn/cascadia_e.php)

Another small plate, the Explorer, is also sliding underneath the North American plate, and at the same time the Juan de Fuca plate is sliding along the Nootka fault. In the north, there is a major transform fault between the Pacific and the North American plates called the Queen Charlotte fault. Therefore, the distinction between long-term tectonic trends and post glacial rebound in this region would be a nontrivial task.

The zero line in the map of VCM nearly follows the Pacific coastal line, with a little curve in the north (Figure 6.12), and such smooth loop of zero line is also seen in $\dot{g}$ map. However, looking at the individual gravity sites in the region, the two sites in Vancouver and Victoria, situated in the northern Cascadia forearc, the values of $\dot{g}$ at these two sites are very different ($+0.65 \pm 0.29$ μGal/a in Vancouver site and -0.77 ± 0.28 μGal/a in Victoria site). Along with the complexity of the area, this region experiences over a metre of precipitation in average per year which leads to large seasonal variations in soil moisture. As a consequence, large peak-to-peak seasonal changes in gravity of about 8 μGal are observed at these sites, and the detection of long term movements in this moist environment from gravity observations would be a daunting task if it were not for the fact that the ground in this region becomes fully saturated each winter. Correcting for the gravitational effect of seasonal variations in soil moisture using various modeling

schemes reduces the seasonal scatter significantly but could bias the long term gravity trend estimates, if not done carefully (Lambert et al., 2001, AGU 2001).

6.5 The ratio of gravity change to height change

The correlation between gravity and height changes is described by the ratio between these two values, which is denoted by $\dot{g} / \dot{H}$. The ratio equals, in the first approximation, the free-air gradient of -0.3086 mGal/m, if no mass changes occur. Deviations from this value are indicators of relative mass changes (Jackson et al., 1984; Berrino et al., 1992; Johnson, 1995).

The adjusted rates of gravity changes which were discussed in section 6.2 are based on the data collected in different years, assuming that the gravity changes are constant in time (Pagiatakis and Salib, 2003). The computed vertical velocities were also assumed to be constant in time. Table 6-2 shows the rates of $\dot{g}$ (GSD and PGC solutions) and $\dot{H}$ in different gravity sites, along with the computed values of $\dot{g} / \dot{H}$. The ratios should be tested statistically to see whether they are significant at a certain confidence interval, and then the physical interpretation can be carried out with some confidence. This study is done in two steps as:

- Studying the $\dot{g} / \dot{H}$ at all the stations,
- Interpreting only the values of $\dot{g} / \dot{H}$ that passed the test and is statistically significant.

6.5.1 Ratio between gravity and height changes for all the points

The ratios of the gravity to height changes in Canadian gravity sites vary between -0.47mGal/m in Ottawa and 2.47 mGal/m in Sept-Iles. To demonstrate the spatial variability of these ratios, $\dot{g} / \dot{H}$ are depicted in Figure 6.15.

The region around Hudson Bay, 700-900 km from ice centre (it is shown by red dot-line in figure 6.15), is rising by about +11.1±0.24 mm/a in Churchill, +5.5±0.24 mm/a in

Nakina, +3.2±0.18 mm/a in Timmins and 3.3±0.42 mm/a in Val d´Or. Corresponding gravity changes of -1.72±0.06 μGal/a, -0.85±0.06 μGal/a, -0.75±0.36 μGal/a and -0.56±0.44 μGal/a are observed at the above sites. The two values for each site correspond to each other excellently if the Bouguer effect (with crustal density) is assumed. The values of $\dot{g} / \dot{H}$ in this region varies between -0.15 to -0.2 mGal/m (See Figure 6.15 for the location of the sites). These values are in good agreements with the findings of Jachens (1978) in which the ratio between gravity and height changes for surface loads (including ice loads) was approximately -0.2mGal/m.

Near the Laurentide ice edge, in Central Canada, the estimates of vertical movements and gravity changes in Thunder Bay and Saskatchewan are +2.3±0.14 mm/a, -0.65±0.39 μGal/a, and 1.3±0.48 mm/a, -0.54±0.34 μGal/a, respectively. The corresponding values of $\dot{g} / \dot{H}$ for these two sites are -0.28mGal/m and -0.39mGal/m. This is consistent with the first approximation of free-air gradient of -0.3 mGal/m.

In the Maritimes, $\dot{g} / \dot{H}$ changes from nearly -0.3mGal/m (free-air effect) to -0.2mGal/m. Small gravity change and large elevation change may have several causes to be speculated upon. The fault slips in Eastern and Western Canada may be causes of the changes of the ratios.

The maximum value of the ratio is experienced at Sept- Iles (2.4mGal/m). The small vertical movement associated with relatively high value of the gravity changes in Sept-Iles is partly due to PGR. This site is located in the postglacial rebound hinge line (zero line) which results in high value for the ratio. The observed $\dot{g}$ in this site is therefore more due to mass changes within the Earth in this area. Knowing that the site is on Lower St Lawrence Seismic Zone, where there is a complex deformation associated with the fault plane, the gravity variations in this site might be also due to the mass changes in the fault system as well as ice load.

Table 6-3: Rates of gravity changes and orthometric height changes along with the ratio between gravity and height changes in gravity sites in Canada.

Site Name	Latitude	Longitude	G-dot(GSD)	G-dot(PGC)	VCM(mm/a)	$\dot{g}/\dot{H}$ (mGal/m)[1]	$\dot{g}/\dot{H}$ (mGal/m)[2]
Calgary	51° 07′ 47′′	114° 00′ 27′′	−1.06 ± 0.24	−1.06 ± 0.24	2.4±0.48	-0.44	-0.44
Charlottetown	46° 16′ 44′′	63° 08′ 00′′	+0.53 ± 0.51	+0.53 ± 0.51	-1.7±0.08	-0.31	-0.31
Churchill	58° 45′ 43′′	94° 05′ 08′′	−1.71 ± 0.06	−1.72 ± 0.08	11.1±0.24	-0.15	-0.15
Edmonton	53° 32′ 04′′	113° 32′ 10′′	−0.79 ± 0.19	−0.83 ± 0.19	3.4±0.48	-0.23	-0.24
Fort Nelson	58° 48′ 02′′	122° 41′ 03′′	+0.31 ± 0.64	+0.26 ± 0.64	4.4±0.77	0.07	0.06
Fort St. John	56° 14′ 42′′	120° 44′ 02′′	−0.24 ± 0.30	−0.26 ± 0.30	4.1±0.47	-0.06	-0.06
Grande Prairie	55° 10′ 16′′	118° 47′ 39′′	+0.09 ± 0.73	+0.07 ± 0.73	2.7±0.46	0.03	0.03
Halifax	44° 44′ 41′′	63° 39′ 26′′	+0.29 ± 0.33	+0.30 ± 0.33	-1.3±0.05	-0.22	-0.23
Hay River	60° 50′ 31′′	115° 45′ 59′′	+0.24 ± 0.47	+0.18 ± 0.47	-3.6±1.04	-0.07	-0.05
Kamloops	50° 41′ 36′′	120° 26′ 30′′	−0.47 ± 0.54	−0.41 ± 0.54	2.3±0.30	-0.2	-0.18
Moncton*	46° 06′ 24′′	64° 41′ 00′′	+1.14 ± 0.83	+1.14 ± 0.83	-0.1±0.13	-7.76	-7.76
Montreal	45° 30′ 30′′	73° 25′ 55′′	−0.65 ± 0.30	−0.67 ± 0.30	2.7±0.30	-0.24	-0.25
Nakina	50° 12′ 54′′	86° 42′ 20′′	−0.85 ± 0.65	−0.85 ± 0.65	5.5±0.24	-0.16	-0.16
Ottawa	45° 23′ 40′′	75° 42′ 49′′	−0.71 ± 0.18	−0.72 ± 0.18	1.5±0.30	-0.47	-0.48
Penticton	49° 28′ 00′′	119° 36′ 00′′	+0.10 ± 0.17	+0.02 ± 0.18	0.9±0.37	0.11	0.02
Prince George	53° 53′ 00′′	122° 40′ 28′′	−0.42 ± 0.43	−0.42 ± 0.43	6.2±0.20	-0.06	-0.07
Prince Rupert	54° 18′ 47′′	130° 19′ 29′′	+0.35 ± 0.55	+0.34 ± 0.55	1.0±0.13	0.34	0.33
Quebec	46° 47′ 25′′	71° 23′ 02′′	+0.36 ± 0.38	+0.36 ± 0.38	2.5±0.21	0.14	0.14
Red Lake	51° 01′ 23′′	93° 49′ 16′′	−0.10 ± 0.36	−0.12 ± 0.36	7.7±0.06	-0.01	-0.02
Regina	50° 26′ 25′′	104° 37′ 03′′	+0.73 ± 0.56	+0.66 ± 0.56	0.9±0.60	0.79	0.72
Roberval	48° 31′ 33′′	72° 13′ 13′′	−0.39 ± 0.37	−0.41 ± 0.37	5.3±0.23	-0.07	-0.08
Saskatoon	52° 10′ 10′′	106° 41′ 22′′	−0.52 ± 0.34	−0.54 ± 0.34	1.3±0.48	-0.39	-0.41
Sault Ste Mari	46° 30′ 30′′	84° 19′ 36′′	+0.05 ± 0.12	+0.05 ± 0.35	1.5±0.11	0.03	0.03
Sept-Iles	50° 13′ 04′′	66° 15′ 50′′	−0.35 ± 0.47	−0.34 ± 0.47	-0.1±0.19	2.80	2.72
St. John’s	47° 34′ 23′′	52° 44′ 02′′	−0.91 ± 0.37	−0.91 ± 0.37	-0.7±0.08	1.30	1.30
Stephenville	48° 32′ 46′′	58° 33′ 52′′	−0.17 ± 0.64	−0.17 ± 0.64	-2.0±0.80	0.09	0.09
Thompson	55° 47′ 50′′	97° 51′ 52′′	−0.66 ± 0.51	−0.67 ± 0.51	9.6±0.41	-0.07	-0.07
Thunder Bay	48° 25′ 59′′	89° 12′ 56′′	−0.65 ± 0.39	−0.65 ± 0.39	2.3±0.14	-0.28	-0.28
Timmins	48° 28′ 38′′	81° 12′ 24′′	−0.75 ± 0.36	−0.76 ± 0.36	3.2±0.18	-0.23	-0.24
Toronto	43° 40′ 14′′	79° 36′ 30′′	−0.18 ± 0.30	−0.19 ± 0.30	0.2±0.12	-0.73	-0.77
Val d’Or	48° 06′ 29′′	77° 46′ 54′′	−0.56 ± 0.44	−0.56 ± 0.44	3.3±0.42	-0.17	-0.17
Vancouver	49° 11′ 44′′	123° 10′ 53′′	+0.65 ± 0.29	+0.62 ± 0.29	1.1±0.07	0.57	0.54
Victoria	48° 38′ 59′′	123° 26′ 59′′	−0.77 ± 0.28	−0.70 ± 0.28	1.5±0.07	-0.50	-0.46
Watson Lake	60° 06′ 49′′	128° 49′ 17′′	+0.42 ± 0.58	+0.40 ± 0.58	3.0±1.02	0.14	0.13
Windsor	42° 19′ 07′′	83° 02′ 38′′	+0.27 ± 0.67	+0.26 ± 0.68	-0.9±0.14	-0.29	-0.28

[1] Rate of Gravity changes is obtained from GSD solution.
[2] Rate of Gravity changes is obtained from PGC solution.
* The anomalous value of gravity changes in this site is associated with relatively high standard deviation, and this value is discarded from the analysis.

Site Name	Latitude	Longitude	G-dot(GSD)	G-dot(PGC)	VCM(mm/a)	$\dot{g}/\dot{H}$ $(mGal/m)^1$	$\dot{g}/\dot{H}$ $(mGal/m)^2$
Winnipeg	49° 48′ 32′′	97° 08′ 15′′	+0.46 ± 0.29	+0.12 ± 0.29	5.8±0.36	0.08	0.02

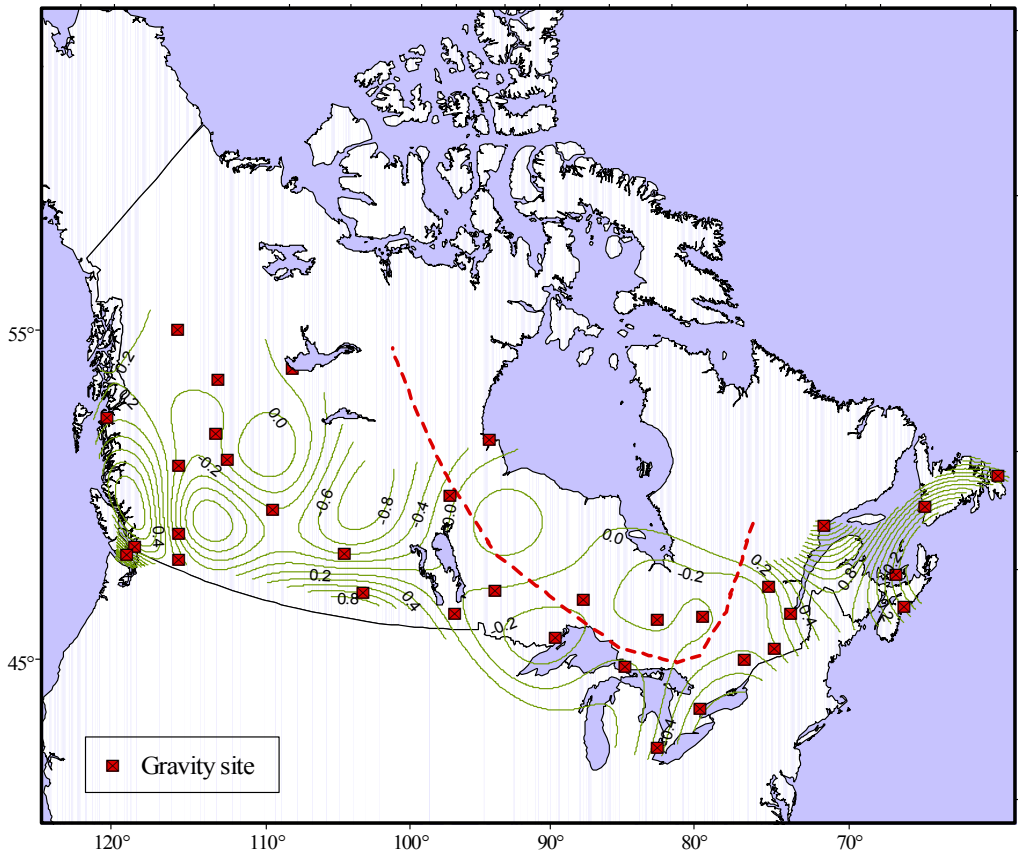

Figure 6.15: The contour map of ratio between gravity and height changes obtained for the values of $\dot{g}$ from GSD solution (Pagiatakis and Salib, 2003) and the map of VCM developed in this study. The contours are in mGal per metre. The region around Hudson Bay, 700-900 km from ice centre is shown by red dot-line. In this area, $\dot{g} / \dot{H}$ is mostly due to PGR.

6.5.2 Statistically significant ratio of gravity changes to height changes

The ratio between gravity and height changes for each station should be confirmed as statistically significant. Following the *t* (Student) distribution (Crow et al., 1960; Vaníček and Krakiwsly, 1986) the significance of the computed ratios was tested at 95% confidence level. The highlighted values in Table 6.3 show the ratio values that passed the test and are used in the physical interpretation that follows. As it is seen, most of the original values were rejected in the test.

The values $\dot{g}/\dot{H}$ in three stations in the area of maximum ice load (Churchill, Edmonton, Timmins), are very close to -0.2mGal/m of the model of PGR (Figure 6.16). It indicates that the mass changes in the area are due to the ice removal.

The dotted line in Fig. 6.16 is a plausible choice for the -0.3086 mGal/m contour and it lies very close to the PGR hinge line.

The values of the ratio in Vancouver and Victoria, even though close, are not consistent and need to be studied further. As discussed in section 6.4.6, this region experiences, over a metre of precipitation per year which leads to large seasonal variations in soil moisture and makes the detection of long-term trends more difficult.

Table 6-4: Rates of gravity changes and orthometric height changes along with the ratio between gravity and height changes in gravity sites in Canada. The information related to the sites with statistically significant ratios are highlighted based on the value for the t-student test.

Site Name	Latitude	Longitude	$\dot{g}$(GSD) (μGal/a)	VCM (mm/a)	$\dot{g}/\dot{H}$ (mGal/m)	$\frac{\dot{g}/\dot{H}}{\sigma_{\dot{g}/\dot{H}}}$
Calgary	51° 07′ 47′′	114° 00′ 27′′	−1.06 ± 0.24	2.4±0.48	-0.44±0.19	-2.34
Charlottetown	46° 16′ 44′′	63° 08′ 00′′	+0.53 ± 0.51	-1.7±0.08	-0.31±0.32	-0.99
Churchill	58° 45′ 43′′	94° 05′ 08′′	−1.71 ± 0.06	11.1±0.24	-0.15±0.01	-15.61
Edmonton	53° 32′ 04′′	113° 32′ 10′′	−0.79 ± 0.19	3.4±0.48	-0.23±0.09	-2.63
Fort Nelson	58° 48′ 02′′	122° 41′ 03′′	+0.31 ± 0.64	4.4±0.77	0.07±0.16	0.45
Fort St. John	56° 14′ 42′′	120° 44′ 02′′	−0.24 ± 0.30	4.1±0.47	-0.06±0.08	-0.73
Grande Prairie	55° 10′ 16′′	118° 47′ 39′′	+0.09 ± 0.73	2.7±0.46	0.03±0.27	0.12
Halifax	44° 44′ 41′′	63° 39′ 26′′	+0.29 ± 0.33	-1.3±0.05	-0.22±0.26	-0.85
Hay River	60° 50′ 31′′	115° 45′ 59′′	+0.24 ± 0.47	-3.6±1.04	-0.07±0.15	-0.44
Kamloops	50° 41′ 36′′	120° 26′ 30′′	−0.47 ± 0.54	2.3±0.30	-0.20±0.26	-0.78
Moncton	46° 06′ 24′′	64° 41′ 00′′	+1.14 ± 0.83	-0.1±0.13	-7.76±12.51	-0.62
Montreal	45° 30′ 30′′	73° 25′ 55′′	−0.65 ± 0.30	2.7±0.30	-0.24±0.11	-2.17
Nakina	50° 12′ 54′′	86° 42′ 20′′	−0.85 ± 0.65	5.5±0.24	-0.16±0.13	-1.24
Ottawa	45° 23′ 40′′	75° 42′ 49′′	−0.71 ± 0.18	1.5±0.30	-0.47±0.12	-3.94
Penticton	49° 28′ 00′′	119° 36′ 00′′	+0.10 ± 0.17	0.9±0.37	0.11±0.24	0.47
Prince George	53° 53′ 00′′	122° 40′ 28′′	−0.42 ± 0.43	6.2±0.20	-0.06±0.07	-0.90
Prince Rupert	54° 18′ 47′′	130° 19′ 29′′	+0.35 ± 0.55	1.0±0.13	0.34±0.57	0.59
Quebec	46° 47′ 25′′	71° 23′ 02′′	+0.36 ± 0.38	2.5±0.21	0.14±0.16	0.88
Red Lake	51° 01′ 23′′	93° 49′ 16′′	−0.10 ± 0.36	7.7±0.06	-0.01±0.05	-0.28
Regina	50° 26′ 25′′	104° 37′ 03′′	+0.73 ± 0.56	0.9±0.60	0.79±1.12	0.71
Roberval	48° 31′ 33′′	72° 13′ 13′′	−0.39 ± 0.37	5.3±0.23	-0.07±0.07	-1.01
Saskatoon	52° 10′ 10′′	106° 41′ 22′′	−0.52 ± 0.34	1.3±0.48	-0.39±0.40	-0.98
Sault Ste Mari	46° 30′ 30′′	84° 19′ 36′′	+0.05 ± 0.12	1.5±0.11	0.03±0.08	0.40
Sept-Iles	50° 13′ 04′′	66° 15′ 50′′	−0.35 ± 0.47	-0.1±0.19	2.80±8.02	0.35
St. John's	47° 34′ 23′′	52° 44′ 02′′	−0.91 ± 0.37	-0.7±0.08	1.30±0.67	1.95
Stephenville	48° 32′ 46′′	58° 33′ 52′′	−0.17 ± 0.64	-2.0±0.80	0.09±0.36	0.24
Thompson	55° 47′ 50′′	97° 51′ 52′′	−0.66 ± 0.51	9.6±0.41	-0.07±0.06	-1.23
Thunder Bay	48° 25′ 59′′	89° 12′ 56′′	−0.65 ± 0.39	2.3±0.14	-0.28±0.19	-1.51
Timmins	48° 28′ 38′′	81° 12′ 24′′	−0.75 ± 0.36	3.2±0.18	-0.23±0.12	-1.87
Toronto	43° 40′ 14′′	79° 36′ 30′′	−0.18 ± 0.30	0.2±0.12	-0.73±1.56	-0.46
Val d'Or	48° 06′ 29′′	77° 46′ 54′′	−0.56 ± 0.44	3.3±0.42	-0.17±0.16	-1.09
Vancouver	49° 11′ 44′′	123° 10′ 53′′	+0.65 ± 0.29	1.1±0.07	0.57±0.29	1.97
Victoria	48° 38′ 59′′	123° 26′ 59′′	−0.77 ± 0.28	1.5±0.07	-0.50±0.20	-2.45
Watson Lake	60° 06′ 49′′	128° 49′ 17′′	+0.42 ± 0.58	3.0±1.02	0.14±0.24	0.58
Windsor	42° 19′ 07′′	83° 02′ 38′′	+0.27 ± 0.67	-0.9±0.14	-0.29±0.76	-0.38
Winnipeg	49° 48′ 32′′	97° 08′ 15′′	+0.46 ± 0.29	5.8±0.36	0.08±0.05	1.44

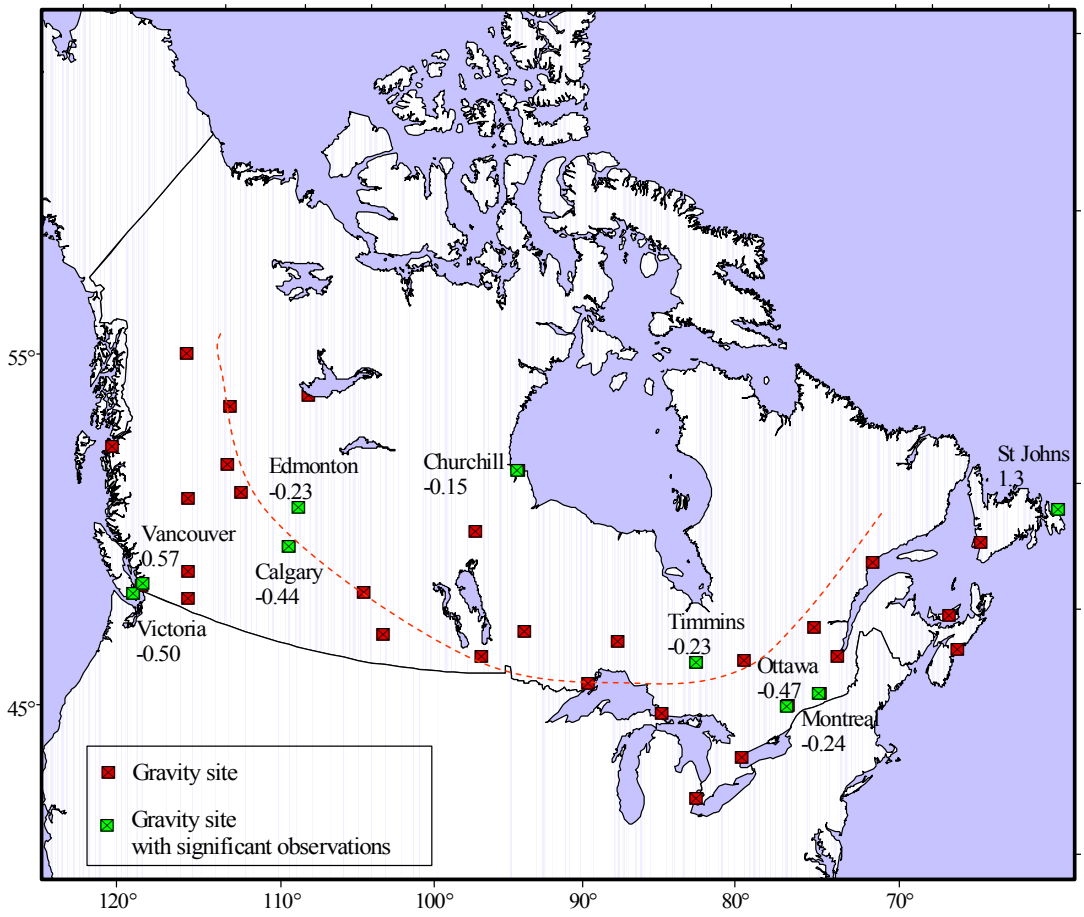

Figure 6.16: The location of gravity sites in Canada. The green squares show the location of those sites with statistically 'significant' gravity observations, along with the values computed for the ratio between gravity and height changes from GSD solution (Pagiatakis and Salib, 2003) and the map of VCM developed in this study.

6.6 Rate of geoidal height changes

Theoretically, the difference between the rate of orthometric and geodetic height changes is equal to the rate of geoidal height changes or $\dot{N}$. It is expected that the long wavelength changes of the geoidal height due to PGR be on the order of 10% of the temporal variations of orthometric height (See Figures 6.1a, b and 6.2a, b). As such, in

Canadian Shield, it is expected to show geoidal height changes at the sub-millimetre per year range.

The difference between VCM and the GPS height changes in Canadian Base Network are computed and depicted in Figure 6.17. The difference varies significantly over Canada. Part of this is due to the variations of the geoidal height, however, the values are generally too large to represent the geoidal changes. The GPS obtained rates of geodetic heights are evidently larger than the VCM in most of Canada. The short duration of GPS observations (less than 10 years), compared to tide gauges with approximately a century long data series, would explain the relatively large standard deviations of the geodetic height changes compared to the standard deviations of VCM, which consequently makes the differences between orthometric and geodetic height changes, rather uncertain. As an example of the uncertainties in the differences, look at southern Saskatchewan which is mostly due to uncertainties in the GPS observations with very short records. This area experience a subsidence of as much as 2-3 mm per year with respect to the ellipsoid from GPS solution, while the same area is seen to have crustal uplift with respect to the geoid, and that makes for a big value for the $\dot{N}$.

There are three other anomalous values for the $\dot{N}$ seen in Eastern Canada (See Figure 6.17). The standard deviations associated with the GPS solution for these particular stations are quite large (See table 6.4), and thus the values for the geoidal height in these stations are not scientifically valid.

Table 6-5: The rate of geoidal height changes computed using the orthometric height changes from VCM and the geodetic height changes from GPS.

GPS site	Latitude (Degree)	Long (Degree)	$\dot{H}$ (mm/a)	$\dot{h}$ (mm/a)	$\dot{N} = \dot{h} - \dot{H}$ (mm/a)	$\sigma_{\dot{N}}$ (mm/a)
3RIV	46.3	-72.6	3.35	2.75	-0.6	1.2
AIS1	55.1	-131.6	-0.85	0.98	1.84	2.9
ALBH	48.4	-123.5	1.71	2.27	0.56	3.8
ALGO	46	-78.1	1.9	3.23	1.32	0
ASBL	49.6	-106	0.74	-3.99	-4.73	5.7
ATLN	59.6	-133.7	-0.55	8.94	9.49	4.1
BAIE	49.2	-68.3	1.21	-3.08	-4.29	8.2
BCFT	45	-77.9	1.21	3.8	2.6	2.1
BCFT	45	-77.9	1.21	3.8	2.6	2.1
BCOM	49.3	-68.2	1.24	4.96	3.72	0.9
BDCK	46.1	-60.8	-2.13	-1.68	0.45	0.6
BEL3	44.2	-77.2	0.62	2.58	1.95	1.8
BLCL	52.4	-126.6	4.92	5.34	0.42	3.4
BLFD	46.8	-64.2	-1.68	-0.58	1.1	1.1

GPS site	Latitude (Degree)	Long (Degree)	$\dot{H}$ (mm/a)	$\dot{h}$ (mm/a)	$\dot{N} = \dot{h} - \dot{H}$ (mm/a)	$\sigma_{\dot{N}}$ (mm/a)
BMTN	51	-93.8	7.66	2.21	-5.46	1.3
BMTN	51	-93.8	7.66	2.21	-5.46	1.3
BNYV	54.6	-111	1.47	1.37	-0.11	6.6
BRDN	49.9	-99.9	4.86	-0.25	-5.11	1.8
BRKS	50.7	-112.1	1.59	-1.77	-3.36	5.7
BSHW	52.7	-113.2	3.73	2.36	-1.38	4.1
BSLR	45.4	-75.9	1.47	3.94	2.47	1.3
BTHT	47.6	-65.8	-1.87	0.88	2.75	0.8
CACU	47.9	-69.5	0.91	3.5	2.59	0.9
CAGS	45.6	-75.8	1.66	1.41	-0.25	1.1
CAL4	51.1	-114.4	2.5	-0.69	-3.19	6.3
CBRK	48.9	-57.9	-0.7	-1.96	-1.26	2.4
CHIB	49.9	-74.4	7.23	9.54	2.3	1
CHIC	48.5	-71.2	3.63	5.78	2.15	1
CHUR	58.8	-94.1	11.12	8.2	-2.92	0.6
CMBR	50.1	-125.3	2.16	4.76	2.6	3.9
CNDA	48.4	-64.6	-2.44	0.48	2.92	1
CNMC	45.4	-73.4	2.63	3.17	0.54	1.3
CNT2	43.5	-80.5	0.06	4.16	4.1	2.4
CP32	50.8	-113.9	1.85	-0.77	-2.62	5.6
CRLV	47.5	-70.3	1.64	3.56	1.92	0.8
CRNB	49.6	-115.7	1.4	-0.41	-1.81	4.3
CVAR	46.4	-62.1	-2.57	-0.84	1.73	1.2
DAUP	51.1	-100	6.58	0.06	-6.53	1.8
DAUP	51.1	-100	6.61	0.06	-6.56	1.8
DFOE	51.7	-104.5	1.6	-1.73	-3.33	5.2
DRAO	49.3	-119.6	0.82	0.95	0.13	0
DSLK	58.4	-130	-0.31	5.7	6	4.1
DUBO	50.3	-95.9	6.61	-2.99	-9.6	0.9
EDMD	47.4	-68.4	-0.08	1.96	2.04	0.5
EDMN	53.6	-113.2	3.37	2.26	-1.1	4
EGMT	54	-113.2	3.01	1.97	-1.04	4.6
FARD	51.6	-98.7	9.28	1.03	-8.25	1.5
FLIN	54.7	-102	0.12	1.48	1.36	0.6
FLMT	45.5	-63.5	-0.69	0.24	0.94	1.2
FNEL	58.8	-122.6	4.42	2.68	-1.74	3.6
FRDN	45.9	-66.7	0.63	-3	-3.63	14.4
FRDT	45.9	-66.7	0.63	-0.98	-1.61	0.6
FTRS	50.8	-115.2	2.29	-0.48	-2.77	6.4
FTSJ	56.2	-120.7	4.1	4.81	0.71	3.1
FTVM	58.5	-116.2	-4.16	7.12	11.27	1.6
FXCR	54.4	-116.8	2.39	2.96	0.58	6.5
GANG	44.3	-76.2	0.65	3.44	2.79	2.5
GDLK	54.6	-94.5	11.96	6.2	-5.75	1.5
GDPR	55.2	-118.5	2.33	2.46	0.14	3
GDRM	46.7	-76	2.71	4.37	1.66	1.3
GDRM	46.7	-76	2.71	4.37	1.66	1.3
GFAL	48.9	-55.7	5.24	-0.98	-6.22	2.6
GLDN	51.3	-117	3.32	-0.71	-4.02	3.6
GNFD	53.6	-114.7	3.34	3.07	-0.27	4
GRAP	53.3	-99.3	9.15	3.04	-6.11	2.5
GRMS	56.4	-117.7	-0.43	7.81	8.24	1.7
HDBY	52.8	-102.4	2.75	1.36	-1.38	1.8
HLAG	45.4	-74.7	1.95	2.08	0.13	1.7
HLFX	44.7	-63.6	-1.36	-1.57	-0.2	0.5
HLTV	46.5	-66.5	0.26	0.77	0.51	1.2
HNTN	53.3	-117.7	3.87	3.53	-0.34	3.3
HRST	49.7	-83.5	4.45	6.36	1.91	1.3
IGNC	49.3	-91.5	3.19	2.74	-0.45	1.6
KATN	51.2	-113.8	2.56	-0.56	-3.12	4.9
KNDL	51.5	-109.2	2.09	-0.67	-2.76	4.6
KNRA	49.7	-94.8	4.54	-0.07	-4.61	1.4
LAVE	46.8	-71.3	2.42	3.3	0.87	1.1
LDMN	53.2	-109.9	2.22	0.57	-1.65	5.8
LETH	49.6	-112.6	0.29	-1.2	-1.49	3.4
LGLK	49.8	-86.5	4.85	6.25	1.4	2.5
LON1	42.9	-81.3	-0.43	3.42	3.85	2.5

GPS site	Latitude (Degree)	Long (Degree)	$\dot{H}$ (mm/a)	$\dot{h}$ (mm/a)	$\dot{N} = \dot{h} - \dot{H}$ (mm/a)	$\sigma_{\dot{N}}$ (mm/a)
LORB	51.2	-106.6	1.32	-1.22	-2.55	4.6
LPCT	47.3	-70	1.25	3.12	1.87	0.6
LSAR	48.8	-79.2	3.23	8.77	5.54	1.4
LTUQ	47.4	-72.8	4.79	5.52	0.73	0.8
LUSE	50.5	-77.4	4.37	12.02	7.66	2.6
MCGT	44.5	-63.9	-1.58	-0.77	0.81	0.8
MDLK	54.1	-108.5	-0.4	1.09	1.48	5.5
MLTN	44.5	-75.9	0.74	2.64	1.9	1.7
MNDR	53.6	-112.4	3.29	1.42	-1.87	4.4
MNTN	46.1	-65	0.01	0.15	0.13	0.7
MPCK	50	-109.5	0.67	-3.21	-3.88	5.6
MRML	45.3	-67.2	0.45	0.25	-0.2	0.9
MTJL	48.5	-68	-0.04	4.3	4.34	0.9
MTJL	48.5	-68	-0.04	4.3	4.34	0.9
NBTF	52.7	-108.2	1.44	-0.12	-1.56	5.4
NRC1	45.5	-75.6	1.61	2.33	0.72	0.6
NRDG	52.5	-116.1	3.97	2.66	-1.31	3.8
PARS	45.4	-80	1.4	4.76	3.36	2.4
PARS	45.4	-80	1.4	4.76	3.36	2.4
PCRT	50.1	-66.8	0.22	5.84	5.62	0.9
PEMB	45.8	-77.2	1.8	3	1.2	2.2
PNTN	54.7	-99	8.62	5.32	-3.3	2.2
PRAL	53.2	-105.9	0.03	2.02	1.99	1.7
PRDS	50.9	-114.3	2.12	-1.32	-3.44	1.1
PRG6	53.9	-122.3	6.1	3.36	-2.73	3.3
PRNT	47.9	-74.6	4.98	8.04	3.05	1.4
PTEG	44.4	-81.4	0.6	4	3.4	2.9
PTER	44.3	-78.3	0.72	2.16	1.44	1.8
REG8	50.3	-104.2	1.02	-3.22	-4.24	4.8
SAK4	52	-106.5	1.39	-3.32	-4.72	1.9
SASG	52.2	-106.4	1.27	1.85	0.58	1.9
SDBY	46.4	-81.2	1.93	4.62	2.7	2.4
SDPT	53.3	-131.8	-0.27	0.68	0.95	3.9
SGTN	49.7	-103	1.57	-1.81	-3.38	1.8
SMTH	54.8	-127.2	3.9	2.41	-1.5	3.8
SPLK	56.4	-95.9	11.18	8.46	-2.72	1.5
SRBK	45.4	-72	2.17	1.25	-0.93	1.2
SRBK	45.4	-72	2.17	1.25	-0.93	1.2
SSMG	46.5	-84.6	1.46	5.03	3.57	2.6
STAN	49.1	-66.5	0.15	3.43	3.28	1
STGO	46	-70.7	1.46	2.24	0.78	1.2
STJG	47.6	-52.7	-0.7	-3.24	-2.54	5
STJH	45.3	-66.1	0.33	0.19	-0.14	0.6
STJO	47.6	-52.7	-0.7	0.38	1.08	0.3
STJV	46.1	-74.6	2.7	3.59	0.88	1.2
STKT	43.1	-79.2	-0.23	0.77	1	2.5
SVLK	50.7	-90.6	6.56	6.14	-0.42	1.4
SWCR	50.2	-107.8	0.69	-3.09	-3.78	4.6
SWNR	52.1	-101.3	5.01	0.27	-4.74	1.9
TBYG	48.5	-89.2	2.46	5	2.54	1.7
THMP	55.8	-98	9.44	6.65	-2.8	2
TIMS	48.5	-81.5	3.26	7.12	3.87	2.1
TMPG	55.4	-98.2	9.52	5.89	-3.63	1.9
TMSC	46.7	-79.1	2.28	4.88	2.6	1.1
TORT	43.7	-79.6	0.25	0.73	0.48	1.8
TSKT	43.9	-66	-2.58	-0.12	2.46	0.9
VALD	48.1	-77.6	3.35	5.24	1.89	0.7
VETN	52	-111.1	3.25	-0.3	-3.54	6.5
VRN4	50.2	-119.3	1.57	0.93	-0.64	3.8
WAWA	48.1	-84.8	2.86	4.09	1.23	2.4
WDSR	42.2	-83	-1	1.97	2.97	2.6
WHTB	47.4	-53.5	0.39	4.36	3.97	4.6
WILL	52.2	-122.2	5.37	2.4	-2.97	1.2
WIN5	50.2	-97.3	6.74	-0.15	-6.89	4.7
WINA	49.9	-97.5	6.1	0.59	-5.5	1.5
WSLR	50.1	-122.9	1.61	9.88	8.27	6.7
WTHL	45.5	-62.7	-1.43	-0.43	1	0.7

GPS site	Latitude (Degree)	Long (Degree)	$\dot{H}$ (mm/a)	$\dot{h}$ (mm/a)	$\dot{N} = \dot{h} - \dot{H}$ (mm/a)	$\sigma_{\dot{N}}$ (mm/a)
WVN3	49.4	-123.3	1.26	2.32	1.07	5

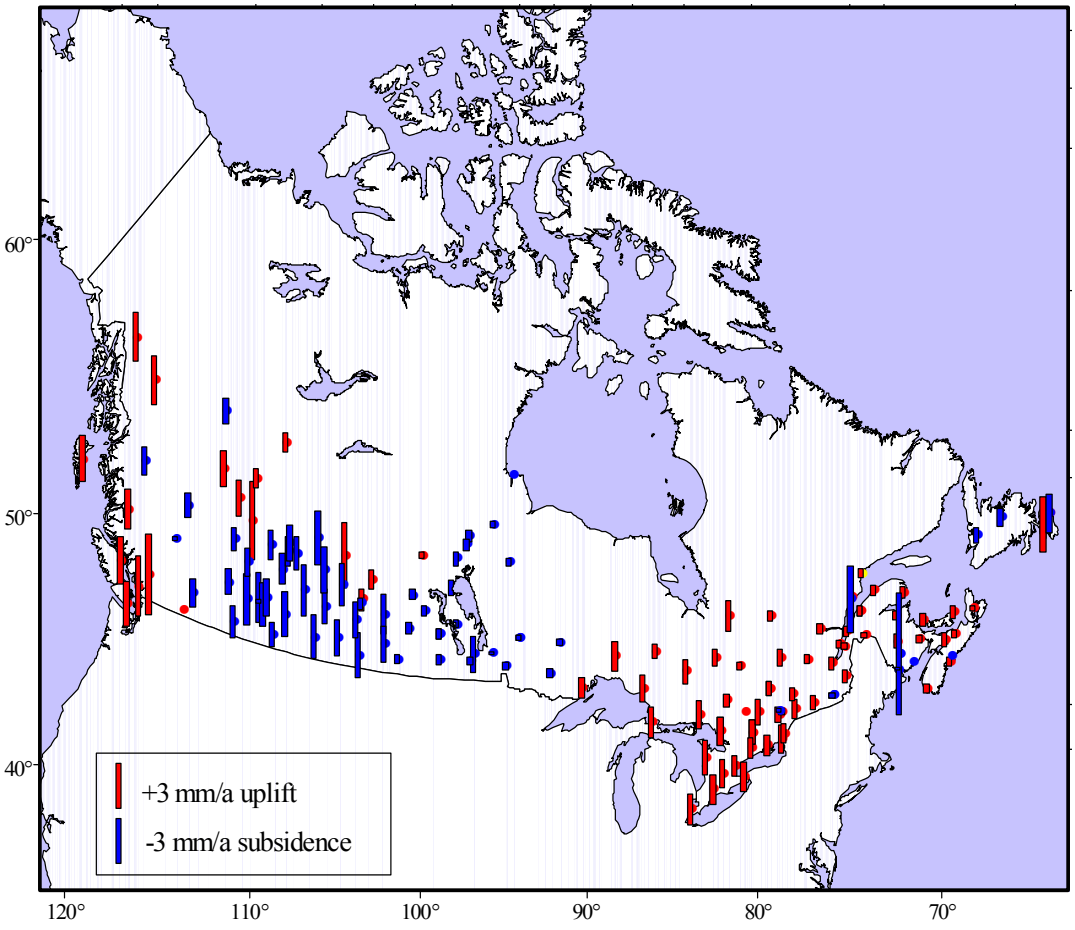

Figure 6.17: The rate of geoidal changes in mm/year. The geoidal changes about 0-2 mm/year in most of Canada, However in southwestern Prairies and in Pacific, the values are ~3-5mm/year either uplift or subsidence.

6.7 VCM as constraint to forward models of GIA

To investigate how VCM can be used as a constraint to GIA models, a sensitivity analysis is performed using forward modeling, and carried out in two steps: 1) Sensitivity of crustal movements to radial viscosity variations; and, 2) Sensitivity of crustal movements to ice thickness. In the first step which will be given in section 6.7.1, the ICE model is fixed, and the standard Earth rheology model is varied by increasing or decreasing the viscosity of the lower and upper mantle. In section 6.7.2, it is assumed that a 7 layer approximation to the standard Earth rheology model is sufficient for our purposes and the ice thicknesses in some areas are varied to find the best fit to the VCM.

6.7.1 Sensitivity of the crustal movements to the radial viscosity variations

Although, the surface geology and seismic tomography clearly show that the Earth properties vary both in the radial and lateral directions, and lateral variations of viscosity have large effects on glacial isostatic adjustment (Sabadini et al., 1986; Wu et al., 1998; Kaufmann and Wu, 2002)[1], most of the published GIA models are computed under the assumption that the Earth viscosity is laterally homogenous.

In this study, the sensitivity of the computed VCM to the radial viscosity variations is investigated, assuming that the Earth is laterally homogenous. This assumption is sufficient only for illustrative purposes.

The elastic structure of the Earth rheology models is given in Table 6-6. The mantle is divided into four depth regions: UM1 (the upper mantle from sub-lithosphere to 420 km

[1] For example, relative sea level (RSL) data near the ice margin is found to be most sensitive to lateral variations in the lithospheric thickness and asthenospheric viscosity, while RSL data near the center of rebound is not sensitive to lateral variations (Kaufmann et al., 2000; Zhong et al., 2003; Latychev et al., 2005).

depth), UM2 (the transition zone from 420 to 670 km depth), LM1 (the shallow part of the lower mantle from 670 to 1330 km depth) and LM2 (the deep part of the lower mantle from 1330 km depth to core-mantle boundary). Figure 6.18 demonstrates diagrammatically the division of the mantle and lithosphere in our studies.

Table 6-6: Maxwell parameters of the reference model (from Wu and van der Wal, 2003)

Earth rheology model	Layer	R(m)	Density ρ(kg/m^3)	Rigidity μ(GPas)
ModW16VA	Lithosphere	6371000	3191.7	0.60192×10^{11}
	Upper Mantle UM1	6256000	3442.1	0.73115×10^{11}
	Transition zone UM2	5971000	3882.4	0.10950×10^{12}
	Lower Mantle LM1	5701000	4527.3	0.18063×10^{12}
	Lower mantle LM2	5200000	5084.2	0.24145×10^{12}
	Core	3480000	10925.0	0.0000

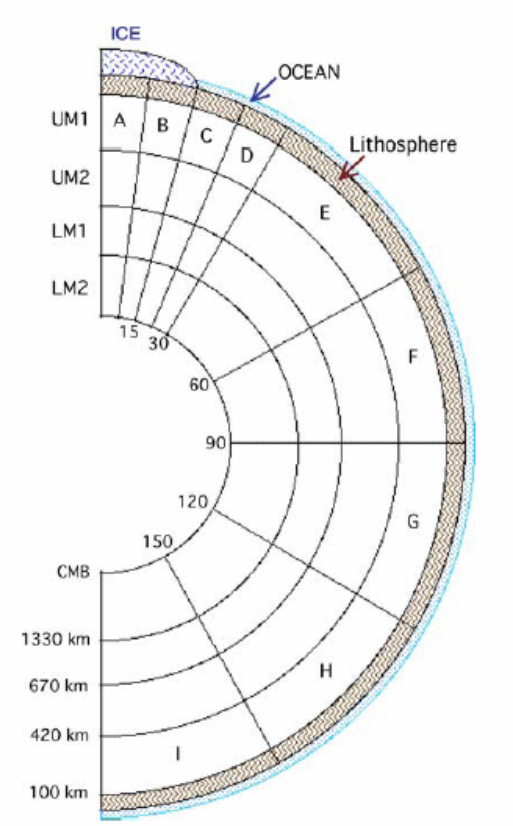

Figure 6.18: Schematic diagram of the spherical Earth rheology model. The mantle is divided into four depth zones: upper mantle (UM1), transition zone (UM2), shallow part of lower mantle (LM1) and deep part of the lower mantle (LM2) (from Wu, 2006).

Sensitivity kernels are normally used in the inversion of mantle viscosity profile from post-glacial rebound observations (Peltier, 1976; Mitrovica and Peltier, 1991, 1993, 1995; and Wu, 2006). It has been shown by Wu (2006), using an inverse kernel, that near the center of rebound, present-day radial velocity is most sensitive to the viscosity in the shallow part of the lower mantle (LM1) and the transition zone (UM2). Just outside the ice margin (15º-22º from the ice center), radial displacement is most sensitive to the viscosity of the transition zone (UM2) and the upper mantle (UM1). Further away, the radial velocity is most sensitive to the viscosity of the lower mantle-either the shallow part (LM1) or the deeper part of the lower mantle (LM2) depending on the location.

Current interest is in the sensitivity of VCM to viscosity changes in certain depth range (e.g., UM1, UM2, LM1 and LM2). For this, eight different Earth rheology models are considered (Table 6-7). These Earth rheology models are chosen to encompass a

viscosity range that still provide a suitable fit to relative sea level observations and approximate the standard VM2 model (Wu, Personal communication). The surface load response of these Earth models was provided to us by W. van del Wal, University of Calgary computed using the Earth code from Dr. L.L.A. Vermeersen, Delft University of Technology (Vermeerson and Sabadinni, 1997).

The forward model of GIA featuring each of these Earth rheology models and adopting the reference ICE3-G and ICE4-G ice history are solved. The rate of present-day crustal variations computed using these test models, and adopted ice histories of ICE-3G and ICE-4G are shown in Figures 6.19-6.34.

Table 6-7 Parameters of the Earth rheology models.

Earth rheology model	Viscosity of Lithosphere v(Pas)	Layer 2 Viscosity(UM 1) v(Pas)	Layer 3 Viscosity(UM2) v(Pas)	Layer 4 Viscosity(LM1) N(Pas)	Layer 5 Viscosit(LM 2) v(Pas)	Layer 6 Viscosity(core) v(Pas)
ModW16VA	1.00×10^{43}	4.00×10^{20}	4.00×10^{20}	2.00×10^{21}	4.00×10^{21}	0.0
ModW17VA	1.00×10^{43}	1.00×10^{23}	1.00×10^{23}	0.20×10^{22}	0.40×10^{22}	0.0
ModW20VA	1.00×10^{43}	4.00×10^{20}	4.00×10^{20}	1.00×10^{22}	1.00×10^{22}	0.0
ModW21VA	1.00×10^{43}	7.00×10^{20}	7.00×10^{20}	2.00×10^{22}	2.00×10^{22}	0.0
ModW23VA	1.00×10^{43}	1.00×10^{21}	1.00×10^{21}	6.00×10^{21}	6.00×10^{21}	0.0
ModW24VA	1.00×10^{43}	7.00×10^{20}	7.00×10^{20}	1.00×10^{22}	1.00×10^{22}	0.0
ModW25VA	1.00×10^{43}	4.00×10^{20}	4.00×10^{20}	6.00×10^{21}	6.00×10^{21}	0.0
ModW26VA	1.00×10^{43}	7.00×10^{20}	7.00×10^{20}	6.00×10^{21}	6.00×10^{21}	0.0

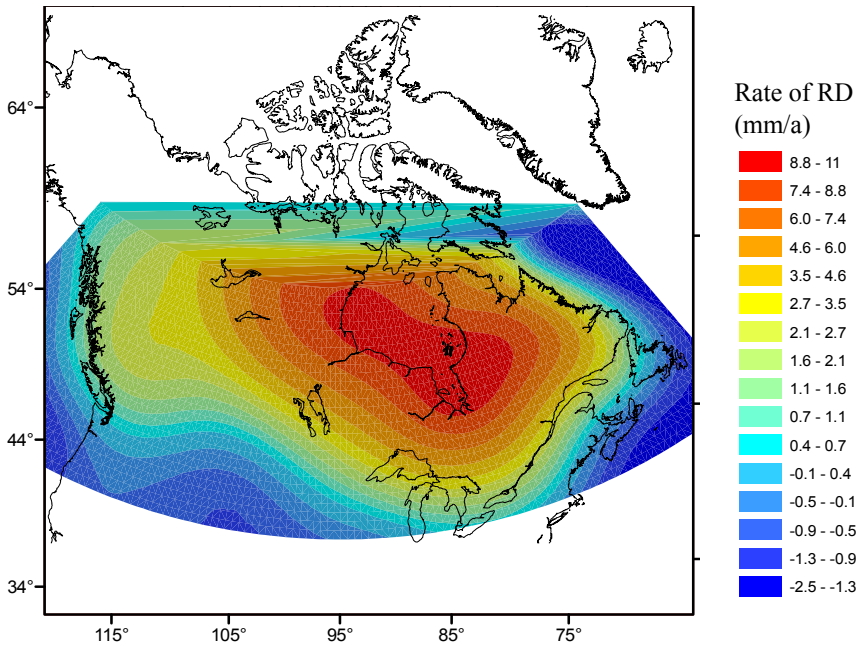

Figure 6.19: The present-day rate of radial displacement of the surface of the solid Earth in North America using Mod16 viscosity model and ICE-3G deglaciation history.

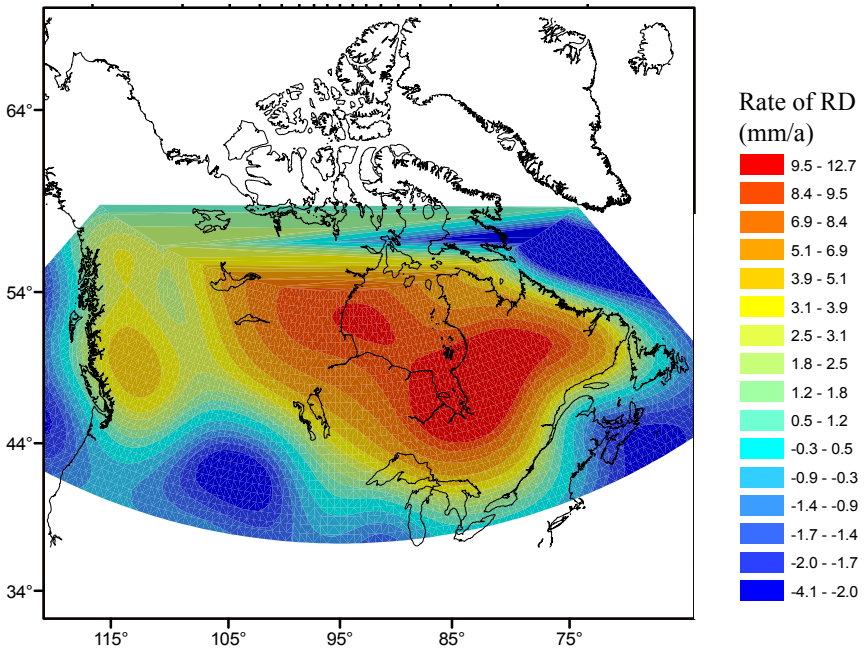

Figure 6.20: The present-day rate of radial displacement of the surface of the solid Earth in North America using Mod17 viscosity model and ICE-3G deglaciation history.

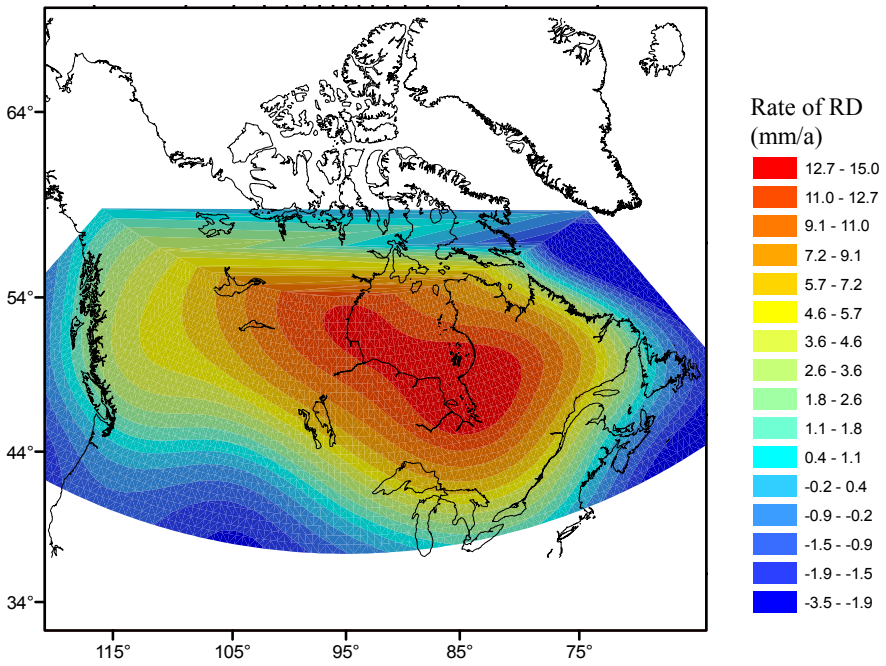

Figure 6.21: The present-day rate of radial displacement of the surface of the solid Earth in North America using Mod20 viscosity model and ICE-3G deglaciation history.

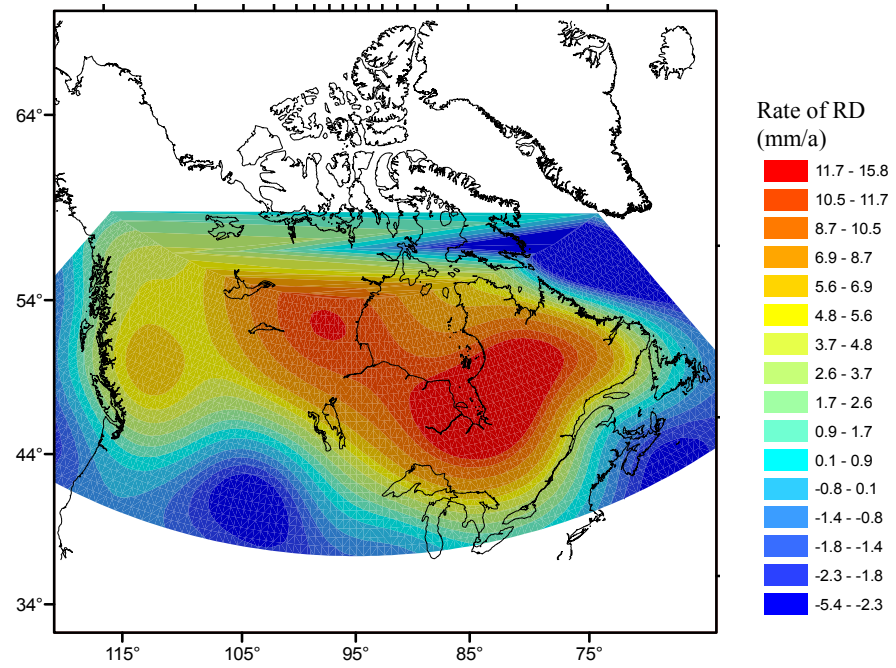

Figure 6.22: The present-day rate of radial displacement of the surface of the solid Earth in North America using Mod21 viscosity model and ICE-3G deglaciation history.

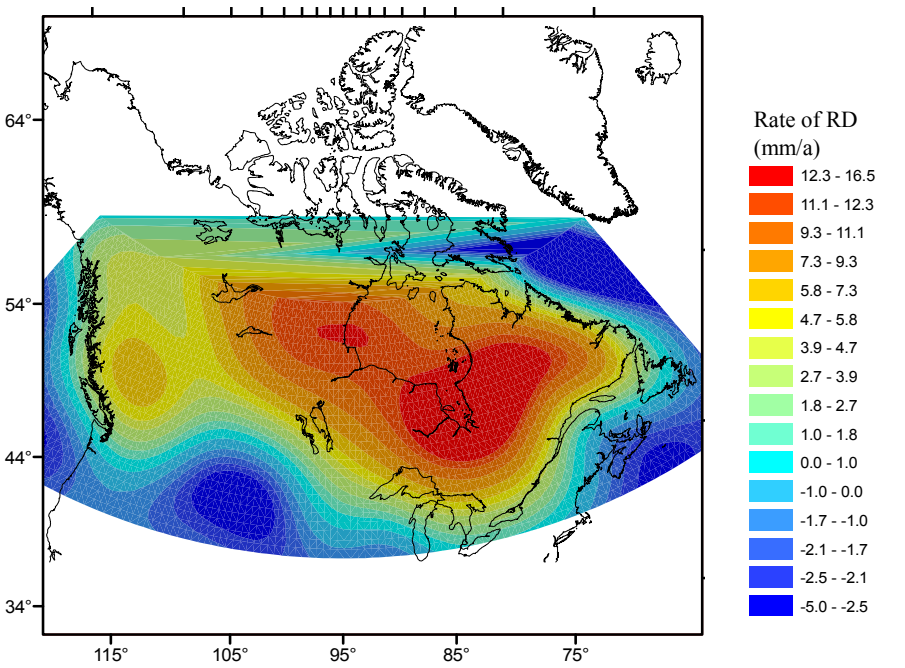

Figure 6.23: The present-day rate of radial displacement of the surface of the solid Earth in North America using Mod23 viscosity model and ICE-3G deglaci

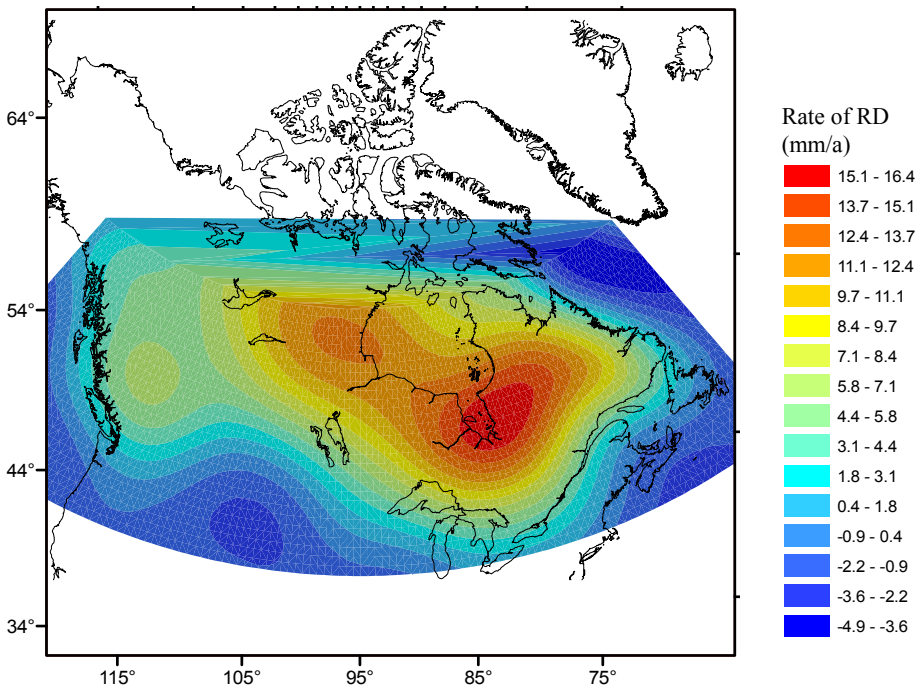

Figure 6.24: The present-day rate of radial displacement of the surface of the solid Earth in North America using Mod24 viscosity model and ICE-3G deglaciation history.

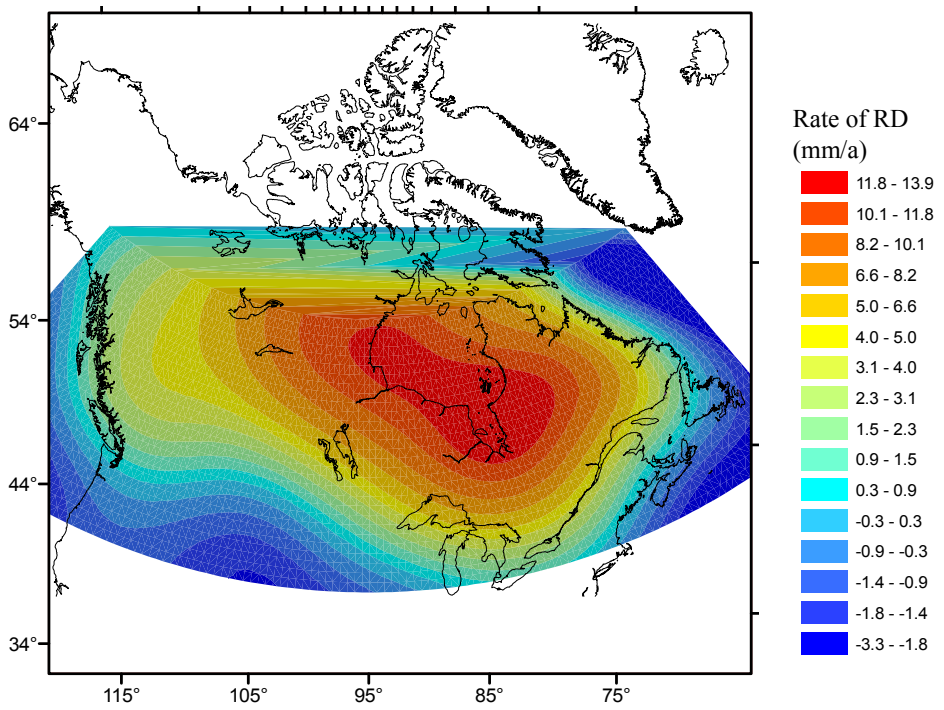

Figure 6.25: The present-day rate of radial displacement of the surface of the solid Earth in North America using Mod25 viscosity model and ICE-3G deglaciation history.

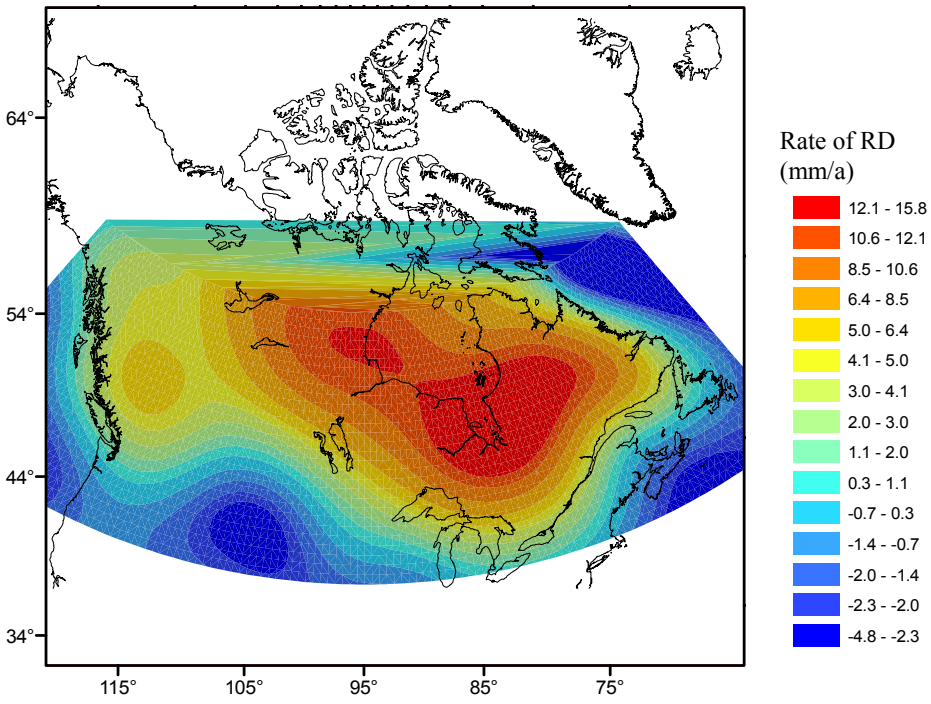

Figure 6.26: The present-day rate of radial displacement of the surface of the solid Earth in North America using Mod26 viscosity model and ICE-3G deglaciation history.

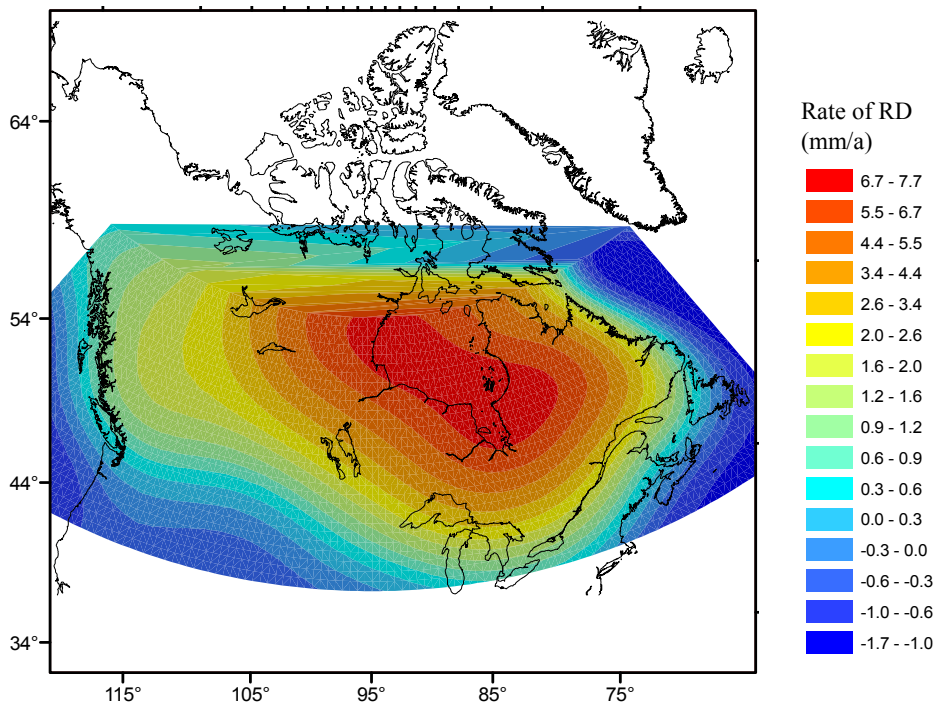

Figure 6.27: The present-day rate of radial displacement of the surface of the solid Earth in North America using Mod16 viscosity model and ICE-4G deglaciation history.

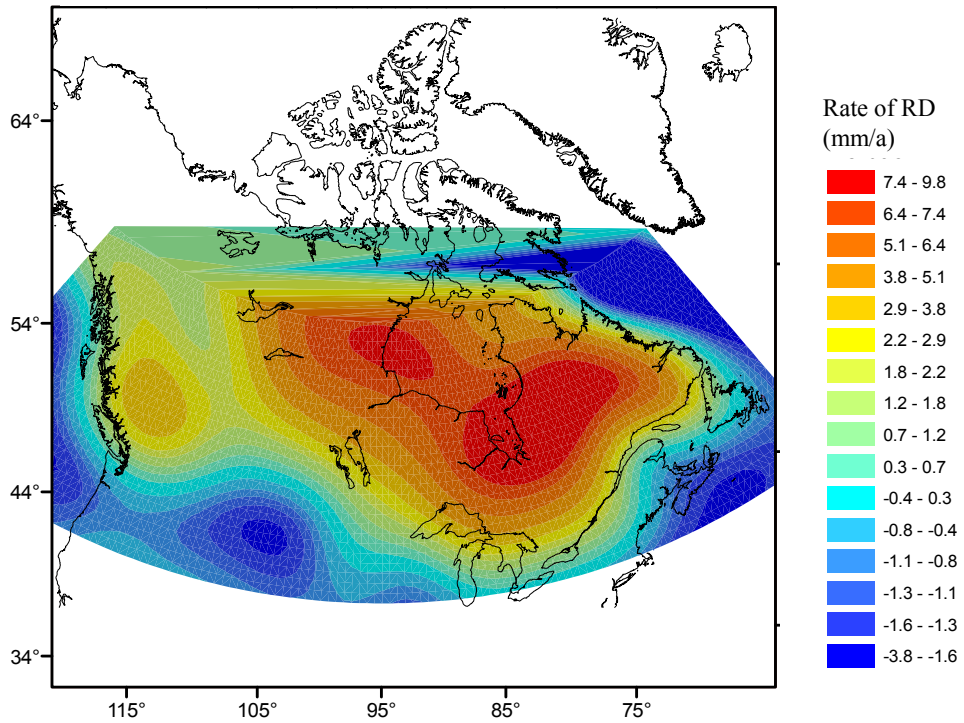

Figure 6.28: The present-day rate of radial displacement of the surface of the solid Earth in North America using Mod17 viscosity model and ICE-4G deglaciation history.

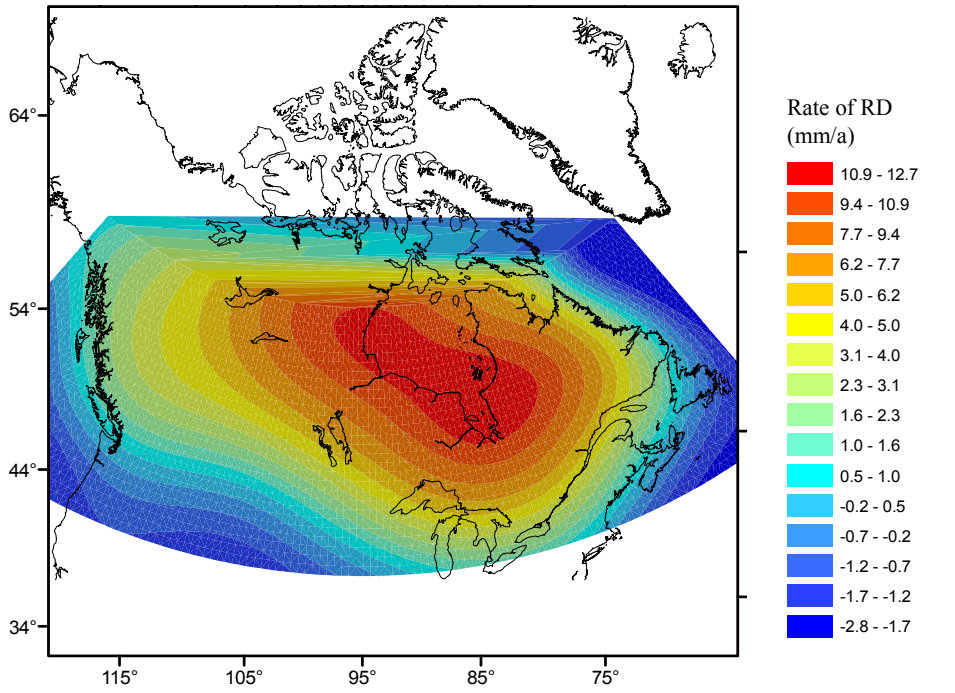

Figure 6.29: The present-day rate of radial displacement of the surface of the solid Earth in North America using Mod20 viscosity model and ICE-4G deglaciation history.

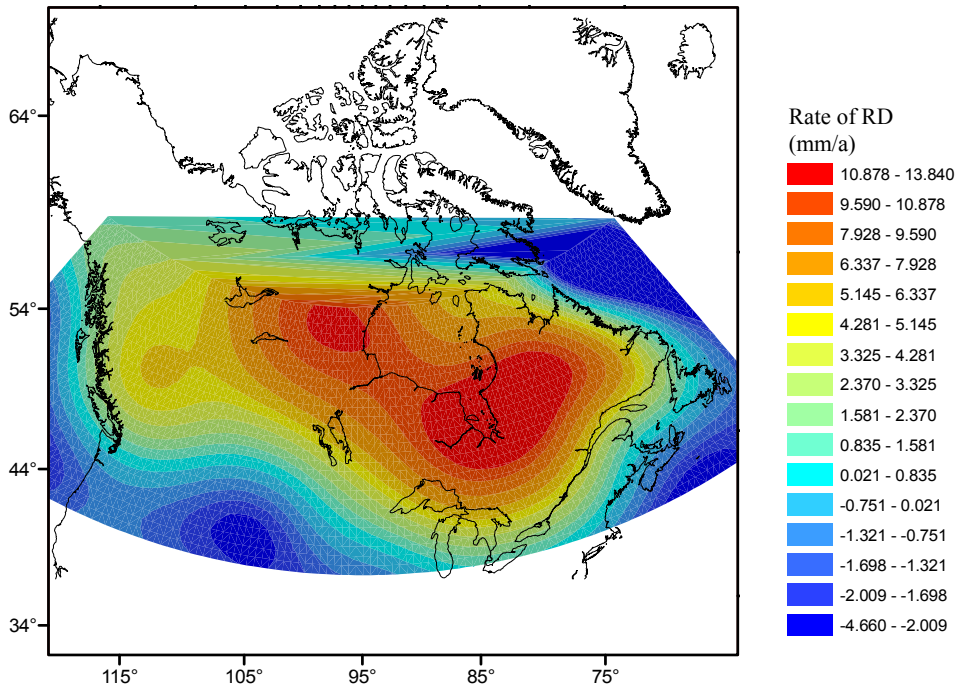

Figure 6.30: The present-day rate of radial displacement of the surface of the solid Earth in North America using Mod21 viscosity model and ICE-4G deglaciation history.

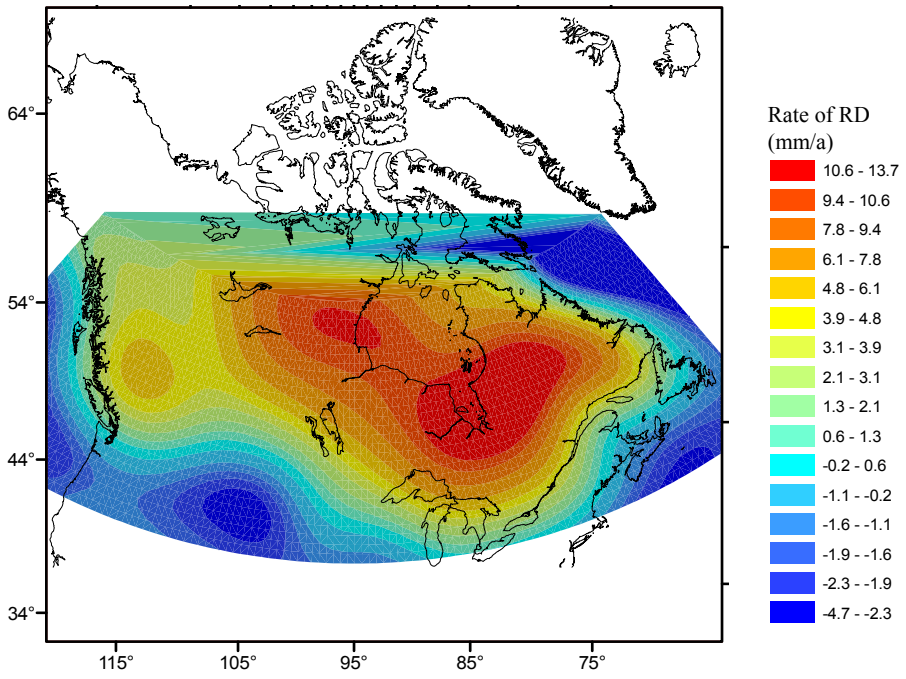

Figure 6.31: The present-day rate of radial displacement of the surface of the solid Earth in North America using Mod23 viscosity model and ICE-4G deglaciation history.

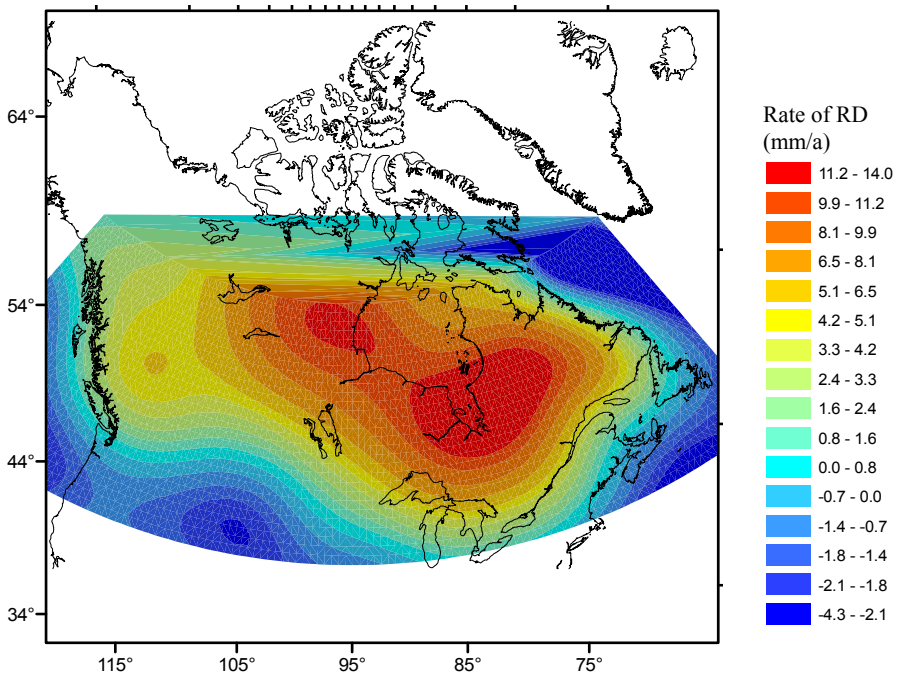

Figure 6.32: The present-day rate of radial displacement of the surface of the solid Earth in North America using Mod24 viscosity model and ICE-4G deglaciation history.

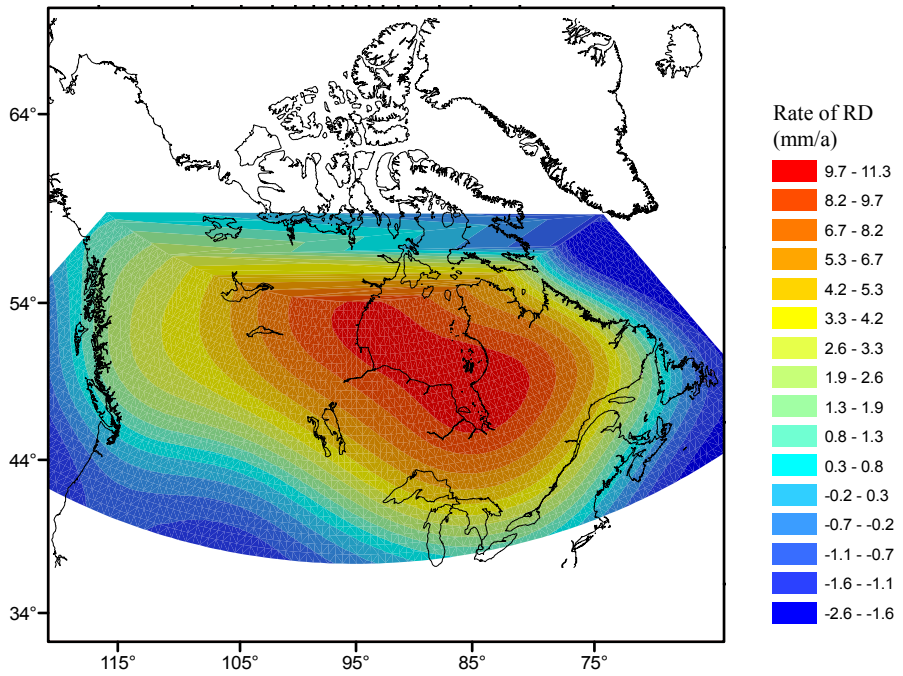

Figure 6.33: The present-day rate of radial displacement of the surface of the solid Earth in North America using Mod25 viscosity model and ICE-4G deglaciation history.

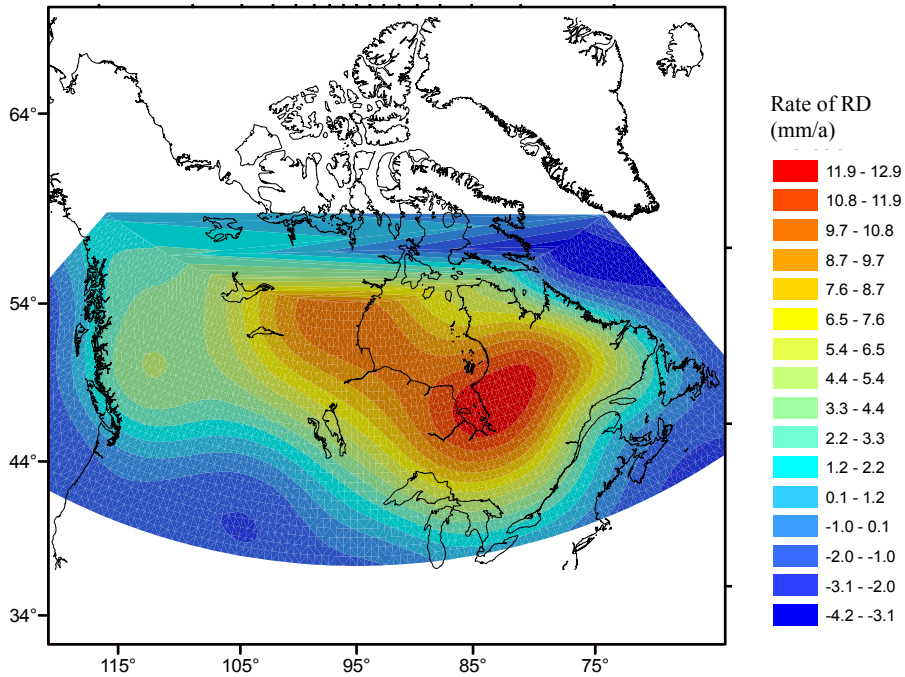

Figure 6.34: The present-day rate of radial displacement of the surface of the solid Earth in North America using Mod26 viscosity model and ICE-4G deglaciation history.

The predictions of present-day vertical crustal changes of the postglacial rebound based on the published ICE3-G and ICE-4G model and the Earth rheology models listed in Table 6-6 are compared with the computed VCM. To carry this out, some sample points in the area of study (where we have compiled VCM) are selected. These test points are selected in different locations with respect to the center of rebound. Also, the points are selected in the areas where the calculated VCM has the lowest standard deviations to assure that the derived rate of orthometric height from the VCM map is not an artifact of the extrapolations in the sparse area. Figure 6.35 shows the location of the selected points and Tables 6-7, 6-8, 6-9 and 6-10 give a list of sample points for the sensitivity analysis along with the rate of present-day radial displacement and geoidal rate of changes obtained from GIA models, using 8 different Earth rheologies, and two adopted standard ice history. The values of radial displacements ($\dot{h}$) and geoidal height rates ($\dot{N}$), from each GIA model in these tables are the direct outputs of the GIA models and should be differenced to obtain the rate of vertical crustal movements with respect to the geoid ($\dot{H}$) for further comparisons with our VCM. In figure 6.35, the points with the same color are the locations where a particular viscosity model leads to a better fit between the values of $\dot{H}$ from the VCM and GIA models. For example, in the area where the points 2, 3 and 4 are located (St. Lawrence area and Quebec), the VCM gives a better fit with a GIA model based on Mod17.

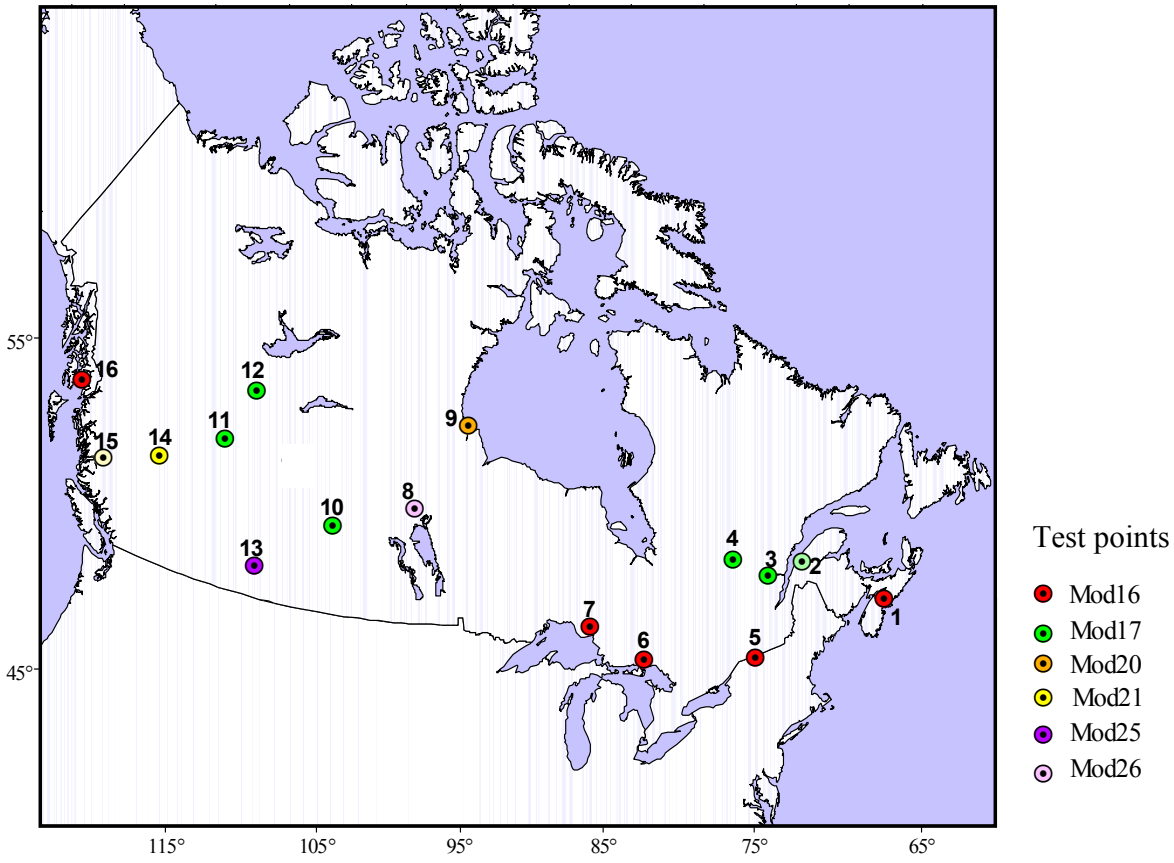

Figure 6.35: Test points for the sensitivity analysis. The points are selected in the coverage of the produced VCM and are chosen to be in regular distribution as possible. The points with the same color are the locations where a particular viscosity model leads to a better fit between the values of $\dot{H}$ from the VCM and GIA models.

Table 6-8: The predicted present-day radial displacement in sample stations using different variation of viscosity of the Earth rheology model, and adopting ICE-3G ice history. The values are in millimetre per year.

Pt.	Latitude (Degree)	Longitude (Degree)	Area of Sampling	RD-Mod16 (mm/a)	RD-Mod17 (mm/a)	RD-Mod20 (mm/a)	RD-Mod21 (mm/a)	RD-Mod23 (mm/a)	RD-Mod24 (mm/a)	RD-Mod25 (mm/a)	RD-Mod26 (mm/a)
1	44.913	-63.984	Eastern Canada, NS	-0.7	-1.95	-0.63	-1.87	-2.07	-1.77	-0.72	-1.85
2	48.394	-68.203	Eastern Canada, St. Lawrence area	2.65	1.11	4.74	3.17	2.44	3.42	4.16	3.06
3	48.394	-71.016	Eastern Canada, St. Lawrence area	3.8	3.54	6.5	5.82	5.5	6.09	5.77	5.63
4	49.787	-73.125	Eastern Canada, St. Lawrence area	6.27	7.81	9.93	10.6	10.72	10.91	8.97	10.32
5	44.913	-73.828	Eastern Canada, St. Lawrence area	1.83	1.93	3.43	3.22	3.29	3.4	2.92	3.02
6	46.305	-81.562	Great Lakes	3.87	4.91	6.6	7.15	7.35	7.4	5.8	6.81
7	48.394	-85.078	Great Lakes	5.38	6.89	8.8	9.57	9.87	9.95	7.84	9.27
8	54.661	-99.141	Manitoba	5.7	6.28	9.1	8.56	8.98	9.23	8.13	8.63
9	58.839	-94.219	Manitoba	9.14	9.47	13.19	11.47	12.26	12.59	12.21	12.25
10	53.269	-106.172	Central Canada, Prairies	2.88	2.74	5.1	4.23	4.5	4.71	4.37	4.2
11	56.054	-117.422	Central Canada, Prairies	2.88	2.66	5.52	5.38	4.87	5.54	4.71	4.87
12	58.839	-116.016	Central Canada, Prairies	3.72	3.45	6.84	6.24	5.83	6.52	5.9	5.86
13	50.483	-111.797	Central Canada, Prairies	0.88	-0.03	1.84	1.03	0.75	1.25	1.43	0.86
14	53.965	-122.344	Western Canada, BC	2.59	4.47	4.54	6.37	6.55	6.32	3.91	5.73
15	52.572	-126.562	Western Canada, BC	1.89	3.78	3.19	5.01	5.24	4.9	2.75	4.45
16	55.358	-131.484	Western Canada, Pacific	1.34	1.72	2.42	3.02	2.68	2.94	2.05	2.59

Table 6-9: The predicted present-day radial displacement in sample stations using different variation of viscosity of the Earth rheology model, and adopting ICE-4G ice history. The values are in millimetre per year.

Pt.	Latitude (Degree)	Longitude (Degree)	Area of Sampling	RD-Mod16 (mm/a)	RD-Mod17 (mm/a)	RD-Mod20 (mm/a)	RD-Mod21 (mm/a)	RD-Mod23 (mm/a)	RD-Mod24 (mm/a)	RD-Mod25 (mm/a)	RD-Mod26 (mm/a)
1	44.913	-63.984	Eastern Canada, NS	-0.23	-1.37	-0.04	-1.08	-1.49	-1.04	-0.17	-1.16
2	48.394	-68.203	Eastern Canada, St. Lawrence area	2.26	1.13	4.44	3.79	2.72	3.78	3.77	3.22
3	48.394	-71.016	Eastern Canada, St. Lawrence area	3.02	3.06	5.77	5.95	5.29	5.91	4.93	5.22
4	49.787	-73.125	Eastern Canada, St. Lawrence area	4.68	6.13	8.33	9.72	9.31	9.65	7.25	8.76
5	44.913	-73.828	Eastern Canada, St. Lawrence area	1.49	1.68	3.11	3.25	3.08	3.22	2.54	2.72
6	46.305	-81.562	Great Lakes	2.93	3.91	5.68	6.7	6.51	6.65	4.77	5.84
7	48.394	-85.078	Great Lakes	4.03	5.46	7.52	8.9	8.67	8.88	6.41	7.92
8	54.661	-99.141	Manitoba	4.09	4.47	7.81	7.79	7.36	7.96	6.57	7.00
9	58.839	-94.219	Manitoba	6.98	7.46	11.51	10.8	10.61	11.34	10.19	10.53
10	53.269	-106.172	Central Canada, Prairies	2.36	2.2	4.86	4.5	4.1	4.61	3.93	3.84
11	56.054	-117.422	Central Canada, Prairies	2.18	2.01	4.72	5.18	4.25	5.03	3.83	4.19
12	58.839	-116.016	Central Canada, Prairies	2.7	2.34	5.79	5.88	4.83	5.78	4.74	4.86
13	50.483	-111.797	Central Canada, Prairies	0.96	0.33	2.03	1.57	1.06	1.59	1.53	1.12
14	53.965	-122.344	Western Canada, BC	1.79	3.46	3.47	5.34	5.43	5.12	2.86	4.46
15	52.572	-126.562	Western Canada, BC	1.21	2.81	2.21	3.86	4.09	3.66	1.83	3.22
16	55.358	-131.484	Western Canada, Pacific	0.92	1.13	1.82	2.39	1.96	2.23	1.47	1.86

Table 6-10: The predicted present-day rate of geoidal changes in sample stations using different variation of viscosity of the Earth rheology model, and adopting ice ICE-3G. The values are in millimetre per year.

Pt.	Latitude (Degree)	Longitude (Degree)	Area of Sampling	GC-Mod16 (mm/a)	GC-Mod17 (mm/a)	GC-Mod20 (mm/a)	GC-Mod21 (mm/a)	GC-Mod23 (mm/a)	GC-Mod24 (mm/a)	GC-Mod25 (mm/a)	GC-Mod26 (mm/a)
1	44.913	-63.984	Eastern Canada, NS	0.23	0.2	0.39	0.43	0.32	0.38	0.31	0.3
2	48.394	-68.203	Eastern Canada, St. Lawrence area	0.64	0.7	1.01	1.03	0.94	1.03	0.88	0.92
3	48.394	-71.016	Eastern Canada, St. Lawrence area	0.75	0.87	1.19	1.24	1.16	1.23	1.04	1.11
4	49.787	-73.125	Eastern Canada, St. Lawrence area	0.96	1.2	1.49	1.58	1.52	1.6	1.32	1.46
5	44.913	-73.828	Eastern Canada, St. Lawrence area	0.52	0.6	0.86	0.91	0.82	0.89	0.73	0.78
6	46.305	-81.562	Great Lakes	0.76	0.92	1.23	1.29	1.24	1.31	1.06	1.18
7	48.394	-85.078	Great Lakes	0.94	1.14	1.5	1.56	1.51	1.59	1.32	1.44
8	54.661	-99.141	Manitoba	1.1	1.26	1.74	1.7	1.66	1.77	1.53	1.61
9	58.839	-94.219	Manitoba	1.37	1.58	2.07	1.99	1.98	2.08	1.85	1.93
10	53.269	-106.172	Central Canada, Prairies	0.79	0.87	1.31	1.28	1.21	1.31	1.12	1.16
11	56.054	-117.422	Central Canada, Prairies	0.68	0.79	1.16	1.24	1.12	1.22	0.99	1.07
12	58.839	-116.016	Central Canada, Prairies	0.81	0.93	1.36	1.41	1.3	1.41	1.16	1.25
13	50.483	-111.797	Central Canada, Prairies	0.49	0.48	0.83	0.84	0.73	0.83	0.68	0.69
14	53.965	-122.344	Western Canada, BC	0.5	0.65	0.86	1.02	0.9	0.98	0.72	0.84
15	52.572	-126.562	Western Canada, BC	0.35	0.48	0.61	0.78	0.66	0.72	0.5	0.6
16	55.358	-131.484	Western Canada, Pacific	0.31	0.37	0.54	0.67	0.54	0.61	0.44	0.5

Table 6-11: The predicted present-day rate of geoidal changes in sample stations using different variation of the viscosity of the Earth rheology model, and adopting ice ICE4-G history. The values are in millimetre per year.

Pt.	Latitude (Degree)	Longitude (Degree)	Area of Sampling	GC-Mod16 (mm/a)	GC-Mod17 (mm/a)	GC-Mod20 (mm/a)	GC-Mod21 (mm/a)	GC-Mod23 (mm/a)	GC-Mod24 (mm/a)	GC-Mod25 (mm/a)	GC-Mod26(mm/a)
1	44.913	-63.984	Eastern Canada, NS	0.18	0.14	0.32	0.37	0.25	0.32	0.26	0.25
2	48.394	-68.203	Eastern Canada, St. Lawrence area	0.48	0.54	0.84	0.93	0.79	0.89	0.71	0.76
3	48.394	-71.016	Eastern Canada, St. Lawrence area	0.56	0.68	1.00	1.11	0.97	1.07	0.84	0.93
4	49.787	-73.125	Eastern Canada, St. Lawrence area	0.72	0.91	1.24	1.41	1.27	1.37	1.06	1.2
5	44.913	-73.828	Eastern Canada, St. Lawrence area	0.4	0.45	0.72	0.8	0.68	0.76	0.6	0.64
6	46.305	-81.562	Great Lakes	0.57	0.7	1.03	1.16	1.03	1.13	0.86	0.97
7	48.394	-85.078	Great Lakes	0.71	0.88	1.27	1.41	1.26	1.37	1.07	1.2
8	54.661	-99.141	Manitoba	0.82	0.94	1.49	1.54	1.38	1.52	1.24	1.32
9	58.839	-94.219	Manitoba	1.03	1.2	1.76	1.79	1.64	1.79	1.51	1.59
10	53.269	-106.172	Central Canada, Prairies	0.61	0.65	1.13	1.18	1	1.15	0.92	0.96
11	56.054	-117.422	Central Canada, Prairies	0.5	0.58	0.97	1.1	0.91	1.04	0.78	0.86
12	58.839	-116.016	Central Canada, Prairies	0.59	0.68	1.13	1.25	1.05	1.19	0.93	1.01
13	50.483	-111.797	Central Canada, Prairies	0.38	0.38	0.71	0.77	0.6	0.71	0.56	0.57
14	53.965	-122.344	Western Canada, BC	0.37	0.48	0.68	0.86	0.71	0.79	0.55	0.65
15	52.572	-126.562	Western Canada, BC	0.25	0.35	0.47	0.63	0.5	0.55	0.37	0.45
16	55.358	-131.484	Western Canada, Pacific	0.23	0.27	0.42	0.56	0.41	0.48	0.33	0.38

In order to carry out a direct comparison between VCM and the crustal deformations predicted by GIA models, two sets of values for the radial displacement and geoidal rate should be subtracted for each test point to obtain the vertical movements with respect to the geoid (equation 5.1).

Tables (6-11) and (6.12) give the values of VCM at the test points along with the corresponding values computed from GIA models described earlier for two standard ICE models, ICE-3G ad ICE-4G respectively.

In Eastern Canada, mainly near St. Lawrence River, the VCM fits better with GIA model using Mod17 Earth rheology model and ICE-3G, in which a higher viscosity is considered for the upper crust (See Tables 6-11 and 6-12). In point (1) further east in N.S., the VCM fits better with GIA model using Mod16 Earth rheology model and ICE-3G. The vertical crustal movements in this region which is the peripheral region to PGR or forbulge, is most sensitive to the viscosity of the upper mantle (UM1, UM2) for both ICE models. This is shown by considering small changes in the viscosity in the upper mantle which leads to relatively large changes in the predicted crustal movements. This agrees with the findings of Wu (2006) to the sensitivity of the crustal velocities in this area to the viscosity of the upper mantle using "inverse kernels".

In the Great Lakes, the VCM has a better agreement with the predictions of GIA computed using Mod16 Earth rheology in which generally there is a lower viscosity for different layers of mantle, compared to other Earth rheology models. The predicted rate of vertical velocities in the Great Lakes using all the Earth and ICE models shows values bigger that what is computed from the VCM. The absolute value of the VCM in this area is controlled more by the Churchill tide gauge record which is affected by temperature and salinity in Hudson Bay and as such the estimated linear trends of this tide gauge may not be all due to PGR.

In Churchill station (Test point# 8 in Tables 6-11, 6-12), which is close to the center of ice loading, the vertical crustal movements in the present time is more sensitive to the variation of the shallow part of the mantle (LM1) and it better fits with the ModW26VA and ModW24VA Earth rheology model, where the lower mantle viscosity is 6×10^{21} Pa.s, and 1×10^{22} Pa s, respectively. This is confirmed by Wu (2006) result of inversion.

This analysis also indicates that near the center of rebound at Churchill station, present day vertical crustal movement is most controlled by the viscosity in the shallow part of the lower mantle (LM1).

In Central Canada and in the Prairies, the predictions of GIA model using Mod17 is closer to the VCM. However, all the predictions are inconsistent with VCM. Either changing the ice thickness in this area (as has been suggested by Lambert, 1998) or using a laterally changing viscosity may be a solution. The former will be investigated in the next section. On the other hand, as it was discussed in section 6.6, this area displays some local movements and as such, the crustal movements in this area are not all due to PGR.

Farther to the west, the VCM has a better agreement with GIA predictions using upper mantle viscosity 7×10^{20} in models Mod23.

Table 6-12: The predicted present-day rate of crustal velocities with respect to geoidal changes in sample stations using different viscosity variation of the Earth rheology model, and adopting ICE-3G ice history along with the computed values from VCM. The values are in millimetre per year.

Pt.	Latitude (Degree)	Longitude (Degree)	Area of Sampling	VCM	$\dot{H}$ Mod16	$\dot{H}$ Mod17	$\dot{H}$ Mod20	$\dot{H}$ Mod21	$\dot{H}$ Mod23	$\dot{H}$ Mod24	$\dot{H}$ Mod25	$\dot{H}$ Mod26
1	44.913	-63.984	Eastern Canada, NS	-0.79	-0.93	-2.15	-1.02	-2.3	-2.39	-2.15	-1.03	-2.15
2	48.394	-68.203	Eastern Canada, St. Lawrence area	0.01	2.01	0.41	3.73	2.14	1.5	2.39	3.28	2.14
3	48.394	-71.016	Eastern Canada, St. Lawrence area	2.95	3.05	2.67	5.31	4.58	4.34	4.86	4.73	4.52
4	49.787	-73.125	Eastern Canada, St. Lawrence area	7.12	5.31	6.61	8.44	9.02	9.2	9.31	7.85	8.86
5	44.913	-73.828	Eastern Canada, St. Lawrence area	0.37	1.31	1.33	2.57	2.31	2.47	2.51	2.19	2.24
6	46.305	-81.562	Great Lakes	1.82	3.11	3.99	5.37	5.86	6.11	6.09	4.74	5.63
7	48.394	-85.078	Great Lakes	3.14	4.44	5.75	7.3	8.01	8.36	8.36	6.52	7.83
8	54.661	-99.141	Manitoba	7.12	4.6	5.02	7.36	6.86	7.32	7.46	6.6	7.02
9	58.839	-94.219	Manitoba	11.01	7.77	7.89	11.12	9.48	10.28	10.51	10.36	10.32
10	53.269	-106.172	Central Canada, Prairies	-0.97	2.09	1.87	3.79	2.95	3.29	3.4	3.25	3.04
11	56.054	-117.422	Central Canada, Prairies	-0.45	2.2	1.87	4.36	4.14	3.75	4.32	3.72	3.8
12	58.839	-116.016	Central Canada, Prairies	-4.77	2.91	2.52	5.48	4.83	4.53	5.11	4.74	4.61
13	50.483	-111.797	Central Canada, Prairies	0.84	0.39	-0.51	1.01	0.19	0.02	0.42	0.75	0.17
14	53.965	-122.344	Western Canada, BC	5.98	2.09	3.82	3.68	5.35	5.65	5.34	3.19	4.89
15	52.572	-126.562	Western Canada, BC	4.99	1.54	3.3	2.58	4.23	4.58	4.18	2.25	3.85
16	55.358	-131.484	Western Canada, Pacific	-0.94	1.03	1.35	1.88	2.35	2.14	2.33	1.61	2.09

Table 6-13: The predicted present-day rate of crustal velocities with respect to geoidal changes in sample stations using viscosity variation of the Earth rheology model, and adopting ICE-4G ice history along with the computed values from VCM. The values are in millimetre per year.

Pt.	Latitude (Degree)	Longitude (Degree)	Area of Sampling	VCM	$\dot{H}$ Mod16	$\dot{H}$ Mod17	$\dot{H}$ Mod20	$\dot{H}$ Mod21	$\dot{H}$ Mod23	$\dot{H}$ Mod24	$\dot{H}$ Mod25	$\dot{H}$ Mod26
1	44.913	-63.984	Eastern Canada, NS	-0.79	-0.41	-1.51	-0.36	-1.45	-1.74	-1.36	-0.43	-1.41
2	48.394	-68.203	Eastern Canada, St. Lawrence area	0.01	1.78	0.59	3.6	2.86	1.93	2.89	3.06	2.46
3	48.394	-71.016	Eastern Canada, St. Lawrence area	2.95	2.46	2.38	4.77	4.84	4.32	4.84	4.09	4.29
4	49.787	-73.125	Eastern Canada, St. Lawrence area	7.12	3.96	5.22	7.09	8.31	8.04	8.28	6.19	7.56
5	44.913	-73.828	Eastern Canada, St. Lawrence area	0.37	1.09	1.23	2.39	2.45	2.4	2.46	1.94	2.08
6	46.305	-81.562	Great Lakes	1.82	2.36	3.21	4.65	5.54	5.48	5.52	3.91	4.87
7	48.394	-85.078	Great Lakes	3.14	3.32	4.58	6.25	7.49	7.41	7.51	5.34	6.72
8	54.661	-99.141	Manitoba	7.12	3.27	3.53	6.32	6.25	5.98	6.44	5.33	5.68
9	58.839	-94.219	Manitoba	11.01	5.95	6.26	9.75	9.01	8.97	9.55	8.68	8.94
10	53.269	-106.172	Central Canada, Prairies	-0.97	1.75	1.55	3.73	3.32	3.1	3.46	3.01	2.88
11	56.054	-117.422	Central Canada, Prairies	-0.45	1.68	1.43	3.75	4.08	3.34	3.99	3.05	3.33
12	58.839	-116.016	Central Canada, Prairies	-4.77	2.11	1.66	4.66	4.63	3.78	4.59	3.81	3.85
13	50.483	-111.797	Central Canada, Prairies	0.84	0.58	-0.05	1.32	0.8	0.46	0.88	0.97	0.55
14	53.965	-122.344	Western Canada, BC	5.98	1.42	2.98	2.79	4.48	4.72	4.33	2.31	3.81
15	52.572	-126.562	Western Canada, BC	4.99	0.96	2.46	1.74	3.23	3.59	3.11	1.46	2.77
16	55.358	-131.484	Western Canada, Pacific	-0.94	0.69	0.86	1.4	1.83	1.55	1.75	1.14	1.48

6.7.2 Sensitivity of the rate of radial displacement and geoidal height to the ice thickness variations

The next task is to investigate the effect of varying the ice thickness history in the predicted vertical crustal movements. The sensitivities of the VCM to the ice thickness in two areas in Canada are investigated. These areas are: 1) Eastern Canada; and, 2) Canadian Prairies.

Figure 6.36 illustrates the location of ice disks from the ICE-4G model in Eastern Canada. In order to have a close look at the value of the ICE thickness in different deglaciation cycle, the deglaciation graphs for disks 147 and 161 are plotted in figure 6.37.

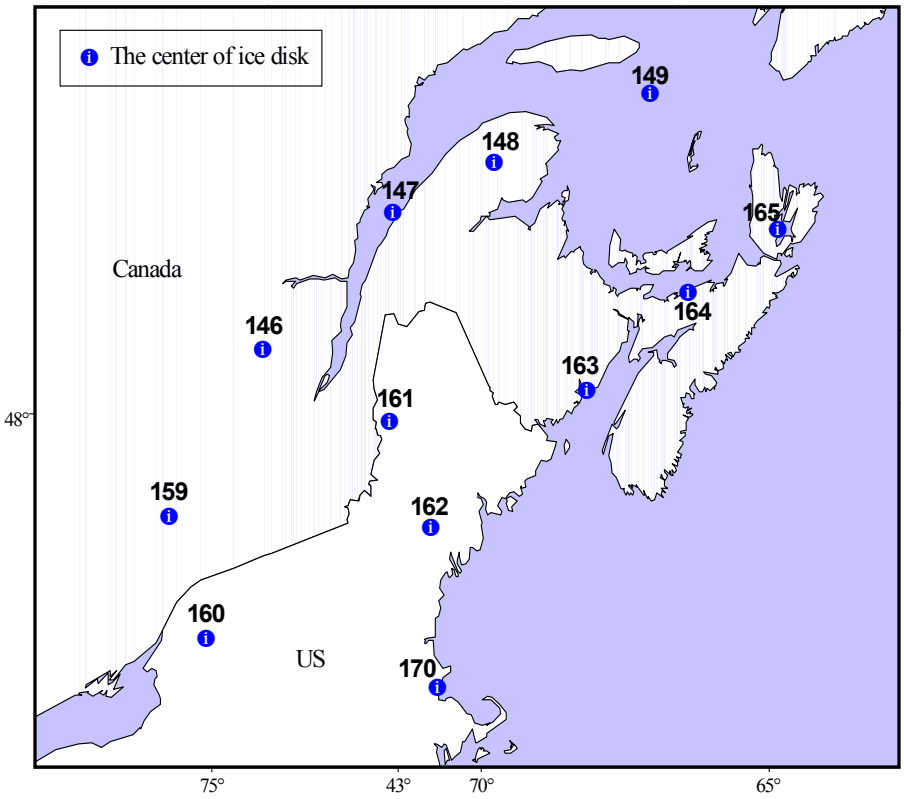

Figure 6.36: The map of the location of ICE-4G disks in Eastern Canada. The symbols show the location of the center of each disk.

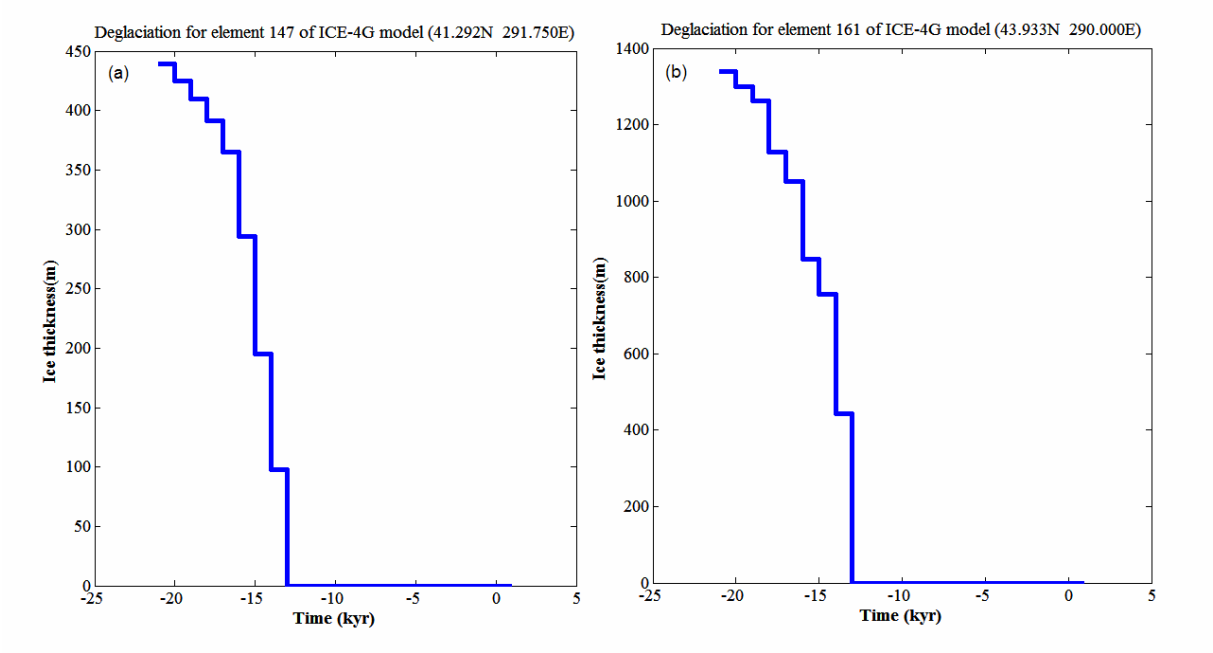

Figure 6.37: Deglaciation history of disk 147(a) and disk 161(b) from ICE-4G model. (Please note the different vertical scales)

It is clear that even though the disks are located within 300 km of each other, the maximum ICE thickness of the two disks is significantly different (1378 m for disk 161, and 400 m for disk 147). Looking at the ice thickness of all disks, it was decided to test first the sensitivity of vertical velocities to the ice thickness of those disks that show significant difference in its ice thickness compared to the adjacent disk. In Eastern Canada, the disks #147 was selected for the analysis. Then, the values of ice thickness in this particular disk were modified. (1.5 times more than the original value for the ice thickness from ICE-4G model). Figure 6.38 shows the deglaciation plots of this ice disk from the original ICE-4G model along with the deglaciation plots of the modified ICE-4G.

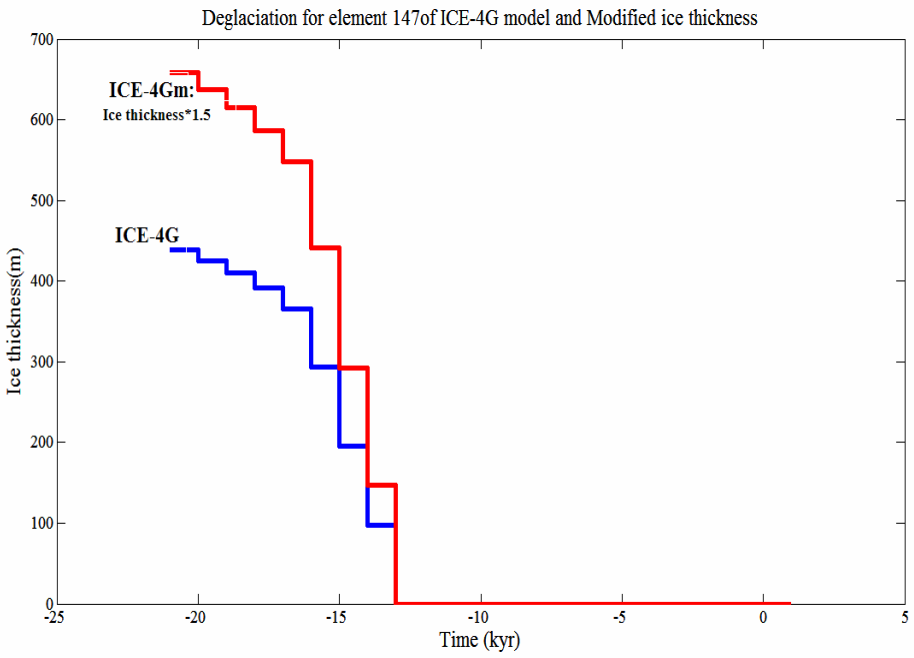

Figure 6.38: Deglaciation history in ice disk#147 from the original ICE-4G ice model and the modified ICE-4G in this particular disk.

Figure 6.39 shows the present-day rate of radial displacement of the surface of the solid Earth in North America using the Mod17 Earth rheology model and modified ICE-4G for disk 147 deglaciation history and Figure 6.40 shows the discrepancies of the rates of radial displacement resulting from the original ICE-4G model and the modified model when adding more ice in the disk 147. The maximum value of the change is 0.12 mm/year, considering the ice increasing factor of 1.5. The figure depicts the fact that changing the ice thickness in one disk only affects the rate of radial displacement of the areas around that disk.

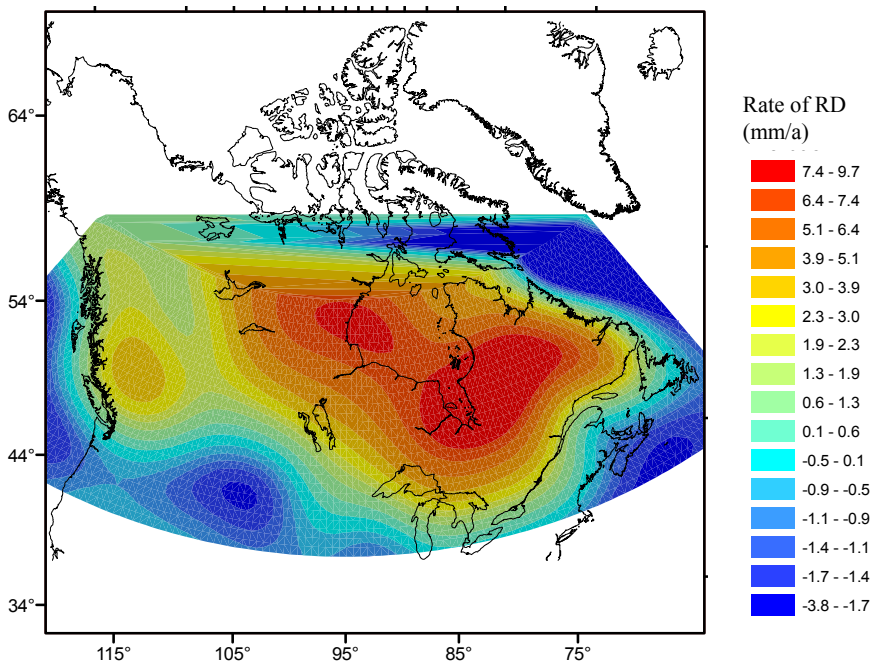

Figure 6.39: The present-day rate of radial displacement (RD) of the surface of the solid Earth in North America using the Mod17 Earth rheology model and modified ICE-4G for disk 147 deglaciation history.

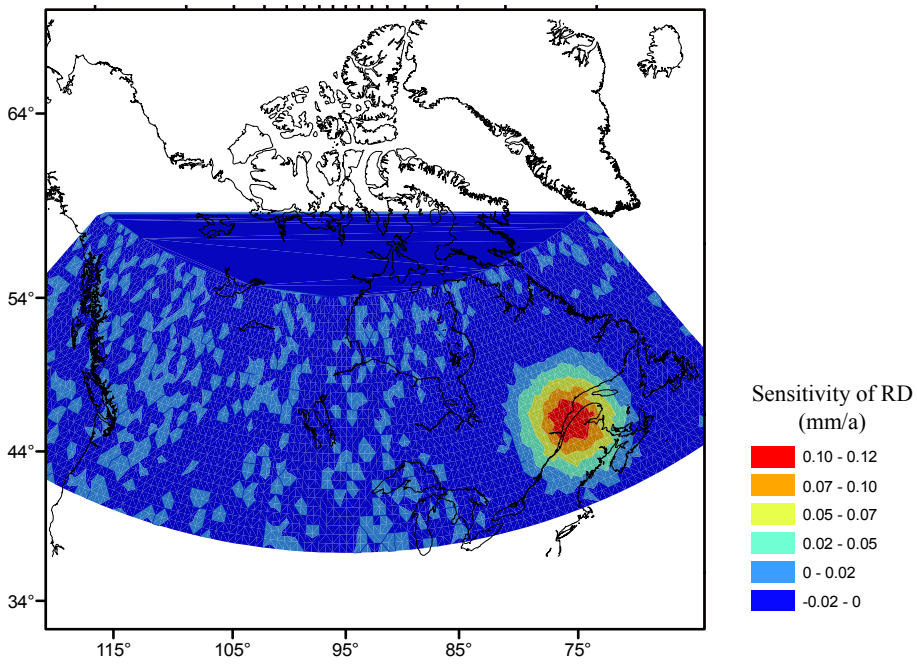

Figure 6.40: The sensitivity of the radial displacement (RD) rate to the changes of ice thickness in disk 147. The maximum peak happens in the position of the modified disk and is equal to 0.15 mm/yr.

The disagreement between the VCM and the present day predictions of the crustal velocities using GIA models in the Prairies was shown in section 6.7.1. The level of uncertainty in GIA models is apparent when the predicted crustal uplift rates for two ICE models, ICE-3G and ICE-4G, are compared in Tables 6-10 and 6-11 (Please see, for instance the predicted value of crustal uplift for test point #12 located in the Prairies). The uncertainty in this area is largely the result of the poor distribution of geological data for making the ICE models. Incorporating crustal velocities from geodetic data might improve the understanding of vertical land movement and may validate the GIA models in this area.

Thinning of Laurentide ice-sheet over the Prairies has been suggested by Lambert (1998) to obtain a better fit for the GIA predictions of crustal movements models with (1) the tilting of Campbell strand line, south and west of Lake Winnipeg, (2) the rate of decrease in absolute gravity values in Manitoba and (3) water level gauge observations in southern Manitoba lakes. In this study, we investigate whether the present day crustal movements are sensitive to the ice thickness in some specific areas, and if so, which GIA model with different ice thicknesses is closer to our VCM, which in turn helps to constrain the ICE models for the GIA analysis. The reference ICE-3G model (Tushingham and Peltier, 1991), and its two modifications, ICE-3G-m1 and ICE-3G-m2, are compared. In these two modified ice models, the southwestern portion of the ice sheet, west of Winnipeg, has been thinned to about 25% and 50% of the original ICE-3G thickness, respectively. The present day crustal velocities using Mod17 Earth rheology model, and adopted modified ice models are then predicted and compared with VCM. Figure 6.41 shows the area of thinning the ice-sheet in this study.

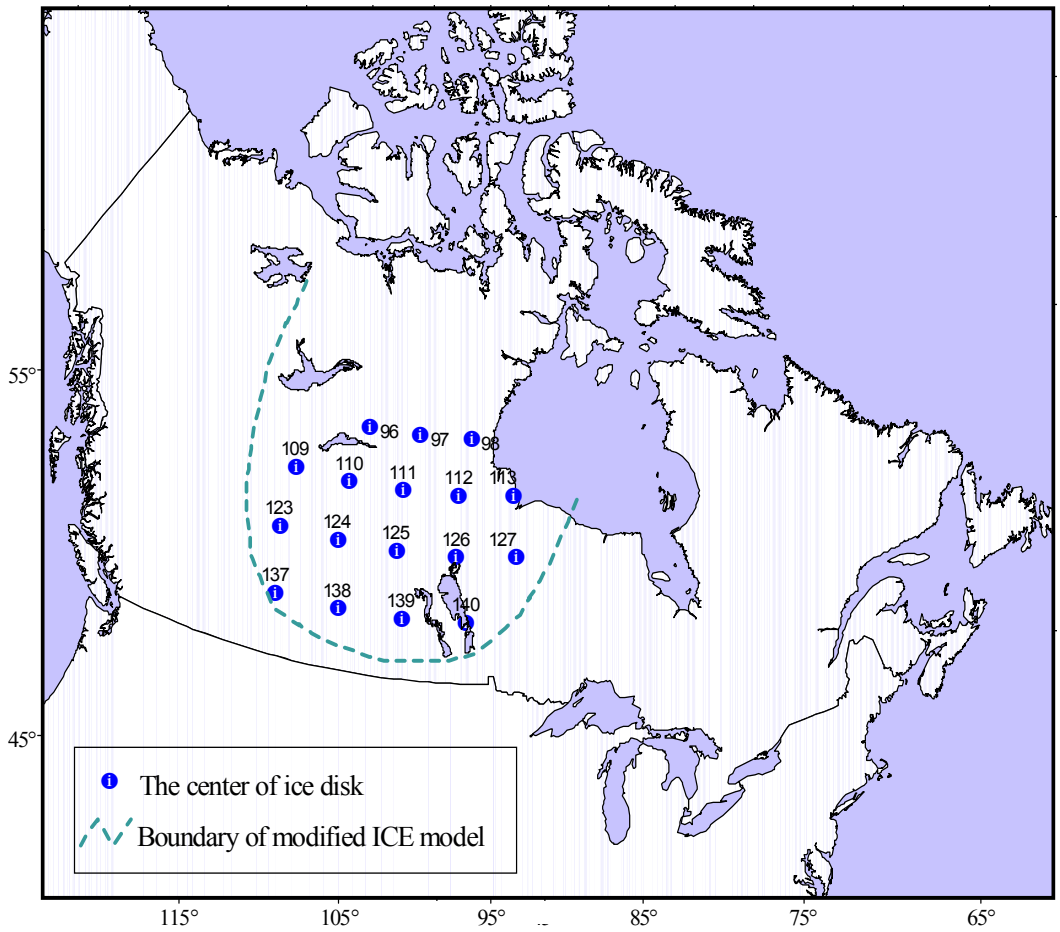

Figure 6.41: The location of ICE-3G disk in the Prairies. The dash line shows the boundary in which the Laurentide ice sheet is thinned.

Figure 6.42 a, b, show the present-day crustal velocities for two models, modified ICE-3G with 25% thinning the ice-sheet in the Prairies and modified ICE-3G with 50% thinning the ice-sheet in the Prairies, respectively.

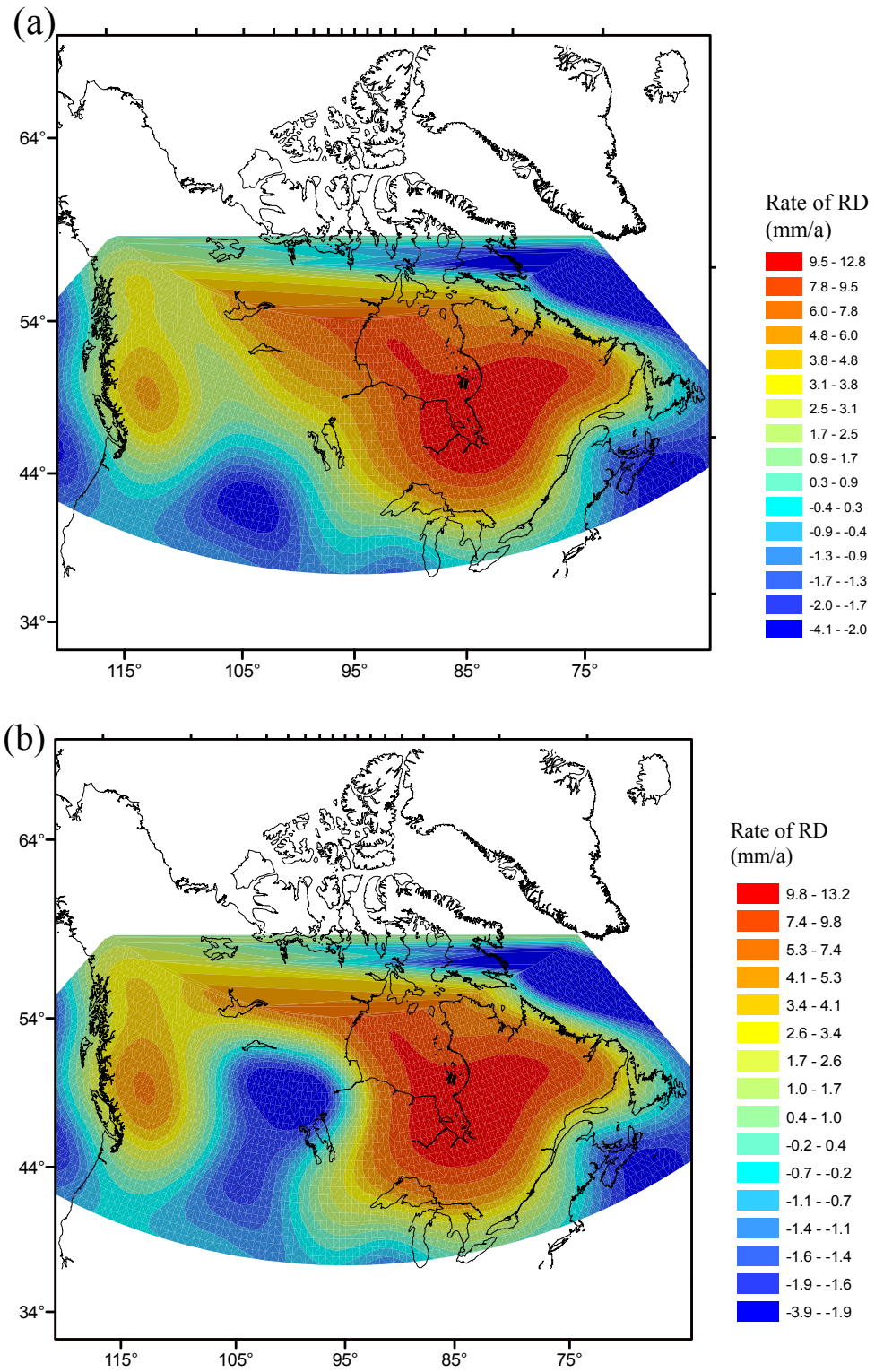

Figure 6.42: a) The present-day radial displacements(RD) using Mod17 Earth rheology model and modified ICE-3G by thinning the ice-sheet in the Prairies as 25% and b) The present-day radial displacements using Mod17 Earth rheology model and modified ICE-3G by thinning the ice-sheet in the Prairies as 50%.

The predicted values of vertical crustal movements using the standard ICE-3G, and two modified ice models are then compared with VCM. It is apparent that thinning the ice sheet in the Prairies results in values of crustal motion which fit better with the VCM in that area. However, it also affects the prediction of crustal motion in other areas close to the Prairies. As such, special attention should be paid to the amount of thinning in the disks. Table 6.13 shows some of the predicted values in sample points in the Prairies.

Table 6-14: The predicted present-day rate of crustal velocities with respect to geoidal changes in sample stations using ICE-3G, ICE-3Gm1 and ICE-3Gm2 ICE models and Mod17 Earth rheology model along with the computed values from VCM. The values are in millimetre per year.

Pt..	Latitude (Degree)	Longitude (Degree)	Area of Sampling	$\dot{H}$ (VCM)	$\dot{H}$ (ICE-3G,Mod17)	$\dot{H}$ (ICE-3Gm1,Mod17)	$\dot{H}$ (ICE-3Gm2,Mod17)
8	54.661	-99.141	Manitoba	7.12	5.02	2.73	-2.29
10	53.269	-106.172	Central Canada, Prairies	-0.97	1.87	0.50	-2.6
11	56.054	-117.422	Central Canada, Prairies	-0.45	1.87	1.66	1.12
12	58.839	-116.016	Central Canada, Prairies	-4.77	2.52	1.89	0.53
13	50.483	-111.797	Central Canada, Prairies	0.84	-0.51	-0.61	-0.96

This study explicitly showed the importance of adopting a thinner ice sheet for the Prairies; however, since the vertical movements can also be the results of some local effects, this statement is just a suggestion for further modeling of PGR from geodetic perspectives.

Chapter 7

Conclusions and Recommendation

7.1 Conclusions

A fitting method of smooth piecewise algebraic approximation (SPAA), was developed in this study to model crustal motions. This method of SPAA avoids many of the limitations associated with traditional approaches of data fitting such as the requirement that the data be of point values, as it is seen in MQ method (Hardy, 1978) and in B-splines (Gregorski et al., 2000; Greiner and Hormann, 1996); or that they should be on grid or at least well distributed (Zhou et al., 1997). SPAA is not restricted to low degree polynomials and the smoothness of the resulting function is guaranteed along the patch boundaries by imposing the continuity and smoothness (zero and first derivative) constraints and the degree of smoothness can be simply controlled by the number and degree of differentiability constraints in the model.

A physically meaningful model of VCM was compiled for Canada in which the method of SPAA was applied. The VCM model is based on the simultaneous approximation by piecewise surfaces to scattered precise re-levelling data and tide gauge records, where constraints are enforced between the parameters of the surfaces.

The VCM model developed in this research gives the details of the crustal movements. Enforcing the continuity and smoothness of the resulting surface in the first derivatives throughout the surface, the VCM model can highlight the long wavelength spatial variations of the crustal motion in Canada. In addition, the model can reveal the complexities in tectonic-prone areas and is flexible in the sense that additional constraints can be imposed if some physical knowledge of the crustal movements is known. Moreover, the VCM model is independent of the choice of nodes. Even by dealing with

scattered data, and ill-conditioned equations system in some patches, a stable solution is obtained by changing the origin of the coordinate system.

The VCM map indicates the location of PGR hinge line, which starts from Gulf of St. Lawrence River in eastern Canada, follows the Atlantic coastlines to the south, passes through the Great Lakes, and loops in the west to follow the Pacific coastline. This is in relatively good agreement with most of the GIA models.

The rate of changes of orthometric height obtained from the map of VCM was compared with the map of gravity changes rate (Pagiatakis and Salib, 2003). The PGR hinge line follows the same pattern in both maps and the close correlation between the map of VCM and $\dot{g}$ map is easily seen.

For the first time in Canada, a map of ratio between gravity and height changes was compiled. Even though the values of gravity changes in most of the gravity stations in Canada are not statistically significant, the value of ratio of gravity changes to height changes is in a fairly close agreement with theoretical models in different areas (Jachens, 1978). The values of ratio between gravity and height changes in areas such as Churchill, Edmonton and Timmins stations, once covered by ice, are very close to -0.2mGal/m of the model of Jachens (1978) for surface load. It shows that the mass redistribution in this area is mainly due to the ice removal. The value of -0.3086 mGal/m for the free-air gradient follows the pattern of PGR hinge line from GIA models. The values of the ratio in the only two significant stations in the west, Vancouver and Victoria, are not consistent and need to be studied further. These two sites are not only located in different tectonic plates which obviously makes it difficult to interpret the $\dot{h}$ and $\dot{g}$, but they also experience, over a metre of precipitation per year which leads to large seasonal variations in soil moisture and makes the detection of long-term trends more difficult.

A map of geoidal height changes was compiled using the VCM and CBN-GPS solution and was physically interpreted. The standard deviations of the GPS solution are generally larger than the standard deviation of the VCM in the area where there are data for the computation. The consistencies and inconsistencies between the values of orthometric and geodetic height changes in CBN were studied. Throughout Canada, the

difference between two values of $\dot{h}$ and $\dot{H}$ are within the range of 10-15% of the crustal movements which is reasonable and it is theoretically related to the geoidal height changes due to PGR.

The maximum inconsistencies are seen in the Prairies, where an average of 3-5mm/year was estimated for the differences between geodetic and orthometric height changes. These values are too large to come from the contribution of PGR, only. Looking at the GPS solution and its standard deviations, it is suspected that the estimations of geodetic height changes in this area might not be precise enough, and longer records for the GPS observations should improve the result. The GPS observations in the Prairies should be tested.

In principle, the map of VCM gives more detail of the crustal movements than the GPS solution. The PGR hinge line in the map of $\dot{h}$ and the long wavelength of the PGR zero line, detectable in the map of VCM, are in good agreement, except that the zero line in our map is more to the north in the Great Lakes which might be due to the tide gauge records in the Churchill station. The trend of this tide gauge record dictates the absolute value of the VCM in the Great Lakes area.

One of the main goals of our research was to investigate how VCM can be used in geophysical models. Thus, the sensitivity of the VCM to the viscosity of the Earth rheology models, and the ice thickness were investigated. The amount of misfit between the VCM and different GIA models obtained using different Earth rheology models were studied.

In Eastern Canada, mainly around the St. Lawrence River, the VCM fits better with GIA model using Mod17 Earth rheology model for ICE-3G history, in which a higher viscosity is considered for the upper crust. Further east in N.S., the model of VCM fits better with GIA model using Mod16 Earth rheology model. The VCM is sensitive to the viscosity of upper mantle in this area. This validates the recent findings of Wu (2006), in which it was shown using inverse kernels, that the crustal velocities near the ice margin area are more sensitive to the viscosity of the upper mantle.

In the Great Lakes, the VCM has a better agreement with the predictions of GIA computed using Mod16 Earth rheology in which generally a lower viscosity for different layers of mantle is considered. The sensitivity analysis in this area revealed once again the uncertainty in the absolute value of VCM in the region mainly obtained from Churchill tide gauge. This study also showed that near the center of rebound at Churchill tide gauge, present day vertical crustal movement is most sensitive to the viscosity in the shallow part of the lower mantle (LM1) and the transition zone (UM2).

In Central Canada and in the Prairies, the inconsistency between the VCM and GIA prediction of crustal movements using one of the standard ice models is shown. The thinning of the Laurentide ice- sheet in the Prairies by much as 25% and 50% of the standard ICE-3G thickness in the Prairies, showed a better agreement with VCM. The prediction of GIA in this area is uncertain and this finding indicates that new parameters in the GIA model for this particular area should be sought.

These analyses suggest the sensitivity of VCM to the lateral variations. Lateral variations of viscosity have large effects on glacial isostatic adjustment and should not be neglected (Sabadini et al., 1986; Wu et al., 1998; Kaufmann and Wu, 2002). It has been shown by Kaufmann et al. (2000); Zhong et al. (2003); Latychev et al. (2005) that relative sea level (RSL) data near the ice margin is very sensitive to the lateral variations in the lithospheric thickness and asthenospheric viscosity. The sensitivity of the VCM to the lateral variation of viscosity and to the ice thickness in different areas should be the next step to follow this investigation.

The value of eustatic sea level is of primary importance in the absolute term of the VCM. Most published values for global sea-level rise are based on tide-gauge data provided by the Permanent Service for Sea Level, adjusted in various ways to account for the non-representative sampling of gauge locations and local rates of uplift or depression of the land caused by the ongoing postglacial rebound. In this study, we adopted the eustatic contribution of the sea level rise from Douglas et al. (2001). In order to apply the most accurate estimates of the global water rise, special studies should be conducted on the global tide gauge records and the observations of the climate-related processes.

The analyses conducted on the tide gauge records showed the values of linear trends close to the previous studies, but with smaller standard deviation. This was explained to be the result of using additional records of the tide gauges than the previous study of Carrera et al., 1991(more than 10 years).

The optimum differencing tree for the tide gauges in Atlantic and Pacific was designed based on the correlations between the records of the adjacent tide gauges. Halifax, Charellettown, Point au Pere were considered to be used as point velocities in Atlantic differencing network, as they have longer records than other tide gauges in the area. In Pacific, Seathle, with more than 100 years of continuous records was considered to be in point velocity mode. Other tide gauges records were treated in differencing mode.

7.2 Recommendation for further studies

The recommendations for future studies are summarized as follow:

1. Further investigation about the $\dot{N}$ in the Prairies.

   The rates of geoidal height changes in the south Prairies need further investigations. GPS solutions in the Prairies need to be checked.

2. Further interpretation of the ratio of $\dot{g} / \dot{H}$

   There are not many resources on this aspect. It is highly recommended that some studies are carried on particularly on the interpretation of the value of the ratio between gravity changes to height changes.

3. The incorporation of U.S. leveling data.

   The incorporation of more data will certainly improve the image. We attempted to retrieve the re-levelling information from the U.S. leveling data. However, their extraction was not completed at the time of submitting this dissertation. The importance of adding these data can be seen as a good support for the southern part of the map of VCM in Canada.

4. It is recommended that the re-leveling survey be conducted for some lines. Knowing that such surveys are expensive, one of the outcomes of this research is the identification of those leveling lines that have higher priorities to be re-leveled. The lines recommended for re-levelling are given in Appendix VI.

5. The use of GIS in multidisciplinary researches and projects.

We took advantage of GIS throughout this research. It is recommended that such tools are used more in geosciences, especially due to the increasing the amount of data.

6. Consideration of Lateral viscosity in the sensitivity analysis of crustal movements to the viscosity.

The surface geology and seismic tomography clearly show that the Earth properties vary both in the radial and lateral directions. This study showed that the lateral variations of the viscosity should be considered to find the best fit between GIA models and VCM. It is recommended that in further investigations, a 3D viscosity model is used in GIA models.

7. Sensitivity analysis of the VCM to the ice thickness in other areas in Canada, as well as sensitivity to the terminal moraine.

There has not been very much work done on the sensitivity of the crustal movements to the ice thickness and the time of the completion of ice. More research should be conducted about this.

8. The use of VCM for inverse problem

The VCM was used as a basis for comparison to the results of forward modeling of crustal movements. The inverse problem should be formulated to accompany the crustal movement models from the geodetic data. The model should be able to use VCM as boundary conditions.

9. The use of SPAA in other applications.

Since, surface modeling is needed in many applications in Geomatics and other disciples; it is strongly recommended that SPAA is considered when dealing with scattered data of any types.

10. The use of other data which contain information on the time gravity changes and covers the whole of Canada.

In particular the GIA signal over Canada is transparent in the time gravity changes detected by GRACE satellites. It is recommended that GRACE gravity data be included for further investigation.

Bibliography

Adams, J., and P. W. Basham (1991). "The seismicity and seismotectonics of eastern Canada", In *Neotectonics of North America*, Eds. Slemmons, D.B. et al., Decade Map Vol. 1, pp. 261–276.

Basham, P. W., D. H. Weichert., F. M. Anglin, and M. J. Berry (1982). "New probabilistic strong ground motion maps of Canada: a compilation of earthquake source zones, methods and results." Publications of the Earth Physics Branch, Open file, 82-33.

Benko, P., G. Kos, T. Varady, L. Andor, and R. Martin (2002). "Constrained fitting in reverse engineering." *Computer Aided Geometric Design*, Vol. 19, pp. 173- 205.

Berrino, G., H. Rymer, G. C. Brown, and G. Corrado (1992). "Gravity-height correlations for calderas at unrest." *Journal of Volcanology and Geothermal research*, Vol. 53, pp. 11-26.

Calais, E., J. Y. Han, C. DeMets, and J. M. Nocquet (2006). "Deformation of the North American plate interior from a decade of continuous GPS measurements." *J. Geophys Research,* Vol. 111. B06402, doi: 10.1029/2005JB004253.

Carrera, G., and P. Vaníček (1988). " A comparison of present sea level linear trends from tide gauges, map of crustal movements and radiocarbon curves in Eastern Canada." *Palaeogeography, palaeoclimatology, palaeoecology*, Vol. 68, pp. 127-134.

Carrera, G., and P. Vaníček (1994). "Compilation of a new map of recent vertical crustal movements in Canada." The 8-th International Symposium on Recent Crustal Movements, Kobe, Japan, December 6-11, 1993.

Carrera, G., P. Vaníček, and M. Craymer (1991). "The compilation of a map of recent vertical movements in Canada. Department of Surveying Engineering." Technical report No. 153, University of New Brunswick, Fredericton, NB. Canada, 106.

Cartwright, D. E. (1968). "A unified analysis of tides and surges round north and east Britain." *Philosophical Transactions R. Soc.* Lond, Vol. 263, pp. 1-55.

Cartwright, D. E. (1983). "On the smoothing of climatological time series, with application to sea- level at Newlyn." *Geophysical journal* R.A.S. Vol. 75, pp. 639-658.

Chrzanowski, A, Y. Q. Chen, and J. M. Secord (1986). "Identification of deformation models in space and time domain." *Surv Rev*, Vol. 33, pp. 518-528.

Church, J. A., J. M. Gregory, P. Huybrechts, M. Kuhn, K. Lambeck, M. T. Nhuan, P. Qin, and P. L. Woodworth (2001). *Climate Change: The Scientific Basis,* Cambridge Univ. Press, New York, pp. 501-555.

Coordinating Committee on Great lakes Basic Hydraulic and Hydrologic Data (1977). Apparent vertical movements over the Great Lakes: Chicago, U.S. Army Corps of Engineers, and Cornwall, Ontario, Environmental Canada, 70p.

Crow, E. L., F. A. Davis, and M. W. Maxfield (1960). Statistics manual. Dover, Minneola, NY.

Crowley, T. J., and G. R. North (1991). *Paleoclimatology*, Oxford Univ., New York.

Dahmen, W. A., R. H. J. Gmelig Meyling, and J. H. M. Ursem (1990)."Scattered Data Interpolation by Bivariate C^1-piecewise Quadratic Functions." *Approximation Theory and its Applications*, Vol. 6, pp. 6–29.

Dierckx, P. (1993). *Curve and Surface Fitting with Splines.* Oxford University Press, 1993.

Dierckx, P., S. Van Leemput, and T. Vermeire (1992). "Algorithms for Surface Fitting using Powell-Sabin Splines." *IMA Journal of Numerical Analysis,* Vol. 12, No. 2, pp. 271–299.

Douglas, C.B. (1991). "Global sea level rise." *J. Geophys. Res.,* Vol. 96, No. C4, pp. 6981-6992.

Douglas, B. C., M. S. Kearney, and S. P. Leatherman (2001). *Sea Level Rise; History and Consequences*, Academic, San Diego.

Dyne, D., D. Levin, and S. Rippa (1986). "Numerical procedures for surface fitting of scattered data by radial functions." *SIAM Journal of Scientific and Statistical Computing*, Vol. 7, No. 2, pp. 639-659.

Ekman, M., and J. Mäkinen (1996). "Recent Postglacial rebound, Gravity change and mantle flow in Fennoscandia." *Geophys. J. Int.* Vol. 126, pp. 229-234.

Forsey, D. R., and R. H. Bartels (1995). "Surface Fitting with Hierarchical Splines." *ACM Transactions on Graphics,* Vol. 14, No. 2, pp. 134–161.

Franke. R. (1982). "Scattered data interpolation: test of some methods." *Mathematics of Computation,* Vol. 38, No. 157, pp. 181-200.

Farrell, W. E., and J. A. Clark (1976). "On postglacial sea level." *Geophys. JR Astron. Soc*, Vol. 46, pp. 647–667.

Godin, G. (1972). *The analysis of tides*. Liverpool, Liverpool Press.

Gregorski, B. F., B. Hamann, and K. I. Joy (2000). "Reconstruction of B-spline Surfaces from Scattered Data Points." *Proc. Computer Graphics International 2000*, pp. 163–170.

Greiner. G., and K. Hormann (1996). "Interpolating and Approximating Scattered 3D Data with Hierarchical Tensor Product Splines." In *Surface Fitting and Multiresolution Methods,* Eds. A. Le M´ehaut´e, C. Rabut, and L. L. Schumaker*,* pp. 163–172.

Haber, J, F. Zeilfelder, O. Davydov, and H. P. Seidel (2001). "Smooth approximation and rendering of large scattered data sets." *Proceedings of the conference on Visualization '01* San Diego, California, 2001, pp. 341 – 348. ISBN ~ ISSN: 1070-2385.

Hardy, R. L. (1978). "The application of multiquadric equations and point mass anomaly models to crustal movements studies." NOAA technical report NOS 76, NGS 11, Rockville, MD.

Henton, J., M. R. Craymer, R. Ferland, H. Dragert, S. Mazzotti, and D. L. Forbes (2006). "Crustal motion and deformation monitoring of the Canadian landmass." *Geomatica,* Vol. 60, No. 2, pp. 173-191.

Holdahl, R. S., and R. L. Hardy (1978). "Solvability and multiquadric analysis as applied to investigations of vertical crustal movements." *Techtonophysics*, Vol. 52, pp. 139-155.

Jachens, R. C. (1978)."The gravity method and interpretive techniques for detecting vertical crustal movements." *Proc. 9th geodesy/ Solid Earth and Ocean Physics*

(GEOP) Research Conference, An Onternational Symposium on the Applications of Geodesy to Geodynamics, Ed. I.I. Mueller. IAG/IUGG and COSPAR, Columbus, U.S.A., October. Department of Geodetic Science Report 280, the Ohio State University, Columbus, U.S.A., 153-155.

Jackson, S. M., R. B. Smith, and T. L. lsen (1984). "Recent Uplift of the Yellowstone Caldera from Precession Gravity Measurements, Eos, trans, Am. Geophy. Union, 65, 45, 1118.

Johnson, D. J. (1995). "Gravity changes on Mauna Loa Volcano in Mauna Loa reveald: Structure, composition, History and Hazards." In *Geophysical Monograph* 92, Eds. J. M. Rhodes, and John P. Lockwood, AGU, pp. 127-143.

Kaufmann, G., and P. Wu (2002). "Glacial isostatic adjustment in Fennoscandia with a three dimensional viscosity structure as an inverse problem." *Earth Planet. Sci. Lett.,* Vol. 197, pp. 1-10.

Kaufmann, G., P. Wu, and G. Li (2000)."Glacial isostatic adjustment in Fennoscandia for a laterally heterogeneous earth." *Geophys. J. Int.,* Vol. 143, pp. 262-273.

Kobbelt, L. P, T. Bareuther, and H. P. Seidel (2000). "Multiresolution shape deformations for meshes with dynamics vertex connectivity." *Computer Graphics Forum*, Vol. 19, No. 3, pp. 249-259.

Koohzare, A., P. Vaníček, and M. Santos (2006a). "The use of smooth piecewise algebraic approximation in the determination of vertical crustal movements in Eastern Canada." *Proc*., *Joint assembly of the IAG, IAPSO and IABO*, Cairns, Australia, 2005, Vol.130.

Koohzare, A., P. Vaníček, and M. Santos (2006b). "Compilation of a Map of Recent Vertical Crustal Movements in Eastern Canada Using Geographic Information System." *Journal of Surveying Engineering*. ASCE, Vol. 132, No. 4, pp. 160-167.

Kumarapeli, P. S. (1985). "Vestiges of Iapeton Rifting in the craton west of the Northern Appalachian." *Geosciences Canada*, Vol. 12, No. 2, pp. 54-59.

Lambert, A ., N. Courtier, G. S. Sasagawa, F. Klopping, D. Winester, T. S. James, and J. O. Liard (2001). "New constraints on Laurentide postglacial rebound from absolute gravity measurements." *Geophys. Res. Lett.*, Vol. 28, pp. 2109-2112.

Lambert, A., N. Courtier, H. Dragert, T.S. James, M. Schmitt, and K. Wang (2001). "Absolute gravity measurements in the Cascadia subduction zone." *American Geophysical Union Conference*. Fall. 2001.

Lambert, A., T. S. James, and L. H. Thorleifon (1998). "Combining geomorphological and geodetic data to determine postglacial rebound tilting in Manitoba." *Journal of Paleolimology*. Vol. 19, pp. 365-376.

Lancaster, P., and K. Salkauskas (1986). *Curve and Surface Fitting*. Academic Press.

Latychev, L., J. X. Mitrovica, M. E. Tamisica, J. Tromp, and R. Moucha (2005). "Influence of lithospheric thickness variations on 3-D crustal velocities due to glacial isostatic adjustment." *Geophys. Res. Lett*., Vol. 32, L01304, doi: 10.1029/2004GL021454.

Lemieux, Y., A. Tremblay, and D. Lavoie (2003). "Structural analysis of supracrustal faults in the Charlevoix area, Quebec: relation to impact cratering and the St-Laurent fault system." *Can. J. Earth Sci./Rev. can. sci. Terre*, Vol. 40, No. 2, 221-235.

Lee, S., G. Wolberg, and S. Y. Shin (1997). "Scattered Data Interpolation with Multilevel B-Splines." *IEEE Transactions on Visualization and Computer Graphics*, Vol. 3, No. 3, pp. 228–244.

Liu, Q. W., and Y. Q. Chen (1998). "Combing the geodetic models of vertical crustal deformation." *Journal of Geodesy*, pp. 673-683. Springer-Verlag.

Liu, Q. W., and T. Parm (1996). "On the vertical deformation models." *Proc 8th FIG International Symposium on deformation measurements*, Hong Kong, 25-28 June.

Lodha, S. K., and R. Franke. (1999). "Scattered Data Techniques for Surfaces." In *Proc. Dagstuhl Conf. Scientific Visualization*, Eds. H. Hagen, G. Nielson, and F. Post, pp. 182-222.

Mainville, A., and M. Craymer (2005). "Present-day tilting of the Great lakes region based on water level gauges." *GSA Bulletin*, Vol. 117, No. 7/8, pp. 1070-1080.

Martinec, Z. (2000). "Spectral–finite element approach to three-dimensional viscoelastic relaxation in a spherical earth." *Geophys. J. Int***,** Vol. 142, pp. 117-137. doi:10.1046/j.1365-246x.2000.00138.x.

Mazzoti, S., T. S. James, J. Henton, and J. Adams (2005). "GPS crustal strain, postglacial rebound, and seismic hazard in eastern North America: The Saint Lawrence Valley example*." J. geophys. Res.,* Vol. 110, B11301, doi: 10.1029/2004JB003590.

Meier, M. F., and J. M. Wahr (2001). "Sea level is rising: Do we know why?" *PNAS, Proceeding of the National Academy of Sciences of the United States of America,* May 14, 2002, Vol. 99, No. 10, pp. 6524-6526.

Meyling, R. H. J. G., and P. R. Pfluger (1990). "Smooth Interpolation to scattered data by bivariate piecewise polynomials of odd degree."*Computer Aided Geometric Design*, Vol. 7, No. 5, pp. 439-458.

Mikhail, E. M. (1976). *Observations and least squares*, New York: IEP.

Mitrovica, J. X., and W. R. Peltier (1991a). "On postglacial geoid subsidence over the equatorial oceans." *J. Geophys. Res*., Vol. 96, No. 20, pp. 53-71.

Mitrovica, J. X., and Peltier W R. (1991b). "A complete formalism for the inversion of post glacial rebound data: resolving power analysis." *Geophys. J. Int.,* Vol. 104, pp. 267-288.

Mitrovica, J. X., and W. R. Peltier (1993). "The inference of mantle viscosity from an inversion of the Fennoscandian relaxation spectrum." *Geophys. J. Int.,* Vol. 114, pp. 45-62.

Mitrovica, J. X., and W. R. Peltier (1995). "Constraints on mantle viscosity based upon inversion of post-glacial uplift data from the Hudson Bay region." *Geophys. J. Int.,* Vol. 122, pp. 353-376.

Moore, D., and J. Warren (1991). "Approximation of dense scattered data using algebraic surfaces." *IEEE, pp.* 681-690.

Morandi, C. M., S. De Marchi, and D. Fasoli (1999). "A Package for Representing C^1 Interpolating Surfaces: Application to the Lagoon of Venice's Bed." *Numerical Algorithms,* Vol. 20, No. 2/ 3, pp. 197–215.

Pagiatakis, S. D. (2003). "Historical relative gravity observations and the time rate of change of gravity due to postglacial rebound and other tectonic movements in Canada." *Journal of geophysical research,* Vol. 108, No. B9, 2406, doi: 1029/2001 JB001676.

Pan, M., and L. E. Sjöberg (1998). "Unification of vertical datums by GPS and gravimetric geoid models with application to Fennoscandia." *Journal of Geodesy*, pp. 64-70, 10.1007/s001900050149.

Park, K., R. S. Nerem, J. L. Davis, M. S. Schenewerk, G. A. Milne, and J. X. Mitrovica (2002). "Investigation of glacial isostatic adjustment in the northeast U.S. using GPS measurements." *Geophys. Res. Lett.,* Vol. 29, No. 11, 1509, doi: 10.1029/2001GL013782.

Peltier, W.R. (1974). "The impulse response of a Maxwell Earth." *Reviews of Geophysics and Space Physics*, Vol. 12, No. 4, pp. 649–669.

Peltier, W. R. (1976). "Glacial isostatic adjustment—II. The inverse problem." *Geophys. J. R. astr. Soc.,* Vol. 46, pp. 669-706.

Peltier, W. R. (1994). "Ice Age Paleotopography." *Science*, Vol. 265, pp. 195-201.

Peltier, W. R. (1996). "Global sea level rise and glacial isostatic adjustment: An analysis of data from the east coast of North America." *geophysical research letters*, Vol. 23, pp. 717-720.

Peltier, W. R. (1998). "The inverse problem for mantle viscosity" *Inverse problems,* Vol. 14, pp. 441-478.

Peltier, W. R. (2001). "Global glacial isostatic adjustment and modern instrumental records of relative sea level history" In *Sea Level Rise: History and Consequences.* Eds. M. S. (EDT) Kearney, S. P. (EDT) Leatherman, B. C. Douglas , Published by Elsevier.

Peltier, W. R. (2002). "On eustatic sea level history: Last Glacial Maximum to Holocene." *Quaternary Science Reviews*, Vol. 21, No. 1, pp.377-396(20).

Peltier, W.R. (2004). "Global glacial isostasy and the surface of the ice-age earth: The ICE-5G (VM2) model and GRACE." *Annual Review of Earth and Planetary Sciences*, Vol. 32, pp. 111-149.doi:10.1146/annurev.earth.32.082503.144359.

Peltier, W. R., and J. T. Andrews (1976). "Glacial isostatic adjustment, I, The forward problem." *Geophys. JR astr. Soc*, Vol. 46, pp. 605-646.

Randot, J. (1968). "Nouvel impact meteoritique fossile, La structure semicirculaire de Charlevoia. " *J. Earth Sci*., Vol. 5, pp. 1305-1317.

Rapp, R. (1994). “Separation between reference surfaces of selected vertical datums.” *Journal of Geodesy*, Vol. 69, doi: 10.1007/BF00807989.

Sabadini, R., D. A. Yuen, and M. Portney (1986). “The effects of upper mantle lateral heterogeneities on postglacial rebound.” *Geophys. Res. Lett.,* Vol. 13, pp. 337-340.

Sella, G. F., T. H. Dixon, and A. Mao (2002). “REVEL: A model for recent plate velocities from space geodesy” *J. Geophys. Res*., Vol. 107(B4), 2081, doi: 10.1029/2000JB000033.

Spada, G., R. Sabadini, D.A. Yuen, and Y. Rocard (1992). “Effects on post-glacial rebound from the hard rheology in the transition zone.” *Geophys. J. Int.*, Vol. 109, pp. 683–700.

Tackmam, G. (1997). Postglacial tilting and lake level changes in Southern Manitoba, PhD thesis, University of Utah, Salt Lake City.

Tait, B. J., and A. P. Bolduc (1985). “An update on rates of apparent vertical movement in the Great Lakes basin.” *Proceedings, Third International Symposium on the North American Vertical Datum*: Rockville, Maryland, National Geodetic Survey, U.S., Department of Commence, 193-206.

Tromp, J., and J.X Mitrovica (1999). “Surface loading of a visco-elastic Earth - i. General theory.” *Geophys. J. Int.*, Vol. 137, pp. 847–855.

Tushingham, A. M. (1992). “Postglacial uplift predictions and historical water levels of the Great Lakes.” *Journal of Great Lakes Research*, Vol. 18, pp. 440-455.

Tushingham, A. M., and W. R. Peltier (1991). “Ice-3G: A new global model of late Pleistocene deglaciation based upon geophysical predications of postglacial relative sea level change.” *J. Geophysics. Res*., Vol. 96, pp. 4497-4523.

Turk, G. (1992). “Re-tiling polygonal surfaces.” In Computer Graphics, Ed. Edwin E. Catmull, *SIGGRAPH '92 Proceedings*, July 1992, Vol. 26, pp. 55- 64.

Van der Wal, W. (2003). **“**Geoid Anomalies due to Low-Viscosity Zones in Glacial Isostatic Adjustment Modeling.” MSc thesis, Delft Institute for Earth-Oriented Space Research, Delft University of Technology.

Vaníček, P. (1976). “Pattern of recent vertical crustal movements in Maritime Canada.” *Can. J. Earth Sci,* Vol. 13, pp. 661-667.

Vaníček, P., and G. Carrera (1993). "Treatment of sea-level records in modeling linear vertical crustal motion." *Proc., CRCM '93*, Kobe, Japan, pp. 305-309.

Vaníček, P., and D. Christodulids (1974). "A method for evaluation of vertical crustal movements from scatted geodetic relevellings." *Can. J. Earth Sci*, Vol. 11, pp. 605-610.

Vaníček, P., and E. Krakiwsky (1986). *Geodesy: The Concepts*, 2nd ed. North-Holland, Amsterdam, Netherlands, 1986.

Vaníček, P., and D. Nagy (1981). "On the compilation of the map of contemporary vertical crustal movements in Canada." *Tectonophysics*, Vol. 71, pp. 75-86.

Vaníček, P., and L. E. Sjöberg (1987). "A note on vertical crustal movement determination techniques." Technical report no. 9, Dept. Geodesy, The Royal Institute of Technology, Stockholm.

Velicogna. I., and J. Wahr (2002). "Postglacial rebound and Earth's viscosity structure from GRACE." *Journal of geophysical research.* 107, NO. 0, XXXX, doi:10.1029/2001JB001735, 2002.

Velímský, J., and Z. Martinec (2005). "Time-domain, spherical harmonic-finite element approach to transient three-dimensional geomagnetic induction in a spherical heterogeneous Earth." *Geophysical Journal International*, Vol. 161, No. 1, pp. 81-101.

Vermeersen, L.L.A., and R. Sabadini (1997). "A new class of stratified visco-elastic models by analytical techniques." *Geophys. J. Int.*, Vol. 139, pp. 530–571.

Warrick, R. A., C. Le Provost, M. F. Meier, J. Oerlemans, and P. A. Woodworth (1996). *Climate Change 1995: The Science of Climate Change*, eds. Houghton, J. T., Meira Filho, L. G., Callander, B. A., Harris, N., Kattenberg, A. & Maskell, K. Cambridge Univ. Press, New York, pp. 359-405.

Wahr J., H. DaZhong and A. Trupin (1995). "Predictions of vertical uplift caused by changing polar ice volumes on a viscoelastic earth." *Geophy. Res. Lett.* , Vol. 22, No. 8, pp. 977–980.

Wolf, D. (1985). "An improved estimate of lithospheric thickness based on a reinterpretation of tilt data from Pleistocene Lake Algonquin" *Can. J. Earth Sci*. Vol. 22, pp. 768-773.

Wolf, D., V. Klemann, J. Wuensch, and F. P. Zhang (2006). "A reanalysis and reinterpretation of geodetic and geological evidence of glacial-isostatic adjustment in the Churchill region, Hudson Bay." *Surv. Geophys*., Vol. 27, pp. 19-61, doi:10.1007/s10712-005-0641-x.

Wu, P. (1978). "The response of a Maxwell Earth to applied surface loads: glacial isostatic adjustment." Master's thesis, University of Toronto.

Wu, P. P. (2002). "Modes coupling in a visco-elastic self-gravitating spherical earth induce by axisymmetric loads and lateral viscosity variations." *Earth and Planet. Sci. Lett.,* Vol. 202, pp. 49-60.

Wu, P. P. (2004). "Using commercial finite element packages for the study of Earth deformation, sea levels and the state of stress." *Geophys. J. Int*., Vol. 158, pp 401. doi:10.1111/j.1365-246X.2004.02338.x

Wu, P. P. (2006). "Sensitivity of relative sea levels and crustal velocities in laurentide to radial and lateral viscosity variations in the mantle." *Geophys. J. Int.* pp, 165-401, 413.doi:10.1111/j.1365-246X.2006.02960.x.

Wu, P. P., Z. Ni, and G. Kaufmann (1998). „Postglacial rebound with lateral heterogeneities: from 2-D to 3-D modeling." In *Dynamics of the ice age earth: a modern perspective*, ed. Wu, P., Trans Tech Publications, Switzerland, pp. 557-582.

Zhong, S., A. Paulson and J. Wahr (2003). "Three-dimensional finite-element modeling of Earth's viscoelastic deformation: effects of lateral variations in lithospheric thickness." *Geophys. J. Int.,* Vol. 155, pp. 679-695.

Zhou. J., N. M. Patrikalakis, S. T. Tuohy, and X. Ye (1997). "Scattered Data Fitting with Simplex Splines in Two and Three Dimensional Spaces." *The Visual Computer, Vol.* 13, No. 7, pp. 295–315.

Appendix I

Gram –Schmidt orthogonalization

According to Gram –Schmidt orthogonalization method, one can write:

$$\forall i = 1 : l : \boldsymbol{\varphi}_i^* = \sum_{j=1}^{i-1} \boldsymbol{\alpha}_{ij} \boldsymbol{\varphi}_j^* + \boldsymbol{\varphi}_i \tag{a. 1}$$

This can be done in the following steps:

- $\boldsymbol{\varphi}_1^* = \boldsymbol{\varphi}_1$ (a. 2)
- $\boldsymbol{\varphi}_2^* = \boldsymbol{\alpha}_{21}\boldsymbol{\varphi}_1^* + \boldsymbol{\varphi}_2 = \boldsymbol{\alpha}_{21}\boldsymbol{\varphi}_1 + \boldsymbol{\varphi}_2$ (a. 3)

But $\left\langle \phi_2^*, \phi_1^* \right\rangle = 0$

$$\begin{aligned} &\Rightarrow \alpha_{21}\left\langle \phi_1^*, \phi_1^* \right\rangle + \left\langle \phi_2, \phi_1^* \right\rangle = 0 \\ &\Rightarrow \alpha_{21} = -\left\langle \phi_2, \phi_1^* \right\rangle / \left\langle \phi_1^*, \phi_1^* \right\rangle \\ &\alpha_{21} = -\left\langle \phi_2, \phi_1^* \right\rangle / \left\| \phi_1^* \right\|^2 \end{aligned} \tag{a. 4}$$

- $\phi_3^* = \alpha_{31}\phi_1^* + \alpha_{32}\phi_2^* + \phi_3 = (\alpha_{31} + \alpha_{32}\alpha_{21})\phi_1 + \alpha_{32}\phi_2 + \phi_3$ (a. 5)

But $\left\langle \phi_3^*, \phi_1^* \right\rangle = 0$ and $\left\langle \phi_3^*, \phi_2^* \right\rangle = 0$

$$\begin{aligned} &\Rightarrow \alpha_{31}\left\langle \phi_1^*, \phi_1^* \right\rangle + \alpha_{32}\left\langle \phi_2^*, \phi_1^* \right\rangle + \left\langle \phi_3, \phi_1^* \right\rangle = 0 \\ &\Rightarrow \alpha_{31}\left\langle \phi_1^*, \phi_2^* \right\rangle + \alpha_{32}\left\langle \phi_2^*, \phi_2^* \right\rangle + \left\langle \phi_3, \phi_2^* \right\rangle = 0 \\ &\Rightarrow \alpha_{31} = -\left\langle \phi_3, \phi_1^* \right\rangle / \left\| \phi_1^* \right\|^2 \\ &\Rightarrow \alpha_{32} = -\left\langle \phi_3, \phi_2^* \right\rangle / \left\| \phi_2^* \right\|^2 \end{aligned} \tag{a. 6}$$

Generally

$$\alpha_{ij} = -\left\langle \phi_i, \phi_j^* \right\rangle / \left\| \phi_j^* \right\|^2 \tag{a. 7}$$

$$\underline{\Phi}^* = \underline{\mathbf{T}}\underline{\Phi}, \tag{a. 8}$$

Where

$$\underline{\mathbf{T}} = \begin{bmatrix} 1 & 0 & \ldots & & 0 \\ \alpha_{21} & 1 & 0 & \ldots & 0 \\ \alpha_{31} + \alpha_{32}\alpha_{21} & \alpha_{32} & 1 & 0 & \ldots & 0 \\ : & : & : & : & & : \\ : & : & : & : & & : \\ \alpha_{u1} + \ldots & \alpha_{u2} + \ldots & \ldots & : & & 1 \end{bmatrix} \qquad \text{(a. 9)}$$

Inverse Trasformation; (De-orthogonalization)

$$\underline{\Phi} = \underline{\mathbf{T}^*}\underline{\Phi}^*, \qquad \text{(a. 10)}$$

Where

$$\underline{\mathbf{T}^*} = \begin{bmatrix} 1 & 0 & \ldots & & 0 \\ -\alpha_{21} & 1 & 0 & \ldots & 0 \\ -\alpha_{31} & -\alpha_{32} & 1 & 0 & \ldots & 0 \\ : & : & : & : & & : \\ : & : & : & : & & : \\ -\alpha_{u1} & -\alpha_{u2} & \ldots & : & & 1 \end{bmatrix} \qquad \text{(a. 11)}$$

Appendix II

A full description of the re-levelling data extraction algorithm

The corrected height differences for all the leveling segments in Canada are in a source file (VERT_DISC_MEAN_ELEV_DIFF.*).The succession of the stations on the levelling lines was obtained by following the link number and section number. A levelling line is divided in link and the link is divided in section and the section is divided in running. Each sequential section number is sequential on the levelling line. The length of a section and link can vary. For example, one link can be found with 2 sections and another link can have 150 sections. The same is for the link. Part of this file is shown in Table b.1.

LINE_ID and STATION_NO in the file give some useful information. In the STATION_NO(For example 69U010), the first 2 characters is the year the BM was put in the ground (not necessarily observed). It may have been observed in 1970 and 1993. The 3rd character tells us the province. The codes are given in the file SDNumbering format in GDS (Please see SDNumbering Format in the levelling database of GSD NRCan). D means the work was levelled by the province of Ontario. The 4-6 or 4-7 characters are a sequential number, numbering the BMs for that year in that province. The 3rd character is also a code for the province. There are also about 80000 permanent first order BMs in Canada (Mainville, Personal communication)

As for LINE_ID (For example 111D74740115), the first 3 characters (here 111) is a number) ranging from 1 to 525, each representing a basic route (almost like a road system) in Canada (There are some special cases though, e.g., the number 885, 886, 887, 888, 889, 998 and 999). The 4th character (here D) is the code for the province, same province code as for STATION_NO. The 5-6 characters is the year the line was first observed here 1974. The 7-8 characters are the year of the current observation. So, 111D7474 means it is the 1st time line 111D is observed. LINE_ID 111D74880443A means the line 111D was re-leveled in 1988. Hence, this is a key to find the re-leveled

sections. The characters 9-12 is a job number, it links all the levelling line done by a party chief that year, e.g. 115 or 443 above. 443A and 443B means that the party chief observed two networks that year.

Table b.1: Part of this file VERT_DISC_MEAN_ELEV_DIFF.

LINE_ID	link#	section#	STATION_1	STATION_2	dh	distance
116M22220335A	2	2	22M*0564	22M*0565	1.63600004	-.62545
116M22220335A	2	3	22M*0565	22M*0566	1.59500003	.94671
116M22220335A	2	4	22M*0566	22M*0567	1.64400005	.28209
116M22220335A	2	5	22M*0567	22M4K	.654999971	3.4351
116M22220335A	2	6	22M4K	22M*0568	1.57500005	-.43312
116M22220335A	2	7	22M*0568	22M*0569	1.42499995	.60076
116M22220335A	2	8	22M*0569	22M5K2	1.44099998	-5.09229
116M22220335A	2	9	22M5K2	22M5K	.846000016	13.27114
116D75890564	4	8	75D8041	89D*0002	2.2349999	-4.63539
116D75890564	4	9	89D*0002	75D8039	1.648	-.51792
116D75890564	4	10	75D8039	75D8038	1.68900001	7.53709
116D75890564	4	11	75D8038	88U526	1.13	-4.98189
116D75890564	4	13	75D8036	75D8035	1.602	10.07133
116D75890564	4	14	75D8035	75D8034	1.66199994	10.28009
116D75890564	4	15	75D8034	75D8033	1.74300003	2.46283
116D75890564	4	16	75D8033	75D8032	2.33599997	.64731
116D75890564	4	17	75D8032	75D8031	1.28900003	-5.62845
116M22220335A	1	1	22M004	22M1K	.833999991	3.53797
116M22220335A	1	2	22M1K	22M*0552	1.31400001	-.99319
116M22220335A	1	3	22M*0552	22M*0553	1.32000005	-.7908
116M22220335A	1	4	22M*0553	22M*0554	1.83000004	.69937
116M22220335A	1	5	22M*0554	22M*0555	1.39199996	-.3717

To retrieve the relevelled segments from this file, the following steps were done:

1- Classifying the file into smaller files for each leveling line surveyed in each year for a specific province, and making an organized database based on the province and levelling line. The output of this step looks as:

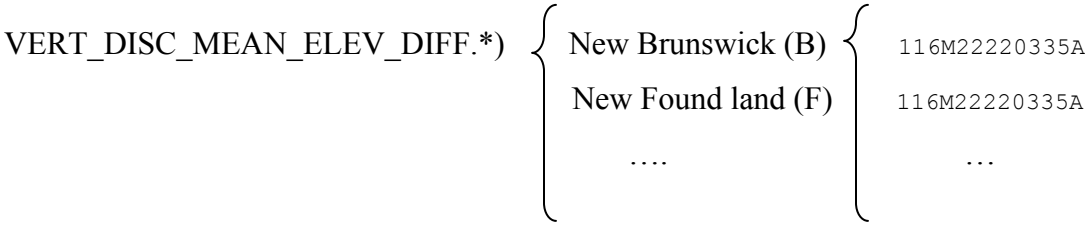

2- Extract those leveling lines that are shown in two different years from the leveling line name. For example, 111D7474 means it is the 1st time line 111D is observed. LINE_ID 111D74880443A means the line 111D was re-leveled in 1988.

3- Sorting the retrieved leveling line as for the link number and section number to facilitate the succession of the stations on the levelling lines. This was one of the main steps. The output of this step is shown diagrammatically in Figure b.1.

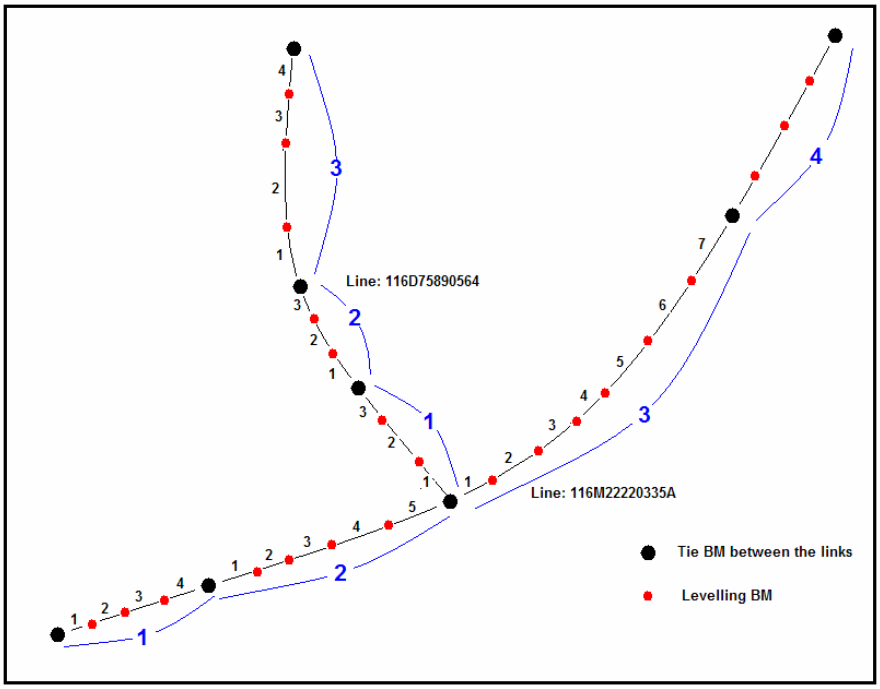

Figure b. 1 Sorting the retrieved leveling line as for the link number and section number

4- Producing a file containing Bm1_id, Bm2_id, Line_id, Cumul_link_no, Cumul_section_no, where Cumul_link_no and Cumul_section_no are all possible first 10 combination of the sections in a leveling line.

In Figure b.2, for example, the levelling information for the following succession were created.

A>B, A>C, A>D, B>C, B>D and C>D

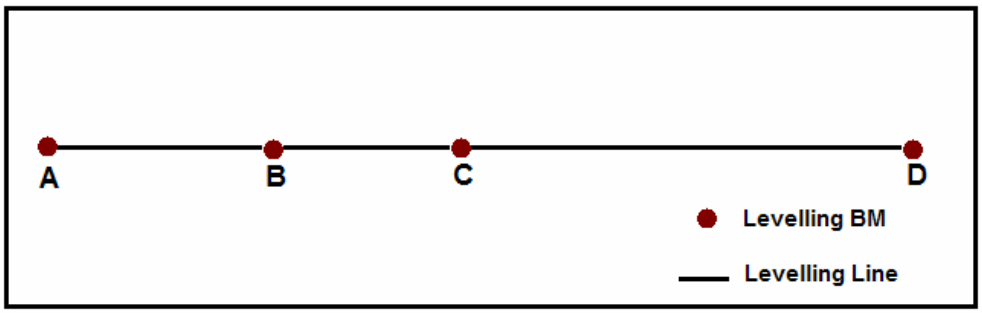

Figure b. 2 combination of leveling segments to retrieve all possible re-leveling information.

```
68S218   , 77S3001  , 001S77770064e.prn,   1,   1,
68S218   , 77S*0001 , 001S77770064e.prn,   1,   2,
68S218   , 77S001   , 001S77770064e.prn,   1,   3,
68S218   , 77S*0012 , 001S77770064e.prn,   1,   4,
68S218   , 68S167   , 001S77770064e.prn,   1,   5,
68S218   , 60S087   , 001S77770064e.prn,   1,   6,
68S218   , 68S166   , 001S77770064e.prn,   1,   7,
68S218   , 60S088   , 001S77770064e.prn,   1,   8,
68S218   , 77S002   , 001S77770064e.prn,   1,   9,
68S218   , 60S089   , 001S77770064e.prn,   1,  10,
68S218   , 77S003   , 001S77770064e.prn,   1,  11,
77S3001  , 77S*0001 , 001S77770064e.prn,   2,   2,
77S3001  , 77S001   , 001S77770064e.prn,   2,   3,
77S3001  , 77S*0012 , 001S77770064e.prn,   2,   4,
77S3001  , 68S167   , 001S77770064e.prn,   2,   5,
77S3001  , 60S087   , 001S77770064e.prn,   2,   6,
77S3001  , 68S166   , 001S77770064e.prn,   2,   7,
77S3001  , 60S088   , 001S77770064e.prn,   2,   8,
77S3001  , 77S002   , 001S77770064e.prn,   2,   9,
77S3001  , 60S089   , 001S77770064e.prn,   2,  10,
77S3001  , 77S003   , 001S77770064e.prn,   2,  11,
77S3001  , 77S004   , 001S77770064e.prn,   2,  12,
77S*0001 , 77S001   , 001S77770064e.prn,   3,   3,
77S*0001 , 77S*0012 , 001S77770064e.prn,   3,   4,
77S*0001 , 68S167   , 001S77770064e.prn,   3,   5,
77S*0001 , 60S087   , 001S77770064e.prn,   3,   6,
```

5- The searching of re-leveled data is done in the combination file, searching all the repeated combinations in two different years, and once the re-leveled section is found, the link number and section number are retrieved to use for cumulation of the height difference and distance.

Table b.2 : The output re-leveled information file

```
-----------------------------------------------------------------------------------------------
77S008    77S009    001S77770064e.prn 001S77930590e.prn -8.381 -8.389 2.5420
77S009    77S013    001S77770064e.prn 001S77930590e.prn -1.289 -1.280 6.6810
77S013    77S015    001S77770064e.prn 001S77930590e.prn -6.876 -6.882 3.3020
77S015    77S016    001S77770064e.prn 001S77930590e.prn -0.042 -0.042 0.8590
77S011    12S7DR    001S77770064e.prn 001S77930590e.prn  0.559  0.558 0.0920
12S7DR    77S012    001S77770064e.prn 001S77930590e.prn -1.494 -1.492 0.6600
```

Appendix III

The use of spatial analysis in finding the adjacency of the close-by tide gauges for differencing analysis

First, GIS is used to find the adjacent tide gauges. Using the adjacency facility in ArcGIS software, the tide gauges which are close to each node station are located. In other words, the closest *n* gauges to each node are determined. The radius of the adjacency can be different from node to node depending on the distribution of the tide gauges locations. In this study, the value of 500 km was set for the adjacency of the gauges to a node site. Figure (c.1) shows the tide gauges that are close to Charlottetown, considered as a node site.

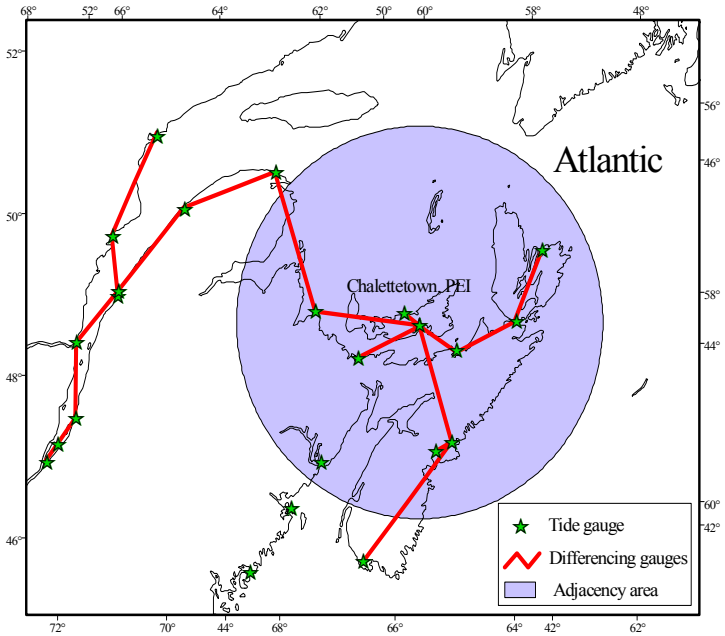

Figure c. 1: The optimum tree diagram of tide-gauges for differencing. The tide gauges inside the circle boundary are adjacent to Charlottetown.

Appendix IV

The time series of monthly mean sea level records of the tide gauges, the linear trends and their standard deviations

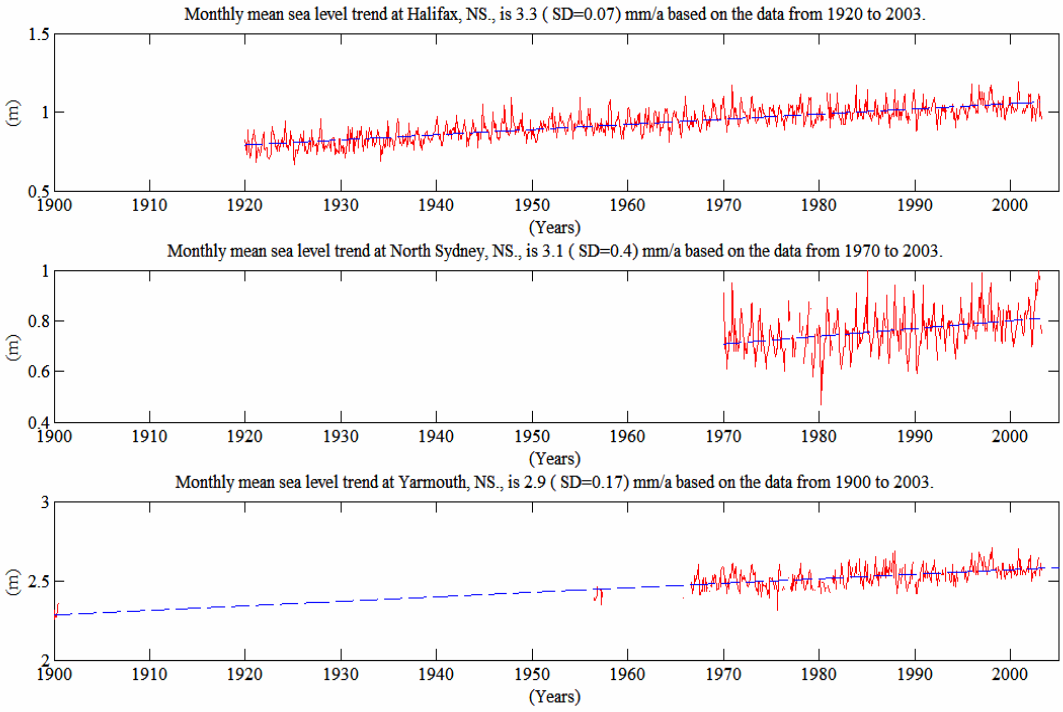

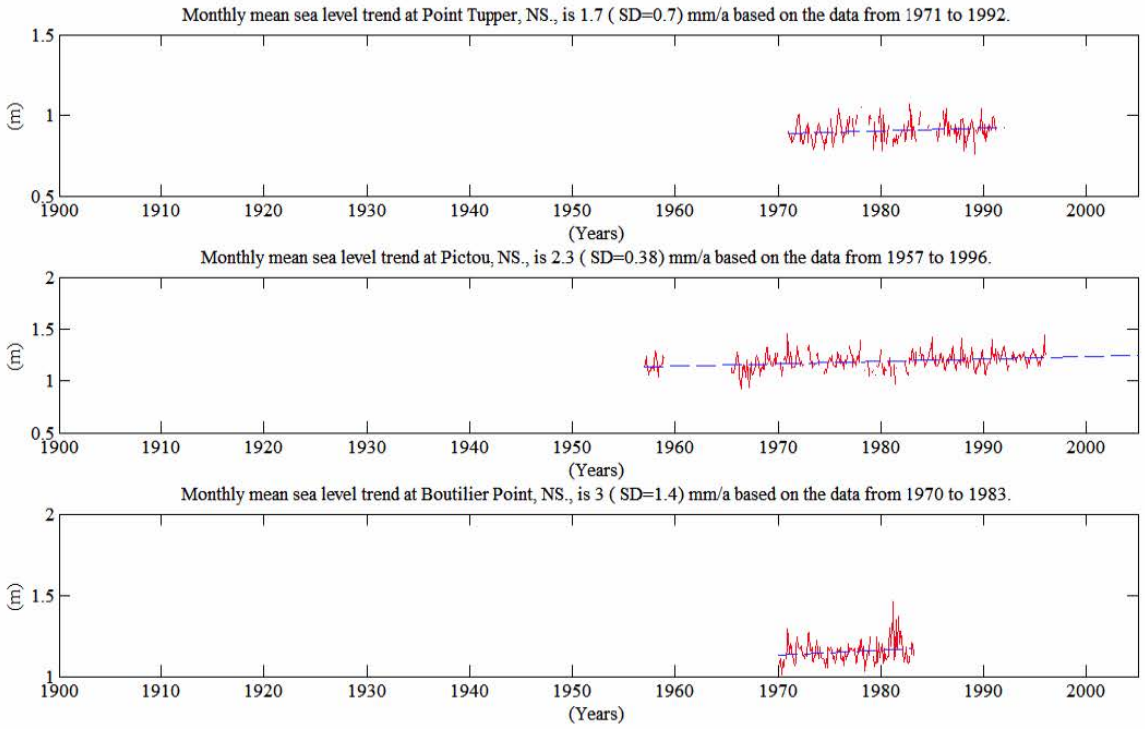
Monthly mean sea level trend at Point Tupper, NS., is 1.7 (SD=0.7) mm/a based on the data from 1971 to 1992.
(m)
(Years)
Monthly mean sea level trend at Pictou, NS., is 2.3 (SD=0.38) mm/a based on the data from 1957 to 1996.
(m)
(Years)
Monthly mean sea level trend at Boutilier Point, NS., is 3 (SD=1.4) mm/a based on the data from 1970 to 1983.
(m)
(Years)

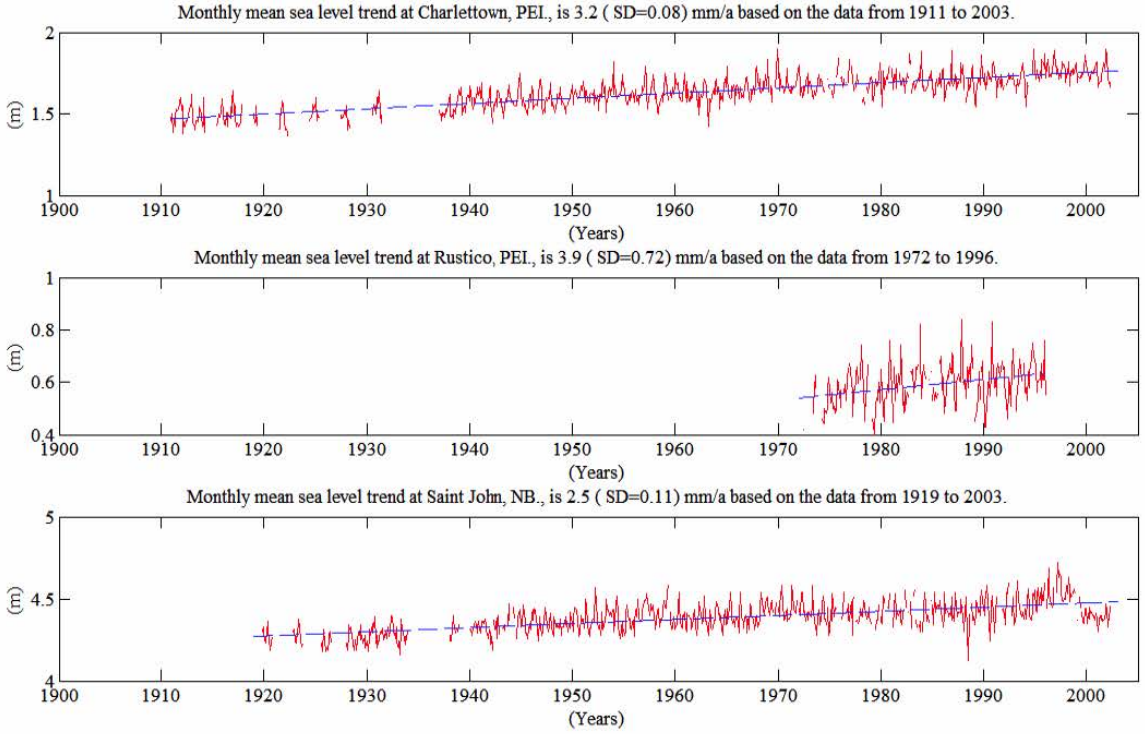
Monthly mean sea level trend at Charlettown, PEI., is 3.2 (SD=0.08) mm/a based on the data from 1911 to 2003.
(m)
(Years)
Monthly mean sea level trend at Rustico, PEI., is 3.9 (SD=0.72) mm/a based on the data from 1972 to 1996.
(m)
(Years)
Monthly mean sea level trend at Saint John, NB., is 2.5 (SD=0.11) mm/a based on the data from 1919 to 2003.
(m)
(Years)

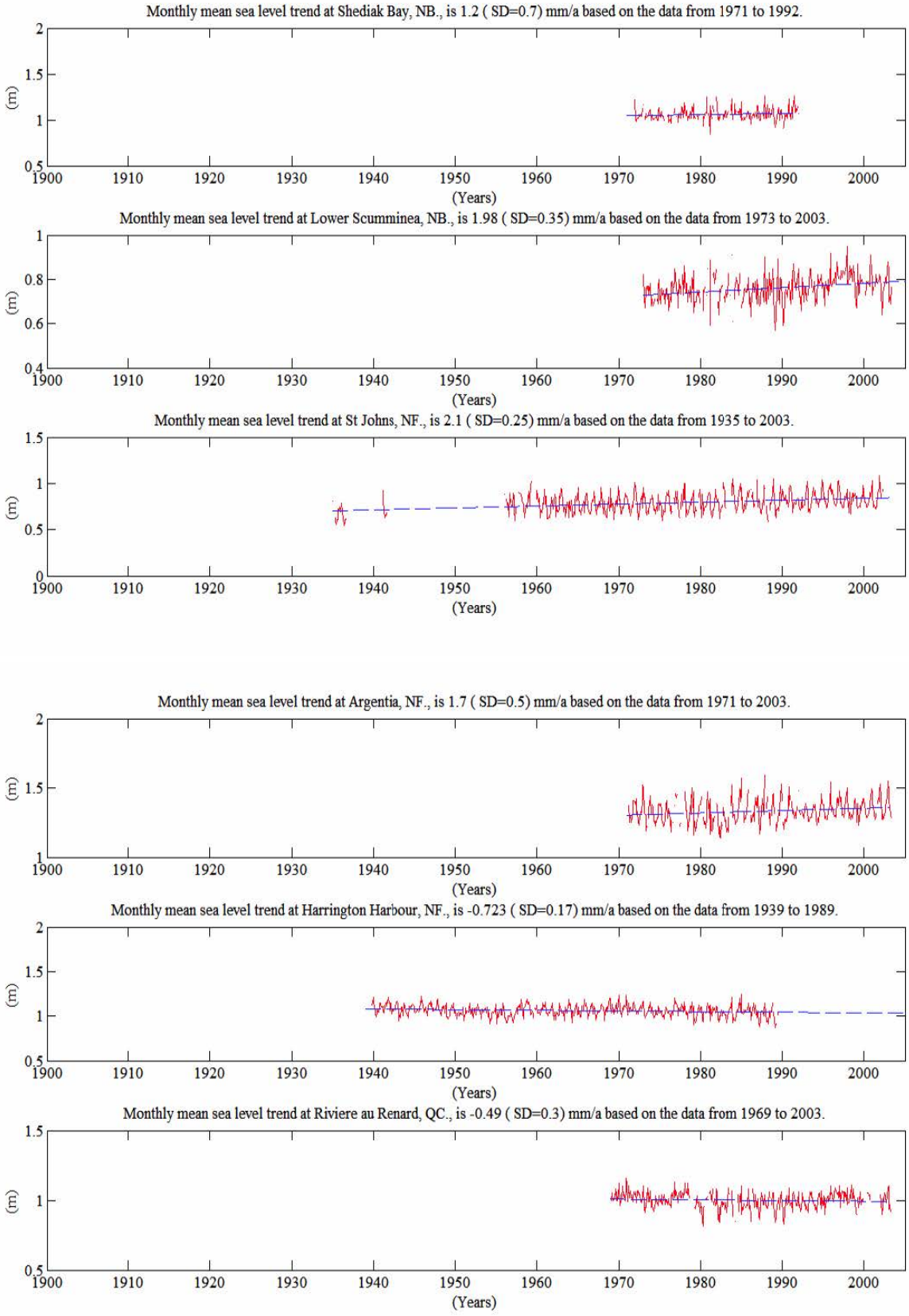
Monthly mean sea level trend at Shediak Bay, NB., is 1.2 (SD=0.7) mm/a based on the data from 1971 to 1992.
(m)
(Years)
Monthly mean sea level trend at Lower Scumminea, NB., is 1.98 (SD=0.35) mm/a based on the data from 1973 to 2003.
(m)
(Years)
Monthly mean sea level trend at St Johns, NF., is 2.1 (SD=0.25) mm/a based on the data from 1935 to 2003.
(m)
(Years)
Monthly mean sea level trend at Argentia, NF., is 1.7 (SD=0.5) mm/a based on the data from 1971 to 2003.
(m)
(Years)
Monthly mean sea level trend at Harrington Harbour, NF., is -0.723 (SD=0.17) mm/a based on the data from 1939 to 1989.
(m)
(Years)
Monthly mean sea level trend at Riviere au Renard, QC., is -0.49 (SD=0.3) mm/a based on the data from 1969 to 2003.
(m)
(Years)

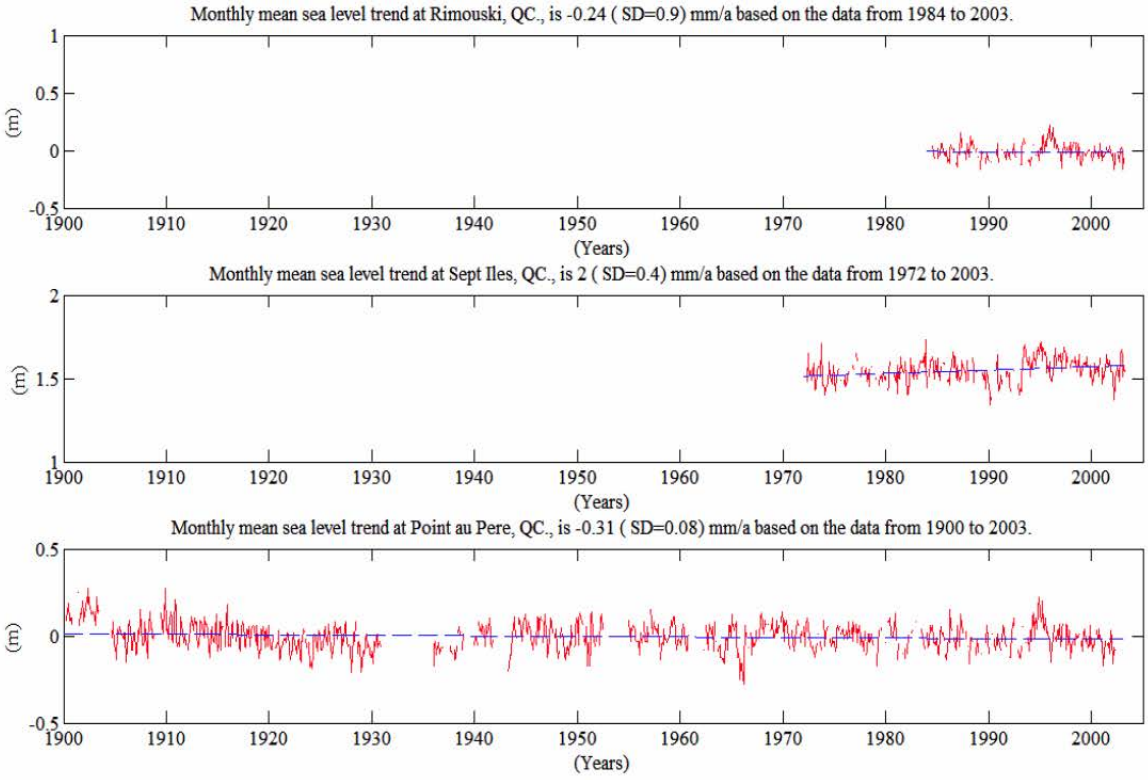
Monthly mean sea level trend at Rimouski, QC., is -0.24 (SD=0.9) mm/a based on the data from 1984 to 2003.
(m)
(Years)
Monthly mean sea level trend at Sept Iles, QC., is 2 (SD=0.4) mm/a based on the data from 1972 to 2003.
(m)
(Years)
Monthly mean sea level trend at Point au Pere, QC., is -0.31 (SD=0.08) mm/a based on the data from 1900 to 2003.
(m)
(Years)

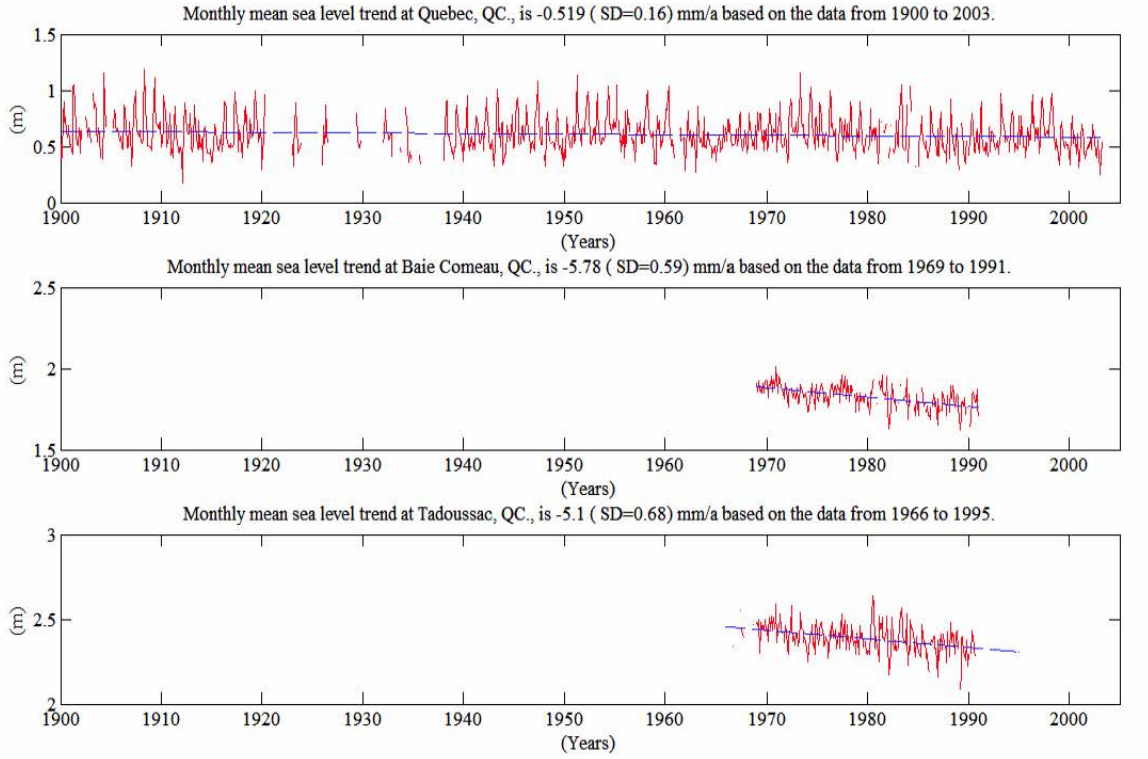
Monthly mean sea level trend at Quebec, QC., is -0.519 (SD=0.16) mm/a based on the data from 1900 to 2003.
(m)
(Years)
Monthly mean sea level trend at Baie Comeau, QC., is -5.78 (SD=0.59) mm/a based on the data from 1969 to 1991.
(m)
(Years)
Monthly mean sea level trend at Tadoussac, QC., is -5.1 (SD=0.68) mm/a based on the data from 1966 to 1995.
(m)
(Years)

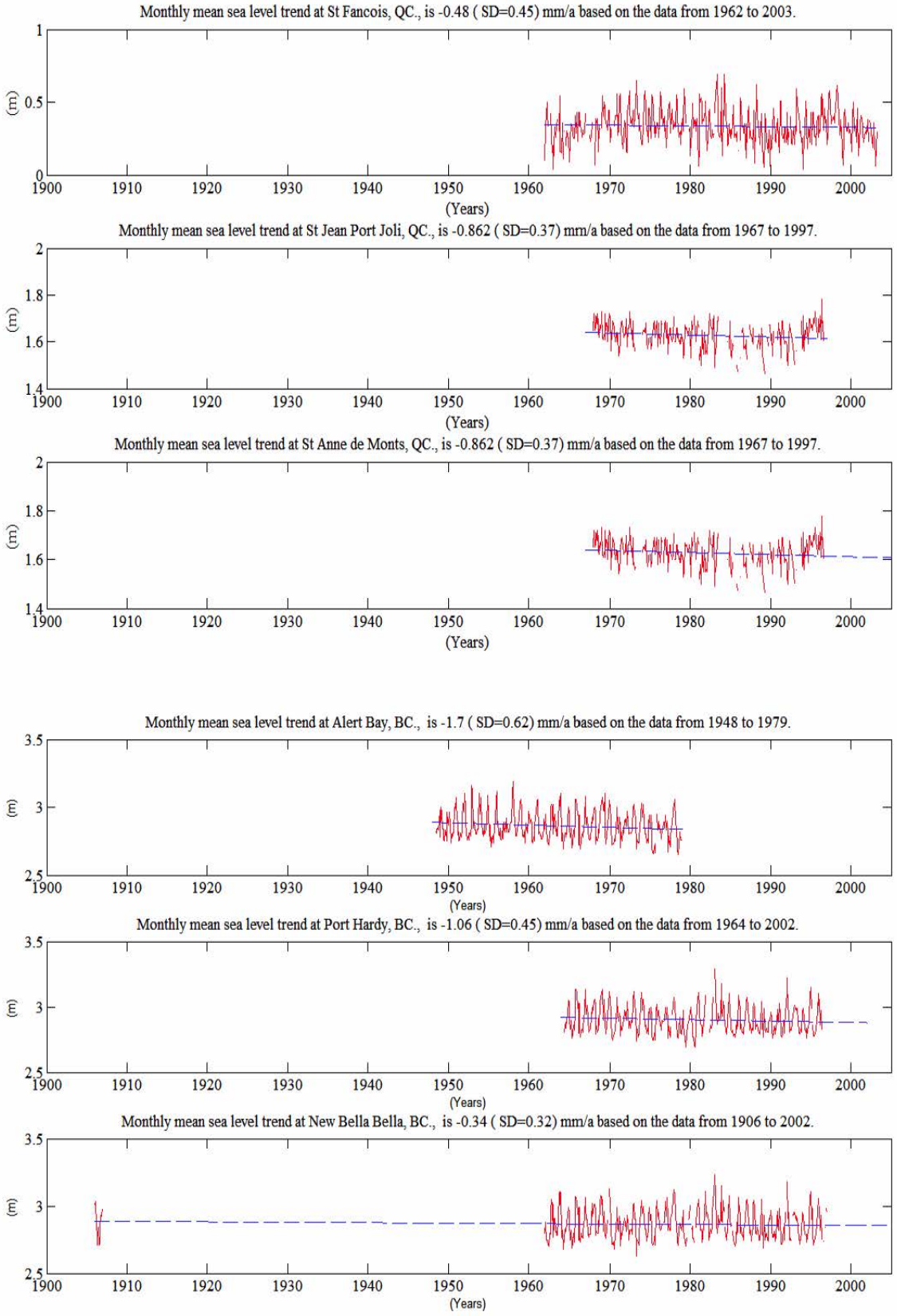
Monthly mean sea level trend at St Fancois, QC., is -0.48 (SD=0.45) mm/a based on the data from 1962 to 2003.
(m)
(Years)
Monthly mean sea level trend at St Jean Port Joli, QC., is -0.862 (SD=0.37) mm/a based on the data from 1967 to 1997.
(m)
(Years)
Monthly mean sea level trend at St Anne de Monts, QC., is -0.862 (SD=0.37) mm/a based on the data from 1967 to 1997.
(m)
(Years)
Monthly mean sea level trend at Alert Bay, BC., is -1.7 (SD=0.62) mm/a based on the data from 1948 to 1979.
(m)
(Years)
Monthly mean sea level trend at Port Hardy, BC., is -1.06 (SD=0.45) mm/a based on the data from 1964 to 2002.
(m)
(Years)
Monthly mean sea level trend at New Bella Bella, BC., is -0.34 (SD=0.32) mm/a based on the data from 1906 to 2002.
(m)
(Years)

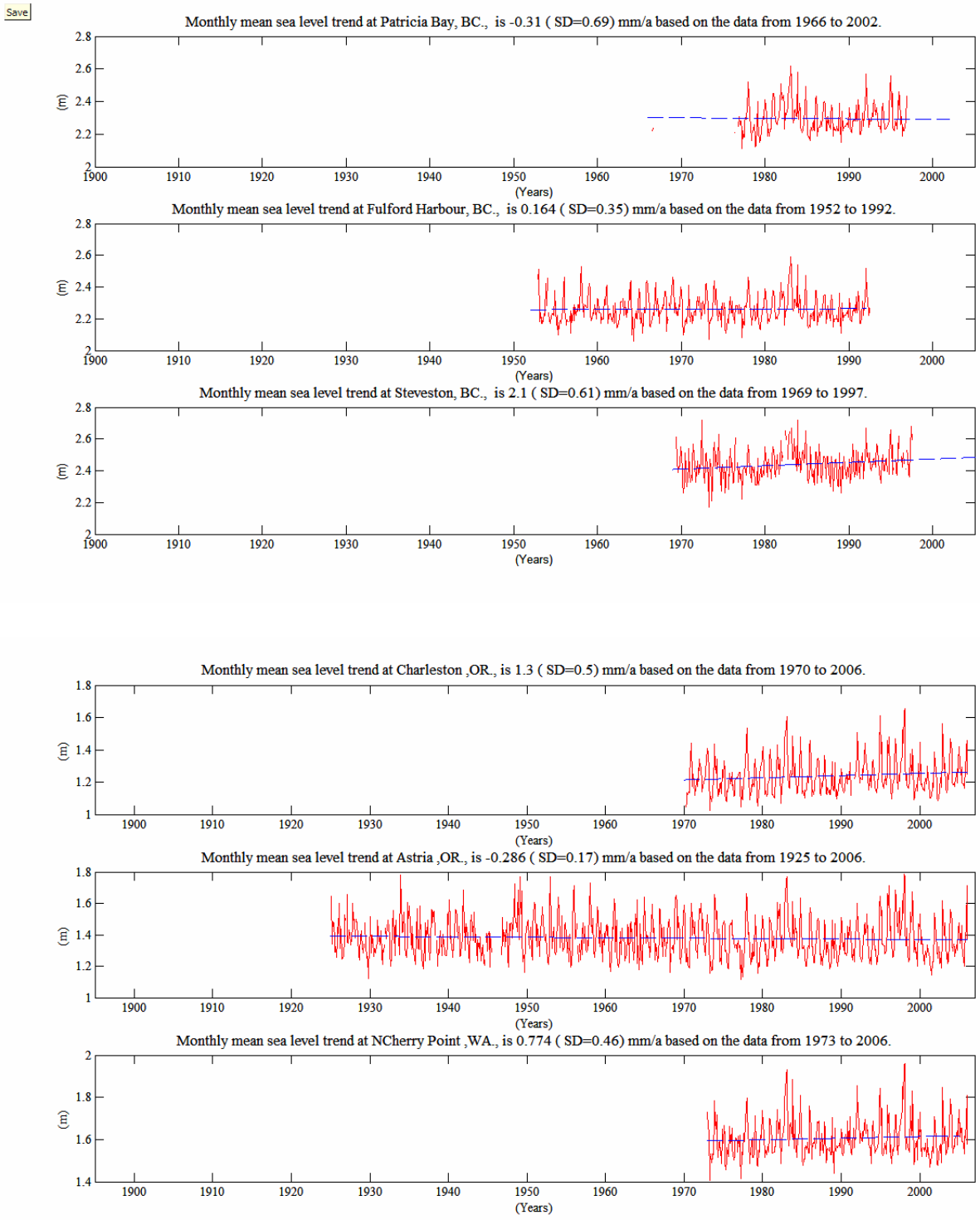
Save
Monthly mean sea level trend at Patricia Bay, BC., is -0.31 (SD=0.69) mm/a based on the data from 1966 to 2002.
Monthly mean sea level trend at Fulford Harbour, BC., is 0.164 (SD=0.35) mm/a based on the data from 1952 to 1992.
Monthly mean sea level trend at Steveston, BC., is 2.1 (SD=0.61) mm/a based on the data from 1969 to 1997.
Monthly mean sea level trend at Charleston ,OR., is 1.3 (SD=0.5) mm/a based on the data from 1970 to 2006.
Monthly mean sea level trend at Astria ,OR., is -0.286 (SD=0.17) mm/a based on the data from 1925 to 2006.
Monthly mean sea level trend at NCherry Point ,WA., is 0.774 (SD=0.46) mm/a based on the data from 1973 to 2006.
(m)
(Years)

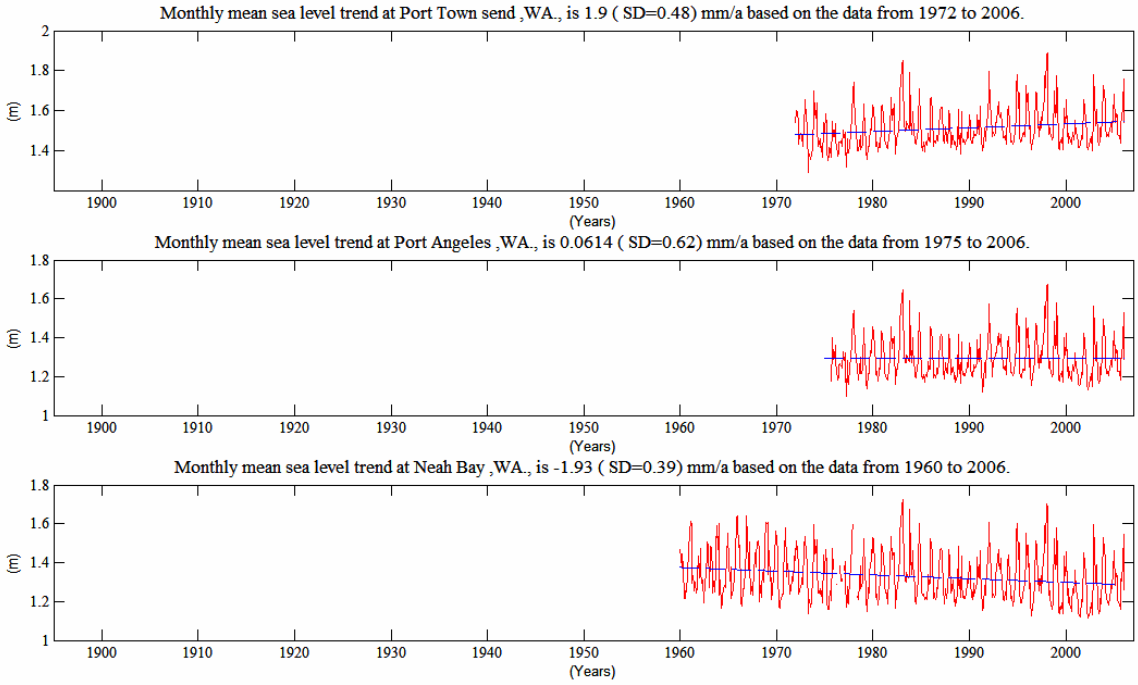
Monthly mean sea level trend at Port Town send ,WA., is 1.9 (SD=0.48) mm/a based on the data from 1972 to 2006.
Monthly mean sea level trend at Port Angeles ,WA., is 0.0614 (SD=0.62) mm/a based on the data from 1975 to 2006.
Monthly mean sea level trend at Neah Bay ,WA., is -1.93 (SD=0.39) mm/a based on the data from 1960 to 2006.
(m)
(Years)

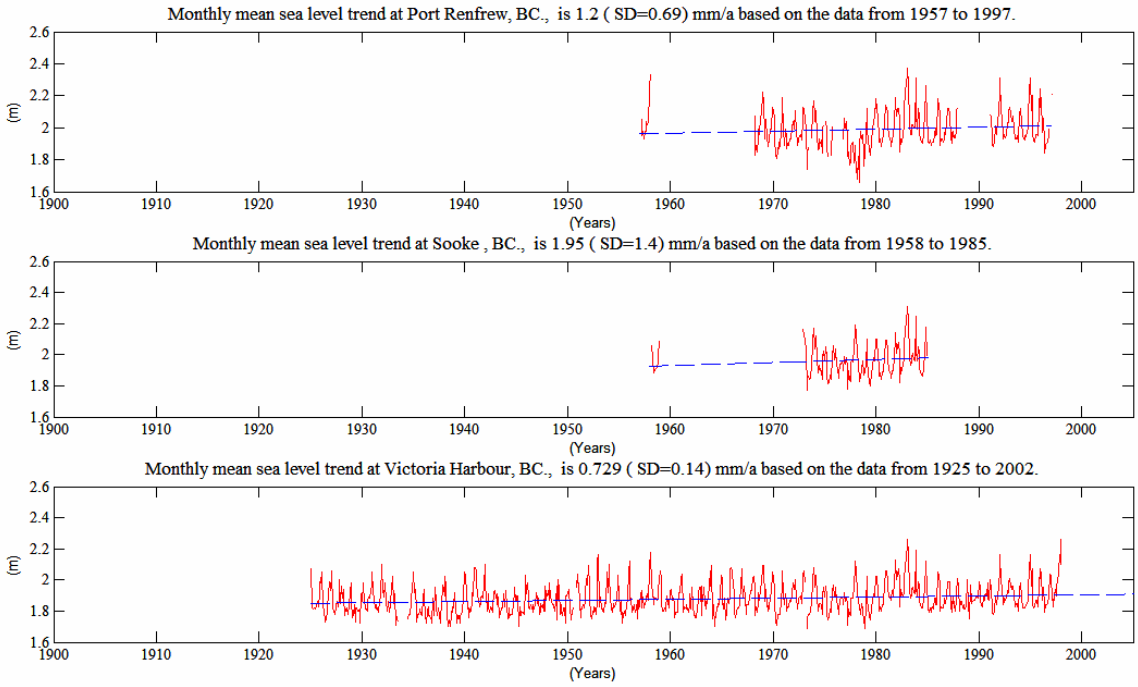
Monthly mean sea level trend at Port Renfrew, BC., is 1.2 (SD=0.69) mm/a based on the data from 1957 to 1997.
Monthly mean sea level trend at Sooke , BC., is 1.95 (SD=1.4) mm/a based on the data from 1958 to 1985.
Monthly mean sea level trend at Victoria Harbour, BC., is 0.729 (SD=0.14) mm/a based on the data from 1925 to 2002.
(m)
(Years)

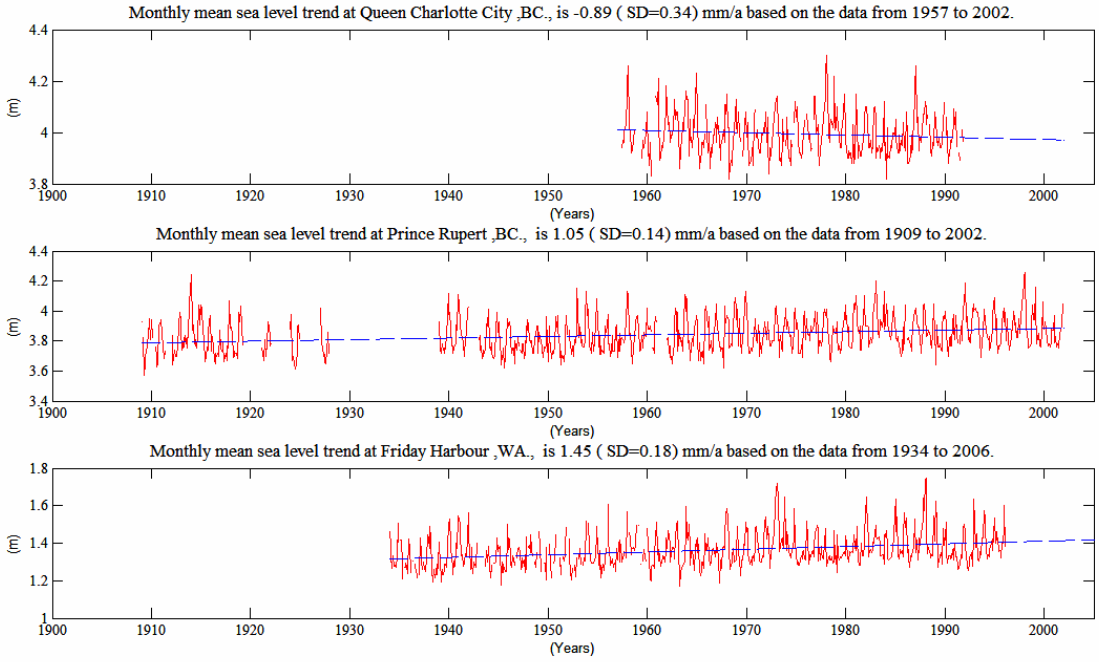
Monthly mean sea level trend at Queen Charlotte City ,BC., is -0.89 (SD=0.34) mm/a based on the data from 1957 to 2002.
Monthly mean sea level trend at Prince Rupert ,BC., is 1.05 (SD=0.14) mm/a based on the data from 1909 to 2002.
Monthly mean sea level trend at Friday Harbour ,WA., is 1.45 (SD=0.18) mm/a based on the data from 1934 to 2006.
(m)
(Years)

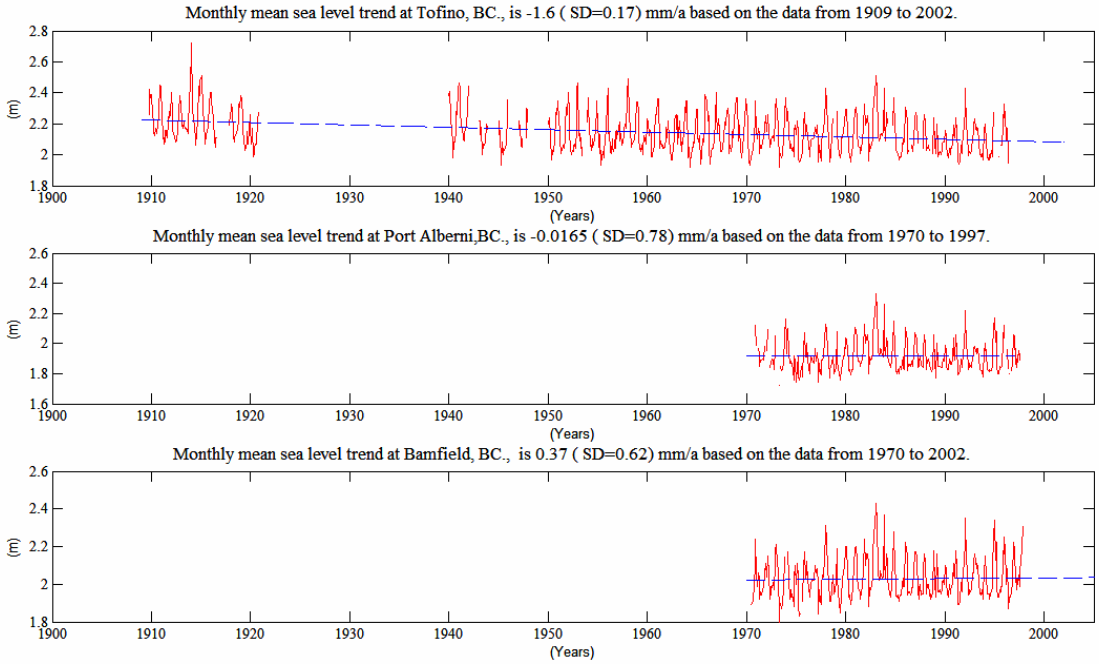
Monthly mean sea level trend at Tofino, BC., is -1.6 (SD=0.17) mm/a based on the data from 1909 to 2002.
Monthly mean sea level trend at Port Alberni,BC., is -0.0165 (SD=0.78) mm/a based on the data from 1970 to 1997.
Monthly mean sea level trend at Bamfield, BC., is 0.37 (SD=0.62) mm/a based on the data from 1970 to 2002.
(m)
(Years)

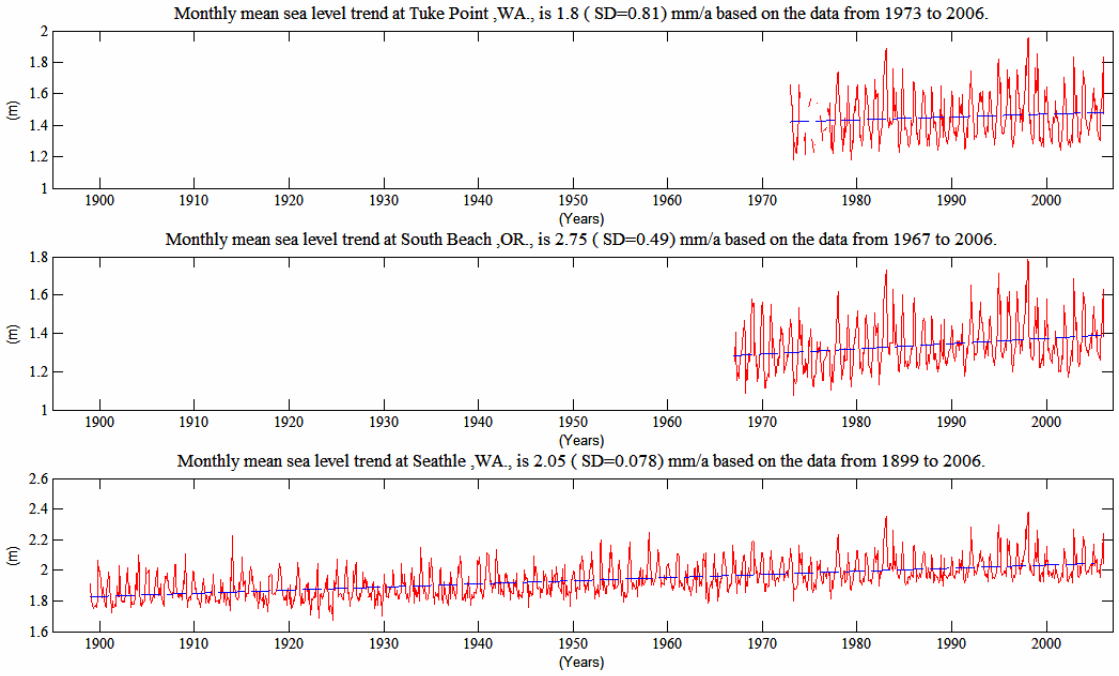
Monthly mean sea level trend at Tuke Point ,WA., is 1.8 (SD=0.81) mm/a based on the data from 1973 to 2006.
Monthly mean sea level trend at South Beach ,OR., is 2.75 (SD=0.49) mm/a based on the data from 1967 to 2006.
Monthly mean sea level trend at Seathle ,WA., is 2.05 (SD=0.078) mm/a based on the data from 1899 to 2006.
(m)
(Years)

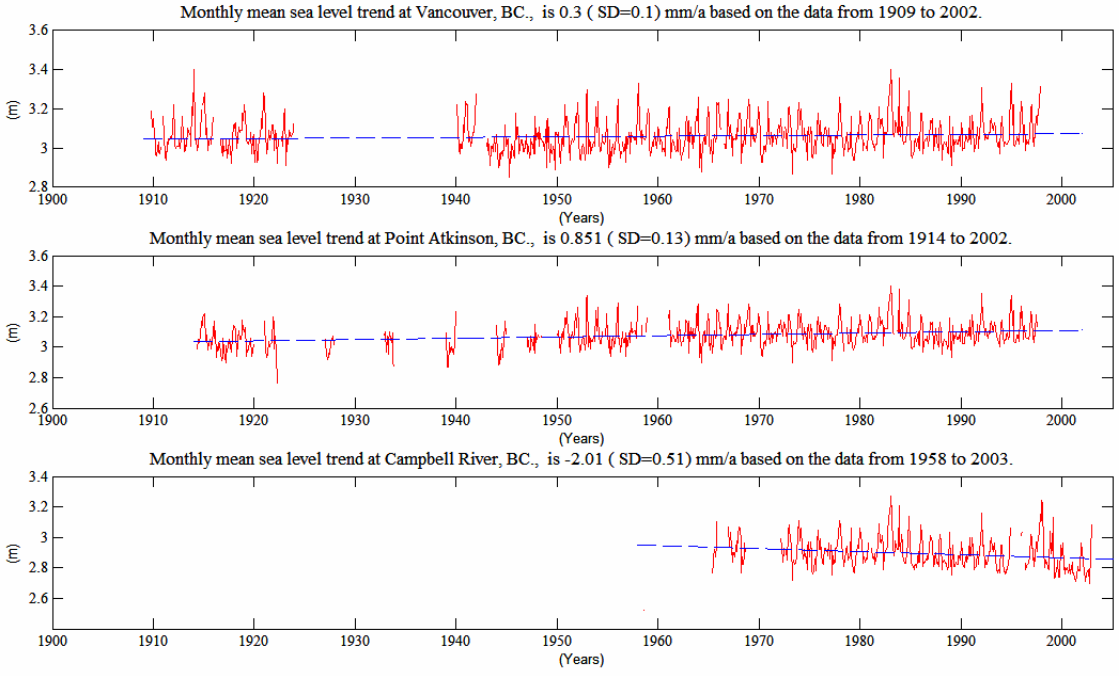
Monthly mean sea level trend at Vancouver, BC., is 0.3 (SD=0.1) mm/a based on the data from 1909 to 2002.
Monthly mean sea level trend at Point Atkinson, BC., is 0.851 (SD=0.13) mm/a based on the data from 1914 to 2002.
Monthly mean sea level trend at Campbell River, BC., is -2.01 (SD=0.51) mm/a based on the data from 1958 to 2003.
(m)
(Years)

Appendix V

Correlation Coefficients between the records of the tide gauges in Atlantic coast, Great Lakes and Pacific coast

==========Atlantic coast==========

r =

Columns 1 through 11

1.0000	0.7934	0.7753	-0.3721	0.9167	0.6414	0.5190	-0.2020	-0.4534	0.5137	0.6502
0.7934	1.0000	0.6116	-0.3846	0.8720	0.6853	0.6929	0.5277	-0.3353	0.2002	0.7092
0.7753	0.6116	1.0000	-0.4639	0.7067	0.5700	0.5771	0.1603	-0.4668	0.3370	0.4731
-0.3721	-0.3846	-0.4639	1.0000	-0.4294	-0.3579	-0.2986	0.0573	0.6080	-0.4345	-0.3807
0.9167	0.8720	0.7067	-0.4294	1.0000	0.7854	0.7950	0.1786	-0.4226	0.5370	0.7087
0.6414	0.6853	0.5700	-0.3579	0.7854	1.0000	0.6180	0.7231	-0.1141	0.6223	0.4920
0.5190	0.6929	0.5771	-0.2986	0.7950	0.6180	1.0000	0.2983	-0.2290	0.4736	0.6513
-0.2020	0.5277	0.1603	0.0573	0.1786	0.7231	0.2983	1.0000	0.4736	-0.3915	-0.2148
-0.4534	-0.3353	-0.4668	0.6080	-0.4226	-0.1141	-0.2290	0.4736	1.0000	-0.6478	-0.5751
0.5137	0.2002	0.3370	-0.4345	0.5370	0.6223	0.4736	-0.3915	-0.6478	1.0000	0.8131
0.6502	0.7092	0.4731	-0.3807	0.7087	0.4920	0.6513	-0.2148	-0.5751	0.8131	1.0000
0.9167	0.8720	0.7067	-0.4294	1.0000	0.7854	0.7950	0.1786	-0.4226	0.5370	0.7087
-0.5071	0.0731	0.1061	0.1443	-0.4026	0.0132	0.2116	0.1143	-0.2029	0.0912	0.1431
0.0328	-0.3150	0.0180	0.0850	-0.0795	0.1045	-0.0208	-0.0693	0.1672	0.0545	-0.1379
0.4304	0.4895	0.2998	-0.1880	0.4101	0.5444	0.2395	0.3955	0.1055	-0.6837	0.4397
0.6378	0.4078	0.5518	-0.2387	0.6718	0.8533	0.5469	0.8020	0.0362	0.5955	0.4151
0.7923	0.7881	0.5915	-0.1534	0.8286	0.5876	0.6567	0.2126	-0.2330	0.3079	0.5747
0.2061	0.1023	0.1317	-0.1606	0.2451	0.6175	0.2660	0.6532	0.5728	-0.2607	-0.2830
0.0642	-0.0966	0.0938	0.0219	0.0717	0.4632	0.1142	0.4144	0.4537	-0.2208	-0.3474
0.1608	-0.2024	0.1579	-0.0050	0.0204	0.2605	0.1314	0.0122	0.1842	0.1163	-0.1015
0.2085	-0.0782	0.3412	0.3830	0.1449	0.3429	0.2453	0.1916	0.1916	-0.0577	-0.2142
0.2778	0.3153	0.1981	-0.2664	0.4053	0.6682	0.3477	0.7274	0.1924	-0.0013	-0.0577
0.4960	0.6752	0.3279	-0.0416	0.3819	0.4661	0.2394	0.4705	0.4705	-0.2494	-0.0735
0.7377	0.8411	0.5990	-0.1277	0.8137	0.7201	0.5842	0.4795	-0.2087	0.5063	0.7064
0.2670	0.0963	0.1105	-0.0168	0.1632	0.5085	0.2745	0.2424	0.0826	0.1196	0.0298
0.5388	0.6222	0.2083	-0.1629	0.6420	0.4493	0.5349	0.3731	0.0055	0.1420	0.3827
0.7339	0.7362	0.5526	-0.0392	0.8062	0.8589	0.6038	0.5669	-0.0189	0.3265	0.5874
0.2773	0.3501	0.0904	0.2871	0.2892	0.1009	0.1849	0.2303	0.2173	-0.1394	0.2253
0.3681	0.2422	0.5044	0.2610	0.2888	0.4658	0.2944	0.4010	0.4010	-0.2545	-0.2717
0.0784	0.1290	0.1085	0.1591	0.0804	0.0446	-0.0019	0.1932	-0.1856	0.0945	0.1219
0.2916	0.1453	0.3592	-0.0878	0.2918	0.5528	0.3745	0.3952	0.3648	0.4695	0.0565

```
    0       0   0.6792   0.1039   0.8086        0        0        0        0        0        0
-0.2214       0   0.0680   0.4893  -0.2913        0  -0.2954  -0.3743  -0.3743  -0.3743  -0.3743
-0.0938       0  -0.0656   0.2110  -0.4231        0  -0.4259  -0.4030  -0.4030  -0.4030  -0.4030
```

Columns 12 through 22

```
 0.9167  -0.5071   0.0328   0.4304   0.6378   0.7923   0.2061   0.0642   0.1608   0.2085   0.2778
 0.8720   0.0731  -0.3150   0.4895   0.4078   0.7881   0.1023  -0.0966  -0.2024  -0.0782   0.3153
 0.7067   0.1061   0.0180   0.2998   0.5518   0.5915   0.1317   0.0938   0.1579   0.3412   0.1981
-0.4294   0.1443   0.0850  -0.1880  -0.2387  -0.1534  -0.1606   0.0219  -0.0050   0.3830  -0.2664
 1.0000  -0.4026  -0.0795   0.4101   0.6718   0.8286   0.2451   0.0717   0.0204   0.1449   0.4053
 0.7854   0.0132   0.1045   0.5444   0.8533   0.5876   0.6175   0.4632   0.2605   0.3429   0.6682
 0.7950   0.2116  -0.0208   0.2395   0.5469   0.6567   0.2660   0.1142   0.1314   0.2453   0.3477
 0.1786   0.1143  -0.0693   0.3955   0.8020   0.2126   0.6532   0.4144   0.0122   0.1916   0.7274
-0.4226  -0.2029   0.1672   0.1055   0.0362  -0.2330   0.5728   0.4537   0.1842   0.1916   0.1924
 0.5370   0.0912   0.0545  -0.6837   0.5955   0.3079  -0.2607  -0.2208   0.1163  -0.0577  -0.0013
 0.7087   0.1431  -0.1379   0.4397   0.4151   0.5747  -0.2830  -0.3474  -0.1015  -0.2142  -0.0577
 1.0000  -0.4026  -0.0795   0.4101   0.6718   0.8286   0.2451   0.0717   0.0204   0.1449   0.4053
-0.4026   1.0000  -0.0287  -0.0016   0.4530   0.2100  -0.1461  -0.0761  -0.0859   0.0010  -0.1962
-0.0795  -0.0287   1.0000  -0.1179   0.0536  -0.0680   0.4886   0.6327   0.9101   0.7207   0.2114
 0.4101  -0.0016  -0.1179   1.0000        0   0.3871   0.3010   0.0984  -0.0563  -0.0096   0.1772
 0.6718   0.4530   0.0536        0   1.0000        0        0        0   0.3189        0        0
 0.8286   0.2100  -0.0680   0.3871        0   1.0000   0.1705  -0.0041   0.0112   0.2182   0.1898
 0.2451  -0.1461   0.4886   0.3010        0   0.1705   1.0000   0.8741   0.6153   0.6788   0.7813
 0.0717  -0.0761   0.6327   0.0984        0  -0.0041   0.8741   1.0000   0.7170   0.7549   0.6319
 0.0204  -0.0859   0.9101  -0.0563   0.3189   0.0112   0.6153   0.7170   1.0000   0.8301   0.3311
 0.1449   0.0010   0.7207  -0.0096        0   0.2182   0.6788   0.7549   0.8301   1.0000   0.3992
 0.4053  -0.1962   0.2114   0.1772        0   0.1898   0.7813   0.6319   0.3311   0.3992   1.0000
 0.3819   0.4826  -0.1122   0.2758        0   0.3489   0.2345   0.1638  -0.0487   0.1411   0.2716
 0.8137   0.1271  -0.1985   0.7065        0   0.7565   0.1965   0.0535  -0.0715  -0.0748   0.3356
 0.1632  -0.0713   0.4959   0.1583   0.8740   0.2433   0.8189   0.7422   0.5656   0.7521   0.6842
 0.6420   0.6751  -0.1817   0.2929      NaN   0.5148   0.2045  -0.0410  -0.1468  -0.0271   0.2996
 0.8062   0.1574   0.0574   0.6684        0   0.6936   0.4491   0.3077   0.1720   0.2318   0.5114
 0.2892  -0.6584  -0.2296   0.3706        0   0.1779  -0.0745  -0.1800  -0.1574  -0.2666   0.0896
 0.2888   0.1098   0.5237   0.1314        0   0.4008   0.7205   0.6469   0.5887   0.8047   0.5590
 0.0804   0.0951  -0.0981   0.0583        0   0.0478   0.1099  -0.0393  -0.0498   0.3465   0.1115
 0.2918  -0.1148   0.5511   0.2617        0   0.1737   0.8412   0.8489   0.7080        0   0.5254
 0.8086   0.1039  -0.3070        0        0        0        0        0        0        0        0
-0.2913  -0.4535   0.6550        0        0  -0.1745  -0.3852   0.1279   0.3712   0.3660   0.1516
-0.4231  -0.0588   0.6288        0        0  -0.3970  -0.2911  -0.5284   0.3171   0.4683  -0.1546
```

Columns 23 through 33

```
 0.4960   0.7377   0.2670   0.5388   0.7339   0.2773   0.3681   0.0784   0.2916        0  -0.2214
 0.6752   0.8411   0.0963   0.6222   0.7362   0.3501   0.2422   0.1290   0.1453        0        0
 0.3279   0.5990   0.1105   0.2083   0.5526   0.0904   0.5044   0.1085   0.3592   0.6792   0.0680
-0.0416  -0.1277  -0.0168  -0.1629  -0.0392   0.2871   0.2610   0.1591  -0.0878   0.1039   0.4893
```

0.3819 0.8137 0.1632 0.6420 0.8062 0.2892 0.2888 0.0804 0.2918 0.8086 -0.2913
0.4661 0.7201 0.5085 0.4493 0.8589 0.1009 0.4658 0.0446 0.5528 0 0
0.2394 0.5842 0.2745 0.5349 0.6038 0.1849 0.2944 -0.0019 0.3745 0 -0.2954
0.4705 0.4795 0.2424 0.3731 0.5669 0.2303 0.4010 0.1932 0.3952 0 -0.3743
0.4705 -0.2087 0.0826 0.0055 -0.0189 0.2173 0.4010 -0.1856 0.3648 0 -0.3743
-0.2494 0.5063 0.1196 0.1420 0.3265 -0.1394 -0.2545 0.0945 0.4695 0 -0.3743
-0.0735 0.7064 0.0298 0.3827 0.5874 0.2253 -0.2717 0.1219 0.0565 0 -0.3743
0.3819 0.8137 0.1632 0.6420 0.8062 0.2892 0.2888 0.0804 0.2918 0.8086 -0.2913
0.4826 0.1271 -0.0713 0.6751 0.1574 -0.6584 0.1098 0.0951 -0.1148 0.1039 -0.4535
-0.1122 -0.1985 0.4959 -0.1817 0.0574 -0.2296 0.5237 -0.0981 0.5511 -0.3070 0.6550
0.2758 0.7065 0.1583 0.2929 0.6684 0.3706 0.1314 0.0583 0.2617 0 0
0 0 0.8740 NaN 0 0 0 0 0 0 0
0.3489 0.7565 0.2433 0.5148 0.6936 0.1779 0.4008 0.0478 0.1737 0 -0.1745
0.2345 0.1965 0.8189 0.2045 0.4491 -0.0745 0.7205 0.1099 0.8412 0 -0.3852
0.1638 0.0535 0.7422 -0.0410 0.3077 -0.1800 0.6469 -0.0393 0.8489 0 0.1279
-0.0487 -0.0715 0.5656 -0.1468 0.1720 -0.1574 0.5887 -0.0498 0.7080 0 0.3712
0.1411 -0.0748 0.7521 -0.0271 0.2318 -0.2666 0.8047 0.3465 0 0 0.3660
0.2716 0.3356 0.6842 0.2996 0.5114 0.0896 0.5590 0.1115 0.5254 0 0.1516
1.0000 0.5178 0.3049 0.2547 0.4389 0.2890 0.3850 -0.0475 0 0 -0.3731
0.5178 1.0000 0.2144 0.4580 0.7734 0.2043 0.0946 -0.0044 0.3234 0 0
0.3049 0.2144 1.0000 0.2812 0.3337 -0.0980 0.7696 0.0996 0.7054 0.2816 0.1562
0.2547 0.4580 0.2812 1.0000 0.3605 0.6510 0.2284 0.3620 -0.3924 0 -0.3365
0.4389 0.7734 0.3337 0.3605 1.0000 0.3386 0.3082 0.0333 0.5304 0 0
0.2890 0.2043 -0.0980 0.6510 0.3386 1.0000 0.1251 0.0498 -0.0822 0 0
0.3850 0.0946 0.7696 0.2284 0.3082 0.1251 1.0000 0.3328 0 0 -0.0098
-0.0475 -0.0044 0.0996 0.3620 0.0333 0.0498 0.3328 1.0000 0.0584 0 0
0 0.3234 0.7054 -0.3924 0.5304 -0.0822 0 0.0584 1.0000 0 0
0 0 0.2816 0 0 0 0 0 0 1.0000 0
-0.3731 0 0.1562 -0.3365 0 0 -0.0098 0 0 0 1.0000
-0.3813 0 0.1241 -0.5445 0 0 -0.0129 0 0 0 0.9860

Column 34

-0.0938
0
-0.0656
0.2110
-0.4231
0
-0.4259
-0.4030
-0.4030
-0.4030
-0.4030
-0.4231
-0.0588
0.6288

0
0
-0.3970
-0.2911
-0.5284
0.3171
0.4683
-0.1546
-0.3813
0
0.1241
-0.5445
0
0
-0.0129
0
0
0
0.9860
1.0000

interval =

Columns 1 through 9

0.0625	0.1020	0.0979	0.0655	0.0699	0.1101	0.0885	0.0885	0.0898
0.1020	0.1004	0.1052	0.1069	0.1046	0.1111	0.1054	0.1063	0.1087
0.0979	0.1052	0.0958	0.1025	0.0996	0.1137	0.1020	0.1036	0.1052
0.0655	0.1069	0.1025	0.0603	0.0689	0.1143	0.0927	0.0929	0.0939
0.0699	0.1046	0.0996	0.0689	0.0661	0.1132	0.0920	0.0930	0.0944
0.1101	0.1111	0.1137	0.1143	0.1132	0.1084	0.1145	0.1151	0.1180
0.0885	0.1054	0.1020	0.0927	0.0920	0.1145	0.0874	0.0908	0.0924
0.0885	0.1063	0.1036	0.0929	0.0930	0.1151	0.0908	0.0877	0.0912
0.0898	0.1087	0.1052	0.0939	0.0944	0.1180	0.0924	0.0912	0.0889
0.0905	0.1097	0.1061	0.0951	0.0947	0.1195	0.0923	0.0929	0.0935
0.0885	0.1057	0.1027	0.0923	0.0927	0.1149	0.0904	0.0912	0.0925
0.0699	0.1046	0.0996	0.0689	0.0661	0.1132	0.0920	0.0930	0.0944
0.0647	0.1037	0.0989	0.0608	0.0681	0.1126	0.0900	0.0901	0.0908
0.0698	0.1034	0.0981	0.0657	0.0686	0.1113	0.0921	0.0920	0.0933
0.1407	0.1411	0.1465	0.1521	0.1449	0.1559	0.1465	0.1441	0.1517
0.3313	0.3361	0.3313	0.3222	0.3180	0.3313	0.3222	0.4497	0.3412
0.1069	0.1225	0.1169	0.1135	0.1094	0.1349	0.1149	0.1128	0.1186
0.1284	0.1346	0.1340	0.1362	0.1353	0.1526	0.1376	0.1327	0.1376
0.1223	0.1290	0.1281	0.1295	0.1290	0.1453	0.1301	0.1270	0.1301
0.0921	0.1023	0.1005	0.0964	0.0941	0.1103	0.0956	0.0964	0.0981

0.1895	0.2139	0.1960	0.2139	0.2000	0.2772	0.2011	0.1913	0.1913
0.1184	0.1225	0.1240	0.1252	0.1245	0.1372	0.1260	0.1218	0.1265
0.1512	0.1657	0.1611	0.1639	0.1628	0.1970	0.1668	0.1545	0.1545
0.1304	0.1307	0.1376	0.1362	0.1346	0.1353	0.1362	0.1315	0.1411
0.0725	0.1130	0.1057	0.0691	0.0755	0.1209	0.0996	0.0992	0.0963
0.1366	0.1746	0.1559	0.1465	0.1411	0.2066	0.1453	0.1453	0.1465
0.1376	0.1393	0.1418	0.1445	0.1411	0.1473	0.1445	0.1422	0.1490
0.1310	0.1340	0.1389	0.1400	0.1379	0.1494	0.1379	0.1346	0.1400
0.1651	0.1904	0.1739	0.1812	0.1775	0.2294	0.1844	0.1675	0.1675
0.1797	0.1812	0.1895	0.1904	0.1820	0.2011	0.1869	0.1886	0.1960
0.1775	0.1739	0.1804	0.1895	0.1767	0.1789	0.1746	0.1820	0.2022
0	0	0.9800	0.1812	0.2922	0	0	0	0
0.2859	0	0.3578	0.3099	0.2859	0	0.2890	0.2922	0.2922
0.2955	0	0.3844	0.3180	0.3222	0	0.3222	0.3267	0.3267

Columns 10 through 18

0.0905	0.0885	0.0699	0.0647	0.0698	0.1407	0.3313	0.1069	0.1284
0.1097	0.1057	0.1046	0.1037	0.1034	0.1411	0.3361	0.1225	0.1346
0.1061	0.1027	0.0996	0.0989	0.0981	0.1465	0.3313	0.1169	0.1340
0.0951	0.0923	0.0689	0.0608	0.0657	0.1521	0.3222	0.1135	0.1362
0.0947	0.0927	0.0661	0.0681	0.0686	0.1449	0.3180	0.1094	0.1353
0.1195	0.1149	0.1132	0.1126	0.1113	0.1559	0.3313	0.1349	0.1526
0.0923	0.0904	0.0920	0.0900	0.0921	0.1465	0.3222	0.1149	0.1376
0.0929	0.0912	0.0930	0.0901	0.0920	0.1441	0.4497	0.1128	0.1327
0.0935	0.0925	0.0944	0.0908	0.0933	0.1517	0.3412	0.1186	0.1376
0.0896	0.0926	0.0947	0.0920	0.0946	0.1540	0.3313	0.1200	0.1433
0.0926	0.0874	0.0927	0.0897	0.0921	0.1494	0.3267	0.1159	0.1369
0.0947	0.0927	0.0661	0.0681	0.0686	0.1449	0.3180	0.1094	0.1353
0.0920	0.0897	0.0681	0.0596	0.0649	0.1437	0.3222	0.1091	0.1298
0.0946	0.0921	0.0686	0.0649	0.0612	0.1441	0.3222	0.1084	0.1318
0.1540	0.1494	0.1449	0.1437	0.1441	0.1386	0	0.1482	0.1517
0.3313	0.3267	0.3180	0.3222	0.3222	0	0.3180	0	0
0.1200	0.1159	0.1094	0.1091	0.1084	0.1482	0	0.1055	0.1393
0.1433	0.1369	0.1353	0.1298	0.1318	0.1517	0	0.1393	0.1273
0.1340	0.1295	0.1290	0.1237	0.1257	0.1469	0	0.1321	0.1304
0.0986	0.0958	0.0941	0.0932	0.0930	0.1396	0.3267	0.1128	0.1304
0.2078	0.2000	0.2000	0.1895	0.1913	0.2360	0	0.2126	0.1990
0.1281	0.1255	0.1245	0.1206	0.1202	0.1550	0	0.1313	0.1407
0.1651	0.1611	0.1628	0.1508	0.1540	0.1836	0	0.1700	0.1617
0.1433	0.1376	0.1346	0.1334	0.1324	0.1617	0	0.1366	0.1564
0.1015	0.0998	0.0755	0.0684	0.0702	0.1628	0.3412	0.1186	0.1437
0.1473	0.1461	0.1411	0.1369	0.1404	0.2066	0.0000 - 1.9600i	0.1559	0.1732
0.1531	0.1457	0.1411	0.1404	0.1415	0.1535	0	0.1469	0.1477
0.1437	0.1396	0.1379	0.1334	0.1346	0.1622	0	0.1396	0.1486
0.1844	0.1775	0.1775	0.1645	0.1657	0.2101	0	0.1820	0.1789

0.2000	0.1960	0.1820	0.1860	0.1877	0.2043	0	0.1913	0.1895
0.1950	0.1852	0.1767	0.1886	0.1820	0.2413	0	0.1804	0.2510
0	0	0.2922	0.1812	0.1508	0	0	0	0
0.2922	0.2922	0.2859	0.2859	0.2859	0	0	0.2922	0.9800
0.3267	0.3267	0.3222	0.2955	0.3222	0	0	0.3222	1.1316

Columns 19 through 27

0.1223	0.0921	0.1895	0.1184	0.1512	0.1304	0.0725	0.1366	0.1376
0.1290	0.1023	0.2139	0.1225	0.1657	0.1307	0.1130	0.1746	0.1393
0.1281	0.1005	0.1960	0.1240	0.1611	0.1376	0.1057	0.1559	0.1418
0.1295	0.0964	0.2139	0.1252	0.1639	0.1362	0.0691	0.1465	0.1445
0.1290	0.0941	0.2000	0.1245	0.1628	0.1346	0.0755	0.1411	0.1411
0.1453	0.1103	0.2772	0.1372	0.1970	0.1353	0.1209	0.2066	0.1473
0.1301	0.0956	0.2011	0.1260	0.1668	0.1362	0.0996	0.1453	0.1445
0.1270	0.0964	0.1913	0.1218	0.1545	0.1315	0.0992	0.1453	0.1422
0.1301	0.0981	0.1913	0.1265	0.1545	0.1411	0.0963	0.1465	0.1490
0.1340	0.0986	0.2078	0.1281	0.1651	0.1433	0.1015	0.1473	0.1531
0.1295	0.0958	0.2000	0.1255	0.1611	0.1376	0.0998	0.1461	0.1457
0.1290	0.0941	0.2000	0.1245	0.1628	0.1346	0.0755	0.1411	0.1411
0.1237	0.0932	0.1895	0.1206	0.1508	0.1334	0.0684	0.1369	0.1404
0.1257	0.0930	0.1913	0.1202	0.1540	0.1324	0.0702	0.1404	0.1415
0.1469	0.1396	0.2360	0.1550	0.1836	0.1617	0.1628	0.2066	0.1535
0	0.3267	0	0	0	0	0.3412	0.0000 - 1.9600i	0
0.1321	0.1128	0.2126	0.1313	0.1700	0.1366	0.1186	0.1559	0.1469
0.1304	0.1304	0.1990	0.1407	0.1617	0.1564	0.1437	0.1732	0.1477
0.1211	0.1240	0.1950	0.1353	0.1559	0.1490	0.1376	0.1628	0.1437
0.1240	0.0908	0.1950	0.1200	0.1559	0.1295	0.1025	0.1429	0.1379
0.1950	0.1950	0.1895	0.2066	0.1950	0.3099	0.2032	0.2234	0.2619
0.1353	0.1200	0.2066	0.1171	0.1633	0.1453	0.1315	0.1789	0.1564
0.1559	0.1559	0.1950	0.1633	0.1503	0.2032	0.1687	0.1904	0.1895
0.1490	0.1295	0.3099	0.1453	0.2032	0.1276	0.1499	0.2164	0.1535
0.1376	0.1025	0.2032	0.1315	0.1687	0.1499	0.0641	0.1503	0.1554
0.1628	0.1429	0.2234	0.1789	0.1904	0.2164	0.1503	0.1366	0.1990
0.1437	0.1379	0.2619	0.1564	0.1895	0.1535	0.1554	0.1990	0.1353
0.1426	0.1327	0.2219	0.1445	0.1797	0.1540	0.1469	0.1895	0.1590
0.1746	0.1719	0.1960	0.1812	0.1732	0.2431	0.1767	0.2089	0.2205
0.1836	0.1812	0.3704	0.2032	0.2667	0.2032	0.2089	0.2413	0.1931
0.2360	0.1753	0	0.2089	0	0.1860	0.2032	0.3704	0.2164
0	0	0	0	0	0	0.1574	0	0
0.5910	0.3099	0.5910	0.8765	0.5658	0	0.2989	0.2922	0
0.6533	0.3520	0.6198	0.9800	0.5658	0	0.3099	0.3313	0

Columns 28 through 34

0.1310	0.1651	0.1797	0.1775	0	0.2859	0.2955
0.1340	0.1904	0.1812	0.1739	0	0	0

0.1389	0.1739	0.1895	0.1804	0.9800	0.3578	0.3844
0.1400	0.1812	0.1904	0.1895	0.1812	0.3099	0.3180
0.1379	0.1775	0.1820	0.1767	0.2922	0.2859	0.3222
0.1494	0.2294	0.2011	0.1789	0	0	0
0.1379	0.1844	0.1869	0.1746	0	0.2890	0.3222
0.1346	0.1675	0.1886	0.1820	0	0.2922	0.3267
0.1400	0.1675	0.1960	0.2022	0	0.2922	0.3267
0.1437	0.1844	0.2000	0.1950	0	0.2922	0.3267
0.1396	0.1775	0.1960	0.1852	0	0.2922	0.3267
0.1379	0.1775	0.1820	0.1767	0.2922	0.2859	0.3222
0.1334	0.1645	0.1860	0.1886	0.1812	0.2859	0.2955
0.1346	0.1657	0.1877	0.1820	0.1508	0.2859	0.3222
0.1622	0.2101	0.2043	0.2413	0	0	0
0	0	0	0	0	0	0
0.1396	0.1820	0.1913	0.1804	0	0.2922	0.3222
0.1486	0.1789	0.1895	0.2510	0	0.9800	1.1316
0.1426	0.1746	0.1836	0.2360	0	0.5910	0.6533
0.1327	0.1719	0.1812	0.1753	0	0.3099	0.3520
0.2219	0.1960	0.3704	0	0	0.5910	0.6198
0.1445	0.1812	0.2032	0.2089	0	0.8765	0.9800
0.1797	0.1732	0.2667	0	0	0.5658	0.5658
0.1540	0.2431	0.2032	0.1860	0	0	0
0.1469	0.1767	0.2089	0.2032	0.1574	0.2989	0.3099
0.1895	0.2089	0.2413	0.3704	0	0.2922	0.3313
0.1590	0.2205	0.1931	0.2164	0	0	0
0.1298	0.2011	0.1970	0.2248	0	0	0
0.2011	0.1633	0.3139	0	0	0.4754	0.5061
0.1970	0.3139	0.1789	0.2800	0	0	0
0.2248	0	0.2800	0.1732	0	0	0
0	0	0	0	0.1441	0	0
0	0.4754	0	0	0	0.2859	0.3267
0	0.5061	0	0	0	0.3267	0.2955

==========Pacific coast==========

r =

Columns 1 through 12

Tofino	1.0000	0.9456	0.9679	0.8269	0.9767	0.9235	0.9325	0.9316	0.5357	0.8437	0.8055	0.9465
Port Alberny	0.9456	1.0000	0.9622	0.8351	0.9559	0.9491	0.9593	0.9499	0.6476	0.9378	0.9242	0.9535
Bamfield	0.9679	0.9622	1.0000	0.8507	0.9828	0.9636	0.9540	0.9468	0.5690	0.9317	0.9114	0.9388
Port Renfrew	0.8269	0.8351	0.8507	1.0000	0.7991	0.8699	0.8311	0.8496	0.5549	0.8485	0.8297	0.7819
Sooke	0.9767	0.9559	0.9828	0.7991	1.0000	0.9575	0.9535	0.9714	0.6334	0.9575	0.9484	0.9367
Victoria	0.9235	0.9491	0.9636	0.8699	0.9575	1.0000	0.9846	0.9662	0.6577	0.9513	0.9142	0.9137
Patricia Bay	0.9325	0.9593	0.9540	0.8311	0.9535	0.9846	1.0000	0.9740	0.7521	0.9643	0.9606	0.9336

Fulford Har	0.9316	0.9499	0.9468	0.8496	0.9714	0.9662	0.9740	1.0000	0.6871	0.9764	0.9733	0.9316
Steveston	0.5357	0.6476	0.5690	0.5549	0.6334	0.6577	0.7521	0.6871	1.0000	0.7819	0.7854	0.6501
Vancouver	0.8437	0.9378	0.9317	0.8485	0.9575	0.9513	0.9643	0.9764	0.7819	1.0000	0.9374	0.9040
Point Atkinson	0.8055	0.9242	0.9114	0.8297	0.9484	0.9142	0.9606	0.9733	0.7854	0.9374	1.0000	0.9228
Campbell	0.9465	0.9535	0.9388	0.7819	0.9367	0.9137	0.9336	0.9316	0.6501	0.9040	0.9228	1.0000
Alert Bay	0.9497	0.8664	0.9424	0.7619	0.9385	0.9296	0.8920	0.8999	0.3878	0.8709	0.8675	0.8440
Port Hardy	0.9643	0.9354	0.9607	0.8379	0.9467	0.9328	0.9224	0.9070	0.5420	0.8929	0.8710	0.9353
Bella Bella	0.9376	0.8901	0.9346	0.7856	0.9114	0.8924	0.8767	0.8722	0.5117	0.8646	0.8420	0.9238
Queen Char	0.4971	0.2866	0.3938	0.2981	0.4306	0.3953	0.2803	0.4272	-0.0176	0.3211	0.3197	0.3475
Prince Rupert	0.7412	0.8150	0.8752	0.7777	0.8374	0.8209	0.8257	0.7932	0.5074	0.7930	0.7611	0.8031
Friday	0.5090	0.3602	0.4087	0.4480	0.4459	0.5960	0.3064	0.3960	0.0362	0.4810	0.4144	0.3357
Toke	0.9310	0.9034	0.9626	0.8220	0.9554	0.9057	0.8894	0.8779	0.5241	0.8697	0.8359	0.8712
South	0.8833	0.8825	0.9531	0.8627	0.9687	0.9223	0.9154	0.9112	0.5268	0.8858	0.8441	0.8250
Seathle	0.6111	0.9320	0.9604	0.8582	0.9747	0.9018	0.9557	0.9416	0.6725	0.8263	0.8768	0.8625
Ptown	0.9170	0.9417	0.9678	0.8511	0.9804	0.9564	0.9575	0.9563	0.6632	0.9509	0.9201	0.8902
Pang	0.9628	0.9633	0.9877	0.8166	0.9915	0.9587	0.9524	0.9582	0.6530	0.9446	0.9259	0.9381
Neah	0.9814	0.9420	0.9730	0.8809	0.9778	0.9128	0.9172	0.9121	0.5117	0.8702	0.8709	0.9519
Char	0.9205	0.8825	0.9516	0.8199	0.9641	0.9276	0.9225	0.9326	0.5383	0.9032	0.8772	0.8789
Astra	0.8365	0.8589	0.8862	0.7656	0.8992	0.7844	0.8702	0.8048	0.6155	0.7895	0.7565	0.8320
ACher	0.9184	0.9407	0.9500	0.8297	0.9718	0.9617	0.9714	0.9859	0.7608	0.9797	0.9714	0.9350

Columns 13 through 24

0.9497	0.9643	0.9376	0.4971	0.7412	0.5090	0.9310	0.8833	0.6111	0.9170	0.9628	0.9814
0.8664	0.9354	0.8901	0.2866	0.8150	0.3602	0.9034	0.8825	0.9320	0.9417	0.9633	0.9420
0.9424	0.9607	0.9346	0.3938	0.8752	0.4087	0.9626	0.9531	0.9604	0.9678	0.9877	0.9730
0.7619	0.8379	0.7856	0.2981	0.7777	0.4480	0.8220	0.8627	0.8582	0.8511	0.8166	0.8809
0.9385	0.9467	0.9114	0.4306	0.8374	0.4459	0.9554	0.9687	0.9747	0.9804	0.9915	0.9778
0.9296	0.9328	0.8924	0.3953	0.8209	0.5960	0.9057	0.9223	0.9018	0.9564	0.9587	0.9128
0.8920	0.9224	0.8767	0.2803	0.8257	0.3064	0.8894	0.9154	0.9557	0.9575	0.9524	0.9172
0.8999	0.9070	0.8722	0.4272	0.7932	0.3960	0.8779	0.9112	0.9416	0.9563	0.9582	0.9121
0.3878	0.5420	0.5117	-0.0176	0.5074	0.0362	0.5241	0.5268	0.6725	0.6632	0.6530	0.5117
0.8709	0.8929	0.8646	0.3211	0.7930	0.4810	0.8697	0.8858	0.8263	0.9509	0.9446	0.8702
0.8675	0.8710	0.8420	0.3197	0.7611	0.4144	0.8359	0.8441	0.8768	0.9201	0.9259	0.8709
0.8440	0.9353	0.9238	0.3475	0.8031	0.3357	0.8712	0.8250	0.8625	0.8902	0.9381	0.9519
1.0000	0.9485	0.8911	0.5811	0.8389	0.5298	0.9142	0.8863	0.8737	0.9160	0.9209	0.9411
0.9485	1.0000	0.9575	0.4186	0.8903	0.4171	0.9365	0.8800	0.8841	0.9204	0.9542	0.9639
0.8911	0.9575	1.0000	0.4493	0.9290	0.4033	0.9165	0.8413	0.8224	0.8749	0.9243	0.9301
0.5811	0.4186	0.4493	1.0000	0.4486	0.3868	0.3918	0.4246	0.3591	0.3196	0.3540	0.4540
0.8389	0.8903	0.9290	0.4486	1.0000	0.5274	0.8846	0.8197	0.7853	0.8421	0.8754	0.8238
0.5298	0.4171	0.4033	0.3868	0.5274	1.0000	0.4319	0.4393	0.6065	0.3570	0.3606	0.3884
0.9142	0.9365	0.9165	0.3918	0.8846	0.4319	1.0000	0.9526	0.9294	0.9491	0.9631	0.9459
0.8863	0.8800	0.8413	0.4246	0.8197	0.4393	0.9526	1.0000	0.9626	0.9696	0.9560	0.8779
0.8737	0.8841	0.8224	0.3591	0.7853	0.6065	0.9294	0.9626	1.0000	0.9906	0.9664	0.8309
0.9160	0.9204	0.8749	0.3196	0.8421	0.3570	0.9491	0.9696	0.9906	1.0000	0.9750	0.9109
0.9209	0.9542	0.9243	0.3540	0.8754	0.3606	0.9631	0.9560	0.9664	0.9750	1.0000	0.9686
0.9411	0.9639	0.9301	0.4540	0.8238	0.3884	0.9459	0.8779	0.8309	0.9109	0.9686	1.0000

0.9090	0.9036	0.8645	0.4313	0.8212	0.4232	0.9259	0.9719	0.9470	0.9482	0.9502	0.9115
0.7676	0.8565	0.7982	0.2891	0.6374	0.4243	0.9153	0.8464	0.6932	0.8938	0.9077	0.8609
0.8933	0.9062	0.8745	0.2854	0.8224	0.2783	0.8820	0.9178	0.9643	0.9607	0.9545	0.9043

Columns 25 through 27

0.9205	0.8365	0.9184
0.8825	0.8589	0.9407
0.9516	0.8862	0.9500
0.8199	0.7656	0.8297
0.9641	0.8992	0.9718
0.9276	0.7844	0.9617
0.9225	0.8702	0.9714
0.9326	0.8048	0.9859
0.5383	0.6155	0.7608
0.9032	0.7895	0.9797
0.8772	0.7565	0.9714
0.8789	0.8320	0.9350
0.9090	0.7676	0.8933
0.9036	0.8565	0.9062
0.8645	0.7982	0.8745
0.4313	0.2891	0.2854
0.8212	0.6374	0.8224
0.4232	0.4243	0.2783
0.9259	0.9153	0.8820
0.9719	0.8464	0.9178
0.9470	0.6932	0.9643
0.9482	0.8938	0.9607
0.9502	0.9077	0.9545
0.9115	0.8609	0.9043
1.0000	0.8300	0.9294
0.8300	1.0000	0.8445
0.9294	0.8445	1.0000

interval =

Columns 1 through 12

0.0702	0.1171	0.1040	0.1178	0.1645	0.0765	0.1182	0.0930	0.1139	0.0712	0.0800	0.1036
0.1171	0.1117	0.1124	0.1247	0.1668	0.1117	0.1273	0.1240	0.1143	0.1120	0.1128	0.1173
0.1040	0.1124	0.1002	0.1216	0.1668	0.1004	0.1132	0.1218	0.1117	0.1004	0.1049	0.1055
0.1178	0.1247	0.1216	0.1128	0.1746	0.1130	0.1382	0.1245	0.1209	0.1132	0.1141	0.1287
0.1645	0.1668	0.1668	0.1746	0.1590	0.1595	0.2000	0.1590	0.1700	0.1595	0.1645	0.1657
0.0765	0.1117	0.1004	0.1130	0.1595	0.0646	0.1128	0.0907	0.1091	0.0726	0.0783	0.1009
0.1182	0.1273	0.1132	0.1382	0.2000	0.1128	0.1126	0.1422	0.1298	0.1128	0.1186	0.1165
0.0930	0.1240	0.1218	0.1245	0.1590	0.0907	0.1422	0.0906	0.1202	0.0912	0.0943	0.1200

0.1139	0.1143	0.1117	0.1209	0.1700	0.1091	0.1298	0.1202	0.1089	0.1094	0.1104	0.1180
0.0712	0.1120	0.1004	0.1132	0.1595	0.0726	0.1128	0.0912	0.1094	0.0657	0.0761	0.1011
0.0800	0.1128	0.1049	0.1141	0.1645	0.0783	0.1186	0.0943	0.1104	0.0761	0.0732	0.1058
0.1036	0.1173	0.1055	0.1287	0.1657	0.1009	0.1165	0.1200	0.1180	0.1011	0.1058	0.1007
0.1069	0.2126	0.2022	0.1782	0.2219	0.1033	0.3844	0.1126	0.1895	0.1039	0.1110	0.1904
0.0954	0.1135	0.1018	0.1176	0.1693	0.0928	0.1149	0.1086	0.1103	0.0932	0.0963	0.1023
0.0931	0.1149	0.1023	0.1186	0.1700	0.0907	0.1153	0.1051	0.1117	0.0912	0.0942	0.1032
0.0946	0.1141	0.1113	0.1151	0.1639	0.0918	0.1273	0.0992	0.1113	0.0924	0.0952	0.1120
0.0725	0.1126	0.1009	0.1137	0.1590	0.0720	0.1135	0.0924	0.1097	0.0686	0.0757	0.1015
0.0843	0.1145	0.1128	0.1151	0.1590	0.0751	0.1284	0.0922	0.1119	0.0798	0.0851	0.1133
0.1106	0.1191	0.1066	0.1313	0.1746	0.1063	0.1135	0.1331	0.1200	0.1063	0.1119	0.1087
0.0980	0.1117	0.1002	0.1151	0.1645	0.0950	0.1132	0.1128	0.1089	0.0951	0.0989	0.1019
0.0702	0.1117	0.1002	0.1128	0.1590	0.0646	0.1126	0.0906	0.1089	0.0657	0.0732	0.1007
0.1061	0.1137	0.1027	0.1255	0.1645	0.1023	0.1132	0.1255	0.1145	0.1025	0.1072	0.1048
0.1137	0.1220	0.1089	0.1369	0.1877	0.1089	0.1132	0.1386	0.1240	0.1091	0.1151	0.1117
0.0899	0.1135	0.1015	0.1161	0.1706	0.0876	0.1137	0.1011	0.1106	0.0880	0.0919	0.1022
0.1037	0.1126	0.1008	0.1216	0.1645	0.1002	0.1141	0.1216	0.1115	0.1003	0.1048	0.1055
0.0773	0.1117	0.1002	0.1132	0.1590	0.0659	0.1126	0.0913	0.1089	0.0737	0.0789	0.1011
0.1081	0.1159	0.1045	0.1287	0.1651	0.1040	0.1132	0.1287	0.1169	0.1040	0.1092	0.1063

Columns 13 through 24

0.1069	0.0954	0.0931	0.0946	0.0725	0.0843	0.1106	0.0980	0.0702	0.1061	0.1137	0.0899
0.2126	0.1135	0.1149	0.1141	0.1126	0.1145	0.1191	0.1117	0.1117	0.1137	0.1220	0.1135
0.2022	0.1018	0.1023	0.1113	0.1009	0.1128	0.1066	0.1002	0.1002	0.1027	0.1089	0.1015
0.1782	0.1176	0.1186	0.1151	0.1137	0.1151	0.1313	0.1151	0.1128	0.1255	0.1369	0.1161
0.2219	0.1693	0.1700	0.1639	0.1590	0.1590	0.1746	0.1645	0.1590	0.1645	0.1877	0.1706
0.1033	0.0928	0.0907	0.0918	0.0720	0.0751	0.1063	0.0950	0.0646	0.1023	0.1089	0.0876
0.3844	0.1149	0.1153	0.1273	0.1135	0.1284	0.1135	0.1132	0.1126	0.1132	0.1132	0.1137
0.1126	0.1086	0.1051	0.0992	0.0924	0.0922	0.1331	0.1128	0.0906	0.1255	0.1386	0.1011
0.1895	0.1103	0.1117	0.1113	0.1097	0.1119	0.1200	0.1089	0.1089	0.1145	0.1240	0.1106
0.1039	0.0932	0.0912	0.0924	0.0686	0.0798	0.1063	0.0951	0.0657	0.1025	0.1091	0.0880
0.1110	0.0963	0.0942	0.0952	0.0757	0.0851	0.1119	0.0989	0.0732	0.1072	0.1151	0.0919
0.1904	0.1023	0.1032	0.1120	0.1015	0.1133	0.1087	0.1019	0.1007	0.1048	0.1117	0.1022
0.1030	0.1508	0.1407	0.1284	0.1052	0.1086	0.2718	0.1668	0.1030	0.2205	0.3313	0.1340
0.1508	0.0926	0.0945	0.1015	0.0932	0.1020	0.1079	0.0961	0.0926	0.1037	0.1108	0.0937
0.1407	0.0945	0.0894	0.0986	0.0911	0.0991	0.1087	0.0969	0.0894	0.1045	0.1115	0.0914
0.1284	0.1015	0.0986	0.0917	0.0934	0.0944	0.1184	0.1042	0.0917	0.1137	0.1225	0.0952
0.1052	0.0932	0.0911	0.0934	0.0660	0.0798	0.1068	0.0954	0.0660	0.1029	0.1096	0.0891
0.1086	0.1020	0.0991	0.0944	0.0798	0.0747	0.1216	0.1054	0.0747	0.1157	0.1257	0.0955
0.2718	0.1079	0.1087	0.1184	0.1068	0.1216	0.1005	0.1005	0.1005	0.1005	0.1039	0.1016
0.1668	0.0961	0.0969	0.1042	0.0954	0.1054	0.1005	0.0908	0.0908	0.0972	0.1029	0.0918
0.1030	0.0926	0.0894	0.0917	0.0660	0.0747	0.1005	0.0908	0.0547	0.0972	0.1029	0.0843
0.2205	0.1037	0.1045	0.1137	0.1029	0.1157	0.1005	0.0972	0.0972	0.0972	0.1029	0.0984
0.3313	0.1108	0.1115	0.1225	0.1096	0.1257	0.1039	0.1029	0.1029	0.1029	0.1029	0.1043
0.1340	0.0937	0.0914	0.0952	0.0891	0.0955	0.1016	0.0918	0.0843	0.0984	0.1043	0.0843
0.1960	0.1015	0.1022	0.1106	0.1004	0.1126	0.1012	0.0953	0.0953	0.0978	0.1036	0.0964

0.1045	0.0929	0.0908	0.0921	0.0732	0.0761	0.1005	0.0910	0.0641	0.0972	0.1029	0.0846
0.2395	0.1055	0.1063	0.1161	0.1045	0.1182	0.1005	0.0986	0.0986	0.0986	0.1029	0.0999

Columns 25 through 27

0.1037	0.0773	0.1081
0.1126	0.1117	0.1159
0.1008	0.1002	0.1045
0.1216	0.1132	0.1287
0.1645	0.1590	0.1651
0.1002	0.0659	0.1040
0.1141	0.1126	0.1132
0.1216	0.0913	0.1287
0.1115	0.1089	0.1169
0.1003	0.0737	0.1040
0.1048	0.0789	0.1092
0.1055	0.1011	0.1063
0.1960	0.1045	0.2395
0.1015	0.0929	0.1055
0.1022	0.0908	0.1063
0.1106	0.0921	0.1161
0.1004	0.0732	0.1045
0.1126	0.0761	0.1182
0.1012	0.1005	0.1005
0.0953	0.0910	0.0986
0.0953	0.0641	0.0986
0.0978	0.0972	0.0986
0.1036	0.1029	0.1029
0.0964	0.0846	0.0999
0.0953	0.0953	0.0992
0.0953	0.0641	0.0986
0.0992	0.0986	0.0986

Appendix VI

The Canadian 1st order leveling lines which need to be re-leveled

Based on the data distribution in each patch to obtain a more stable VCM solution for that patch, the leveling lines that need to be surveyed for crustal motion analysis are identified. Figure g.1, depicts the leveling lines and re-leveled segments in Canada. In this figure, the green dot-lines show the Canadian levelling network, and the red dot-lines represent the re-leveled segments. The leveling lines that need to be re-leveled are marked by their name in the figure. Table g. 1 list these leveling lines and their length.

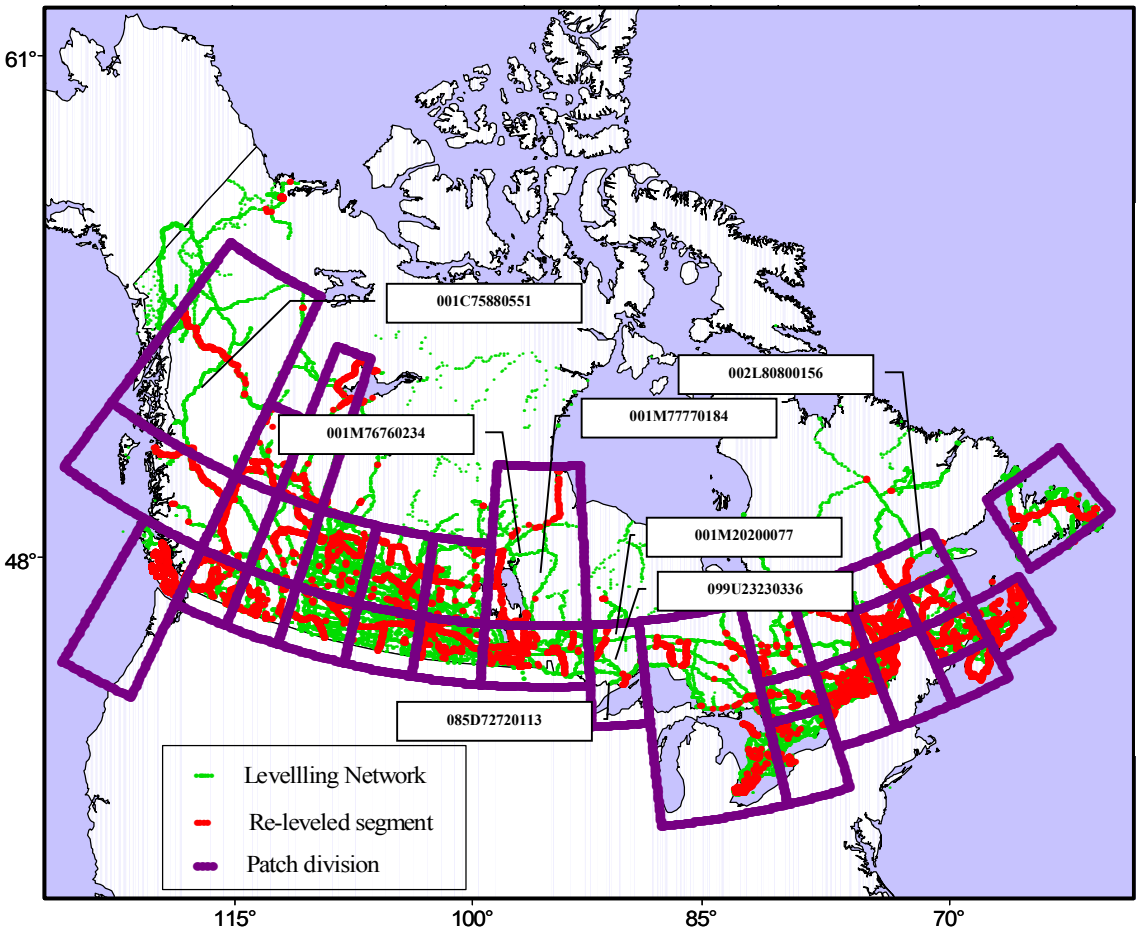

Figure g.1: The distribution of leveling and re-leveled data in Canada.

Table g.1: List of leveling lines that are recommended to be re-leveled for the crustal motion analysis.

Levelling line	**Length** (km)
001M76760234	170
100M20200077	190
099U23230336	186
085D72720113	168
001M77770184	410
001C75880551	398
002L80800156	145

Appendix VII

A sample of ICE models

The given ICE-4G model

It gives the coordinates of the center of each element along with the ice thickness in every discrete ice history deglaciation.

1 6.657 282.500 0.277 2.500 893. 893. 893. 893. 893. 893. 893. 893.
893. 744. 596. 447. 179. 0. 0. 0. 0. 0. 0. 0. 0. 0. 0.
2 6.657 287.500 0.277 2.500 1056.1056.1056.1056.1056.1056.1056.1056.
1056. 897. 737. 578. 191. 0. 0. 0. 0. 0. 0. 0. 0. 0. 0.
3 6.657 292.500 0.277 2.500 888. 888. 888. 888. 888. 888. 888. 888.
888. 740. 592. 444. 178. 0. 0. 0. 0. 0. 0. 0. 0. 0. 0.
4 7.250 280.000 0.316 2.500 1214.1214.1214.1214.1214.1214.1214.1214.
1214.1016. 817. 619. 261. 23. 23. 23. 23. 23. 23. 23. 23. 23. 23.
5 7.250 285.000 0.316 2.500 1056.1056.1056.1056.1056.1056.1056.1056.
1056. 951. 846. 741. 431. 225. 225. 225. 225. 225. 225. 225. 225. 225.
6 7.250 290.000 0.316 2.500 1310.1310.1310.1310.1310.1310.1310.1310.
1310.1143. 976. 810. 390. 110. 110. 110. 110. 110. 110. 110. 110. 110.
7 7.250 294.000 0.316 1.500 1286.1286.1286.1286.1286.1286.1286.1286.
1286.1122. 957. 793. 317. 0. 0. 0. 0. 0. 0. 0. 0. 0. 0.
8 7.450 297.000 0.116 1.500 1186.1186.1186.1186.1186.1186.1186.1186.
1186.1022. 857. 693. 317. 0. 0. 0. 0. 0. 0. 0. 0. 0. 0.
9 7.910 276.000 0.344 2.500 1376.1376.1376.1376.1376.1376.1376.1376.
1376.1206.1036. 866. 350. 6. 6. 6. 6. 6. 6. 6. 6. 6. 6.
10 7.910 281.000 0.344 2.500 1551.1551.1551.1551.1551.1551.1551.1551.
1551.1323.1094. 866. 395. 81. 81. 81. 81. 81. 81. 81. 81. 81. 81.
11 7.910 286.000 0.344 2.500 1454.1454.1454.1454.1454.1454.1454.1454.
1454.1284.1114. 944. 517. 233. 233. 233. 233. 233. 233. 233. 233. 233. 233.
12 7.910 291.000 0.344 2.500 1475.1475.1475.1475.1475.1475.1475.1475.
1475.1291.1107. 923. 471. 170. 170. 170. 170. 170. 170. 170. 170. 170. 170.

Curriculum Vita

AZADEH KOOHZARE, Ph.D.

Dep. of Geodesy and Geomatics Engineering
University of New Brunswick
P.O. Box 4400, Fredericton, NB E3B 5A3
a.koohzare@unb.ca

EMPLOYMENT

Research Assistant, University of New Brunswick	2003-2007
Instructor, University of New Brunswick	2006-2007
Instructor, K. N. Toosi University of Technology, Tehran	2001-2003
Research Assistant, K. N. Toosi University of Technology, Tehran	2001-2002
Geodetic Survey Division, National Cartographic Center, Tehran	1999-2003

EDUCATION

Ph.D. ***Geodesy and Geomatics*** **2003-2007**
Dept. Geodesy and Geomatics Engineering
University of New Brunswick (UNB), Fredericton, NB
Thesis title: 'A physically meaningful model of vertical crustal movements in Canada using smooth piecewise algebraic approximation, Constraints for Glacial Isostatic Adjustment Models'
GPA: 4.3

M.Sc. ***Geodesy and Geomatics*** **1999-2001**
Dept. Geodesy and Geomatics Engineering
K. N. Toosi University of Technology, Tehran (KNTU)
Thesis title: 'Geodynamics modeling and geodetic observations of Arabia-Eurasia collision zone'
Thesis GPA: **4.3**
Course GPA: 4.0

B.Sc. ***Civil-Surveying Engineering,*** **1995-1999**
K.N.Toosi University of Technology, Tehran
GPA: **4.0**

ACADEMIC HONOURS AND AWARDS

- **First Prize** for the best presentation in Canadian Geophysical Union conference, Banff, 2005.
- **Distinction:** Research fellowship from the research network of Geomatics for Informed Decisions (GEOIDE) Canada, to work as a *visiting scientist* in the Dept. Of Earth Sciences, University of Calgary, Canada, 2005.
- **First Prize** for the best presentation in 2004 Student Technical Conference. University of New Brunswick, 2004.

WORK EXPERIENCES

University of New Brunswick (UNB) **Feb 2003-Present**
Research Assistant

Geodetic Survey Division, National Cartographic Center, Tehran, Iran **Oct 1999-Jan 2003**
Professional Geomatic Engineer

K.N. Toosi University of Technology, Tehran **Oct 2000-Oct 2002**
ITC Assistant *(Part-time)*

TEACHING EXPERIENCES

- ***Geodesy I,*** University of New Brunswick, Fredericton, NB, Canada, 2006.
- ***Geodesy II,*** University of New Brunswick, Fredericton , NB, Canada, 2004 and 2005
- ***Kinematics Positioning,*** University of New Brunswick, Fredericton , NB, Canada, 2005
- ***Dini 12-22,*** National cartographic Center, Tehran, Iran, 2002.
- ***Theory of errors and Statistics***, K. N. Toosi University of Technology, Tehran, 2002
- ***Differentional Geometry,*** K. N. Toosi University of Technology, Tehran, Iran, 2001

TEACHING DEGREE AND HOUNORS

- Honoured **Diploma in University Teaching, University of New Brunswick**, 2005.
- Completion of the training program for Mentoring and Tutoring to students with disabilities. Project: Successful Transition Employment Program (STEP), University of New Brunswick, 2005.

PUBLICATIONS

Refereed Publications:

Koohzare, A., Vaníček, P., and Santos, M. (2007). Geodetic modeling and geophysical interpretation of recent vertical crustal movements and gravity changes over Canada, *IUGG XXIV 2007, Joint assembly, Perugia, Italy (Accepted).*

Koohzare, A., P. Vanícek and M. Santos (2006). Compilation of a map of recent vertical crustal movements in eastern Canada using GIS. *Journal of Surveying Engineering. ASCE*, *Vol.132, No.4, pp. 160-16.*

Koohzare, A., Vaníček, P., and Santos, M. (2006). The use of smooth piecewise algebraic approximation in the determination of vertical crustal movements in Eastern Canada. *Proc., Joint assembly of the IAG, IAPSO and IABO, Cairns, Australia, 130.*

Koohzare, A., Vaníček, P., and Santos, M. (2006). Smooth Piecewise Algebraic Approximation as applied to large-scale 2D scattered geodetic data fitting, *Computers and Geosciences, (in review)*

Koohzare, A., Vaníček, P., and Santos, M. (2006). Pattern of recent vertical crustal movements in Canada, *Journal of Geodynamic (in review).*

Koohzare, A., Vaníček, P. and Santos, M (2006). Comparison of the recent vertical crustal movements with the rate of gravity changes and GPS heights in Canada. *(To be submitted to Journal of Geodynamic).*

Koohzare. A, P. Vanícek, Santos, M. (2005). Compilation of a map of vertical crustal movements in Eastern Canada using Spline polynomials. *Ellements Vol 23, no. 2. pp30-34.*

Koohzare.A. and N. R. Nazari (2001). The consideration of different terms of Molodenskij solution in determining height anomaly. *Proceedings Geomatics 80 conference, National Cartographic. Geomatic80 Proceeding. Tehran. Iran.*

Koohzare, A., F. Tavakoli and M. Sedigh (2000). The determination of vertical crustal movements in North Tehran fault using precise levelling data". *Proceeding*, *ASC Seismology, Earthquake Hazard Assessment and Earth's Interior Related Topics, 2000".Publisher: University of Tehran. Tehran. Iran.*

Non-refereed Publications and Papers Presented at Professional and Technical Meetings:

Koohzare A., P. Vanícek and M. Santos (2007). Geodetic modeling and geophysical interpretation of recent vertical crustal movements and gravity changes over Canada*, IUGG XXIV 2007, joint Assembly, perugia, Italy (Accepted)*

Koohzare A., P. Vanícek and M. Santos (2006). Radial basis functions fitting methods and smooth piecewise algebraic approximation to determine postglacial tilting in the Canadian Prairies, Canadian Geophysical Union conference. Banff, 2005.

Koohzare. A., P. Vanícek and M. Santos (2006). The Contribution of Northern US Geodetic Data to the Study of Vertical Deformations of the Crust in Canada, American Geophysical Union, Baltimore 2006.

Koohzare, A., P. Vanícek and M. Santos (2005). Compilation of the map of vertical crustal movements in Eastern Canada using spline polynomials. Canadian Geophysical Union conference. Banff, 2005.

Koohzare, A., P. Vanícek and M. Santos (2004). Glacial Isostatic Adjustment Observed using Historical Tide Gauge Records and Precise Relevelling Data in Eastern Canada. *American Geophysical Union (AGU) and Canadian Geophysical Union (CGU) join assembly. Montreal, 2004*.

Koohzare, A., P. Vanícek and M. Santos (2004). Spatial Analysis and Treatment of sea Level records using GIS. *GEOIDE Annual Conference, Ottawa, 2004*.

Koohzare, A., P. Vanícek and M. Santos (2004). GIS data structure for crustal deformation studies: How GIS can help geodesy? *Geomatics Atlantics, Fredericton, N.B. 2004* (poster presentation).

Koohzare. A. (1999). Orbit determination and its improvement for GPS satellites. *The first seminar of surveying engineering and Geomatics, Conference Proceeding. Isfahan University*.

Books or part of Books

Koohzare. A, and M. Choobchian (2000) Digital levels Dini10, 12, 22. *National Cartographic Center. (NCC) Tehran, Iran.*

Invited talk:

Geodetic Survey Division, National Resource of Canada. Modeling Vertical Crustal Movements in Canada using Smooth Piecewise Algebraic Approximation (Modeler le mouvement vertical de la croûte terrestre au Canada en utilisant la méthode "Smooth Piecewise Algebraic Approximation"), July 2006

REFERENCES AVAILABLE UPON REQUEST